

**Development of Methods for Assessment of the Effects of Sterilisation on Acellular
Vascular Grafts**

Jake Christopher Milton-Barker

Submitted in accordance with the requirements for the degree of
Doctor of Philosophy

The University of Leeds
Institute of Medical and Biological Engineering

September, 2015

The candidate confirms that the work submitted is his/her own and that appropriate credit has been given where reference has been made to the work of others.

This copy has been supplied on the understanding that it is copyright material and that no quotation from the thesis may be published without proper acknowledgement.

The right of Jake Milton - Barker to be identified as Author of this work has been asserted by him in accordance with the Copyright, Designs and Patents Act 1988.

© 2015 The University of Leeds and Jake Christopher Milton - Barker

Acknowledgements

Firstly I would like to thank my supervisors Professor Eileen Ingham, Professor John Fisher, Dr Stacy-Paul Wilshaw and Dr Helen Berry. Together they have been instrumental to the success, of both myself and the completion of my Ph.D thesis. I would also like to thank my fellow Ph.D and post-doctoral researchers, Japareng Lalung, Helen Lee, Eirini Tsagkaraki, Will Vickers, Chris Serna, Andrew Aldridge, Jennifer Edwards, Mark Hepples, Iraklis Papageorgiou, Lindsay Parker, Carl Maguire, Keeley Tomkinson and Natalie Hakes to name but a few as their support, knowledge and advice has been invaluable over the past few years both on a personal and academic level. I would also like to thank Dan Thomas and the laboratory technicians for all of their help and support that was equally essential to the success of this study.

I would like to thank Jamie Roberts and Sally-Anne Poyser for providing me with not just a place to live but a place to call home for the most part of my study. Two of the best friends that without, none of this would have been possible.

Finally I would like to thank the support of my family whose guidance and security equipped me with the tools to progress this far in life. A special thank you to Keith Milton – Barker who my every success is a credit to your persistence and dedication as a father.

Abstract

Cardiovascular disease is the highest cause of morbidity worldwide, encompassing blood vessel disorders such as coronary artery and peripheral arterial disease. For small diameter applications (less than 6 mm) a tissue engineered commercial product is yet to be produced. Previously, a process for the production of acellular porcine carotid arteries was developed which showed excellent potential for clinical translation as vascular bypass grafts. Medical products, however, need to be sterilised to a sterility assurance level of 10^{-6} before they can be used clinically.

The aim of this thesis was firstly to produce acellular vascular grafts from porcine carotid arteries using previously developed decellularisation technology. Secondly, to develop robust methods capable of evaluating the effects of different sterilisation methods on the biological and mechanical characteristics of acellular vascular grafts and finally to determine the compatibility of the main stream industrially available sterilisation processes (Gamma and E-Beam irradiation and ethylene oxide treatment) with acellular vascular grafts.

Decellularisation of porcine carotid arteries was evaluated by determination of DNA content and histology. Biocompatibility was assessed using contact cytotoxicity. Acellular arteries were then subjected to 30 kGy (25 kGy min) E-Beam or Gamma irradiation or ethylene oxide treatment. The effects of sterilisation were determined using histology, immunohistochemistry, second harmonic generation multiphoton imaging, differential scanning calorimetry, denatured collagen content and determination of mechanical properties compared to non-sterilised acellular arteries. Mechanical properties were assessed using uniaxial tensile testing at a low strain rate to failure and burst pressure and compliance testing

Histologically, the architecture of the arteries was retained post decellularisation and DNA content was reduced by greater than 95 %. The arteries were not cytotoxic. Stress strain mechanics were also retained but compliance testing showed a significant reduction.

Post sterilisation with both Gamma irradiation and E-beam irradiation, there was a significantly increased stiffness of the elastin and collagen modulus of the acellular arteries. Ethylene oxide treatment significantly increased the elastin and collagen modulus. E-Beam irradiation and ethylene oxide treatment reduced compliance excessively. Histology showed the architecture of gamma and E-beam sterilised arteries to be consistent with acellular arteries and that ethylene oxide treated arteries exhibited some layer separation. Multiphoton imaging showed damage to all sterilised samples with Gamma sterilised acellular arteries the least affected. There were no significant differences in denaturation temperature.

These results were in partial agreement with previously reported data on the effects of Gamma and E-beam sterilisation on tendons. Gamma, E-beam [30 kGy] irradiation and ethylene oxide treatment caused detrimental effects to the mechanical properties of acellular porcine carotid arteries. E-beam irradiation and ethylene oxide treatment caused severe reduction in the compliance of acellular porcine carotid arteries. Compliance mismatch is a known failure mechanism of vascular grafts, therefore E-Beam irradiation and ethylene oxide treatment were not compatible with acellular vascular grafts. Gamma irradiation caused the least damaging effects and is the most likely candidate of the three that could potentially be optimised for sterilising acellular vascular grafts.

Table of Contents

Acknowledgements	iii
Abstract	iv
Table of Contents	vi
List of Tables	xii
List of Figures	xiv
Chapter 1 Vascular Disease and Small Diameter Vascular Grafts	1
1.1 Introduction.....	1
1.2 The vascular system.....	2
1.2.1 Physiology of Blood Vessels.....	4
1.2.2 Extracellular Matrix and its Components.....	5
1.3 Vascular disease, risk, incidence and therapies	7
1.3.1 Atherosclerosis, Thrombosis and Hypertension.....	9
1.3.2 Incidence and Risk of Cardiovascular Disease	13
1.3.3 Therapies.....	14
1.4 Small Diameter Vascular Grafts.....	16
1.4.1 Synthetic SDVG	17
1.4.1.1 PET and ePTFE (Dacron and Terylene, Teflon and Gore- Tex).....	17
1.4.1.2 Polyurethanes	19
1.4.2 Regenerative Scaffolds.....	19
1.4.2.1 Biodegradable synthetics	20
1.4.2.2 Natural scaffolds	20
1.4.2.3 Collagen scaffolds.....	21
1.4.2.4 Elastin	21
1.4.2.5 Fibrin.....	22
1.4.2.6 Autologous synthesised ECM scaffolds	22
1.4.2.7 Allogeneic grafts.....	22
1.4.2.8 Decellularised natural scaffold	23
1.4.2.9 Overview of Small Diameter Vascular grafts	27
1.4.3 Mechanical Concepts and their role in Vascular Grafts	28
1.4.4 Compliance.....	28
1.4.5 Stress Strain	31
1.5 Sterilisation of Medical Devices	32

1.5.1 Micro-Organisms.....	32
1.5.1.1 Gram positive and Gram negative bacteria	32
1.5.1.2 Mycobacteria.....	33
1.5.1.3 Viruses	33
1.5.1.4 Prions.....	34
1.5.2 Microbial Susceptibility To Sterilisation	34
1.5.3 Sterility Assurance and Biological Indicator Organisms	35
1.5.4 Viral Clearance and Porcine Model Viruses.....	35
1.5.5 Sterilisation Techniques for Soft Tissues	36
1.5.6 Chemical Sterilisation Methods.....	37
1.5.6.1 Ethylene oxide.....	37
1.5.6.2 Hydrogen peroxide.....	39
1.5.6.3 Peracetic Acid	39
1.5.6.4 Electrolyzed Water	39
1.5.6.5 Ozone	40
1.5.7 Physical Sterilisation Methods	40
1.5.7.1 Radiation.....	40
1.5.7.2 Gamma Radiation	40
1.5.7.3 E-Beam Radiation	42
1.5.7.4 Plasma	43
1.5.7.5 Supercritical Carbon Dioxide.....	44
1.6 Summary	46
1.7 General Aims and objectives	46
1.8 Experimental Approach	46
1.8.1 Porcine Scaffold.....	46
1.8.2 Sterilisation	47
1.8.3 Assessment Methods.....	47
Chapter 2 : General Materials and Methods	49
2.1 Equipment	49
2.2 Chemicals and Reagents.....	49
2.3 Consumables.....	49
2.4 Cell Lines.....	49
2.5 Antibodies.....	49
2.6 Methods.....	50
2.6.1 Glassware Disinfection	50

2.6.2 Equipment and Reagent Sterilisation	50
2.6.3 Measurement of Ph.....	50
2.6.4 Aseptic Technique and Cabinets	50
2.6.5 Microbiological Plating Technique.....	50
2.6.6 Histological Analysis	51
2.6.6.1 Tissue fixation and embedding.....	51
2.6.6.2 Sectioning of paraffin wax embedded tissue samples.....	52
2.6.6.3 Haematoxylin and eosin staining.....	52
2.6.6.4 DAPI staining	53
2.6.6.5 Immunohistochemical labelling of paraffin embedded tissue sections using monoclonal antibodies specific for collagen IV	54
2.6.7 Isolation and Quantification of DNA	56
2.6.8 Cell Culture and Maintenance.....	57
2.6.8.1 Culture medium.....	57
2.6.8.2 Cell resurrection	57
2.6.8.3 Cell passaging.....	58
2.6.8.4 Determination of cell number and cell viability using Trypan blue	58
2.6.8.5 Cryopreservation of cell lines	58
2.6.9 Biocompatibility Assays of Arteries	59
2.6.9.1 Sterility testing of samples	59
2.6.9.2 Contact cytotoxicity	59
2.6.10 Denatured Collagen Assay	59
2.7 Statistical Analysis.....	61
Chapter 3 Production of Porcine Carotid Acellular Arteries	62
3.1 Introduction.....	62
3.1.1 Leeds Decellularisation Method.....	62
3.2 Aims and Objectives.....	63
3.3 Materials and Methods	64
3.3.1 Tissue Procurement and Dissection	64
3.3.2 Decellularisation Process.....	65
3.3.3 Tissue Sampling For Biological And Mechanical Evaluation.....	68
3.3.4 Determination Of The Effectiveness Of The Decellularisation Process And The Biocompatibility Of Acellular Porcine Carotid Arteries.....	71
3.4 Results.....	71
3.4.1 Sterility Testing Of Acellular Porcine Carotid Arteries	72

3.4.2 Histological Analysis	73
3.4.3 Immunohistochemical Labelling Of Collagen IV	74
3.4.4 DNA Content.....	75
3.4.5 Contact Cytotoxicity	76
3.4.6 Summary Of Data On Determination Of The Effectiveness Of Decellularisation Of The Four Different Batches Of Acellular Porcine Carotid Arteries	77
3.5 Discussion	77
Chapter 4 Development of Mechanical Testing Methods	80
4.1 Introduction.....	80
4.2 Aims and Objectives	81
4.3 Materials and Methods	82
4.3.1 Tissue Procurement And Dissection	82
4.3.2 Decellularisation Of Native Porcine Carotid Arteries	82
4.3.3 Development Of Compliance And Burst Pressure Testing	82
4.3.3.1 Preliminary analysis of methods.....	82
4.3.3.2 Reproducibility.....	84
4.3.3.3 Sensitivity Analysis.....	84
4.3.3.4 Compliance testing of native and acellular arteries	84
4.3.4 Uniaxial Tensile Testing	84
4.4 Results.....	87
4.4.1 Development Of Compliance And Burst Pressure Test Method	87
4.4.1.1 Preliminary analysis of methods.....	87
4.4.1.2 Reproducibility of the Constant Weight Method for Measurement of Compliance	89
4.4.1.3 Sensitivity Analysis to Investigate the Impact of Load on Compliance	90
4.4.1.4 Determination of Compliance of Native and Acellular Porcine Carotid Arteries	92
4.4.2 Investigation Of The Effects Of Preloading In Tensile Testing Of Native And Acellular Porcine Carotid Artery Tissue	94
4.4.2.1 Effects of Varying Preload on Individual Parameters Extracted from Stress Strain Curves	94
4.4.2.2 Preload Selection	97
4.4.2.3 Comparison of parameters derived from low strain rate to failure testing of native and acellular arteries at 0.01 N.....	97
4.5 Discussion	99

Chapter 5 Mechanical properties of Sterilised Acellular Porcine Carotid Arteries.....	105
5.1 Introduction.....	105
5.2 Aims and objectives.....	106
5.3 Materials and Methods	106
5.3.1 Arteries	106
5.3.2 Irradiation Sterilisation	107
5.3.3 Freeze Drying	108
5.3.4 Ethylene Oxide Sterilisation	108
5.3.5 Rehydration Of Arteries	108
5.3.6 Mechanical Testing Of Samples	108
5.4 Results.....	110
5.4.1 Mechanical Properties of Gamma and E-Beam Irradiated Acellular Porcine Carotid Arteries.....	110
5.4.1.1 Uniaxial Tensile Testing of Gamma and E-Beam Irradiated Acellular Porcine Carotid Arteries.....	110
5.4.1.2 Compliance Testing of Gamma and E-Beam Irradiated Acellular Porcine Carotid Arteries.....	113
5.4.2 Mechanical Properties Of Freeze-Dried and Freeze-dried Ethylene Oxide Treated Acellular Porcine Carotid Arteries.....	115
5.4.2.1 Uniaxial Tensile Testing of Freeze-Dried and Freeze-Dried Ethylene Oxide Treated Acellular Porcine Carotid Arteries	115
5.4.2.2 Compliance	118
5.5 Discussion	120
Chapter 6 Biological Assessment of Acellular Porcine Arteries after Sterilisation using Different Methods.....	125
6.1 Introduction.....	125
6.2 Aims and objectives.....	127
6.3 Materials and Methods	127
6.3.1 Arteries and Sampling.....	127
6.3.2 Irradiation Sterilisation	127
6.3.3 Freeze Drying	128
6.3.4 EO Method.....	128
6.3.5 Sterility Testing	128
6.3.6 Histological and Immunohistochemical Analysis.....	128
6.3.7 Multiphoton Imaging.....	128
6.3.8 Contact Cytotoxicity	128
6.3.9 Differential Scanning Calorimetry.....	128

6.3.10 Denatured Collagen Assay	129
6.4 Results.....	130
6.4.1 Sterility of Sterilised Acellular Porcine Carotid Arteries	130
6.4.2 Histological Evaluation of Sterilised Acellular Porcine Carotid Arteries.....	131
6.4.3 Biocompatibility of Sterilised Acellular Porcine Carotid Arteries	133
6.4.4 Immunostaining For Collagen IV in Sterilised Acellular Porcine Carotid Arteries	135
6.4.4.1 Gamma Irradiation Artefacts Without Support Scaffold	135
6.4.4.2 Gamma Irradiation Effects with Support Scaffold.....	137
6.4.5 Multiphoton Imaging of Sterilised Acellular Porcine Carotid Arteries	138
6.4.6 Differential Scanning Calorimetry.....	143
6.4.7 Denatured Collagen Content	144
6.5 Discussion	145
Chapter 7 Discussion.....	148
List of References	159
Appendix A	177
A.1 Equipment.....	177
A.2 Chemicals and Reagents	178
A.3 Consumables	180
Appendix B	182
B.1 Statistical Analysis	182

List of Tables

Table 1.1 : Genetic and environmental factors that increase the risk of atherosclerosis.....	13
Table 1.2 : Number and type of coronary artery bypass/replacement procedures.	17
Table 1.3:Physical, Chemical and Enzymatic Methods of Decellularisation.	26
Table 1.4 : Micro-organisms in order of sterilization resistance.....	34
Table 1.5 : Sterilisation processes and their indicator organism.....	35
Table 1.6 : Common model viruses used for porcine tissue.	36
Table 1.7 : Desired attributes for a sterilisation process	37
Table 1.8 : Effects of radiation dose on HIV with varying temperatures and materials.....	41
Table 2.1 : Cell lines, <i>Cell lines with type species and NCTC catalogue number.</i>	49
Table 2.2 : Tissue processing steps.	51
Table 2.3 : Haematoxylin and Eosin staining procedure.	52
Table 2.4 : DAPI staining procedure.	53
Table 2.5 : Dewaxing and rehydration of sections.	55
Table 2.6 : Dehydration of sections.	56
Table 2.7 : Denatured collagen assay standards.....	61
Table 3.1: Antibiotic concentrations in the disinfection solution.	66
Table 3.2 : Decellularisation process for porcine carotid arteries	68
Table 3.3 : Overview of the sampling process for each batch and each sterilisation/process.....	69
Table 3.4 : Summary of analysis of four batches of acellular arteries for the effectiveness of the decellularisation process.	77
Table 4.1 : Average Percentage Diameter Change of Native and Acellular Arteries at 100 mmHg.....	93
Table 4.2 : Average Percentage Length Change of Native and Acellular Arteries at 100 mmHg.....	93
Table 4.3 : The Average Transition Strain for Native and Acellular Arteries in the Circumferential and Axial Direction at Varying Levels of Preload	95
Table 4.4 : The Average Transition Stress for Native and Acellular Arteries in the Circumferential and Axial Direction at Varying Levels of Preload	95
Table 4.5 : The Average Ultimate Tensile Strain for Native and Acellular Arteries in the Circumferential and Axial Direction at Varying Levels of Preload.....	96
Table 4.6 : The Average Ultimate Tensile Stress for Native and Acellular Arteries in the Circumferential and Axial Direction at Varying Levels of Preload.....	96

Table 4.7 : The Average Collagen Modulus for Native and Acellular Arteries in the Circumferential and Axial Direction at Varying Levels of Preload	96
Table 4.8 : The Average Elastin Modulus for Native and Acellular Arteries in the Circumferential and Axial Direction at Varying Levels of Preload	96
Table 4.9 : Changes in the mechanical parameters of porcine carotid arteries post decellularisation in the circumferential and axial directions.	98
Table 4.10 : Patency Rates and Compliance Values of Clinically Used Vascular Grafts.....	101
Table 5.1:Sample Sizes for sampling method I and II for each batch of acellular arteries	107
Table 5.2 : Intended (I) and Actual (A) Sample Sizes for Mechanical Testing	109
Table 5.3 : Parameters Extracted from Stress Strain Curves Derived from Low Strain Rate to Failure Uniaxial Tensile Testing in the Circumferential Direction Of Native, Acellular, Gamma and E-Beam Irradiated Porcine Carotid Arteries.	111
Table 5.4 : Parameters Extracted From Stress Strain Curves Derived From Low Strain Rate To Failure Uniaxial Tensile Testing In The Axial Direction Of Native, Acellular, Gamma And E-Beam Irradiated Porcine Carotid Arteries.	112
Table 5.5 - Average Percentage Diameter Change Native, Acellular, Acellular Gamma and E-Beam Irradiated Arteries at 100 mmHg.....	114
Table 5.6 - Average Percentage Length Change of Native, Acellular, Acellular Gamma and E-Beam Irradiated Arteries at 100 mmHg.....	114
Table 5.7 : Parameters Extracted From Stress Strain Curves Derived From Low Strain Rate To Failure Uniaxial Tensile Testing In The Circumferential Direction Of Native, Native Freeze-Dried, Acellular, Acellular Freeze-Dried And Ethylene Oxide Treated Porcine Carotid Arteries.....	116
Table 5.8 : Parameters Extracted From Stress Strain Curves Derived From Low Strain Rate To Failure Uniaxial Tensile Testing In The Axial Direction Of Native, Native Freeze-Dried, Acellular, Acellular Freeze-Dried And Ethylene Oxide Treated Porcine Carotid Arteries.	117
Table 5.9 - Average Percentage Diameter Change Native, Native Freeze-dried, Acellular, Acellular Freeze-dried and Ethylene Oxide Treated Arteries at 100 mmHg	119
Table 5.10 - Average Percentage Length Change Native, Native Freeze-dried, Acellular, Acellular Freeze-dried and Ethylene Oxide Treated Arteries at 100 mmHg	119

List of Figures

Figure 1.1 : Schematic of the cardiovascular system	2
Figure 1.2 : Anatomy and circulation of the heart.	3
Figure 1.3 : Relationship between average blood pressure, total cross-sectional area and velocity between arteries to veins.....	3
Figure 1.4 : Image depicting the relative layers in arteries and veins.	4
Figure 1.5 : The formational changes of elastin in stretched or relaxed states.....	6
Figure 1.6 : Collagen helix structure.....	6
Figure 1.7 : Location and orientation of GAGs in relation to a protein core.	7
Figure 1.8 : Stenotic artery.	7
Figure 1.9 : Vasculature of the heart.....	8
Figure 1.10 : Vasculature of the brain.....	8
Figure 1.11 : Images depicting the femoral, popliteal and tibial arteries of the leg.....	9
Figure 1.12 : Build up of plaque within a blood vessel lumen.....	9
Figure 1.13 : Thrombosis and embolus development.....	10
Figure 1.14 : Aortic arch and carotid and subclavian bifurcations.	10
Figure 1.15 : Endothelial cells subjected to either turbulent or laminar flow.....	11
Figure 1.16 : Formation of foam cells.....	12
Figure 1.17 : Haematoxylin and eosin stained arteries showing normal (A)and hypertension (B)states.....	12
Figure 1.18 : Chart of death incidences per 100 000 worldwide from cardiovascular diseases.	13
Figure 1.19 : Number of bypass/replacement grafts performed on coronary arteries, iliac and femoral arteries and arteriovenous shunts in the UK 2010-2011.	14
Figure 1.20 : Image depicting the greater saphenous vein and its tributaries of the leg.....	15
Figure 1.21 : Diagram of routine CABG surgery	15
Figure 1.22 : Image depicting femoropopliteal bypass graft surgery.	15
Figure 1.23 : Two versions of arteriovenous graft in forearm.	16
Figure 1.24 : Primary patency rates of synthetic and autograft saphenous vein at 2 and 5 years. ASV – Autograft saphenous vein.	18
Figure 1.25 : Diagram showing how tissue regeneration should take over support from scaffold.....	20
Figure 1.26 : Antigen recognition in acute rejection, depicting the direct, indirect and semi-direct pathway.....	24

Figure 1.27 : Relationship between vein and artery wall thickness, volume and pressure.	29
Figure 1.28 : End to side anastomosis.	31
Figure 1.29 : Stress-Strain behaviour of an artery during loading and unloading.	32
Figure 1.30 : a graph showing the temperature and pressure at which carbon dioxide change phase to a supercritical fluid.	44
Figure 1.31 : Porcine cardiovascular system identifying vasculature.	47
Figure 2.1 Streaking pattern, streaking pattern used during sterility checks of suspensions.	50
Figure 3.1 : Dissected porcine carotid artery.	65
Figure 3.2 : Image depicting sampling method I of porcine carotid arteries.	69
Figure 3.3 : Image depicting sampling method II of porcine carotid arteries.	70
Figure 3.4: Representative images of histological sections of fresh porcine common carotid arteries from two different suppliers.	72
Figure 3.5 : Images of sterility tests carried out on batch 1 of acellular arteries.	72
Figure 3.6 : Representative images of histological sections of native and acellular porcine common carotid arteries from batch 1.	73
Figure 3.7 : Representative images of sections of native and acellular porcine common carotid arteries (batch 1) labelled using immunohistochemistry with an antibody to collagen IV.	74
Figure 3.8 : Total DNA content of native and acellular porcine carotid arteries from batch 1.	75
Figure 3.9 : Representative images captured using phase contrast microscopy of BHK and L929 cells growing in contact with acellular porcine carotid artery samples from batch 1.	76
Figure 3.10 : Representative images captured using light microscopy of BHK and L929 cells stained with geimsa growing in contact with acellular porcine carotid artery samples from batch 1.	76
Figure 4.1 : Image of the equipment setup used for determination of the compliance and burst pressure testing.	82
Figure 4.2 : Compliance and Burst Pressure Rig Setup.	83
Figure 4.3 : Schematic of the purpose built rig for tensile testing of arteries.	85
Figure 4.4 : Image of porcine carotid artery loaded to failure using a purpose built rig placed in a waterbath.	85
Figure 4.5 : Chart representing the six parameters derived from stress strain curves from uniaxial tensile testing.	86
Figure 4.6 : Percentage diameter change in arteries with increasing pressure determined using four methods of compliance measurement.	87
Figure 4.7 : Representative images of arteries captured during testing using the four different methods of measuring compliance.	88

Figure 4.8 : Reproducibility of percentage diameter increase of porcine carotid arteries tested using the constant weight method.	89
Figure 4.9 : Sensitivity Analysis of Load on Percentage Diameter Change of Arteries with Increasing Pressure.....	90
Figure 4.10 : Sensitivity Analysis of Load on Percentage Length Change of Arteries with Increasing Pressure.....	91
Figure 4.11 : Average Percentage Diameter Change of Native and Acellular Arteries with Increasing Pressure.....	92
Figure 4.12 : Average Percentage Length Change of Native and Acellular Arteries with Increasing Pressure.	93
Figure 4.13 Average Stress Strain Curves of Native and Acellular Arteries Tested in the Circumferential Direction at Varying Levels of Preload	94
Figure 4.14 Average Stress Strain Curves of Native and Acellular Arteries Tested in the Axial Direction at Varying Levels of Preload	95
Figure 4.15 : Force Extension Curves of Native and Acellular Porcine Carotid Arteries in the Circumferential and Axial Directions.....	97
Figure 4.16 : Average Stress Strain Curves of Native and Acellular Arteries Tested in the Circumferential Direction at 0.01 N preload.	98
Figure 4.17 : Average Stress Strain Curves of Native and Acellular Arteries Tested in the Axial Direction at 0.01 N preload.....	99
Figure 4.18 : Proposed Method to Calculate the Transition Strain Using a Line of Equal Angle Between the Tangents of the Collagen and Elastin Slopes.	103
Figure 5.1 : Diagram of the artery support for packaging.....	107
Figure 5.2 : Acellular Artery on PEG Support Structure and Vacuum Sealed in Inner Foil Membrane and Outer Tyvek	107
Figure 5.3 : Freeze Dried Acellular Arteries on PEG Support Structure	108
Figure 5.4 : Average Stress Strain Curves Derived From Low Strain Rate To Failure Uniaxial Tensile Testing In The Circumferential Direction Of Native, Acellular, Gamma And E-Beam Irradiated Porcine Carotid Arteries.....	111
Figure 5.5 : Average Stress Strain Curves From Parameters Extracted From Stress Strain Curves Derived From Low Strain Rate To Failure Uniaxial Tensile Testing In The Axial Direction Of Native, Acellular, Gamma And E-Beam Irradiated Porcine Carotid Arteries.	112
Figure 5.6 : Average Percentage Diameter Change of Native, Acellular, Acellular Gamma and E-Beam Irradiated and NBF fixed Arteries with Increasing Pressure.	113
Figure 5.7 : Average Percentage Length Change of Native, Acellular, Acellular Gamma and E-Beam Irradiated and NBF fixed Arteries with Increasing Pressure.	114
Figure 5.8 Average Stress Strain Curves Derived From Low Strain Rate To Failure Uniaxial Tensile Testing In The Circumferential Direction Of Native, Native Freeze-Dried, Acellular, Acellular Freeze-Dried And Ethylene Oxide Treated Porcine Carotid Arteries	116

Figure 5.9 Average Stress Strain Curves Derived From Low Strain Rate To Failure Uniaxial Tensile Testing In The Axial Direction Of Native, Native Freeze-Dried, Acellular, Acellular Freeze-Dried And Ethylene Oxide Treated Porcine Carotid Arteries	117
Figure 5.10 : Average Percentage Diameter Change Native, Native Freeze-dried, Acellular, Acellular Freeze-dried, Ethylene Oxide Treated and NBF Fixed Arteries with Increasing Pressure.....	118
Figure 5.11 : Average Percentage Length Change Native, Native Freeze-dried, Acellular, Acellular Freeze-dried, Ethylene Oxide Treated and NBF Fixed Arteries with increasing pressure.....	119
Figure 6.1 : The Second Harmonic Generation of Light.....	126
Figure 6.2 : Images of sterility tests carried out on batches of acellular arteries post sterilisation.....	130
Figure 6.3 Representative images of histological sections of native, acellular, Gamma and E-Beam irradiated and freeze-dried EO treated porcine porcine common carotid arteries in the circumferential direction.....	131
Figure 6.4 : Representative images of histological sections of native, acellular, Gamma and E-Beam irradiated and freeze-dried EO treated porcine porcine common carotid arteries in the longitudinal direction.	132
Figure 6.5: Representative images captured using phase contrast microscopy of L929 cells growing in contact with acellular, Gamma and E-Beam irradiated and freeze-dried EO treated acellular porcine carotid arteries from batches 3 and 4.	133
Figure 6.6: Representative images captured using phase contrast microscopy of BHK cells growing in contact with acellular, Gamma and E-Beam irradiated and freeze-dried EO treated acellular porcine carotid arteries from batches 3 and 4.	133
Figure 6.7: Representative images captured using light microscopy of L929 cells stained with Geimsa growing in contact with acellular, Gamma and E-Beam irradiated and freeze-dried EO treated acellular porcine carotid arteries from batches 3 and 4.....	134
Figure 6.8: Representative images captured using light microscopy of L929 cells stained with Geimsa growing in contact with acellular, Gamma and E-Beam irradiated and freeze-dried EO treated acellular porcine carotid arteries from batches 3 and 4.....	134
Figure 6.9 : Representative images of collagen IV immuno-stained sections of native (A) , acellular (B) and acellular Gamma (C, D) irradiated porcine carotid arteries. Acellular Gamma irradiated isotype control (F) and antibody diluent control (E).	136
Figure 6.10 : Representative images of collagen IV immune-labelling in sections of native (A), acellular (B, C) , acellular Gamma (D) irradiated, acellular E-Beam (G) irradiated, acellular EO (J) treated porcine carotid arteries. Isotype controls (E, H, K) and antibody diluent controls (F, I, L).	137
Figure 6.11 Second harmonic image generation of (A) Native, (B) Acellular, (C) Boiled and (D) NBF fixed porcine carotid arteries.....	139

Figure 6.12 : Second harmonic image generation of Gamma irradiated acellular porcine carotid arteries (A,B).	139
Figure 6.13 : Second harmonic image generation of E-Beam irradiated acellular porcine carotid arteries (A,B).	140
Figure 6.14 : Second harmonic image generation of freeze-dried acellular porcine carotid arteries.....	140
Figure 6.15 : Second harmonic image generation of freeze-dried EO treated acellular porcine carotid arteries (A, B).....	141
Figure 6.16 : Z stacked Second harmonic image generation of acellular (A), Gamma (B) and E-Beam (C) irradiated and EO (D) treated acellular porcine carotid arteries.....	142
Figure 6.17 : Bar chart depicting denaturation temperatures of native, boiled and NBF fixed, acellular, Gamma irradiated, E-Beam irradiated, freeze-dried EO treated acellular porcine carotid arteries.	143
Figure 6.18 : Bar chart of denatured collagen content in native, acellular, acellular Gamma and E-Beam irradiated, EO treated, boiled and NBF fixed porcine carotid arteries.....	144

Chapter 1 Vascular Disease and Small Diameter Vascular Grafts

1.1 Introduction

Cardiovascular disease (CVD) is the highest cause of morbidity worldwide (W.H.O., 2011), CVD encompasses a range of heart and blood vessel disorders such as coronary artery disease (CAD) and peripheral arterial disease (PAD). Both are characterised by reduced blood supply caused primarily by severely stenotic arteries. Vascular grafts are used to replace damaged arteries and reinstate normal blood flow and function to the vascular system. There has been moderate success in bypass surgery of large diameter blood vessels with synthetic grafts, however this does not translate to small diameter blood vessels <6mm. The gold standard for coronary artery bypass surgery (CABG) or peripheral arterial disease is an autograft of either vein or artery, commonly the saphenous vein (SV). If insufficient native artery is available due to previous surgery or disease, then Dacron or expanded polytetrafluoroethylene (ePTFE) synthetic grafts are used; both of these are associated with low patency rates due to early occlusion and increased risk of infection (Teebken & Haverich, 2002; van Det *et al.*, 2009). This has led to intensive research in tissue engineered small and medium diameter vascular grafts.

Acellular allogeneic and xenogeneic (porcine and bovine) vascular grafts have been developed using patented platform decellularisation technology (Ingham *et al.*, 2010). The process removes the native cells and cellular debris including the genetic material whilst also maintaining the mechanical integrity. These scaffolds have the potential for clinical use in-vivo (Wilshaw *et al.* 2012). The initial clinical use of acellular artery technology will be either a peripheral artery bypass or arteriovenous graft to build confidence in the technology.

All medical devices must be supplied sterile. Sterilisation is vitally important for the safety of the patient and the success of the arterial graft. Current sterilisation techniques such as peracetic acid (PAA) treatment require that the tissue is aseptically transferred following chemical sterilisation and this is not ideal for a manufacturing process, a process that can sterilise the product in its final packaging is preferable (terminal sterilisation). Moreover, it has been shown that PAA treatment has an adverse effect on the basement membrane of porcine common femoral arteries, in particular the expression of collagen IV as determined by immunohistochemistry and increased thrombogenicity (Personal communication; Dr S.P. Wilshaw).

The choice of sterilisation technique implemented should not alter the mechanical properties out of a preferential range, reduce biocompatibility or increase thrombogenicity. Ideally for a commercial product a terminal sterilisation process is required so that there is no risk of contamination post sterilisation. The two main terminal sterilisation processes currently used

for tissue grafts are ethylene oxide and Gamma radiation, followed by two newer processes: E-Beam radiation and supercritical carbon dioxide. The four processes sterilise via different mechanisms and will be discussed in detail in Sections 1.5.6 and 1.5.7, however they all result in breaking chemical bonds, producing crosslinking and chain scission of polymers via the formation of free radicals. It is therefore necessary to optimise one of these methods in order to reduce the amount of graft damage. The aim of this study was to develop robust methods for the assessment of the effects of different sterilisation methods on acellular vascular grafts and to produce a terminally sterilised acellular vascular product.

1.2 The vascular system

The cardiovascular system is a closed loop system of tubular vessels called veins and arteries carrying blood to and from the heart respectively. The heart being the driving force of the system pumping the flow of blood around the body (Figure 1.1) (Johnson & Byrne, 1998).

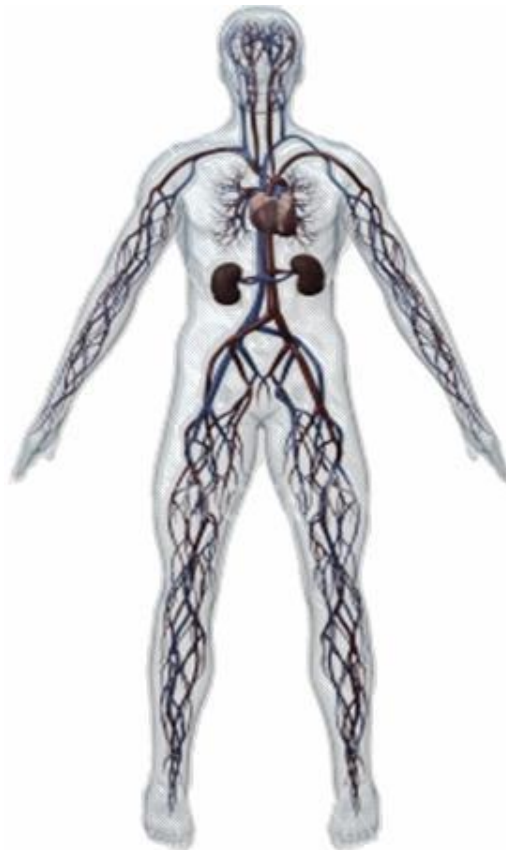


Figure 1.1 : Schematic of the cardiovascular system
Adapted from Kaulitzki (2011)

The heart can be considered as two pumps; the left and right heart, each consisting of a ventricle and atrium (Figure 1.2). The right heart circulates blood around the pulmonary system at pressures of 10/24 mmHg (diastolic/systolic) and the left heart circulates blood around the systemic system at pressures of 80/120 mmHg. The flow of blood between the atria and ventricles is controlled by atrio-ventricular valves and the flow between the

ventricles and exit vessels (pulmonary artery, aorta) is controlled by the semi-lunar valves (Johnson & Byrne, 1998).

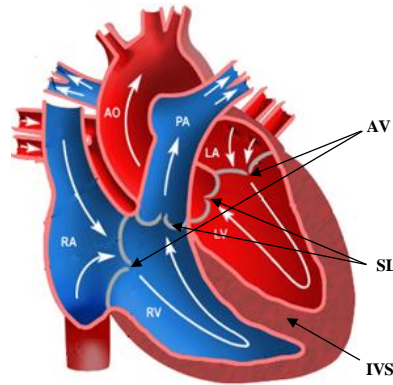


Figure 1.2 : Anatomy and circulation of the heart.

RA-right atrium; LA-left atrium; RV-right ventricle; LV-left ventricle; AO-aorta; PA-pulmonary artery; AV-atrio-ventricular valves; SL-semi-lunar valves; IVS-inter-ventricular septum. Adapted from Preventing-a-Heart-attack.com (2011)

The aorta and large arteries are under the highest pressure, peaking at around 120 mmHg in normal healthy adults. They have a lower distensibility than veins and undergo vasoconstriction to maintain an overall small cross-sectional area that helps propagate the flow at high velocities (approximately 30 cm/s) around the body. As the arteries branch into smaller arteries and arterioles, the cross sectional area increases. The reduction in the radius increases the resistance and the distensibility increases reducing the pulsatility. This leads to a quick reduction in blood velocity and pressure (Klabunde, 2005).

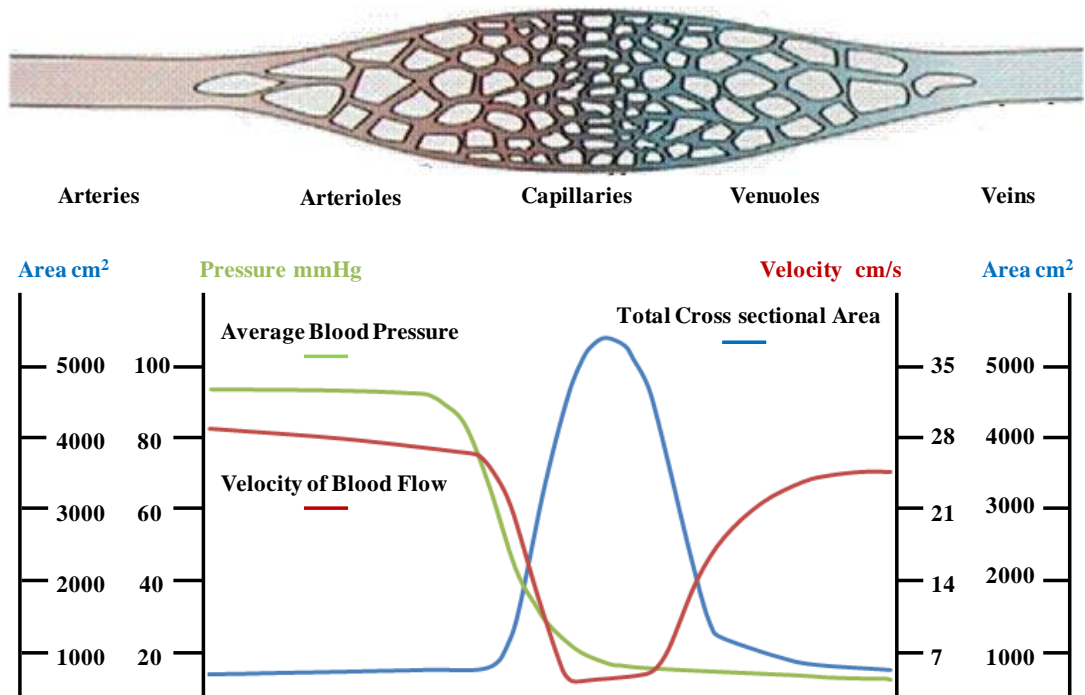


Figure 1.3 : Relationship between average blood pressure, total cross-sectional area and velocity between arteries to veins.

As the blood flows into the capillaries, the pressure ranges from around 10-25 mmHg. The pulsatility is reduced and the velocity drops to its lowest (approximately 0.05 cm/s). This is because of the increased resistance created by the small lumen radii of capillaries although the total cross sectional area of the capillaries is larger than that of the arteries or veins. This allows high rates of gas and molecule exchange. As the flow now proceeds into the venules and veins their ability to distend allows the low pressure to drive large volumes of blood at increasing velocities around the body (Figure 1.3) (Carlson *et al.*, 2008; Jan, 2010).

1.2.1 Physiology of Blood Vessels

Veins and arteries have three distinct layers (Figure 1.4); the tunica intima (1), tunica media (2) and tunica adventitia (3). In comparison to veins, arteries have much thicker media layers, which are rich in elastin and collagen, this provides higher strength and elasticity to resist high blood pressures. In addition the smooth muscle content and the small lumen diameter of arteries help to propagate the strength of the pulse and maintain pressure. Veins have a larger luminal diameter for transporting high blood volumes under low pressure; they also incorporate one way valves in order to maintain unidirectional blood flow, towards the heart without backflow. Capillaries are generally single cell-thick layers of endothelial cells and the main location of nutrient transfer to tissues.

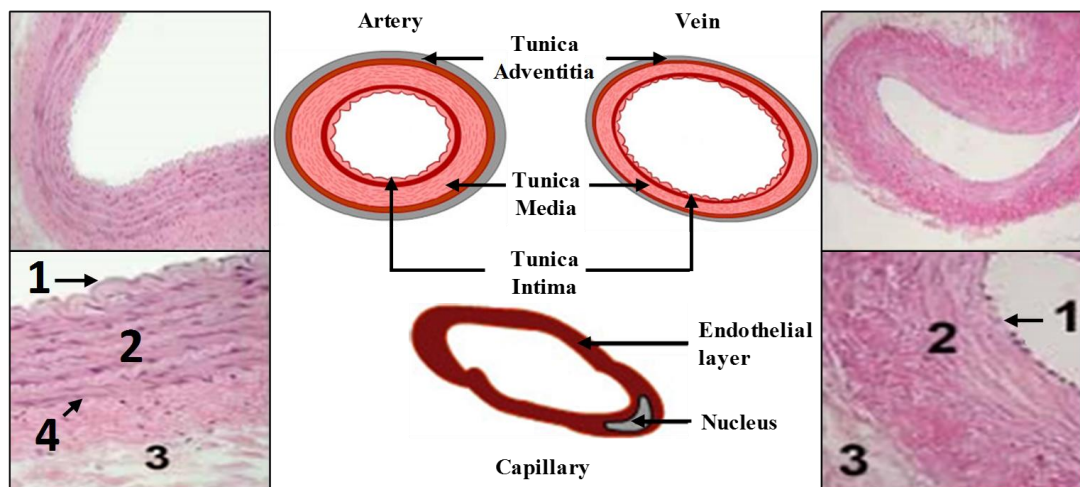


Figure 1.4 : Image depicting the relative layers in arteries and veins.

Haematoxylin and eosin stained arteries (left) and veins (right). (1) tunica intima, (2) tunica media, and (3) tunica adventitia (4) internal elastic lamina. Image adapted from www.vascularconcepts.com (2011)

The tunica adventitia is the external layer of the vessels; its main function is to provide an anchorage to nearby tissues and organs. Its primary constituents are extracellular matrix (ECM) proteins including; elastin fibres, collagen type I and III, proteoglycans, glycoproteins, and hyaluronan and fibro-elastic connective tissue (Stenmark *et al.*, 2006). Most of which are produced by a heterogeneous population of myofibroblastic cells. The tunica adventitia is entwined with a network of smaller thin walled blood vessels called the vasa-vasorum that provides a supply of oxygen and nutrients to the wall of the vessel more readily than diffusion from the vessel lumen. This also makes the adventitial layer a key area of vascular

inflammation. In between the adventitia and the media layers there is an intervening layer of elastic connective tissue called the external elastic lamina (Wagenseil & Mecham, 2009). Studies have also shown that the adventitia may contribute to sensing and detecting injury of the blood vessel (Schulze-Bauer *et al.*, 2002), and within developing vessels may also stimulate progenitor cells to differentiate into smooth muscle cells (SMC), that can then replenish the media, and endothelial cells (Hu *et al.*, 2004).

The tunica media is the thickest layer of blood vessels and contains predominately smooth muscle cells, elastin fibres and collagen types I and III. The smooth muscle cells are highly organised along the circumferential orientation and are responsible for propagating the pulse of the blood by contracting and reducing the lumen size. The elastin fibres contribute largely to the compliance of the vessels. Between the media and intima layers there is an intervening layer of connective tissue called the internal elastic lamina (Dingemans *et al.*, 2000).

The tunica intima is a single-cell-thick layer of endothelial cells (EC), making it the thinnest of the three layers. The cells are orientated longitudinally along the direction of flow, and are stimulated by blood flow-induced shear. This layer rests upon the basement membrane which incorporates the basal lamina, a layer of ECM with high concentrations of collagen type IV and anchoring fibrils of collagen type VII extending from the lamina (Davis, 1993). The basement membrane provides simultaneous flexibility and stability for the endothelial cells, allowing them to withstand blood flow-induced deformation of the vessel, as well as acting as a mechanical barrier. In capillaries, the EC layer also contains pericytes and multi-potent stem cells (Bou-Gharios *et al.*, 2004). The outer surface of the EC layer is a charged surface due to the expression of glycoproteins collectively called glycocalyx. This creates a highly negatively charged surface which aids in restricting the movement of blood cells and plasma proteins through the EC layer (Liu & Yang, 2009). The EC layer helps prevent thrombosis and coagulation by controlling blood-wall interactions and plays an important role in inflammation (Sumpio *et al.*, 2002).

1.2.2 Extracellular Matrix and its Components

There are three main structural components of the extracellular matrix: elastin, collagen and glycosaminoglycans (GAG). The combination of these three constituents dictates the vessel strength, elasticity and reaction to haemodynamic forces.

Elastin is primarily responsible for the elasticity and compliance of a particular tissue, it is very stable, highly insoluble and particularly difficult to synthesise, it has a compact branched three-dimensional structure with cross-links existing between molecules forming an elastin fibre (Debelle & Tamburro, 1999); tissues and organs undergoing large amounts of reversible deformation have particularly high elastin content. In relation to blood vessels elastin aids in recoiling the vessel back to its original diameter (Figure 1.5)(Cooper, 2000).

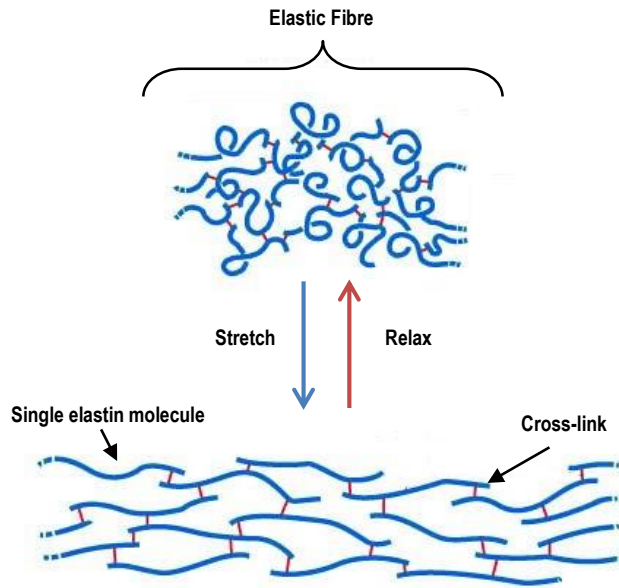


Figure 1.5 : The formational changes of elastin in stretched or relaxed states.
Adapted from Bruce Alberts *et al.* (2004)

Collagen provides the majority of the tensile stiffness and is the main load carrying component in the blood vessels. It is responsible for the structural integrity and, therefore, its ultimate tensile strength (UTS) (Meyers *et al.*, 2008). Collagen has a triple helix structure (Figure 1.6). Each protein strand is made up of amino acids, and demonstrates an α -helical left handed twist of 0.87 nm per turn. The combination of these form an overall right handed helical twist of 8.6 nm, with an average length of one triple helix being about 300 nm. The tensile stiffness and strength of a tissue increases with its collagen content, but the tensile strength and stiffness are also highly dependent on collagen fibre orientation and amount of cross-linking between individual fibres. Cross-linking occurs between the glycine residues and hydroxyl groups forming strong covalent bonds (Fung, 1993). Fibre-forming collagens form fibrils which vary in length, they have a staggered formation allowing the head of one fibre to bond with the tail of another (Figure 1.6) (Cooper, 2000).

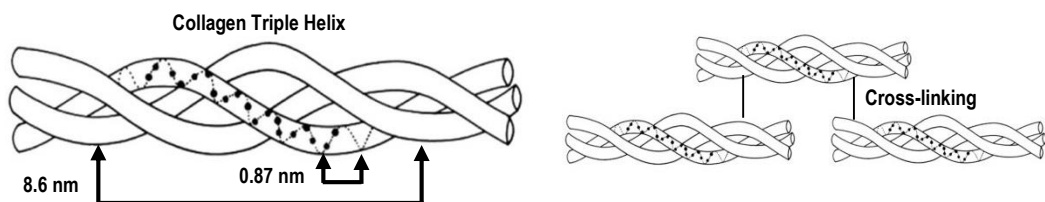


Figure 1.6 : Collagen helix structure.
Image adapted from Fung (1993)

Glycosaminoglycans (GAGs) are long un-branched polysaccharides, usually attached to a protein core (Figure 1.7) in the form of proteoglycans. GAGs account for about 2-5 % of dry weight in blood vessels. Although GAGs represent only a small percentage of the mass of blood vessels they have a large effect on viscoelasticity, compressibility, wall permeability,

haemostasis and thrombosis (Wight, 1989). GAGs are highly negatively charged and draw large influxes of positive ions, creating a large osmotic gradient. This gradient allows GAGs to attract and contain large volumes of water, it is this property that affects the compressibility of a vessel and gives it the ability to endure compressive forces.

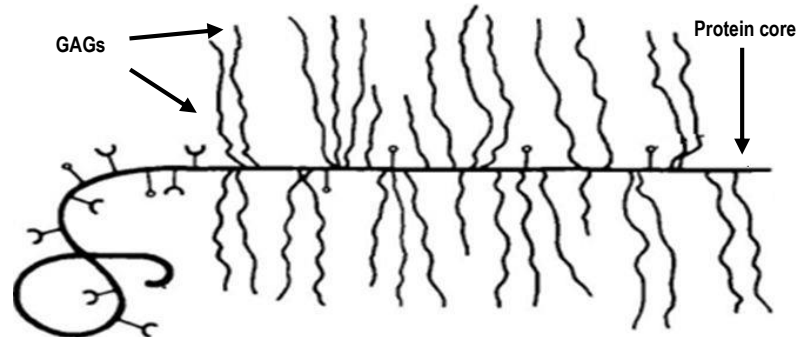


Figure 1.7 : Location and orientation of GAGs in relation to a protein core.
Image adapted from Fung (1993)

1.3 Vascular disease, risk, incidence and therapies

Ischemic heart disease (coronary artery disease) is the world's leading cause of death (Finegold *et al.*, 2013). The major underlying condition leading to vascular diseases such as coronary artery disease, cerebrovascular disease and peripheral vascular disease are stenotic blood vessels caused by atherosclerosis and hypertension. A stenosis is the narrowing of a blood vessel (Figure 1.8), which leads to reduced blood flow downstream, when flow is reduced by 70 % it is known as ischemia (Hertzer *et al.*, 1984). The lack of blood supply reduces the nutrient exchange to the surrounding tissues. In the absence of oxygen and glucose cellular metabolism slows down and waste by-products build up. This cessation of metabolic activity leads to cell necrosis (premature cell death) and the release of cytokines into the intracellular space inciting an inflammatory response. This inflammatory response prevents the influx of phagocytes to remove cellular components by phagocytosis leading to the build up of decomposing tissue.



Figure 1.8 : Stenotic artery.
Image adapted from www.mayfieldclinic.com (2011)

In ischemic heart disease the afflicted arteries are the coronary arteries (Figure 1.9), when the surrounding heart tissue is denied oxygen the cells begin to die of necrosis; this is known

as myocardial infarction (Heart attack). The affected area conducts electrical impulses at a slower rate than healthy heart tissue and causes arrhythmias such as ventricular fibrillation and ventricular tachycardia. The dead cells are not replaced and collagen scarring occurs; damage to the myocardium in this way is one form cardiomyopathy. Myocardial scarring also increases the risk of a ventricular aneurysm forming.

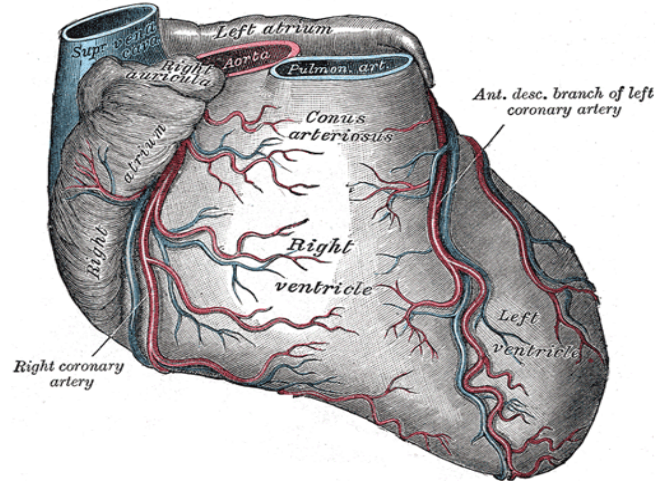


Figure 1.9 : Vasculature of the heart.
Image adapted from Gray *et al.* (1973)

In cerebrovascular disease the afflicted arteries are the small arteries in the brain (Figure 1.10), when the blood flow is reduced in these arteries an ischemic stroke occurs. The lack of oxygen and subsequent necrosis of brain cells prevents the brain from functioning correctly and reduces the electrical output causing muscular paralysis and lack of conscious control.

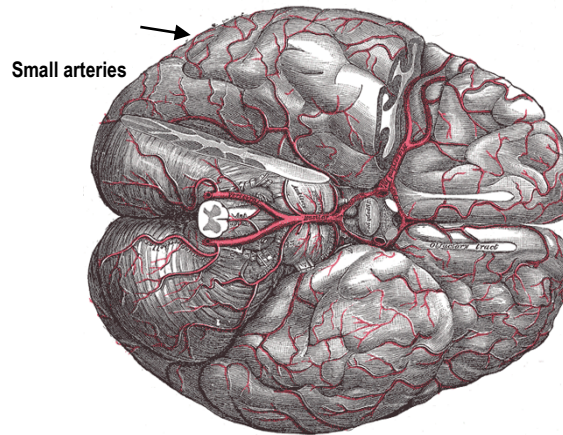


Figure 1.10 : Vasculature of the brain.
Image adapted from Gray *et al.* (1973)

In peripheral vascular disease the afflicted arteries are large arteries not within the coronary, aortic arch or cerebral vasculature; usually this disease is concerned with the lower extremities affecting the femoral, popliteal or tibial artery of the leg. The popliteal artery is the continuation of the femoral artery that runs through the popliteal fossa and then divides into the anterior and posterior tibial arteries (Figure 1.11). Necrosis of tissues in the lower

extremities leads to (in increasing order) claudication (limping), resting pain, Ischemic ulceration and finally sever ulceration and gangrene.

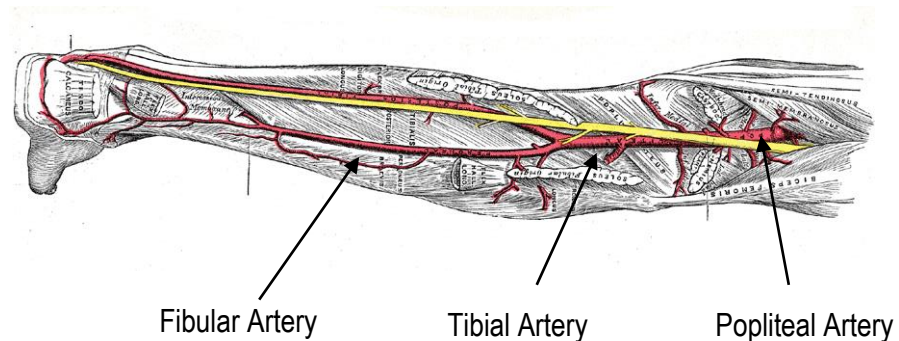


Figure 1.11 : Images depicting the femoral, popliteal and tibial arteries of the leg.
Image adapted from Gray *et al.* (1973)

1.3.1 Atherosclerosis, Thrombosis and Hypertension

As mentioned previously the main cause of vascular disease is atherosclerosis. Atherosclerosis is characterised by the formation of plaques in the blood vessel wall. It is initiated predominantly as a result of the subendothelial deposition of low density lipoproteins (LDL). The lesions develop and grow into the luminal area (Figure 1.12), reducing blood flow and altering the haemodynamics of the vessel.



Figure 1.12 : Build up of plaque within a blood vessel lumen.
Image adopted from www.vwmin.org (2011)

As the lesion continues to develop there is an increasing risk of rupture or erosion of the lesion, this leads to blood clotting and the development of a thrombus, and parts of this blood clot can break away causing an embolus (Figure 1.13). When embolus travels through the blood stream it can cause acute occlusion in the smaller diameter vessels of the heart or brain triggering a myocardial infarction or stroke.

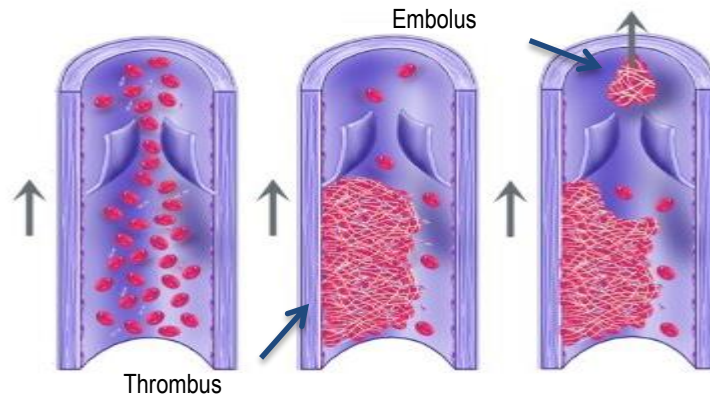


Figure 1.13 : Thrombosis and embolus development.

Image adopted from www.veininfo.co.uk (2011)

Laminar flow (Particulates flow in parallel layers) and high shear stress prevent the deposition of LDL in the blood vessel wall. In areas of non-laminar flow and low shear stress such as stagnation and recirculation points found in arterial branching, bifurcations and curvatures there is increased deposition of LDL (Figure 1.14) (Zarins *et al.*, 1983).



Figure 1.14 : Aortic arch and carotid and subclavian bifurcations.

Image adopted from hms.harvard.edu (2011)

The endothelial cells experiencing laminar flow have an ellipsoid morphology aligned with direction of blood flow, in areas of low shear or turbulent flow the ellipsoid morphology is reduced into random polygons of no particular orientation (Figure 1.15). These areas of altered morphology have increased permeability to macromolecules. Due to the altered hemodynamics, a larger concentration of circulating LDL accumulates, leading to increased passive diffusion across the endothelium (Lusis, 2000). LDLs are retained in the subendothelial matrix by interactions between apolipoprotein B and proteoglycans in the intramural space. Lipoprotein(a) is also retained in the subendothelial matrix via apolipoprotein B and contributes to the development of lesions by inhibiting transforming growth factor β (TGF- β , inhibits the proliferation of SMC), allowing the proliferation of SMCs (Grainger *et al.*, 1994).

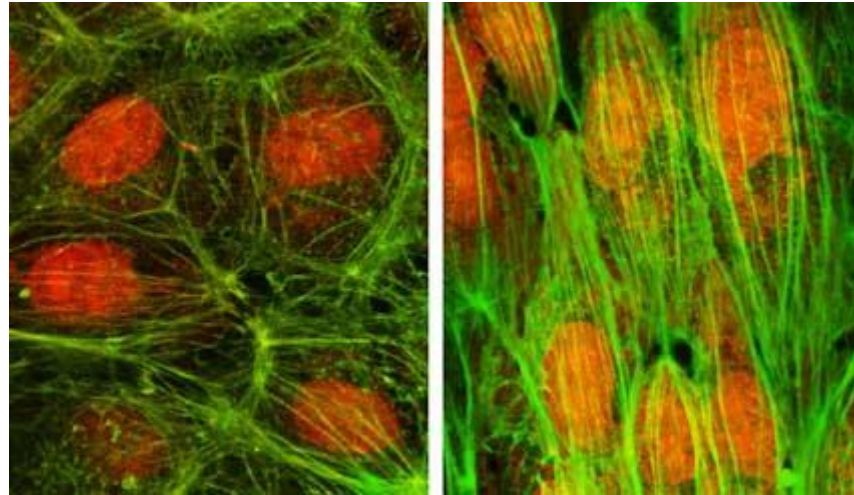


Figure 1.15 : Endothelial cells subjected to either turbulent or laminar flow.
Image adopted from hms.harvard.edu (2011)

When LDLs accumulate in the intramural space between the endothelium and the media they can undergo many modifications including oxidation, lipolysis, proteolysis and aggregation, one of the most significant being oxidation. Cellular processes create reactive oxygen species such as hydroperoxyeicosatetraenoic acid (HPETE) that migrate across cell membranes and oxidise the LDL (Cyrus *et al.*, 1999). The build-up of oxidised LDL activates the endothelial cells and initiates chronic inflammation (Mestas & Ley, 2008). Activated ECs express growth factors and adhesion molecules such as P-selectin, vascular cell adhesion molecule-1 and intracellular adhesion molecule-1 (Dong *et al.*, 1998; Collins *et al.*, 2000). These molecules and factors help the recruitment of monocytes by increasing the adhesion potential to the endothelium when rolling. Following monocyte adherence, monocytes transmigrate to the intramural space. Once monocytes enter the intramural space they differentiate into macrophages, aided by growth factors such as macrophage colony-stimulating factor (M-CSF) (Smith *et al.*, 1995). Macrophages engulf highly oxidised LDL and form 'foam cells' (Figure 1.16), which can be visualised as fatty streaks. LDLs reach a highly oxidised state through reactive oxygen species from cellular waste as well as enzymatic pathways such as myeloperoxidase, sphingomyelinase, secretory phospholipase and NADPH oxidase (Li & Glass, 2002; Saha *et al.*, 2009). Two scavenger receptors SR-A and CD36 on the surface of macrophages have been shown to be important in the development of lesions (Suzuki *et al.*, 1997; Febbraio *et al.*, 2000). The scavenger receptors aid in the transport of highly oxidised LDL into the macrophage. Normally, excess cholesterol is transported to the liver via the reverse cholesterol transport chain and removed from the body in biliary excretion, however in the presence of excess highly oxidised LDL, cholesterol and fatty acids build up within the macrophage (Li & Glass, 2002). The macrophages eventually die from necrosis (Hegyí *et al.*, 1996) leaving cellular debris, that increases the inflammation response further. The extracellular lipid accumulation and cell debris develops into a necrotic core. As the lesion becomes larger, SMCs migrate from the media into the intramural space and produce a fibrous cap around the lesion. The SMC migration and proliferation is propagated by an influx

of activated T-cells producing cytokines such as IFN- γ and TNF- α , these also further exaggerate the inflammatory response (Collins *et al.*, 2000). As the plaque grows in size it bulges into the lumen leading to reduced blood flow and ultimately occlusion of the vessel.

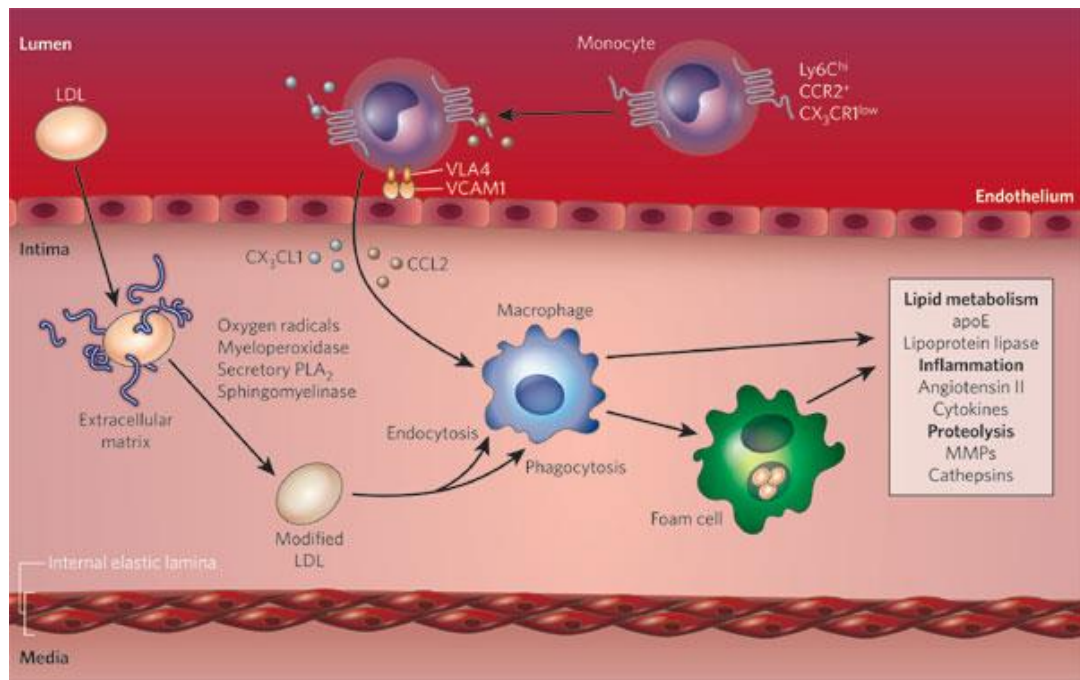


Figure 1.16 : Formation of foam cells.

Image adopted from Rader & Daugherty (2008)

A symptom of atherosclerosis is hypertension. Hypertension is characterised by high blood pressure and affects the pulmonary and systemic systems differently. The common significant change is an increase in wall thickness (Figure 1.17) due to the increased smooth muscle mass, proteoglycans and collagen in the vessel wall as well as reduced lumen diameter. This is a combination of hypertrophy (increase in cell size) and hyperplasia (increase in cell number) (Humphrey & Taylor, 2008).

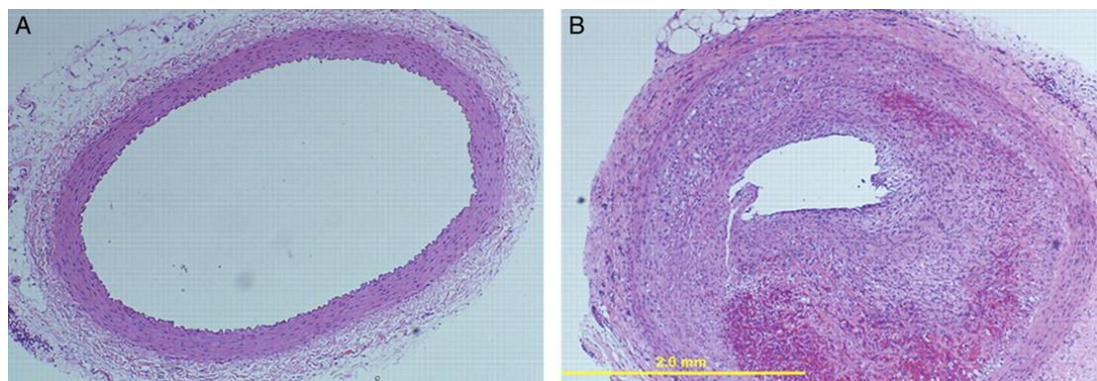


Figure 1.17 : Haematoxylin and eosin stained arteries showing normal (A) and hypertension (B) states.

Adapted from Laing & McPherson (2009)

1.3.2 Incidence and Risk of Cardiovascular Disease

Cardiovascular diseases account for roughly 25 % of all deaths in the age range 5 to 70 with ischemic heart disease being the number one cause of morbidity in the world accounting for approximately 11 % of all deaths with strokes following shortly behind with approximately 9% (W.H.O., 2011). There is a higher incidence of all forms of heart disease in males than in females (Figure 1.18).

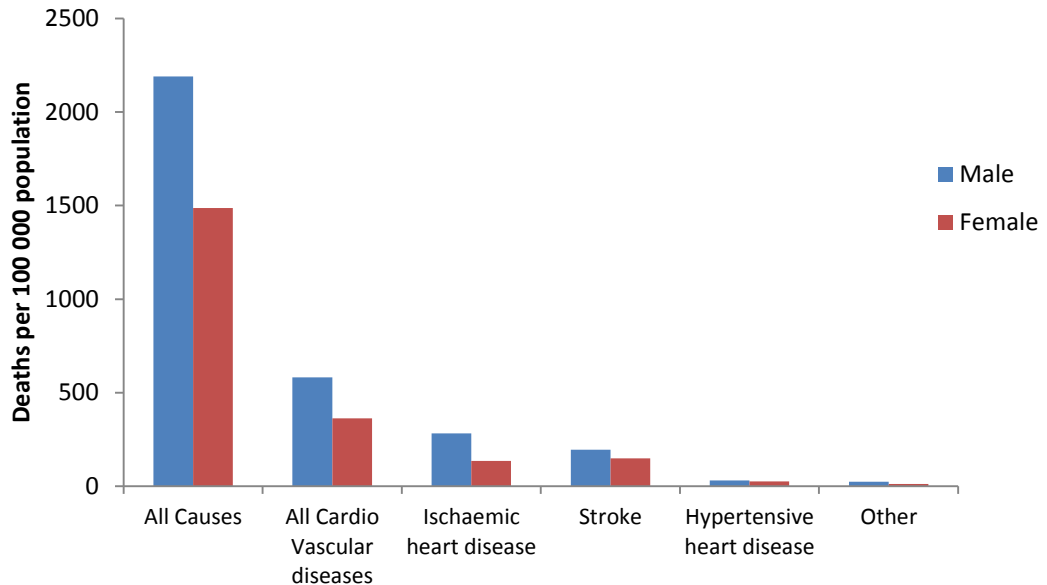


Figure 1.18 : Chart of death incidences per 100 000 worldwide from cardiovascular diseases.
Adapted from W.H.O. (2011).

As well as gender there are a number of other genetic and environmental factors that contribute to an increased risk of the development of atherosclerosis (Table 1.1).

Table 1.1 : Genetic and environmental factors that increase the risk of atherosclerosis.

Genetic	Environmental
Elevated levels of LDL/VLDL	Depression and other behavioural traits
Reduced levels of HDL	High-fat diet
Elevated levels of lipoprotein	Smoking
Elevated blood pressure	Low antioxidant levels
Elevated levels of homocysteine	Lack of exercise
Family history	Infectious agents
Diabetes and obesity	
Gender	
Systemic inflammation	
Metabolic syndrome	
Age	

1.3.3 Therapies

Atherosclerosis is initially treated by increased regular exercise and cessation of smoking, both of which should reduce the amount of LDL in the blood stream. If problems persist pharmacological methods are employed and at the extremities of functional disability surgical intervention is required. Pharmacological therapies include statins, antioxidants, blood thinners and dietary supplements as well as emerging methods utilising antibodies and receptor proteins. Surgical methods available include endarterectomy, which involves the surgical removal of plaque; angioplasty, where a balloon is inflated within the vessel lumen and used to expand the narrowed artery; insertion of a stent (a metal frame to prevent closure of the artery) and ultimately a bypass or replacement graft. For large diameter vessels there are number of clinical products on the market, both synthetic and natural grafts, which are used routinely. Dacron, polyethylene terephthalate (PET) and polytetrafluoro ethylene (PTFE) are synthetic options often used with good patency rates in large diameter vessels. However, for small diameter vessels (< 6mm) these same materials experience early failure and rapid occlusion due to increased thrombogenicity and compliance mismatch (Tilanus *et al.*, 1985; Hoenig *et al.*, 2005). For small diameter vascular graft (SDVG) surgery the main categories are coronary artery, below the knee femoropopliteal bypass as well as arteriovenous shunts for kidney dialysis in established renal failure (ERF)(Figure 1.19).

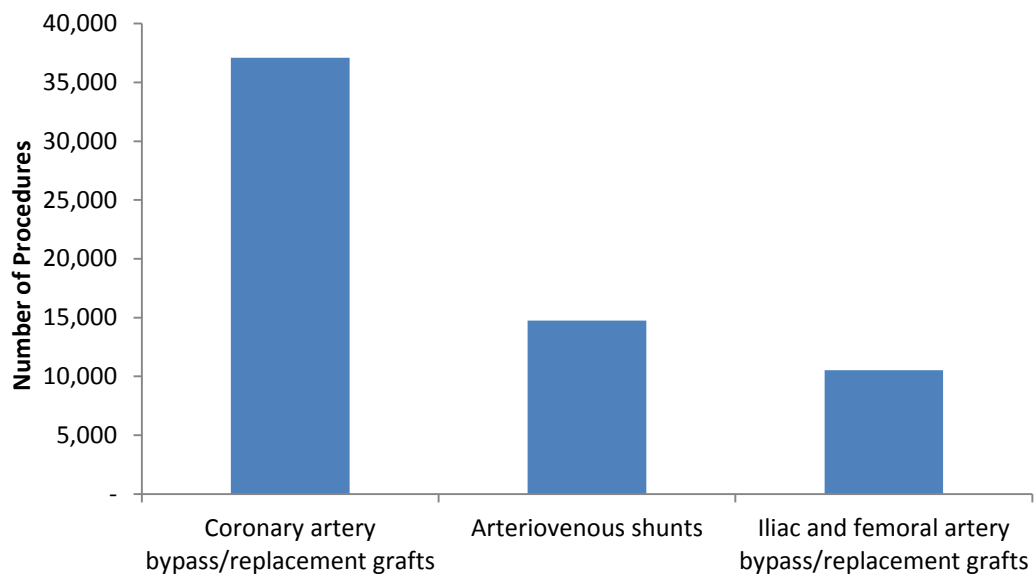


Figure 1.19 : Number of bypass/replacement grafts performed on coronary arteries, iliac and femoral arteries and arteriovenous shunts in the UK 2010-2011.

Adapted from H.S.C.I.C. (2011)

The gold standard for small diameter vascular grafts is autologous vascular tissue, usually saphenous vein (Figure 1.20). Despite this, the procedure is associated with low patency rates and approximately 40 % of patients do not have adequate tissue for the procedure due to vascular disease, size mismatch or previous operations (DeWeese *et al.*, 1966; Veith *et al.*, 1979).

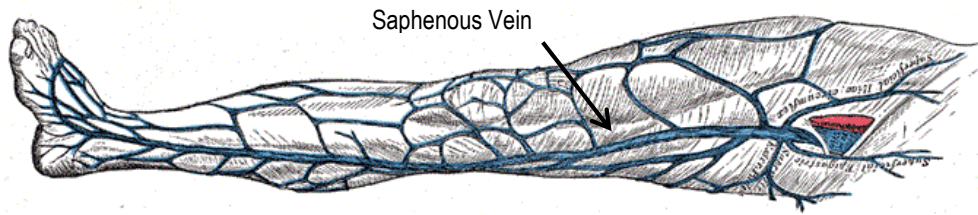


Figure 1.20 : Image depicting the greater saphenous vein and its tributaries of the leg.
Adapted from Gray *et al.* (1973)

Coronary artery bypass grafts (CABG) are most likely to consist of a mammary anastomosis from the left subclavian artery to the left anterior descending coronary artery (1), accompanied by a replacement bypass graft from the aortic arch to the right anterior descending coronary artery (2) (Figure 1.21). A mammary anastomosis is the most common form of CABG followed by saphenous vein bypass, it is also quite likely that multiple coronary arteries will be bypassed (H.S.C.I.C., 2011).

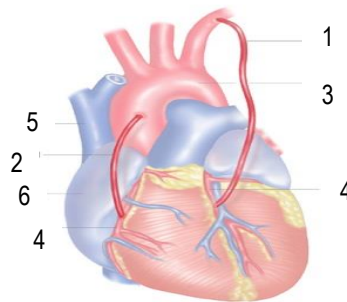


Figure 1.21 : Diagram of routine CABG surgery

(1) bypass originating from subclavian artery , (2) bypass originating from aortic arch, (3). Aorta, (4) coronary artery, (5). vena cava, (6). Auricle. Image adapted from www.nhs.uk (2011).

A femoropopliteal bypass graft can either be above or below the knee depending on the location of the stenotic artery. Above the knee the bypass begins and ends in the femoral artery and below the knee begins in the femoral artery ending in the popliteal artery. Below the knee femoropopliteal bypass grafts are generally SDVGs.

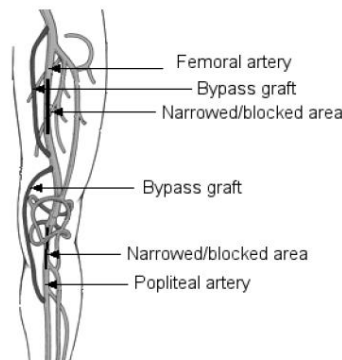


Figure 1.22 : Image depicting femoropopliteal bypass graft surgery.
Image adapted from www.shinonglobal.com (2011)

People suffering from established renal failure require repeated kidney dialysis (filtration) of the blood. The blood is accessed via an arterio-venous fistula (Figure 1.23) which over time becomes stenotic and occludes. Established renal failure requiring vascular access has risen over the past decade and plateaued by 2010 at about 107 per million population. A SDVG could be a potential solution to providing accesses to the patient's blood (L'Heureux *et al.*, 2007a; McAllister *et al.*, 2009).

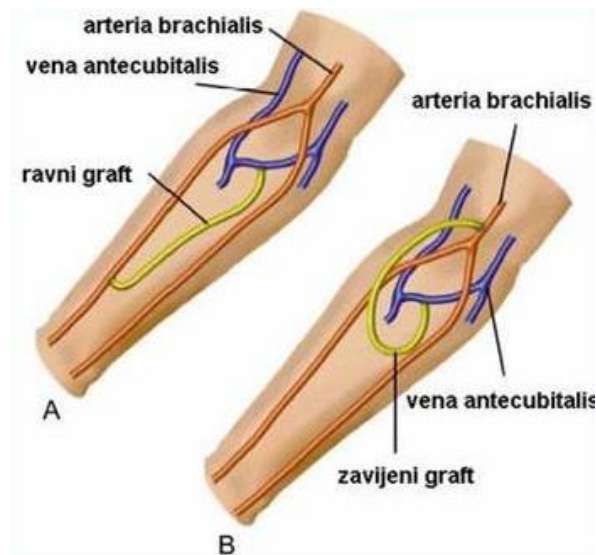


Figure 1.23 : Two versions of arteriovenous graft in forearm.
Image adapted from www.intechopen.com (2011)

1.4 Small Diameter Vascular Grafts

The final stage of therapy for ischemia is a small diameter vascular graft classed as less than 6 mm internal diameter and that the gold standard for this therapy is the use of autologous saphenous vein. A blood vessel is considered patent when it is less than 30 % occluded, although some authors have reported their own conditions for patency in publications. Even as the gold standard the primary patency rates using saphenous vein are low and there is an indication that arterial autografts supersede venous autografts. A study of randomised controlled trials reported venous grafts for above-knee femoropopliteal bypass had primary patency rates of 80 and 74 % at 2 and 5 years respectively (Klinkert *et al.*, 2004) and in CABG the internal mammary artery has been shown to have an 85 % patency rate vs 61 % for autologous saphenous vein at 10 years (Goldman *et al.*, 2004). Although veins undergo structural changes including increasing SMC's in a process called arterialisation, an intact arterial structure appears to be superior to a venous structure. Further to this 40 % of patients do not have adequate tissue for the procedure due to vascular disease, size mismatch or previous procedures. Encompassing these problems creates a market for another source of small diameter vascular graft. To date there is still no comparative alternative to the autografts and this is reflected by the number of surgeries being performed with alternative

grafts compared to autografts. In the UK there are over 37,000 coronary artery replacements or bypass grafts each year and nearly all of these surgeries are autografts with saphenous vein or thoracic arteries, less than one percent are prosthetic grafts (Table 1.2).

Table 1.2 : Number and type of coronary artery bypass/replacement procedures.

Data also includes mean age of patient, adapted from H.S.C.I.C. (2011).

Procedure description	All procedures #	Mean age
Connection of thoracic artery to coronary artery	17,641	67
Saphenous vein graft replacement	17,640	68
Other autograft replacement of coronary artery	1,494	65
Other replacement of coronary artery	284	68
Prosthetic replacement of coronary artery	18	69
Allograft replacement of coronary artery	13	64
Other bypass of coronary artery	6	57

Aside from graft infection, the significant causes for graft failure have been identified: lack of comparable mechanical properties to the native artery such as compliance and strength (Tiwari *et al.*, 2003), anastomotic neointimal hyperplasia and lack of an anti-thrombogenic endothelial layer. The ideal graft should have mechanical properties that match the native artery as well as be non thrombogenic and promote neointimal growth (combination of ECs and basement membrane). One factor that has been reported to promote neointimal growth is the porosity of the graft material and it has been suggested that the pore size should range from large (20-60 μm) at the luminal surface to small (5 μm) on the adventitial surface in order to promote the growth of the vasa vasorum (Sarazin *et al.*, 2004). It is generally thought that compliance should be close to that of the surrounding native artery at physiological pressures (Zilla & Greisler, 1999; Greenwald & Berry, 2000) which ranges from approximately 5.9 % diameter change per 100 mmHg for host arteries to 4.4 % diameter change per 100 mmHg for saphenous vein (Walden *et al.*, 1980). Burst pressure also should be similar to native arteries ranging from approximately 5000 mmHg for carotid arteries to approximately 2000 mmHg for saphenous vein (Teebken & Haverich, 2002). Ideally vascular grafts should also have a long shelf life, and be easily sterilised with the need for minimal preparation time prior to operation (Zhang *et al.*, 2007).

1.4.1 Synthetic SDVG

The advantages of synthetic grafts are that they can be produced cheaply and have consistent microstructures, porosity and strength (Pankajakshan & Agrawal, 2010). Unfortunately they lack growth and regenerative potential and have also been reported to have a higher potential for infection compared to biological grafts .

1.4.1.1 PET and ePTFE (Dacron and Terylene, Teflon and Gore-Tex)

The two most commonly used synthetic materials over the past 50 years are polyethyleneterephthalate (PET) (Dacron or Terylene) and expanded polytetrafluoroethylene

(ePTFE), (Teflon or Gore-Tex) (Chlupác *et al.*, 2009). When PET or ePTFE have been used as SDVGs the patency rates have been found to be significantly lower when compared to autografts. There are two main failure modes; Early failure has been reported to develop as a result of thrombosis and long term failure from anastomotic intimal hyperplasia. Both modes of failure have been recognised to be influenced greatly by the lack of an endothelial layer and smooth muscle cell proliferation. Where as in some animal models complete endothelialisation of the grafts occurs, in humans the healing process develops a thrombotic acellular fibrous lining along the length of the graft and in some cases islands of endothelial cells are observed in the mid region, but in general cellular infiltration is limited to a few millimetres of outgrowth at the anastomoses (Berger *et al.*, 1972; Sauvage *et al.*, 1974). A study of randomised controlled trials of bypasses using PET and PTFE showed no statistical difference in patency rates at approximately 60 and 40 % at 2 and 5 years respectively (Roll *et al.*, 2008), this is substantially lower than autograft saphenous vein (Figure 1.24). Compliance mismatch has been postulated as another reason for failure in SDVG's. The compliance of Dacron and ePTFE are 0.019 and 0.016 % diameter change per mmHg which are both low in comparison to host arteries and saphenous vein (Walden *et al.*, 1980). In summary PTFE and Dacron are suitable conduits for large diameter grafts but in small diameter grafts have suboptimal patency rates in comparison to autografts. A large mismatch in mechanical properties compared to native artery tissue and lack of endothelialisation are the key reasons for failure.

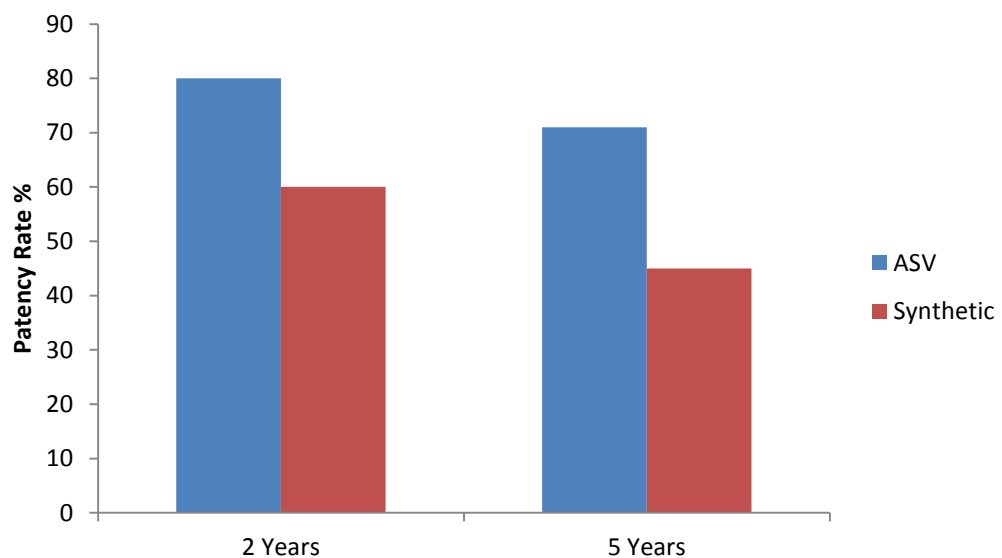


Figure 1.24 : Primary patency rates of synthetic and autograft saphenous vein at 2 and 5 years. ASV – Autograft saphenous vein.

1.4.1.2 Polyurethanes

Over the last ten years polyurethane (PU) has been investigated as an alternative material to PET and PTFE due to its increased elasticity and potentially improved biocompatibility (Tiwari *et al.*, 2002). The composition of PU can be easily configured to provide polymers of varying compliance making it ideal to address the precedence of compliance mismatch in earlier synthetic vascular grafts. Unfortunately first generation PU suffered from inconsistent biodegradability from oxidative and hydrolytic stresses, leading to aneurysm formation and increased thrombogenicity as well as increased infection rates (Brothers *et al.*, 1990). Newer generations of PU have been modified either chemically or used in combination with other materials in attempts to stabilise their structure to these stresses. In short and long term animal models results showed modified PUs developed a layer of complete endothelialisation compared to PTFE which became calcified, thrombogenic and developed increased intimal hyperplasia (Jeschke *et al.*, 1999; Soldani *et al.*, 2010). Findings like this gave rise to a series of clinical trials as kidney dialysis access grafts all achieving subpar patency rates compared to PTFE. An ester modified PU arterial graft “Vectra” achieved a primary graft patency of 42 % at 1 year, a PU arterial graft coated with gelatine and reinforced with knitted polyester achieved primary patency rates of 53.2 % at 1 year (Nakagawa *et al.*, 1995) and a PU arterial graft “Myolink” went into phase one clinical trials (Tiwari *et al.*, 2002) but has not yet published its findings (Desai *et al.*, 2011). To date there has been several clinical trials using PU arterial grafts none of which have shown any clear superiority to PTFE or PET synthetic grafts. Promising work has been carried forward into improving mechanical properties and addressing compliance mismatch issues but PU still suffer from thrombogenic surfaces that lack the promotion of a functioning endothelial layer.

1.4.2 Regenerative Scaffolds

New approaches in the research and development of vascular grafts aim to develop scaffolds which are biodegradable with a view to regeneration *in vivo* or by seeding of autologous cells prior to implantation. In this approach, ideally the scaffold material should degrade at a rate that is inversely proportional to the regeneration of an ECM (Figure 1.25) by either seeded cells or host cells, thus scaffold materials should attract and promote the growth of cells and not induce an immune response. Likewise degradation products of such scaffolds should be bio absorbable and non-cytotoxic or -immunogenic (Berglund *et al.*, 2003).

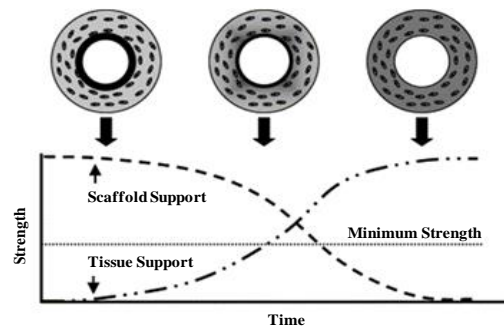


Figure 1.25 : Diagram showing how tissue regeneration should take over support from scaffold.
As a scaffold material degrades over time, so does its load bearing capacity. As the tissue regenerates around the scaffold it produces structural proteins such as collagen; this increases its load bearing capacity.
Image adopted from Berglund *et al.* (2003)

1.4.2.1 Biodegradable synthetics

For biodegradable synthetic scaffolds, degradation rates should be controllable, and the scaffold needs to be designed to promote cell growth, without any residual material left after regeneration of the ECM. A wide range of synthetic scaffolds have been investigated singularly or as copolymers. These include scaffolds fabricated from polyglycolic acid (PGA), polylactic acid (PLA) and poly-L-lactic acid (PLLA), polyε-caprolactone (PCL), polyethylene glycol (PEG), polylactic acid-co-lysine, polyhydroxyalkanoate (PHA), poly-4-hydroxybutyrate (P4HB), and polydioxanone (PDS). PGA is the most commonly used biodegradable polymer scaffold when its used on its own PGA degrades in the body within two weeks, so is only feasible when used as a copolymer (Kannan *et al.*, 2005). There have been animal studies using SDVGs such as a PGA-PLA co-polymer and a polydioxanone composite implanted in a rabbit aorta model that showed 100 % patency at 1 year (Greisler *et al.*, 1988) and a polydioxanone-polypropylene composite implanted in a canine aorto-iliac model that showed 86% patency at 1 year (Greisler *et al.*, 1991), despite these early results there have been no resulting clinical trials. In addition to this biodegradable polymers can require a lengthy conditioning times in order to obtain adequate mechanical properties. PGA scaffolds were seeded with bovine SMC and EC and subjected to pulsatile conditions in a bioreactor, the burst pressure increased from 570 mmHg after 3 weeks to 2150 mmHg after 8 weeks (Niklason *et al.*, 2001). Mechanical properties of some polymers have been modified to attain UTS and compliance to reach ranges of approximately 1.5 to 7 MPa and 0.012 to 0.056 % diameter change per mmHg (Barnes *et al.*, 2007). Poor mechanics, lengthy preconditioning times adding to the lack of “off the shelf” availability and limited animal model and clinical trials data, highlight the infancy of biodegradable polymers compared to autologous tissue and non-biodegradable synthetic materials.

1.4.2.2 Natural scaffolds

Natural scaffolds have the advantage that the material is readily accepted by the body and potentially remodelled easily *in vivo*. Natural scaffolds can be fabricated from natural proteins,

produced by cells *in vitro* or generated through the decellularisation of natural human or animal tissues.

1.4.2.3 Collagen scaffolds

Scaffolds made from collagen have been investigated extensively, since collagen is the major structural component of tissues and has low immunogenicity. Early collagen scaffolds were shown to support good growth of EC and SMCs, and cells cultured on collagen scaffolds were shown to produce ECM proteins; von Willebrand factor (vWF, a protein involved in homeostasis primarily preventing blood coagulation) and prostacyclin (PGI₂, lipid preventing platelet clotting) but lacked sufficient burst pressures (~20-80 mmHg) and were devoid of elastin (Weinberg & Bell, 1986). L'Heureux *et al.* (1993) developed a novel method of contracting a collagen gel around central mandrel with cultured human SMCs, followed by embedding fibroblasts which increased burst pressures. Tranquillo *et al.* (1996) used a magnetic field to align SMCs embedded in a collagen gel in the circumferential direction to better emulate natural cell alignment. Significant improvements to mechanics were made when incorporating biodegradable polymers in the scaffolds such as PGA or PLA, in addition polymer and SMC embedded collagen scaffolds have shown elastin deposition (Park *et al.*, 2009). A 2 mm diameter and 1 cm length scaffold comprised of two layers of collagen Type I of different pore sizes was seeded with SMCs and ECs. They were implanted into rat vena cava and the grafts were harvested at 6 and 12 weeks. After 12 weeks the original collagen had been completely degraded and regenerated with neovascular tissue. The implanted grafts were shown to have a UTS and modulus close to that of arteries and showed no signs of occlusion (Wu *et al.*, 2007). Tillman *et al.* (2009) developed SDVG using PCL and collagen to increase the mechanical properties of the collagen, the implants were used as aorta-iliac bypass grafts in rats and were patent at explantation after one month, however, tensile properties of the graft reduced over the month with degradation of the scaffold. Scaffolds fabricated from collagen alone or with support structures in general, exhibit very low burst pressures, scaffolds with increased burst pressures are those that have been seeded with cells and conditioned for long periods. This makes collagen an impractical protein for the production of arterial scaffolds despite its natural biocompatibility and the reason no long term animal or clinical studies have been conducted.

1.4.2.4 Elastin

The mechanical properties of elastin make it a vital component of blood vessels, so using it as a scaffold has potential benefits. However, scaffolds made of elastin alone have demonstrated very small burst pressures (162±36 mmHg). Elastin-only scaffolds are difficult to use due to the high insolubility of the protein and have demonstrated weak mechanical properties. However, elastin is a necessity within a natural scaffold to achieve compliance similar to native arteries.

1.4.2.5 Fibrin

Fibrin is the body's natural ECM protein involved in wound healing and is easily extracted in the form of fibrinogen from blood. Fibrinogen can then be formed into an autologous scaffold (Fussenegger *et al.*, 2003). Scaffolds based on SMC embedded fibrin gels have been shown to promote increased collagen synthesis compared to scaffolds based on SMC embedded collagen gels (Grassl *et al.*, 2002). A 4 mm SDVG was developed (Swartz *et al.*, 2005) from fibrin matrix embedded with SMC and ECs. The grafts were implanted as interpositional grafts in jugular veins of lambs and explanted after 15 weeks. After the 15 week period mechanical properties were low, the tissue was showing good regeneration and remained patent. Fibrin-based scaffolds have shown good remodelling of the ECM and production of elastin and collagen, but their burst pressures have been reported as far too low, even when incorporated with other biodegradable polymers (460 mmHg)(Tschoeke *et al.*, 2009). However a fibrin scaffold reinforced with a polylactide mesh, seeded with autologous ECs, SMCs and fibroblasts remained patent for six months in sheep carotid arteries (Koch *et al.*, 2010) after which the polymer mesh was almost completely degraded.

1.4.2.6 Autologous synthesised ECM scaffolds

As mentioned previously L'Heureux *et al.* (1993) developed a novel technique of culturing sheets of SMCs and fibroblasts in vitro. Following one month in culture, the seeded SMCs and fibroblasts had developed their own ECM. The sheet of SMCs was wrapped around a tubular support, then the fibroblast sheet was wrapped around the SMC sheet, after maturation of the cells, ECs were seeded on the luminal surface creating a three tiered blood vessel. The burst pressure of the vessel was in excess of 2000 mmHg, similar to that of native veins, and the endothelium produced vWF and PGI₂. They also demonstrated good suturability, but they only had a patency rate of 50 % when implanted as femoral arteries in the canine model. Further trials as arteriovenous access grafts showed early favourable results. One patient died on day 39 due to unrelated cause, a second graft lasted 13 months, and a third one failed after 12 weeks, due to low postoperative flow rate. These grafts have shown good burst pressures of 3340 ± 849 mmHg and compliance (3.1 to 15.0 % per 100 mmHg, 2.3 to 6.2 % per 100 mmHg) and developed a working confluent endothelial layer (L'Heureux *et al.*, 2007b; McAllister *et al.*, 2009). However, the production of this type of graft required a long culture period of over three months, an approach that is not practical nor economically viable.

1.4.2.7 Allogeneic grafts

Allogeneic grafts that have been investigated for use as SDVG replacements include glutaraldehyde treated human umbilical vein and cryopreserved veins. The umbilical vein graft is now in its third decade of clinical use and has shown patency rates at 5 years comparable with that of saphenous veins (Dardik *et al.*, 1988), initially there were concerns

over the glutaraldehyde treatment causing increased calcification and aneurism formation, though in the second decade of its use aneurysm formation was not to be seen (Dardik *et al.*, 2002). This was attributed to improved production methods as well as previous aneurysm formation being caused by patient related diseases. Despite its clinical success the product was taken off the market in 2004 due to changes in FDA regulations on the implantation of tissue with respect to source identification and testing, and the consequent affects this had on tissue procurement and processing (Dardik 2006). Nevertheless, glutaraldehyde treated tissues prevent the ingress of cells and the potential for regeneration of the tissue by host cells. Limited clinical trials have been carried out with cryopreserved allograft veins. Cryopreserved cadaver femoral veins from Synergraft, (CryoLife, Marietta, GA) were used in a clinical trial before being stopped by the FDA, limited results showed no benefit of using the graft and that it was potentially aneurismal (Madden *et al.*, 2005). Cryopreserved saphenous vein allografts were intended to reduce antigenicity but have historically underperformed (Martin *et al.*, 1994) and no change has been seen in recent studies, achieving primary patency rates of 56 %, 32 % and 17 % at 1,3 and 5 years respectively for infrapopliteal bypasses (Randon *et al.*, 2010). Using the L'Heureux *et al.* (1993) method of fusing sheets of fibroblasts and SMCs to form a blood vessel, an allogeneic renal access graft was implanted into 3 human patients. The luminal side was partially “devitalised” by dehydration bringing into question whether this is an allogeneic graft or decellularised graft. The study reports that host immune responses were minimal to the graft and panel reactive antibodies weren't elevated compared to normal allografts that increase levels as much as 80 % at 3 months. It was suggested the lack of host response was due to the graft being constructed from cultured fibroblasts that don't express MHCII antigens and no xeneogenic cells present in the tissue. Although the paper questions the need for complete decellularisation on this basis. Grafts failed at 3 and 5 and 11 months. And in addition it was not a sufficiently large enough trial to evaluate patency (Wystrychowski *et al.*, 2014)

1.4.2.8 Decellularised natural scaffold

A decellularised natural scaffold is an allogeneic or xenogeneic tissue devoid of all native cells, antigens and cellular debris including the genetic material, leaving only the structural materials of ECM matrix providing a natural histo-architecture retaining similar mechanical integrity to the desired tissue.

The main cause of failure in allogeneic grafts is typically acute rejection initialising a few days post-surgery. The response is primarily governed by the adaptive immune system; firstly alloantigens must be presented to CD4+ T-lymphocytes in the appropriate context, secondly activation of lymphocytes and in turn an exponential proliferation and differentiation of lymphocytes. It is this activation, proliferation and differentiation that cause a time delay in the response. Alloantigen recognition is enabled through three pathways (Figure 1.26) direct, indirect and semi direct (Ponticelli, 2012). Recognition in the direct pathway is facilitated by

donor antigen presenting cells (APC). The donor APCs migrate to secondary lymphoid tissue and present donor MHCs/peptides to CD4+ and CD8+ T-cells. The indirect pathway is facilitated by recipient APCs engulfing donor MHCs that were shed during apoptosis or necrosis of donor cells. Epitopes of the donor MHC are presented on recipient APC MHCs. The recipient APCs then migrate to the secondary lymphoid tissue and present donor peptides on recipient APC MHCs to CD4+ T-cells. The semi direct pathway is facilitated by transfer of intact donor MHCs/peptides to recipient APCs via cell-cell contact or exosomes. Recipient APCs then migrate to the secondary lymphoid tissue and present donor MHC/peptides and recipient MHC with donor peptides to CD4+ and CD8+ T-cells. Once CD4+ T-cells become activated using interleukin 2 they then help activate the clonal expansion of CD8+ T-cells specific to donor epitopes and B-cells specific to donor antigens. Cytotoxic CD8+ T cells, helper CD4+ T-cells and alloreactive antibodies then migrate to the donor site causing a considerable inflammatory response. The cell-mediated effector cells combined with activation of elements from the innate immune response result in necrosis and failure of the donor graft (Sagoo *et al.*, 2012). Donor APCs eventually subside and chronic rejection can occur through indirect or semi-direct pathways.

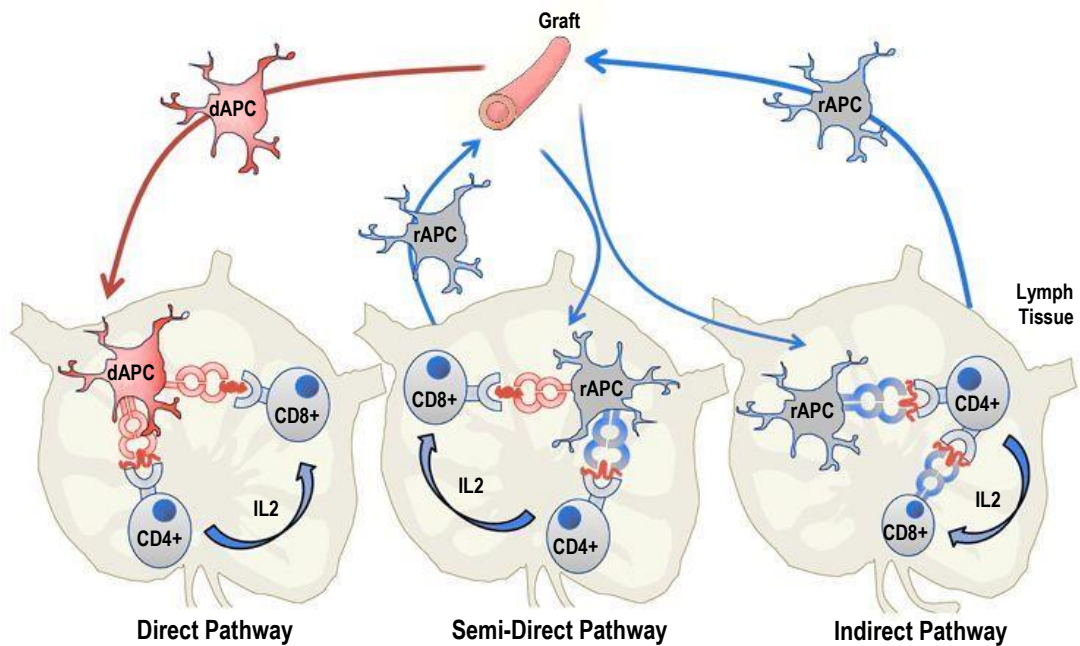


Figure 1.26 : Antigen recognition in acute rejection, depicting the direct, indirect and semi-direct pathway.

The direct pathway is an immune response initiated by the graft APC's and MHC/antigen complexes. The semi-indirect pathway is an immune response initiated by host APC's and graft MHC/antigen complexes. The indirect pathway is an immune response initiated by the host APC's and MHC's which form complexes with the donor antigens. Image adapted from Sagoo *et al.* (2012).

The main cause of failure in xenogeneic grafts is the result of a mixture of intense hyperacute and the aforementioned acute rejection. The hyperacute rejection is governed by the humoral immune system; complement activation is mediated by xenoreactive natural antibodies (XNAs). The intense inflammatory response is due to a high content of IgG and IgM antibodies specific to the galactosyl- $\alpha(1,3)$ galactose (α Gal) epitope. The anti- α Gal antibodies

are the major initiator in the complement activation pathway. The α Gal epitope is expressed on membrane glycoproteins and glycolipids on xenogeneic cells but is not expressed in humans or old world monkeys (Galili & Swanson, 1991). The high antibody titres are thought to be due to constant exposure to intestinal bacteria expressing the α Gal epitope. Tissues and organ grafts require a blood supply to maintain cells, the antibodies bind to α Gal epitopes on the endothelial cells activating the complement activation process; this causes thrombosis of the vasculature leading to oxygen depleted cells and necrosis in the graft ultimately resulting in failure (McPherson *et al.*, 2000). Following the hyperacute rejection response, acute vascular rejection may develop within days or weeks, similar to that of the acute rejection in allogeneic grafts, the complete mechanism is not understood however the synthesis of XNAs has an important role (Parker *et al.*, 1996). It is therefore essential to remove donor cells from allogeneic and xenogeneic grafts to avoid graft rejection response.

In particular for vascular grafts it is also important to remove all nuclear material in the decellularisation process. Firstly as an indicator that the cellular remnants are being removed and secondly because DNA is a contributing factor to calcification (Shanahan, 2013). Glutaraldehyde fixation is used on porcine bioprosthetic heart valves (and other xenografts) in order to reduce the immunogenicity of the grafts; the main cause of failure of glutaraldehyde fixed grafts is calcification (Schoen, 1987). Fixation causes rupture of the donor cells but cellular debris is retained in the graft (Courtman *et al.*, 1994) these cell remnants (Valente *et al.*, 1985) and cell membranes (Maranto & Schoen, 1988) have been linked to increased calcium deposition caused by the release of phosphate from the phospholipid bilayer and other cell debris including DNA and RNA (Neven & D'Haese, 2011). Decellularised scaffolds have been shown to have less calcification formation compared to fresh and glutaraldehyde fixed tissues (Vesely *et al.*, 1995), but incomplete decellularisation can lead to rapid failure of grafts with increased calcification. SynerGrafts model 500 and 700 decellularised porcine heart valves failed rapidly in clinical trials and the product withdrawn. Of the four implanted, one lasted 1 year post operatively, the explant had been encapsulated and showed signs of calcification. The valve was shown to have incomplete decellularisation causing activation of the hyperacute response, they postulate that the calcification was nucleated by the collagen matrix itself but it may also have been compounded by the presence of foreign nuclear material (Simon *et al.*, 2003).

The removal of α Gal epitopes and xenoreactive species in xenogeneic grafts and alloreactive species in allogeneic grafts as well as the complete removal of foreign DNA should allow tolerance of the scaffold with minimal calcification; this is the basic premise of decellularised scaffolds. Therefore decellularisation technique itself is crucial to the success of the implant; whilst causing minimal damage to the ECM matrix the process must remove all immunogenic, calcific and thrombogenic material of the donor (Wilshaw *et al.*, 2012). This also subsequently makes it difficult to assess the constituents of the graft. Varying types of chemical and enzymatic agents have been used alongside physical conditions to achieve decellularisation (

Table 1.3).

Table 1.3: Physical, Chemical and Enzymatic Methods of Decellularisation.

Extra cellular matrix (ECM), glycosaminoglycan (GAG), sodium dodecyl sulphate (SDS), adapted from Gilbert *et al.* (2006).

Method	Mode of action	Effects on ECM
Physical		
Snap Freezing	Intracellular ice crystals disrupt cell membrane	ECM can be disrupted or fractured during rapid freezing
Mechanical agitation	Can cause cell lysis, but more commonly used to facilitate chemical exposure and cellular removal	Aggressive agitation or sonication can disrupt ECM as the cellular material is removed
Chemical		
Acid	Solubilises cytoplasmic components of cells: disrupts nucleic acids	Removes GAGs
Non-ionic detergents Triton X-100	Disrupts lipid-lipid and lipid protein interactions, while leaving protein-protein interactions intact	Mixed results: efficiency dependant on tissue, removes GAGs
Ionic detergents: Sodium dodecyl sulphate (SDS)	Solubilises cytoplasmic and nuclear cell membranes, tends to denature proteins	Removes nuclear remnants and cytoplasmic proteins: tends to disrupt native tissue structure
Sodium deoxycholate Triton X-200		More disruptive to tissue than SDS Yielded efficient cell removal when used with zwitterionic detergents
Zwitterionic detergents CHAPS	Exhibit properties of non-ionic and ionic detergents	Efficient cell removal with ECM disruption similar to that of Triton X-100
Hypertonic and hypotonic solutions EDTA / EGTA	Cell lysis by osmotic shock Chelating agents that bind divalent metallic ions thereby disrupting cell adhesion to ECM	Efficient for cell lysis, but does not effectively remove cellular remnants No isolated exposure, typically used with enzymatic methods
Enzymatic		
Trypsin	Cleaves peptide bonds on C-side of Arg and Lys	Prolonged exposure can disrupt ECM. Removes laminin, fibronectin, elastin and GAGs
Nucleases	Catalyse hydrolysis of interior and terminal bonds of ribonucleotide and deoxyribonucleotide chains	Difficult to remove from the tissue and could invoke an immune response

These agents and conditions need to be optimised specifically to the properties of a particular tissue (Badylak *et al.*, 2009). The small intestinal submucosa (SIS) was one of the early decellularised scaffolds that has been used as a vascular graft (Lantz *et al.*, 1993). Lantz *et al.* (1990) used SIS in the replacement of 36 canine carotid and femoral arteries, and overall graft patency over 82 weeks was 75 %. Of those that remained patent no infections, thrombi or intimal hyperplasia were observed, although 4 grafts showed aneurismal dilation. Huynh *et al.* (1999) developed acellular 4 mm SDVGs made from the intestinal collagen layer of the SIS material impregnated with a thin layer of type I bovine collagen, they were also treated with heparin and cross-linked. Eighteen grafts were implanted into rabbit carotid arteries and all grafts remained patent at explant periods of 28, 53 and 90 days. Remodelling of the arteries was demonstrated and burst pressures were lower than adequate 931 ± 284 mmHg. Zhao *et al.* (2010) also developed SDVGs by seeding decellularised ovine carotid arteries with mesenchymal stem cells and ECs then implanting them into ovine carotid arteries. The implants attained burst pressures of 1800 mmHg, all the grafts were patent after 5 months and had developed an endothelium layer as well as smooth muscle, collagen and elastin. Schaner *et al.* (2004) decellularised human saphenous vein, the grafts of 7mm diameter were implanted as canine carotid interposition grafts and explanted after 2 weeks. The grafts showed an intact basement membrane, burst pressures of 2380 ± 620 mmHg and were all patent at explantation. A decellularised bovine ureter scaffold was also developed for use as a haemodialysis access graft which has been shown to be less immunogenic than cryopreserved allografts (Madden *et al.*, 2002). Assessment of explants of failed bovine ureters produced by their proprietary Synergraft™ technique showed that the implants contained residual cells and residual α GAL epitope leading to graft failure, aneurismal dilation and thrombosis (Spark *et al.*, 2008), and had a primary patency rate of 14 % at 1 year (Das *et al.*, 2011). A clinical study of decellularised cross-linked Artergraft Bovine Carotid Arteries™ showed primary patency rates of 60.5 %, compared to 10.1 % in PTFE, however secondary patency rates were not significantly different (Kennealey *et al.*, 2011). Decellularised scaffolds have been shown to mimic native mechanical properties but limited clinical trials have been conducted. Decellularisation methods are still under optimisation to achieve complete decellularisation including calcification factors and immunogenic epitopes whilst maintaining a functional histo-architecture, some success has been shown in progressing from synthetic grafts but not to the desired level of competing with autografts.

1.4.2.9 Overview of Small Diameter Vascular grafts

Autologous vein remains the gold standard for SDVG replacement, usually the saphenous vein, studies have highlighted that preferentially an arterial autograft would be superior to venous autograft but are not as abundant or replaceable as veins. The long history using standard synthetic replacements such as Dacron and ePTFE may be improving surgeon

experience and increasing patency rates but are still a long stretch from meeting the same standard as autografts. PU replacements are yet to be seen as a practical alternative and have shown substandard results to date. In the field of biodegradable synthetics a large range of polymer compositions are being tuned to reach desired mechanical properties and porosities although to attain this, long preconditioning times have been needed in some cases making them an unrealistic off the shelf product. Similar to biodegradable scaffolds natural scaffolds of collagen, elastin and fibrin require composite scaffolds in order to attain desired characteristics and the development of a potential off the shelf product seems unlikely in the near future. The allogenic glutaraldehyde treated scaffolds experienced over thirty years of clinical use and patency rates comparable to saphenous vein but there have been concerns over aneurismal formation from the grafts and increased calcification commonly associated with gluteraladheyhe fixed tissues. The use of cryopreservation is also providing a limited increase to the potential of allogeneic grafts and has not sufficiently reduced antigenicity. Decellularised scaffolds have shown the ability to retain natural architecture and mechanics. Clinically trialled products being used have received mixed views and failed grafts contain residual cells and immunogenic agents suggesting that complete decellularisation is not being fully achieved. A competent clinical solution has not yet been developed and ASV remains the gold standard for SDVG.

1.4.3 Mechanical Concepts and their role in Vascular Grafts

Determination of the mechanical properties of vascular grafts is an important aspect to be considered. In order for a graft to be suitable for use it should have adequate strength to resist extremes of physiological pressure it should also have a compliance similar to that of analogous tissue. Compliance mismatch has been attributed to failure in vascular grafts. A graft that is too compliant is likely to stimulate aneurysm formation and an artery that it is non-compliant promotes intimal hyperplasia leading to occlusion of the graft. Too weak a material and the graft may rupture.

1.4.4 Compliance

Compliance in its simplest form is the relative change in volume to change in pressure. A compliant vessel subjected to the equal pressure will dilate more and accommodate an increased volume compared to a non compliant vessel. This relationship is described as:

$$\text{Equation 1-1} \qquad C = \Delta V / \Delta P$$

Veins for example are more distensible than arteries and therefore under the same pressure expand more and allow a larger volume of blood to pass through the vessel (Figure 1.27). The relationship between pressure, lumen size, wall thickness and wall stress can be described by an adaption of Laplace law (Westerhof *et al.*, 2010):

$$\text{Equation 1-2} \qquad \tau = Pr/w$$

Where r is the lumen radius and w the wall thickness. This relationship demonstrates how a vessel will increase its wall thickness when subjected to increased pressure and lumen radius

to maintain wall normal shear stress and is postulated as one of the causes contributing to intimal thickening.

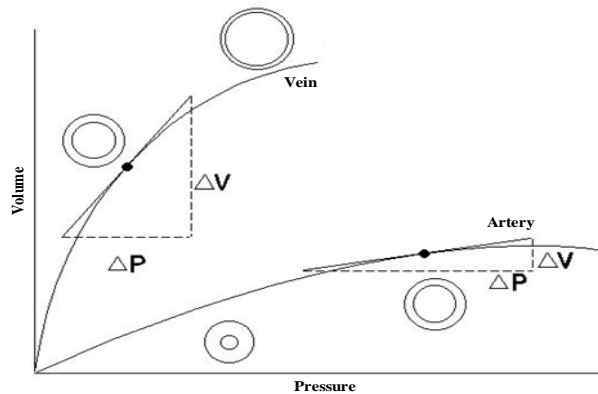


Figure 1.27 : Relationship between vein and artery wall thickness, volume and pressure.
Image adopted from www.columbia.edu (2011)

In clinical applications often the dynamic compliance is calculated in the physiological ranges using systolic and diastolic diameters and pressures, described as:

$$\text{Equation 1-3} \quad C = \frac{(D_s - D_d)}{D_d(P_s - P_d)}$$

The value is converted to a percentage and presented as percentage compliance per millimetre of mercury (% mmHg⁻¹) (Schmitz-Rixen *et al.*, 1993). In static compliance it is possible to calculate the circumferential (CC), longitudinal (LC), cross-sectional (XC) and volumetric compliance (VC)(Salacinski *et al.*, 2001) as well as the physiological compliance. These can be calculated incrementally, cumulatively or over the physiological range as described below, where D = diameter, L = length, A = area, V = volume and 2 and 1 represent final and initial respectively:

$$\text{Equation 1-4} \quad CC = \frac{(D_2 - D_1)}{D_1(P_2 - P_1)}$$

$$\text{Equation 1-5} \quad LC = \frac{(L_2 - L_1)}{L_1(P_2 - P_1)}$$

$$\text{Equation 1-6} \quad XC = \frac{(A_2 - A_1)}{A_1(P_2 - P_1)}$$

$$\text{Equation 1-7} \quad VC = \frac{(V_2 - V_1)}{V_1(P_2 - P_1)}$$

There have been many studies into the effects of compliance mismatch in reference to vascular grafts and its contribution to graft failure. It is now widely accepted that non-compliant (stiffer) grafts in comparison to the host artery at the site of implant contribute to the increase in intimal hyperplasia/thickening and grafts that are excessively compliant can become aneurysmal. Intimal hyperplasia is an increase in thickness of the intima causing

reduced lumen diameter; it is characterised by the migration of smooth muscle cells into the tunica media and the subsequent generation of extra cellular matrix (Newby & Zaltsman, 2000; Mitra *et al.*, 2006).

Generally vascular bypass graft surgery utilises end to side attachment (Figure 1.28 at the anastomoses compared to end to end and this should be taken into consideration when comparing models on intimal hyperplasia formation. End to end anastomoses experience far less intimal hyperplasia than end to side anastomoses, so end to end models can provide conflicting results. A computational model of end to end and end to side anastomosis which simulated grafts of decreasing compliance has shown how peak stresses occur at suture penetrations and the suture line. In end to end anastomoses there is no significant difference in stress regardless of graft compliance. In models of end to side anastomoses, decreasing graft compliance from native arteries to the compliance of Dacron increases mean stress by 40 % providing evidence that excessive stress at sutures could be a signal transduction mechanism that is increased in end to side anastomoses (Ballyk *et al.*, 1998).

Animal models using the end to side technique of implanting various vascular graft materials have shown that intimal hyperplasia occurs preferentially to the toe and heel regions of the distal anastomosis and the bed of the host artery opposing the outflow of the graft. The amount of intimal hyperplasia was constant on the host bed irrespective of material, the heel and in particular the toe region was significantly larger in less compliant grafts. This supports that the less compliant grafts contribute to the pathogenesis of distal anastomosis intimal hyperplasia, but also that a second model, haemodynamics has more influence on bed formation of intimal hyperplasia (Sottiurai *et al.*, 1989; Bassiouny *et al.*, 1992; Trubel *et al.*, 1994). On the bed floor of the host artery opposite the graft outflow, a stagnation point occurs creating areas of low shear stress. It is at these areas of low shear stress and long particle residence times that create conditions suitable for intimal hyperplasia (Morinaga *et al.*, 1985); The importance of compliance as a factor was further confirmed, as one of the animal models used solely autograft tissue and simulated compliance by wrapping an external mesh around the graft, this provided end to side anastomosis and varying levels of graft compliance whilst eliminating an immunogenic/foreign body response as a dominating factor of intimal hyperplasia (Trubel *et al.*, 1994). It is also important to note that that compliance mismatch alone is not sufficient to initiate intimal hyperplasia and surgical healing at an anastomosis is required this was identified in an end to end simulation where external occlusion was induced in an animal model (Okuhn *et al.*, 1989).

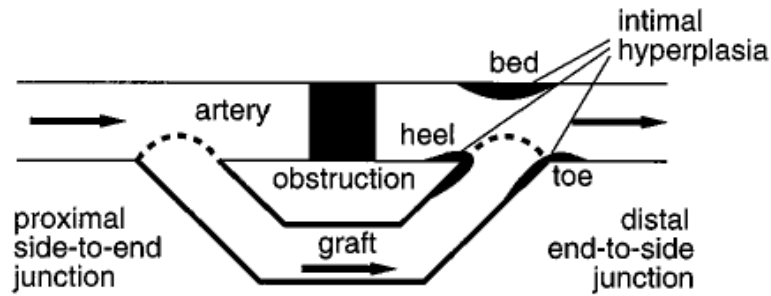


Figure 1.28 : End to side anastomosis.
Image adapted from Ballyk *et al.* (1998)

The majority of aneurysm formation in relation to bypass grafts is pseudo aneurysms forming at the anastomosis due to pooling of blood from poor suture technique, however less compliant arteries have not been considered for implantation due to the likelihood of aneurysm formation so minimal literature is available to review this. Late onset of true aneurysms occurred in a small number of Dacron grafts where the material has stretched due to material fatigue and degradation (Khaira & Vohra, 2002; Van Damme *et al.*, 2005). The relationship of increased compliance and true aneurysm formation is supported by literature investigating aneurysm formation by enzymatic removal of collagen from arteries, this results in an increase in artery compliance and aneurysm simulation (Hamilton *et al.*, 1988).

1.4.5 Stress Strain

When subjected to stress-strain analysis there is a non-linear elasticity in blood vessels (Figure 1.29). The non-linearity is due firstly to the elastin bearing the load and causing large deformations (elastin phase). Subsequently, as the weight bearing is transferred to the collagen in the transition phase, the collagen begins to un-crimp, eventually bearing the entire load. At this point the strength of the collagen can be observed with small deformations with increased load (collagen phase). If the collagen is stretched further, failure will occur. If the tissue is unloaded [before it fails] it will return to its original dimension, showing elastic mechanical properties. However, unloading does not follow the same path as loading. This is called hysteresis and is a result of the viscoelastic properties. Blood vessels are highly anisotropic, demonstrating different stress-strain behaviour when loaded along perpendicular axes (Meyers *et al.* 2008).

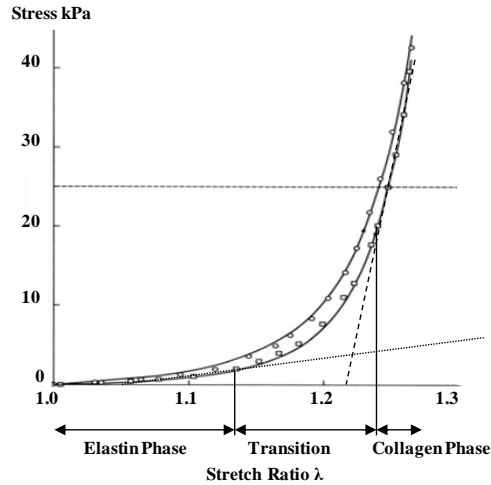


Figure 1.29 : Stress-Strain behaviour of an artery during loading and unloading.
Image adapted from Fung (1993)

1.5 Sterilisation of Medical Devices

Although there is a large emerging research focus on SDVG there is very little investigation and mention of the sterilisation process that must inevitably be carried out. For any medical device or tissue engineered implant intended for clinical use, sterilisation is essential. Microorganisms such as viruses and bacteria can be present in the implant or contaminate the implant during processing/production and they have the potential to infect the recipient, with potentially life threatening consequences as well as cause failure of the implant. Terminal sterilisation is the process of killing or inactivating all types of microorganisms prior to storage, transfer or use of an implant in order to prevent infection or transmission of diseases (Nather *et al.*, 2007).

1.5.1 Micro-Organisms

Microorganisms can be subdivided into unicellular forms and noncellular forms. Unicellular microorganisms may be eukaryotes or prokaryotes. Eukaryotes have a cell nucleus whereas prokaryotes do not. Examples of eukaryotic microorganisms are fungi and protozoa, prokaryotes are microorganisms such as bacteria and archaea. Noncellular microorganisms such as viruses rely on the host cell to survive

1.5.1.1 Gram positive and Gram negative bacteria

Bacteria may be categorised into two groups Gram positive and Gram negative bacteria. They are distinguished using a staining method (Gram stain). In general Gram-positive bacteria have a much denser cell wall rich in peptidoglycans compared to Gram negative bacteria. It is this compositional difference that allows the differentiation of Gram-positive and negative bacteria in the Gram stain. Also specific to Gram positive bacteria are teichoic and teichuronic acids present in some cell walls. In general Gram negative bacteria have a thin layer of peptidoglycans in the cell wall, far less dense than Gram positive bacteria, this layer is

connected by lipoproteins to an external outer membrane, the space between the two layers is called the periplasm. The outer membrane is similar in structure to that of the cytoplasmic membrane but additionally contains lipopolysaccharides, these are part of endotoxins and play a role in bacterial infection.

1.5.1.2 Mycobacteria

Mycobacteria typically stain Gram positive and are then further differentiated using an acid-fast stain. Their cell wall has a unique hydrophobic structure creating a strong permeability barrier. This barrier effectively gives a higher resistance to biocides and antibiotics.

1.5.1.3 Viruses

Viruses are non-cellular micro-organisms. They are small (less than 5 μm), obligate intracellular parasites. Viruses cannot survive on their own and require the use of prokaryotic and eukaryotic host cells in order to replicate. There are many different virus structures, and for the purpose of this discussion of biocides they will be classed into two categories, enveloped and non-enveloped viruses. Common to all viruses is a central nucleocapsid made up of single or double stranded RNA or DNA encircled by a protein capsid built of units called capsomers. Non-enveloped viruses are limited to this structure and are considered hydrophilic. Enveloped viruses have an additional external lipid bi-layer membrane, providing protection and aiding attachment to target cells.

Although there are many differences between viruses, there are several common stages followed by viruses during the course of viral replication: attachment to the host cell, penetration, synthesis of biological molecules, assembly and release. Firstly in order to enter a cell the virus must attach to the cell surface, this is assisted by specific proteins on the capsid or lipid bilayer membrane. These proteins interact with specific receptors on the target cell surface, so the type and number of these receptors determines the sensitivity of the cell to infection by a particular virus. Once the virus is attached it must penetrate the membrane of the target cell. There are varying mechanisms by which viruses do this, the virus can inject or release the nucleocapsid/nucleic acid into the cell or another method is to be endocytosed or fused into the cell, common in enveloped viruses.

Now within the host cell the virus replicates its nucleic acid using the cell's biochemical pathways and synthesises specific viral proteins to allow the virus to replicate itself. Viral replication continues until the cell bursts or lyses to release its viral particles or alternatively the virus uses the host's own cell membrane to form its own viral envelope in a process called budding, this process eventually results in cell death of the host cell. Some viruses have the capacity for latency by incorporating their genetic information into the host genome. The genetic information may then be replicated as the host cell divides. The virus may reactivate at a later stage.

1.5.1.4 Prions

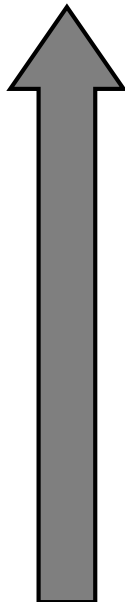
Prions are proteins which have no cellular component and have no recognisable form of associated nucleic acid. Prions are abnormal forms of normal cellular proteins. The normal and abnormal forms have the same primary structure but they differ in their secondary or tertiary structure. It is this change in conformation of the protein that prevents the abnormal form from being degraded in the body and this can lead to accumulation of the protein causing cellular and tissue pathology. Prions in particular affect neural tissues and can accumulate to form amyloid deposits on the brain. Although prions are very resistant to sterilisation they are a very rare cause of disease.

1.5.2 Microbial Susceptibility To Sterilisation

Due to the different composition and structure of microorganisms, they have different susceptibility to sterilisation processes and antibiotics. A general guide to the order of sterilisation resistance is as follows, starting with the most resistant; prions, bacterial spores, mycobacteria, small non-enveloped viruses, Gram negative bacteria, large non-enveloped viruses, Gram positive bacteria, enveloped viruses (Table 1.4)

Table 1.4 : Micro-organisms in order of sterilization resistance.
Adapted from McDonnell (2007)

Resistance	Microorganism	Examples
	Prions	Scrapie, Creutzfeldt-Jakob disease, chronic wasting disease
	Bacterial Spores	Bacillus, Geobacillus, Clostridium
	Protozoal oocysts	Cryptosporidium
	Helminth eggs	Ascaris, Enterobius
	Mycobacteria	Mycobacterium tuberculosis, M. terrae, M. chelonae
	Small, nonenveloped viruses	Poliovirus, parvoviruses, papillomaviruses
	Protozoal cysts	Giardia, Acanthamoeba
	Fungal spores	Aspergillus, Penicillium
	Gram-negative bacteria	Pseudomonas, Providencia, Escherichia
	Vegetative fungi and algae	Aspergillus, Trichophyton, Candida, Chlamydomonas
	Vegetative helminthes and protozoa	Ascaris, Cryptosporidium, Giardia
	Large, nonenveloped viruses	Adenoviruses, Rotaviruses
	Gram-positive bacteria	Staphylococcus, Streptococcus, Enterococcus
	Enveloped viruses	Human immunodeficiency virus, Hepatitis B virus, Herpes simplex virus



1.5.3 Sterility Assurance and Biological Indicator Organisms

In healthcare applications products that interact with broken/damaged skin, normally sterile tissue or are implanted surgically require a sterility assurance level (SAL) of 10^{-6} (ANSI, 2011). This is the probability that from a bio burden of 10^6 colony forming units (CFU) a sterilization technique can reduce the bio burden to less than one in a million (6 log reduction).

The bacteria which are most resistant to a particular sterilisation process are used as an indicator of sterilisation efficacy. Sporulating bacteria are generally more resistant such as *Bacillus atrophaeus* and *Bacillus pumilus* spores. A list of standard indicator organisms for a particular sterilisation process is shown in (Table 1.5).

Table 1.5 : Sterilisation processes and their indicator organism.
(Parisi & Antoine, 1974; Europe, 2004; F.D.A, 2007)

Sterilisation method	Indicator organism
Steam	<i>Geobacillus stearothermophilus</i>
Dry Heat	<i>Bacillus atrophaeus</i>
ethylene Oxide	<i>Bacillus atrophaeus</i>
Liquid Hydrogen Peroxide	<i>Bacillus atrophaeus</i>
Gaseous Hydrogen Peroxide	<i>Geobacillus stearothermophilus</i>
Liquid and Gaseous Peracetic Acid	<i>Geobacillus stearothermophilus</i>
Irradiation	<i>Bacillus pumilus</i>

1.5.4 Viral Clearance and Porcine Model Viruses

For any product using animal tissue or their derivatives there is a risk of zoonotic contaminants, it is therefore required that the sterilisation process is assessed and validated against model viruses endogenous to the particular tissue (EMA, 1996; ICH, 1997; ISO, 22442-3:2007).

For porcine tissue the following viruses (Table 1.6) are often investigated Encephalomyocarditis (EMC), porcine parvovirus (PPV), porcine reovirus, porcine pseudorabies virus (PRV) and murine leukemia retrovirus (LRV). Murine leukemia retrovirus is often used as a representation of porcine endogenous retroviruses due to the lack of robust assays to detect porcine endogenous retroviruses (Hodde & Hiles, 2002).

Table 1.6 : Common model viruses used for porcine tissue.

Virus	Host	Genome	Envelope	Size	Family
Pseudorabies (PRV)	Porcine	dsDNA	✓	120-200 nm	<i>Herpesviridae</i>
Parvovirus (PPV)	Porcine	ssDNA	x	18-24 nm	<i>Parvoviridae</i>
Endogenous retrovirus (PERV)	Porcine	ssRNA	✓	80-100 nm	<i>Retroviridae</i>
Leukemia retrovirus (LRV)	Porcine	ssRNA	✓	80-110 nm	<i>Retroviridae</i>
Encephalomyocarditis (EMC)	Porcine	ssRNA	x	20-30 nm	<i>Picornaviridae</i>
Reovirus	Porcine	dsRNA	x	60-80 nm	<i>Reoviridae</i>

It is accepted that for viral clearance a 6 log reduction must be achieved for sterility and that the log reduction effect of individual steps of a process is cumulative. Since various microorganisms are more or less susceptible to sterilisation, a common method of measurement must be applied to compare the efficacy of the process. These are commonly suspension tests and the most widely used is the determination of the D-value (also known as Time-Kill). A basic D-value test involves subjecting a known concentration of the indicator organism to the sterilisation process for a length of time, over which at intervals, samples are removed to determine the population density of microorganisms remaining. This data can then be used to calculate the reduction in the population density of the microorganisms. A D-value is the time it takes to reduce the population by 90% (1 log unit) under a given set of conditions.

1.5.5 Sterilisation Techniques for Soft Tissues

The two main branches of sterilisation are chemical and physical sterilisation. Physical sterilisation incorporates thermal treatments such as moist heat, dry heat and tyndallisation and non-thermal techniques such as filtration, osmotic pressure, ionising and non-ionising radiation. Chemical sterilisation includes various treatments or process with chemicals such as aldehydes, halogens, alcohols, phenolics, heavy metals, quaternary ammonium compounds and oxides/peroxides. The type of sterilisation technique implemented is dependent on the application, more vigorous techniques may be applicable for sterilisation of equipment but not for use on heat or pressure sensitive tissues and medical devices, therefore the choice of technique is a balance between microbial killing efficacy and compatibility with the product. A list of some of the desired properties is shown below (Table 1.7).

Table 1.7 : Desired attributes for a sterilisation process

Desired attributes for a sterilisation process
<i>Activity against a wide range if not all microorganism</i>
<i>Rapid activity</i>
<i>Efficacy in the presence of contaminating organic or inorganic materials which can inhibit activity</i>
<i>No residual cytotoxic, mutagenic or carcinogenic effect</i>
<i>Minimal alteration to mechanical or biological structures</i>

1.5.6 Chemical Sterilisation Methods

1.5.6.1 Ethylene oxide

There has been a long practice of ethylene oxide (EO) sterilisation in industry as a result of its bactericidal and virucidal ability (Phillips & Kaye, 1949; Jordy *et al.*, 1975), because of this popularity it has since made its transition into sterilisation of tissue engineered products. The majority of recent studies are on the effects on bone and tendon allografts, though there are also studies on its effects on dura mater, fascia lata, aortic wall and sub intestinal submucosa.

EO is highly reactive and combusts spontaneously in just 3 % air, it also has a high diffusivity allowing deep penetration. Its mechanism of action is direct alkylation; it replaces hydrogen atoms within a susceptible functional group with a hydroxyethyl radical. This process results in cross-linking between functional proteins, enzymes and nucleic acids, leading to damage of virus and cell structures and function, eventually causing inactivation.

Bactericidal ability at low temperatures (30 - 40 °C) has been demonstrated by inactivation of *Bacillus subtilis* (Ijiri *et al.*, 1994), *Bacillus atrophaeus* (*Bacillus subtilis* var. *niger*) strips sandwiched between freeze-dried skin, dura mater, amnion, cortical and cancellous bone (Kearney *et al.*, 1989; Kearney *et al.*, 1993).

Few studies have investigated virucidal ability but it has been demonstrated at low temperatures (~30 °C) by spiking non freeze-dried musculoskeletal tissues with HIV-1, bovine viral diarrhea, reovirus type 3, duck hepatitis B, poliomyelitis, canine parvovirus, all achieving complete inactivation (Moore *et al.*, 2004).

It is also well known that EO leaves toxic residuals in the material being sterilised, such as ethylene chlorohydrin (ECH) in the presence of chloride ions, and ethylene glycol (EG) formed by its reaction with water; both are considered mutagenic and carcinogenic (Vangsness *et al.*, 2003). The maximum dose of EO and ECH due to a permanently implanted medical device is described in ISO 10993-7:2008, a maximum dose for EG is not

set, as sufficient control of EO residues will prevent formation of EG (ISO, 10993-7:2008). Various methodologies have been introduced to reduce toxic residues. Pre sterilisation, a defatting treatment such as a chloroform and methanol wash (Arizono *et al.*, 1994) or irrigation with deionised water (Prolo *et al.*, 1980) followed by a prolonged freeze drying period. Post sterilisation, prolonged aeration (Kakiuchi *et al.*, 1996) and rinsing with saline solution (500 ml for 10 minutes) is used before implantation (Kaku *et al.*, 2002).

The extent of EO residuals on cytotoxicity has been investigated in various studies. Arizono *et al.* (1994) measured mean concentration of EO residuals by gas chromatography in human femoral head chips subjected to either defatting, freeze drying and EO sterilisation or defatting and EO sterilisation. The process including freeze drying had a mean concentration of 2.61 ± 1.3 ug/g of EO and the process without freeze drying had a mean concentration of 18.1 ± 3.8 ug/g of EO. Cytotoxicity was determined by quantification of fibroblasts grown in medium shaken with each type of bone chips. Fibroblast growth was inhibited by both groups compared to non EO sterilised bone chips. Fibroblast number reduced by 22 % when incubated with the freeze dried group compared to 43 % reduction when incubated with the non-freeze dried group. This is an indication of the impact of freeze drying on EO sterilised products. Jackson *et al.* (1990) found that 6.4 % of patients with freeze dried EO sterilised bone-patellar tendon-bone allografts developed a chronic inflammatory intraarticular reaction that subsided when the grafts were explanted. It was not determined if the inflammatory response was a result of allosensitisation or EO residuals. In response, Lomas *et al.* (2001) found that microparticles from EO sterilised mineralised and demineralised bone matrices incited an inflammatory response in-vitro and not ECH residuals. Similarly EO and Gamma sterilised chitosan membranes showed no cytotoxic effect on Vero cells in-vitro (Marreco *et al.*, 2004).

The effects on mechanical properties by EO sterilisation and the difference in the effects between hard and soft tissues is still in contention. Smith *et al.* (1996) showed that repetitive freeze thaw cycles significantly decreased the collagen modulus in tendons (possibly due to autolysis), but subsequent freeze-drying and freeze-drying then EO sterilisation did not further alter properties and that no step significantly altered the UTS. It is important to note that immediate freezing after dissection has been shown not to significantly affect the mechanical properties of tendon (Ker, 1981). Similarly Bechtold *et al.* (1994) found no significant differences in UTS between frozen, frozen/freeze-dried and frozen/freeze-dried/EO sterilised tendon however, a significant decrease in collagen modulus was found after freeze-drying tendon from a frozen state, and then a return to non-significantly different levels collagen modulus after EO sterilisation. This could suggest that the freeze drying process was damaging collagen and then the EO sterilisation process was causing cross-linking to mask the damage. Olde Damink *et al.* (1995) showed that EO reacted with the amino-groups in dermal sheep collagen, increasing the pH and decreasing the helical stability of the collagen

as shown by the resulting decrease in shrinkage temperature, however no significant differences were found in tensile strength before or after EO sterilisation.

Due to the prevalence of negative publications on EO sterilisation on tissue regarding cytotoxicity and mechanics, tissue banks have decreased EO sterilisation and leaned towards ionising radiation. However modern techniques and improved equipment can reduce residual levels and potentially reduce or eliminate cytotoxic effects. The effects of EO sterilisation on mechanical properties for different tissues must be investigated individually as different tissues have different structures and different susceptibilities to EO, in addition the necessity to use a freeze-drying process may cause differing levels of damage to a particular tissues structure. This may be of particular concern to vascular tissues where compliance is a significant factor in graft failure.

1.5.6.2 Hydrogen peroxide

Hydrogen peroxide (H_2O_2) is a powerful oxidising agent, it is a broad spectrum biocide. Liquid H_2O_2 at low concentrations is effective against bacteria or fungi but higher concentrations are required to be effective against bacterial spores. To increase efficacy it is often used in combination with peracetic acid. Gas or plasma H_2O_2 has rapid activity against bacterial spores and is less damaging to surfaces. Liquid H_2O_2 can be made into a gas by vaporisation and distributed using a vacuum, increasing penetration can be achieved by the pumping of air or nitrogen into sterilisation chambers. During the process ozone and other free radicals are produced such as $\cdot OH$ and $\cdot OOH$ these complement the biocidal activity. Advantages of H_2O_2 are that it has shorter cycle times compared to EO and breaks down in the environment to water and oxygen (McDonnell, 2007).

1.5.6.3 Peracetic Acid

Liquid PAA is a broad spectrum rapid biocide, it acts as a sterilant during quick cycle times at temperatures between 40 – 60 °C. PAA is an oxidising agent. It causes oxidation of key cellular components by breaking down peptide bonds, free radicals are also produced to complement biocidal activity. It effects bacterial cell walls and membrane permeability, denatures proteins and enzymes in particular sulfhydryl and sulphur bonds and nucleic acids making it effective against viruses. Gaseous PAA is more effective at low concentrations than its liquid form. Sterilisation cycles with PAA are usually performed in a vacuumed process with controlled humidity and temperature. Humidity ranges are around 30 – 80 % and the temperature range is around 40 – 50 °C. PAA breaks down into water and acetic acid and requires constant aeration to remove the build-up of toxic residues (McDonnell, 2007).

1.5.6.4 Electrolyzed Water

Electrolyzed water is a developing technology; it is the process of electrolysis of water by applying a voltage between an anode and cathode separated by an ion permeable barrier. This creates two solutions: a reduced alkaline solution at the cathode and an oxidised acidic

solution at the anode. The acidic solution has a high oxidising potential (~1,100 mV) which is highly biocidal. It has good activity against biofilms but is slower on bacterial spores and it has been shown to have no effect against prions. The primary mechanism of action is due to chlorine in particular hypochlorous acid, again complementary radicals increase the biocidal action. This process causes damage to cell walls, membranes, intracellular components and damages the surface of spores and viruses (McDonnell, 2007).

1.5.6.5 Ozone

Ozone is used in a low temperature process at about 30 – 35 °C, where either air or high concentrations of pure oxygen are passed through a high energy source causing ionisation. Ozone is a broad spectrum biocide, the process requires high humidity between 70 – 95 % to be effective and is distributed using a vacuum. Ozone breaks down in the environment to oxygen and water with no toxic residues (McDonnell, 2007).

1.5.7 Physical Sterilisation Methods

1.5.7.1 Radiation

Depending on the mechanism utilised, electron excitation from either the atomic nucleus or from orbitals surrounding the target atoms in a compound, causes energy in the form of particles or electromagnetic waves to be released. High energy or ionizing radiation such as Gamma irradiation, X-rays and electron beams are required for a sterilisation process as they produce greater specimen penetration and higher microbial killing efficacy. Gamma and X-ray radiation are forms of electromagnetic radiation and electron beams produce beta-particle radiation

1.5.7.2 Gamma Radiation

Gamma radiation produces high energy photons, it releases electrons from the atomic nucleus giving rise to the formation of isotopes. Isotopes decay to stable non-radioactive elements after a period of time measured as the half-life. The decay causes the release of energy in the form of alpha or beta particles or as waves of Gamma irradiation. Different isotopes release Gamma radiation at different wavelengths causing different levels of sterilisation efficacy. Gamma radiation is a rapid biocide. The process mainly affects nucleic acids, it also produces free radicals to compliment effectiveness.

It is generally accepted that a dose of 25 kGy is sufficient to sterilise a product. Standards developed by the British Standards Institute (BSI) and published by the International Standard Organisation (ISO) provide four methods for selecting a radiation sterilisation dose (RSD) for health care products (ISO, 11137-2:2012):

1. VD_{max} 25 - a dose of 25 kGy for a bioburden of less than 1000 cfu/product,
2. VD_{max} 15 - a dose of 15 kGy for a bioburden of 1.5 cfu/product,
3. Methods 1 – specific dose based on product bioburdens

4. Method 2 – specific dose based on product bioburdens

Regarding Gamma irradiation and tissue grafts there are controversial arguments for and against using higher or lower doses than those recommended by the standard. The arguments relate to the source of the tissue, the conditions in which the tissue is being sterilised and the effects of the process on the tissue structure.

For tissues sterilised in liquid mediums containing radical scavengers at room temperature it has been found that viral and bacterial inactivation is possible at RSD of 25 kGy for a wide range of viruses and bacteria including Echovirus I1, Influenza virus A, Poliovirus III Leon (Sullivan *et al.*, 1971), HIV (Spire *et al.*, 1985) and Bacillus pumillus. Controversially, other literature has indicated that higher doses are required for viral inactivation. The effectiveness of Gamma irradiation has been shown to be reduced in freeze dried or frozen conditions, due to pathogens becoming more resistant in the absence of water. Freezing at -80 °C is common practice in tissue banks, Fideler *et al.* (1994) found that when cadaveric frozen bone patellar ligament bone allografts maintained at a temperature of -70 °C using dry ice were irradiated at 30 kGy HIV was inactivated to undetectable levels and that at 25 kGy the virus was still detectable. Campbell & Li (1999) found that in dry ice conditions that 35 kGy was required to inactivate HIV and 89 kGy was required to achieve a SAL of 10⁻⁶ for the bioburden of bone grafts. In a study by Hiemstra *et al.* (1991) the inactivation of HIV in plasma was investigated at -80 °C and 15 °C. The results showed that 25 kGy was sufficient to inactivate the virus to SAL at 15 °C but at -80 °C doses in excess of 50 kGy were required (Table 1.8).

Table 1.8 : Effects of radiation dose on HIV with varying temperatures and materials

Dose	Temp	Material	Inactivation	Author
20 kGy	- 70 °C	bone-patellar ligament-bone	HIV DNA still present	Fideler <i>et al.</i> (1994)
25 kGy	- 70 °C	bone-patellar ligament-bone	HIV DNA still present	Fideler <i>et al.</i> (1994)
30 kGy	- 70 °C	bone-patellar ligament-bone	No HIV DNA present	Fideler <i>et al.</i> (1994)
40 kGy	- 70 °C	bone-patellar ligament-bone	No HIV DNA present	Fideler <i>et al.</i> (1994)
50 kGy	- 80 °C	Plasma	5-6 log10 reduction	Hiemstra <i>et al.</i> (1991)
25 kGy	15 °C	Plasma	5-6 log10 reduction	Hiemstra <i>et al.</i> (1991)
25 kGy	37 °C	T-Lymphocytes	No HIV DNA present	Spire <i>et al.</i> 1985

Collagen has been shown to be susceptible to alteration by Gamma irradiation even at levels as low as 10 kGy (Cheung *et al.* 1990). Gamma irradiation causes peptide fragmentation via chain scission resulting in shorter collagen chains and reduced number of alpha chains. It has also been reported that the damage via chain scission is masked when performing stress strain analysis due to the increased levels of collagen cross-linking. Gouk *et al.* (2008) carried out 2-30 kGy radiation on freeze dried acellular cadaver dermis (AlloDerm). After rehydration mechanical testing showed reduced ultimate tensile strength and Young's modulus, in tissues subjected to doses greater than 15 kGy. This was reversed in lower doses all doses showed large reductions in extensibility. One explanation for the flip in behaviour over a certain dose

is that in lower doses cross-linking is having a more prominent effect and that as dosage increases the effects from chain scission outweigh the cross linking effect. Sun & Leung (2008) also carried out 2-30 kGy radiation on freeze dried acellular cadaver dermis and found that after rehydration collagen denaturation temperature decreased with increasing dose determined by differential scanning calorimetry. Effects caused by Gamma radiation on tendon mechanical properties has been shown to be less deleterious than its effects on dermis. Smith *et al.* (1996) Gamma (25 kGy) irradiated frozen tendon (maintained temperature with dry ice) and found no significant differences in ultimate tensile stress, strain or Young's modulus. This highlights that different tissues containing different amounts and structures of collagen are susceptible to varying effects from radiation.

One proposed way in which to reduce the adverse effects of Gamma irradiation on collagen structure is to introduce radioprotectants. Radioprotectants and radical scavengers act as antioxidants to combine with free radicals to prevent protein fragmentation and chain scission. Some of the radioprotectants that have been used are ascorbic acid (Lee & Song, 2002) riboflavin (Seto *et al.*, 2009) and L-tyrosine. A solution of propylene glycol, dimethyl sulfoxide, mannitol and trehalose was used as a radioprotectant or semitendinosus tendons irradiated at a dose of 50kGy at -50 °C, and the irradiated tendons showed no significant structural differences from untreated controls. Inactivation of Sindbis virus, porcine parvovirus and *Clostridium sordellii* was also demonstrated (Grieb *et al.*, 2006).

The majority of the literature on tissue irradiation is concerned with sterilisation of bone and tendon allografts. The structure and density of these tissues may require higher RSD's compared to softer lighter tissues such as arteries and dermis. Also due to tissue banking storage procedures irradiation is usually performed on frozen tissue and at low temperatures, also creating another tissue specific variant that should be investigated. It is also apparent that lower RSDs could be effective if there were a lower bioburden identified for a particular tissue. This method is not as easy to implement in a research environment due the sample size required for validation with ISO standards. Taking this into consideration a RSD of 25 kGy at room temperature might be predicted to achieve sterilisation of vascular tissues. The use of irradiation causes damage to collagen structure but to different extents depending on tissue and dosage, therefore the effects of radiation should be investigated per tissue. Damaging effects may also be reduced by using certain radioprotectants or as discussed below for E-Beam, the use of an oxygen depleted atmosphere to prevent free radical formation as well as the possibility of using a fractionated dose.

1.5.7.3 E-Beam Radiation

Electron beam irradiation is an alternative to Gamma irradiation, with shorter exposure times and greater control over application, but with limitations of reduced penetration depth (Hogstrom & Almond, 2006) and a short lived but rapid increase in temperature up to 40 °C above ambient. It is thought that with reduced exposure time required with E-Beam, that there

will be reduced structural damage to collagen in tissues. However there have been reports to suggest that E-Beam causes similar damage to collagen in tendons as that caused by Gamma irradiation determined by stress-strain parameters (Seto *et al.*, 2009) or increased damage to collagen in sub intestinal submucosa compared to EO or Gamma irradiation (Grimes *et al.*, 2005). More recent work by Hoburg *et al.* (2010) showed that no significant difference was caused to the mechanical properties determined by stress-strain parameters of bone patellar tendon grafts, when subjected to 10, 25 and 34 kGy of E-Beam irradiation with the exception of a significant reduction in failure load when subjected to 34 kGy. The bone patellar tendon grafts were deep frozen at -70 °C and irradiated under these conditions with the use of dry ice. A novel technique of protecting the tissue from increased radical formation in the presence of oxygen was used, by surrounding the tissue in CO₂ gas, based on findings from the lacquer and coatings industry (Klose, 2007; Baulmann, 1985; Scherzer & Beckert, 1997). Further research by Hoburg *et al.* (2011) investigated the use of a fractionated dose of E-Beam. Evidence from radiotherapy had shown that a fractionated dosage was as effective at microbe elimination as continuous dosage (Gerbi *et al.*, 2009). The dosage was applied at 3.4 kGy 10 times for a period of 30s and the total process took around 12 minutes. The results from this showed no difference in mechanical properties compared to non-irradiated specimens of bone patellar tendon bone and less deleterious effects than a single dose of Gamma or E-Beam radiation. This suggests a fractionated dose reduced total damage caused to the collagen structures. There is little research into the differences in effects between Gamma and E-Beam irradiation on tissues. E-Beam appears to have some distinct benefits over Gamma irradiation such as shorter exposure time, tighter control over ambient temperature conditions, reduced cost and use of fractionated dose. One of the major causes for concern in the use of E-Beam is whether the rapid increase in temperature will have a substantial effect on the collagen in arterial tissues or whether it will be negligible as it is only for a short exposure time. The concept of using a fractionated dose is extremely appealing as this, in theory, should reduce the amount of radiation damage while maintaining sterilisation. Again the use of an oxygen depleted atmosphere to prevent radical formation is an appealing concept, however the extent to which the radicals contribute to sterilisation is undetermined and a higher radiation dose may be required and this has yet to be investigated in the literature. There is also an increased cost and complexity in implementing an oxygen depleted atmosphere into a sterilisation procedure.

1.5.7.4 Plasma

Plasma is a state in which atoms in a gas are excited to the extent at which the orbital electrons are released giving rise to a mixture of charged nuclei and free electrons and other reactive agents such as free radicals. These species are highly reactive and causes essential structural degradation and disruption to functions needed for bacterial and virus survival. Also, as isotopes are formed just like in radiation techniques, as they return to their natural

states photons or heat are released complementing efficacy. Plasmas which have potential for use in tissue sterilisation include oxygen, hydrogen peroxide, peracetic acid, aldehydes and halogens. Plasmas are generated via heat at very high temperatures (~3000 °C) or electromagnetic radiation from microwaves or high-energy radio frequencies at low temperatures (30-50 °C) in a gas vacuum (0.001 to 0.15 kPa). Improvements in technology allow plasmas to be produced at room temperature using a process called dielectric barrier discharge. Dielectric barrier discharge works by passing the gas through a pair of electrodes barriered by a dielectric material which prevents arcing (breakdown of plasma) (McDonnell, 2007).

1.5.7.5 Supercritical Carbon Dioxide

When a liquid is heated to slightly above the critical temperature for the transition phase between liquid and a gas the substance exhibits properties of both a liquid and a gas. CO₂ is becoming an increasingly popular choice as a super critical fluid for use as a sterilisation method. This is attributed to the ability of CO₂ to easily attain a super critical state at low pressures (7.49 MPa) and low temperatures (31.1 °C) (Figure 1.30) as well as high penetration ability, non-toxicity and its easy removal by out gassing and depressurisation (White *et al.*, 2006).

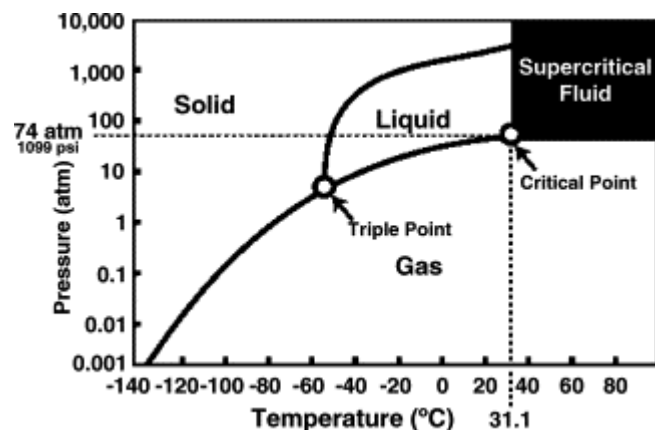


Figure 1.30 : a graph showing the temperature and pressure at which carbon dioxide change phase to a supercritical fluid.

Adopted from (White *et al.*, 2006)

Unfortunately SCCO₂ has shown poor inactivation of bacterial spores and viruses unless used in high temperature and pressure conditions which are detrimental to natural tissues (Kamihira *et al.*, 1987; Ishikawa *et al.*, 1997; Ballestra & Cuq, 1998; Spilimbergo & Bertucco, 2003). This has made it difficult to achieve SAL's of 10⁻⁶. As a result, most SCCO₂ methods are classed as high level disinfectants (Spilimbergo & Bertucco, 2003). Those methods that have shown effectiveness as a terminal sterilisation process are those which have used SCCO₂ in combination with PAA or H₂O₂ which could cause damaging effects to the ECM or leave toxic residuals.

White *et al.* (2006) found that by itself SCCO₂ was incapable of inactivating *B.subtilis* endospores or *B.stearothermophilus* endospores, but when combined with either 5 % PAA or trifluoroacetic acid (TFA) for a period of one hour at 60 °C and 10.34 MPa, that greater than 6.4 log reduction in CFU's was possible, achieving a SAL of 10⁻⁶ with a D-value of 3.25. A mixture analysis also showed that within the dynamic equilibrium of PAA to AA and H₂O₂ that it was the PAA that was responsible for the inactivation of bacterial endospores.

Zhang *et al.* (2006a) also found that SCCO₂ by itself was not effective at inactivating *B.atrophaeus* spores, but by using SCCO₂ with 30% H₂O₂ (200ppm) at a pressure of 27.5 MPa and temperature of 60 °C for a period of 4 hours it was possible to inactivate *B. pumilus* achieving a 6.28 log reduction meeting the industry requirements of a SAL of 10⁻⁶. No analysis of the effects on tissue were performed. Further work by the group (Zhang *et al.*, 2006b) used a similar process on *B.atrophaeus* spores at a lower temperature of 40 °C in attempts to provide evidence for the mechanism of inactivation. This study showed that there was damage to the permeability barrier and internal structures of the spores.

Studies on the virucidal effects of SCCO₂ using any of the aforementioned additives is rare, Qiu *et al.* (2009) used a SCCO₂ method with added PAA (final concentration ~55 ppm) to sterilise acellular porcine dermal matrix for no longer than one and a half hours at temperature and pressure of 35 – 41°C and 9.41-10.03 MPa respectively. The study investigated inactivation of the viruses; Encephalomyocarditis virus (EMC), porcine parvovirus (PPV), porcine pseudorabies virus (PRV), and murine leukemia retrovirus (LRV) as well as *B. atrophaeus* spores. For the spores, a 6 fold log reduction was achieved after 52 minutes reaching sufficient SAL's with a calculated D-Value of 6.3 minutes, EMC was completely inactivated with a log reduction of 6.44, showing that the process was capable of inactivating viruses as well as bacterial spores. The effects of the process on the mechanical properties of the matrix were investigated using a SCCO₂ run time of 1.5 hours by susceptibility to enzymatic digestion and tensile testing. The enzymatic digestion showed that the treated samples were less susceptible to digestion but were not statistically significant from controls. For the tensile tests, the maximum load and stress of the treated matrix was increased compared to the control and the elasticity decreased, but only the elasticity was significantly different. Together, the data showed that there was some change in the matrix architecture.

SCCO₂ has shown potential for use as a terminal sterilisation process. It has been shown that with the addition of additives SCCO₂ can sterilise to industry standards at acceptable temperatures and pressures. The effect of different additives on the possible damage to collagen and the basement membrane would need to be assessed for the process to be used as an industrial terminal sterilisation method for vascular scaffolds.

1.6 Summary

Cardiovascular disease is the highest cause of morbidity worldwide, encompassing blood vessel disorders such as coronary artery and peripheral arterial disease. Due to lack of autograft tissue and low patency rates of synthetic alternatives there is a huge clinical need for an off the shelf small diameter (less than 6 mm) vascular graft. Advances in synthetic materials are promising but are yet to establish a graft with desired mechanical and biological properties. A large focus has been directed at the tissue engineering approach, but similarly there is yet no commercial product available that has comparable clinical outcome to autograft tissue. Previously, a process for the production of acellular porcine carotid arteries has been developed which shows excellent potential for clinical translation as vascular bypass grafts.

Medical products need to be sterilised to a sterility assurance level of 10^{-6} before they can be used clinically. Terminal sterilisation whereby the product is sterilised in its final packaging is desirable for an implantable product. The primary source of literature related to the sterilisation of grafts comes from tissue banks. The sterilisation processes currently used are Gamma and E-Beam irradiation and ethylene oxide treatment. There is much contention on the effects of each of these processes on the mechanical and biological effects on proteinaceous materials and grafts. It is therefore necessary to assess the effects of sterilisation processes on the mechanical and biological properties of the specific type of graft under research and development.

1.7 General Aims and objectives

It was the aim of this thesis to develop a range of robust test methods that enable evaluation of the effects of sterilisation methods on the mechanical and biological properties of acellular vascular grafts. Then using these test methods, determine the compatibility of terminal sterilisation processes, Gamma and E-Beam irradiation and Ethylene oxide treatment with acellular vascular grafts.

1.8 Experimental Approach

1.8.1 Porcine Scaffold

In the search for a small diameter vascular graft porcine vessels are being investigated. Pigs have similar physiological and genomic features to humans and have similar flow rates in the vascular system (Rothschild *et al.*, 2011) as well as a high availability through the meat industry. The left and right porcine carotid artery (Figure 1.31) have an internal diameter of ~ 6 mm at the proximal end narrowing to ~ 3 mm at the distal end with a length of ~ 150 mm depending on age and weight. This makes the porcine carotid arteries a suitable candidate

for a small diameter vascular graft model with future potential as a coronary artery bypass graft. The free graft length in CABG range 8-24 cm with an average 17.7 cm (Mills & Everson, 1989). Therefore in this study acellular vascular grafts will be derived from porcine carotid arteries.

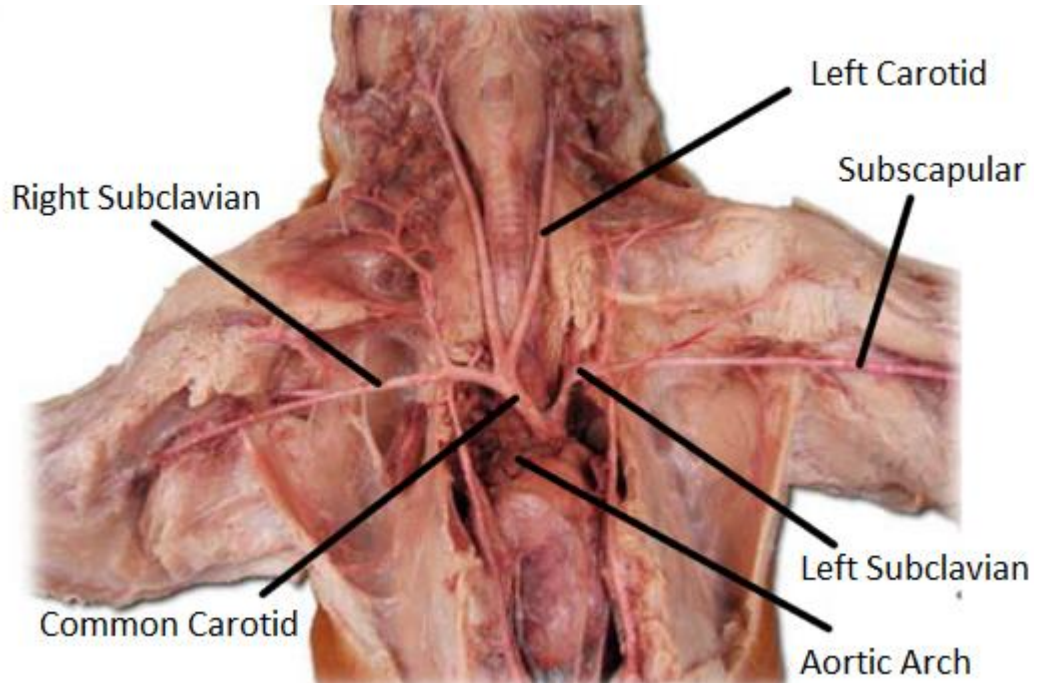


Figure 1.31 : Porcine cardiovascular system identifying vasculature.

1.8.2 Sterilisation

In order to translate the acellular vascular grafts into a clinical product they must first be sterilised in accordance with the medical device directive. As a medical device, to be deemed sterile a SAL of 10^{-6} must be achieved. It is also beneficial to have the product terminally sterilised i.e. sterilised whilst in its final packaging to prevent contamination post sterilisation.

The three highly profiled and industry available sterilisation methods currently being used are Gamma and E-Beam irradiation and ethylene oxide treatment. The effects of each sterilisation method on the biomechanical and biological properties of acellular porcine grafts must be investigated to determine a compatible method

1.8.3 Assessment Methods

Once mechanical and biological quality checks have been passed acellular arteries will be sterilised using Gamma or E-Beam irradiation or ethylene oxide. After which a range of methods will be used to assess and build up an overall picture of the effect of each sterilisation process. These methods have been categorised into three categories:

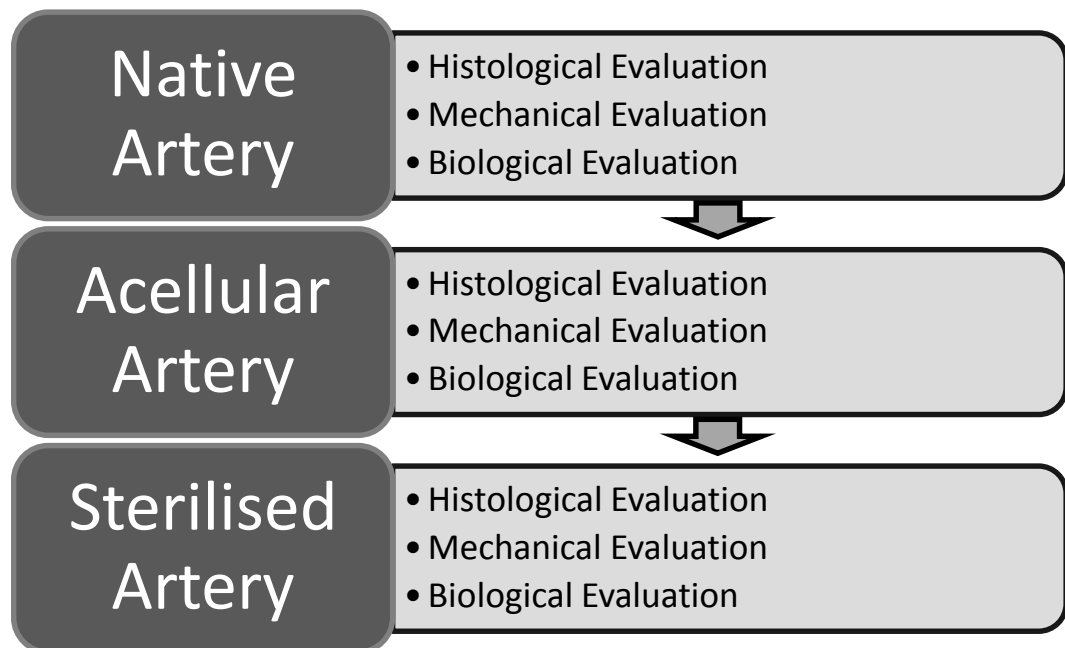
- Histological evaluation
- Mechanical evaluation
- Biological evaluation

Histological evaluation involves haematoxylin and eosin staining, immunohistochemical labelling of collagen IV and multiphoton imaging of acellular sterilised porcine carotid arteries.

Mechanical evaluation involves determination of mechanical properties via uniaxial tensile testing at low strain rate to failure and burst pressure and compliance testing of acellular sterilised porcine carotid arteries.

Biological evaluation involves determination of biocompatibility, denatured collagen content and denaturation temperature (differential scanning calorimetry) of acellular sterilised porcine carotid arteries.

Although all assessments will be carried out to enhance the understanding of the effects caused by the particular sterilisation process, a success failure criteria can be applied for some methods.



Chapter 2 : General Materials and Methods

2.1 Equipment

A list of equipment used throughout this project and the manufacturer is presented in Appendix A; Table A-1.

2.2 Chemicals and Reagents

A list of reagents used throughout this project and their supplier is presented in Appendix A; Table A-2.

2.3 Consumables

A list of consumables used throughout this project and their supplier is presented in Appendix A; Table A-3.

2.4 Cell Lines

Mammalian cell lines used in biocompatibility assays are listed in Table 2.1.

Table 2.1 : Cell lines, *Cell lines with type species and NCTC catalogue number.*

Cell lines	Type	Species	Cat No.
BHK	Fibroblast	Hamster	93120840
L929	Fibroblast	Murine	85103115

2.5 Antibodies

Monoclonal antibody CIV22 (DAKO, M0785) with specificity to collagen IV epitope was used in immunohistochemical labelling. The isotype control protein used to detect background staining of the Fc receptor was Mouse, IgG1 (Dako, X0931) and was used in equal concentration to the primary antibody (1.6 mg.L⁻¹). An antigen retrieval step of incubation with citrate buffer was used to enable antibody binding to the epitope.

2.6 Methods

2.6.1 Glassware Disinfection

Glassware was disinfected by immersion in a 1 % (v/v) solution of Neutracon® followed by rinsing in distilled water.

2.6.2 Equipment and Reagent Sterilisation

All equipment or solutions prior to contact with tissue were sterilised by either dry heat, moist heat (autoclave) or filter sterilisation. Dry heat sterilisation was carried out in a hot air oven at a temperature of 180 °C for 4 hours. Autoclave sterilisation was carried out for 20 minutes at 121 °C and 15 psi (0.1034MPa). Filtered solutions were passed through a 0.2 µm pore size filter in a class II safety cabinet.

2.6.3 Measurement of Ph.

A Jenway 3020 pH meter was used to determine the pH of solutions. Solutions of pH 4, 7 and 10 made from buffer tablets (Merck Chemicals Ltd.) dissolved in de-ionised water were used to calibrate the pH meter. The pH of solutions was altered using varying molarities of hydrochloric acid and sodium hydroxide added drop-wise whilst stirring. Temperature compensation was employed.

2.6.4 Aseptic Technique and Cabinets

All work requiring aseptic technique was carried out in Class II safety cabinets

2.6.5 Microbiological Plating Technique

Plating techniques for detection of single colonies of microorganisms in sterility checks used the pattern shown in Figure 2.1 . A microbiological loop was heated to red hot in a blue Bunsen flame and allowed to cool, the loop was then submersed in the suspension in question and streaked.

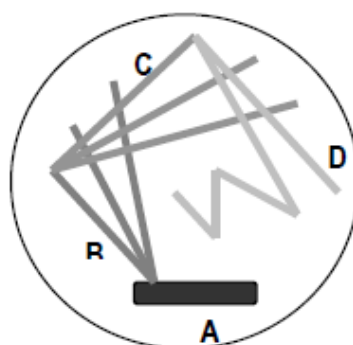


Figure 2.1 Streaking pattern, streaking pattern used during sterility checks of suspensions.

Streaks began from the initial inoculation point (A) which was streaked using a microbiological loop in multiple lines circumferentially; the final line was streaked to the centre of the plate.

2.6.6 Histological Analysis

2.6.6.1 Tissue fixation and embedding

Reagents:

Zinc fixative solution

Trizma base (12.1 g) was dissolved into 1000 ml of distilled water using a magnetic stirrer and stirrer bar. Calcium acetate (0.5 g) was added and dissolved. The pH was adjusted to 7.0-7.4 by adding 6 M hydrochloric acid or 6 M sodium hydroxide drop wise. Zinc acetate (5.0 g) was dissolved into the solution followed by zinc chloride (5.0 g).

Method:

Approximately 3.0 mm length of tissue was dissected and placed into individual plastic cassettes and labelled using a pencil. Cassettes were submerged in zinc fixative for 16-24 hours at room temperature. The cassettes were placed into a metal holding basket and placed in the tissue processor and run on program three (Table 2.2).

Table 2.2 : Tissue processing steps.

Station Number	Contents	Time
1	N/A	0 Hours
2	70% Alcohol	1 Hour
3	90% Alcohol	1 Hour
4	100% Alcohol	1 Hour
5	100% Alcohol	1 Hour
6	100% Alcohol	1 Hour
7	Xylene	1 Hour
8	Xylene	1 Hour
9	Xylene	1 Hour
10	Molten Wax	1 Hour
11	Molten Wax	1 Hour

The program was completed after eleven hours. Upon completion the histology cassettes were removed and transferred to fresh molten wax. The individual specimens were orientated with the circumference face down into metal moulds filled with molten wax. The cassette base was placed on top of the mould and additional wax was used to fill the cassette. The cassettes were then left to cool and harden at room temperature. Once hard, the excess wax was removed and the block stored at room temperature.

2.6.6.2 Sectioning of paraffin wax embedded tissue samples

Method:

The hotplate and water bath were turned on and set to 55-60 °C and 45-50 °C, respectively. A paraffin wax block to section was selected; the angle of the blade of the microtome was set to 2.5 ° and the section thickness to 5 µm. The handle of the microtome was turned in a clockwise direction smoothly cutting the wax block into thin sections. The sections were removed using two sets of fine tip forceps and floated on the surface of the water bath until any wrinkles in the wax disappeared. The floating sections were then removed onto Superfrost or Superfrost plus slides. They were removed in a vertical motion to allow as much water as possible to run off the slide. The slides were labelled and recorded accordingly before being placed onto the hotplate. Samples were left on the hot plate for a minimum of 60 minutes and stored at room temperature until stained.

2.6.6.3 Haematoxylin and eosin staining

Method:

Slides plus sections to be stained were placed into a slide holder and then immersed in a series of reagents for different periods of time (Table 2.3). Sections were dewaxed, rehydrated, stained then dehydrated.

Table 2.3 : Haematoxylin and Eosin staining procedure.

Step	Solution	Time
1	Histo-clear III	10 Minutes
2	Histo-clear III	10 Minutes
3	100% Ethanol	3 Minutes
4	100% Ethanol	2 Minutes
5	100% Ethanol	2 Minutes
6	70% Ethanol	2 Minutes
7	Running tap water	3 Minutes
8	Haematoxylin	1 Minute
9	Running tap water	Until water ran clear
10	Eosin	1 Minute
11	70% Ethanol	5 Seconds
12	100% Ethanol	1 Minute
13	100% Ethanol	2 Minutes
14	100% Ethanol	3 Minutes
15	Histo-clear III	10 Minutes
16	Histo-clear III	10 Minutes

Sections were then mounted using DPX mountant and left to for a minimum of four hours inside a fume hood. Sections were then viewed using an upright microscope under normal Koehler illumination and images captured with a digital camera and Image Pro Plus V5.1.

2.6.6.4 DAPI staining

Reagents:

Dulbecco's phosphate buffered saline (DPBS)

Five Oxoid Dulbecco's PBS tablets were dissolved in 500 ml distilled water. The pH was adjusted to 7.2 – 7.4 using 6 M hydrochloric acid or 6 M sodium hydroxide drop wise whilst using a magnetic stirrer. The solution was sterilised by autoclaving.

Dye buffer (10 mM Tris, 1 mM Na₂EDTA, 1 mM NaCl)

Trizma base (1.211 g), disodium ethylenediaminetetraacetic acid (0.3724 g) and sodium chloride (0.058 g) were dissolved in 1000 ml of distilled water. The solution was sterilised by autoclaving. The pH was adjusted immediately before use to 7.4 using 6 M hydrochloric acid or 6 M sodium hydroxide drop wise whilst using a magnetic stirrer.

DAPI dye solution (1 mg.ml⁻¹)

DAPI (10 mg) was added to 10 ml of nuclease free water and stored at – 20 °C in a foil wrapped container.

Working dye solution (0.1 µg.ml⁻¹)

DAPI dye solution (20 µl) was added to 200 ml of dye buffer in a dark bottle and mixed by inversion.

Method:

Slides plus sections to be stained were placed into a slide holder and then immersed a series of reagents for different periods of time Table 2.4. Sections were dewaxed, rehydrated then stained.

Table 2.4 : DAPI staining procedure.

Step	Solution	Time
1	Histo-clear III	10 Minutes
2	Histo-clear III	10 Minutes
3	100% Ethanol	3 Minutes
4	100% Ethanol	2 Minutes
5	100% Ethanol	2 Minutes
6	70% Ethanol	2 Minutes
7	Running tap water	3 Minutes
8	DAPI working solution (DARK)	10 Minutes

Step	Solution	Time
9	DPBS (DARK)	10 Minutes
10	DPBS (DARK)	10 Minutes
11	DPBS (DARK)	10 Minutes

Sections were then mounted using Dako fluorescence mounting medium and left to set in the dark for a minimum of four hours. Sections were then viewed using an upright microscope using fluorescent microscopy with a DAPI filter and images captured with a digital camera and Image Pro Plus V5.1.

2.6.6.5 Immunohistochemical labelling of paraffin embedded tissue sections using monoclonal antibodies specific for collagen IV

Reagents:

Sodium hydroxide solution (6 M)

Sodium hydroxide (120 g) was dissolved into 500 ml of distilled water using a magnetic stirrer and stirrer bar.

Dulbecco's phosphate buffered saline (DPBS)

See section 2.6.6.4

Hydrogen peroxide solution (3 %; v/v)

Hydrogen peroxide (20 ml 30 %; v/v) was added to 180 ml of DPBS and mixed by inverting (used immediately, excess discarded)

Citrate Buffer (10 %; w/v)

Anhydrous citrate buffer (1.92 g) was dissolved into 1 L of distilled water.

Sodium chloride solution (3 M)

Sodium chloride (175.32 g) was dissolved into 1000 ml of distilled water using a magnetic stirrer and was sterilised by autoclaving.

Tris solution (2M)

Trizma base (242.26 g) was dissolved into 500 ml of distilled water using a magnetic stirrer; the pH was adjusted to 7.6 using 6M hydrochloric acid or 6 M sodium hydroxide drop wise whilst using a magnetic stirrer. The volume was then made up to 1000 ml using distilled water. The solution was sterilised by autoclaving.

Tris buffered saline (TBS)

Tris solution (25 ml, 2 M) was mixed with 50 ml of 3 M sodium chloride solution using a magnetic stirrer, and the volume made up to 1000 ml using distilled water. The pH was adjusted to 7.6 using 6 M hydrochloric acid or 6 M sodium hydroxide drop wise whilst using a magnetic stirrer. The solution was sterilised by autoclaving.

TBS containing 0.05 % (w/v) Tween 20 (TBS-T)

Tween 20 (500 µl) and 1000 ml of TBS were mixed using a magnetic stirrer.

BSA solution (5 %; w/v BSA)

Bovine serum albumin (0.25 g) was dissolved into 50 ml of DPBS using a magnetic stirrer and stirrer bar, the solution was then passed through a 0.2 µm filter into a sterile collection container in a class II cabinet. Volumes (5 ml) were then aliquoted into sterile universals and frozen at -20 °C

Antibody diluent (TBS, 0.1 % (w/v) BSA, 0.1 % (w/v) sodium azide)

Sodium azide (6 ml), 300 µl of 5 % (w/v) BSA solution and 40 ml of tris buffered saline were mixed together using a magnetic stirrer. The pH was adjusted to 7.6 using 6 M hydrochloric acid or 6 M sodium hydroxide whilst stirring with a magnetic stirrer, the volume was made up to 60 ml with TBS.

Antibody solution

A ratio of 1:50 of 80 mg.L⁻¹ collagen IV mouse monoclonal antibody was added to antibody diluent, the volume made up was approximately 20 µl per section.

Antibody isotype solution

A ratio of 1:63 of 100 mg.L⁻¹ mouse IgG1 Kappa was added to antibody diluent, the volume made up is approximately 20 µl per section.

Method:

Firstly the slides plus section to be labelled were processed by dewaxing and rehydrating as shown in Table 2.5.

Table 2.5 : Dewaxing and rehydration of sections.

Step	Solution	Time
1	Histo-clear III	10 Minutes
2	Histo-clear III	10 Minutes
3	100% Ethanol	3 Minutes
4	100% Ethanol	2 Minutes
5	100% Ethanol	2 Minutes
6	70% Ethanol	2 Minutes
7	Running tap water	3 Minutes

Tissue sections then underwent antigen retrieval using 10 % citrate buffer (w/v) for 10 minutes followed by blocking using 3 % (v/v) H₂O₂ for 10 minutes at room temperature and subsequent washing under running tap water. Slides were then placed into four well plastic slide holders and a hydrophobic marker pen was used to circle the sections to reduce the

volume of solution used. Subsequent steps were carried out on a shaker at 20 rpm until dehydration. Sections were rinsed in TBS and incubated with dual endogenous enzyme block (V Block; Ultravision kit) for ten minutes. The monoclonal antibody for collagen IV and the isotype control IgG1 Kappa were diluted with antibody diluent (1:50; 1:63 respectively) to suitable and equal concentrations and incubated for 1 hour, antibody diluent served as a second control. Sections were then washed with TBS-T for ten minutes (x2) followed by TBS for ten minutes (x2). Sections were then incubated for thirty minutes in the dark with labelled polymer-HRP (HRP Polymer; Ultravision kit). The sections were again washed in TBS-T (x2) followed by TBS (x2) for ten minutes each. Sections were then incubated with 3,3 – diaminobenzidine (DAB) plus chromogen (Ultravision Kit) for ten minutes at room temperature. Sections were then washed under running tap water before being counterstained with haematoxylin for 15 seconds and washed again under running tap water until water ran clear. Dehydration of the tissues was carried out as shown in Table 2.6. The sections were then mounted using DPX mountant and air dried for four hours. The sections were viewed using an upright microscope under normal Koehler illumination and images were captured using a digital camera and Image Pro Plus V5.1.

Table 2.6 : Dehydration of sections.

Step	Solution	Time
1	70% Ethanol	5 seconds
2	100% Ethanol	1 Minute
3	100% Ethanol	2 Minutes
4	100% Ethanol	3 Minutes
5	Histo-clear III	10 Minutes
6	Histo-clear III	10 Minutes

2.6.7 Isolation and Quantification of DNA

Method:

DNA was extracted using a commercially available DNeasy blood and tissue kit from QIAgen. Native artery (25-50 mg), acellular (100-250 mg) or sterilised acellular artery (100-250 mg) was macerated and placed in a sterile 2 ml microcentrifuge tube. Buffer ATL (180 µl, native; 360 µl, acellular) and proteinase K (20 µl, native; 40 µl, acellular) from the QIAgen kit were then added, the solution was vortexed and incubated at 56 °C for a minimum of three hours or until the tissue was completely digested. Following digestion premixed Buffer AL (200 µl, native; 400 µl, acellular) from the QIAgen kit and ethanol (100 %; v/v; 200 µl, native; 400 µl, acellular) were added and vortexed. The samples were then centrifuged at 6000 x g for one minute in DNeasy mini spin columns in 600 µl volumes until all the sample had filtered through the column. The flow through was discarded and a new collection tube replaced; 500 µl of Buffer AW1 was filtered through the spin column at 6000 x g for one minute. The flow through was discarded and a new collection tube replaced; 500 µl of Buffer AW2 was filtered

through the spin column at 20 000 x g for three minutes. The flow through was discarded and a new collection tube replaced. Buffer AE (200 µl) was filtered through the column twice to elute the DNA. The concentration of DNA was determined by loading 2 µl samples onto a nanodrop spectrophotometer and determining absorbance at 260 nm (Buffer AE was used as a blank). The concentration of each sample was normalised for volume and initial tissue mass to determine DNA concentration in ng.mg⁻¹.

2.6.8 Cell Culture and Maintenance

2.6.8.1 Culture medium

Reagents:

Tryptone phosphate broth stock solution (TPB; 29.5 g/l)

Tryptone phosphate broth (7.38 g) was dissolved in 250 ml of distilled water and filtered through a 0.2 µm filter unit. Aliquots of 20 ml were stored at – 20 °C for up to six months.

DMEM (10 % FBS, 2 mM L-glutamine, pen/strep 100 U / 100 µg.ml⁻¹)

Fetal bovine serum (FBS, 10 ml; 10 % (v/v)), L-glutamine (1 ml; 1 % (v/v)) , penicillin (2 ml; 2 % (v/v)) and streptomycin (2 ml; 2 % (v/v)) were added to Dulbecco's minimal essential medium (DMEM) (87 ml) and mixed by inversion.

GMEM (5 % FBS, 10 % TPB, pen/strep 100 U / 100 µg.ml⁻¹, 2 mM L-glutamine)

Fetal bovine serum (FBS, 5 ml; 5 % (v/v)), tryptone phosphate broth stock solution (10 ml; 10% (v/v)), L-glutamine (1 ml, 1% (v/v)), Penicillin (2 ml, 1% (v/v)) and streptomycin (2 ml; 2% (v/v)) were added to Glasgow's minimal essential medium (GMEM) (82 ml) and mixed by inversion.

Method:

Cell lines (Section 2.4) were cultured in either DMEM or GMEM with specific additives for each cell line. L929 cell lines were cultured in supplemented DMEM and BHK cell lines were cultured in supplemented GMEM. All medium and reagents were allowed to equilibrate to 37 °C and all medium changes were performed aseptically.

2.6.8.2 Cell resurrection

Relevant culture medium was warmed to 37 °C in water bath. Cells stored in liquid nitrogen and frozen in cryopreservation medium (Section 2.6.8.5) were located from the cell log sheet and removed from Dewar's and thawed in 37 °C water bath. When defrosted 9 ml of culture medium was added to a universal followed by the defrosted cell stock (1 ml). The suspension was then spun down at 150 g for 10 minutes and the supernatant discarded. The cell pellet was resuspended in 1 ml of fresh culture medium then diluted as necessary. The diluted cell suspension was then transferred to a T 75 culture flask and incubated at 37 °C in 5 % (v/v)

CO₂ in air, the medium was subsequently changed approximately every 48 hours until confluent.

2.6.8.3 Cell passaging

When 80 % confluence was observed (microscopically) the cells were passaged. The medium was aspirated from the flask and the cell layer was washed in PBS without calcium and magnesium. The cells were then incubated with 3 ml of trypsin/EDTA solution for 5 minutes at 37 °C in 5 % (v/v) CO₂ in air to detach the cells from the flask. The cells were then suspended in 10 ml of medium to neutralise the trypsin and centrifuged at 150 g for 10 minutes. The supernatant was removed and the cell pellet resuspended in 1 ml of fresh medium at which point a viable cell count (Section 2.6.8.4) was performed if necessary and the cell suspension separated into multiple flasks as needed, or cryopreserved (Section 2.6.8.5).

2.6.8.4 Determination of cell number and cell viability using Trypan blue

Trypan blue dye stains dead cells determined by loss of membrane function and live cells remain clear as can be seen microscopically. The cell viability was determined by mixing a volume (100 µl) of cell suspension and Trypan blue dye in a bijou at a ratio of 1:1 (dilution factor of 2). A small volume (~14 µl) was then pipetted between a glass slide and haemocytometer and viewed under an inverted light microscope. The four 1 mm² corner squares of the grid were counted and the cell count per ml was calculated as follows, where df = dilution factor:

$$\text{Equation 2-1} \quad \text{Num of cells. ml}^{-1} = \frac{\text{viable cell count}}{\text{number of squares counted (4)}} \times 10^4 \times df$$

2.6.8.5 Cryopreservation of cell lines

Reagents:

Cryopreservation medium; DMEM (20 % FBS, 10 % DMSO)

Fetal bovine serum (2 ml; 10 % (v/v)), DMSO (1ml; 10 % (v/v)) were added to Dulbecco's minimal essential medium (DMEM) (7.7 ml) and mixed by inversion.

Method:

The cell density was adjusted to 10⁶.ml⁻¹ in cryopreservation medium. The suspension was immediately aliquoted in 1 ml volumes into cryovials and placed into an isopropanol containing cryo freeze pot before being frozen at – 80 °C for 24 hours. Once frozen cryovials were transferred into liquid nitrogen for long-term storage. DMSO was used to prevent ice crystal formation during the freezing process; and cell suspensions were frozen immediately to reduce its toxic effect.

2.6.9 Biocompatibility Assays of Arteries

2.6.9.1 Sterility testing of samples

A 5 mm² sample was removed from acellular and acellular/sterilised arteries and incubated in nutrient broth at 37 °C for 48 hours. Sterility was determined by observation of a lack of turbidity compared to positive and negative controls. The positive control was nutrient broth exposed to human commensals and the negative control was sterile nutrient broth exposed to the HEPA filtered air.

2.6.9.2 Contact cytotoxicity

Reagents:

Tryptone phosphate broth stock solution (29.5 g/l)

See section 2.6.8.1

DMEM (10 % FBS, 2 mM L-glutamine, pen/strep 100 U / 100 µg.ml⁻¹)

See section 2.6.8.1

GMEM (5 % FBS, 10 % TPB, pen/strep 100 U / 100 µg.ml⁻¹, 2 mM L-glutamine)

See section 2.6.8.1

Method:

Samples of arteries ~ 5 mm² were attached to six-well tissue culture plates using steri strips, cyanoacrylate and steri strips were used as positive and negative controls respectively. The wells were washed three times in PBS without calcium and magnesium and then seeded with 500,000 cells of BHK or L929 cells in 2 ml of culture medium and incubated at 37 °C in 5 % (v/v) CO₂ in air until confluent (~ 48 hours). Phase contrast images were then taken of the cell sample interface. Medium was aspirated and cells were washed with PBS containing calcium and magnesium; cells were then fixed with neutral buffered formalin (NBF) for 10 min and stained with Giemsa solution (2 ml per well) for 5 min after which bright field images were taken. Images were captured through an upright microscope BX40 Olympus UK using a Digital colour camera XC50 Olympus UK. Images were used to view any changes in cell morphology and confluency.

2.6.10 Denatured Collagen Assay

Reagents:

Sodium hydroxide solution (6 M)

See section 2.6.6.5

Digest buffer

Trizma base (1.21 g) and calcium chloride (0.15 g) were added to 100 ml of distilled water using a magnetic stirrer and stirrer bar. The pH was adjusted to 7.8 using 6 M hydrochloric acid or 6 M sodium hydroxide whilst stirring with a magnetic stirrer. The solution was sterilised by autoclaving.

α -Chymotrypsin solution

α -Chymotrypsin was dissolved at 5 mg.ml⁻¹ into digest buffer using a magnetic stirrer and stirrer bar and used immediately

Assay buffer

Citric acid (13.3 g), glacial acetic acid (3.2 ml), sodium acetate (32 g) and sodium hydroxide (9.1 g) were dissolved into 220 ml of distilled water using a magnetic stirrer and stirrer bar. Propan-1-ol (80 ml) was added and the solution made up to 300 ml using distilled water. The pH was adjusted to 6-6.5 using 6 M hydrochloric acid or 6 M sodium hydroxide whilst stirring with a magnetic stirrer. The final volume was adjusted to 400 ml using distilled water.

Chloramine T

Chloramine T (1.41 g) was dissolved into 220 ml of distilled water. The solution was used immediately and any excess was disposed of.

Ehrlich's reagent

P-dimethylaminobenzaldehydeT (7.5 g) was dissolved into 30 ml of propan-1-ol using a magnetic stirrer and stirrer bar. Perchloric acid 60 % (v/v) (13.4 ml) and distilled water were added and stirred using a magnetic stirrer until fully dissolved. Solution was used within one hour and excess disposed of.

Primary assay standard (1 mg.ml⁻¹)

Trans-4-hydroxy-L-proline (25 mg) was added to assay buffer (25 ml) and mixed by inversion.

Secondary assay standard (100 mg.ml⁻¹)

Primary assay standard (1 ml) was added to assay buffer (9 ml) and mixed by inversion.

Method:

Lyophilisation and digestion of tissue

Acellular and acellular/sterilised arteries were macerated (50 mg) and placed into a sterile bijou. The sample was lyophilised to a constant weight using a freeze dryer. Each sample was then incubated with 5 ml α -chymotrypsin solution (5 mg.ml⁻¹) at 30 °C for 24 hours. Samples

were then centrifuged at 600 g for ten minutes; the supernatant (4 ml) was then transferred to a sterile glass universal along with 4 ml of 6 M hydrochloric acid and sealed. Each tube was autoclaved at two bars for four hours and then allowed to cool to room temperature. Samples were neutralised to pH 7.0 by adding 6 M sodium hydroxide drop wise with stirring.

Assay procedure

A range of standards (50 µl) (Table 2.7) and test solutions (50 µl) were added to a clear flat-bottomed 96 well plate. Chloramine T (100 µl) solution was added to each well and then shaken at 60 rpm for five minutes using a plate shaker at room temperature. Ehrlich's reagent was then added to each well and sealed using a topseal cover then incubated for 45 minutes at 60 °C. Optical density was measured using a microplate spectrophotometer at 570 nm. Blank values were subtracted from all standards and unknown samples, then standard curves plotted and used to interpolate the concentration of denatured collagen in the artery.

Table 2.7 : Denatured collagen assay standards.

Standard Concentration (µg.ml⁻¹)	Volume of secondary standard (µl)	Volume of buffer (µl)
30	750	1750
25	625	1875
20	500	2000
15	375	2125
10	250	2500
8	200	2300
6	150	2350
4	100	2400
2	50	2450
0	0	2500

2.7 Statistical Analysis

A list of basic statistical terms used throughout the project can be found in Appendix B. Confidence limits at 95 % ($\alpha = 0.05$) were calculated with a minimum of n=3 using the equation shown:

$$\text{Equation 2-2} \quad 95 \% CL = \text{Standard error} \times t - \text{value}$$

Comparison between groups were analysed using one way analysis of variance (ANOVA) and differences between group means were calculated using the minimum significant difference at $\alpha = 0.05$ (Sokal & Rohlf, 1981). All statistical analysis and manipulation of data was carried out using either Microsoft excel 2010 or Origin Pro 8.6.

Chapter 3 Production of Porcine Carotid Acellular Arteries

3.1 Introduction

As discussed in Chapter 1 there is a clinical need for “an off the shelf” small diameter vascular graft. The approach that is the subject of this study is through the decellularisation of xenogeneic blood vessels that may be repopulated with autologous cells in vitro or in vivo with the potential to regenerate the extracellular matrix over time.

3.1.1 Leeds Decellularisation Method

There are many approaches taken to achieve successful decellularisation of tissues, incorporating a range of physical, chemical and enzymatic processes. At the University of Leeds, in the Institute of Medical & Biological Engineering, a patented (Fisher *et al.*, 2001; Ingham *et al.*, 2010) decellularisation process has been developed.

The proprietary decellularisation process was first established for use in porcine heart valves with the hypothesis that an acellular scaffold (seeded or non-seeded) would regenerate in vivo and grow with the recipient, creating a valve that would be beneficial to younger patients. Several decellularisation protocols were investigated with a variety of reagents and then assessed histologically. The valves were aseptically dissected and washed in disinfection solution then stored in phosphate buffered saline (PBS) containing protease inhibitors, ethylenediaminetetraacetic acid (EDTA) and aprotinin. EDTA is a chelating agent of metal ions; it has a high affinity for calcium ions, EDTA sequesters the calcium ions used by integrins involved in cell adhesion to the ECM. EDTA also has a high affinity for zinc ions making it a potent metalloproteinase inhibitor. The EDTA sequesters magnesium, calcium and zinc ions reducing cell attachment to the extracellular matrix and preventing auto digestion from metalloproteinases. Aprotinin is a broad spectrum inhibitor of serine proteinases; the use of aprotinin prevents released cellular enzymes auto digesting the scaffold.

The first step in the process is to lyse the cells using a hypotonic buffer, again in the presence of protease inhibitors. The hypotonic buffer causes the cells to swell and burst through osmotic pressure. Secondly a series of detergents were assessed for their ability to remove the cells and cellular debris and the minimum concentration at which the detergents would achieve this. Thirdly scaffolds were washed repeatedly in isotonic buffer with proteinase inhibitors to remove residual reagents and cellular debris. Of the reagents tested, two ionic detergents were shown to decellularise porcine aortic valve leaflets, SDS and deoxycholate. SDS and deoxycholate are ionic detergents that cause disruption to the phospholipid bi-layer of cell membranes and form micelles around lipids. Decellularisation was achieved at

concentrations of 0.03 % (w/v) SDS and 0.5 % (w/v) deoxycholate for valve leaflets, but to decellularise aortic roots as well as leaflets the SDS concentration was increased to 0.1 % (w/v). Histological analysis showed decellularisation, intact histo-architecture and the collagen, elastin and GAG content appeared preserved. Contrary to other published work using SDS for the decellularisation of tissues, deleterious effects were not observed. This was possibly due to the inhibition of proteinases since increased concentrations of 1 % (w/v) SDS caused no damage to the ECM (Booth *et al.*, 2002). Mechanical characterisation of the acellular tissue showed no significant effects on the strength of the valve leaflets but a small increase in the extensibility, shrinkage, thickness and hydration was observed (Korossis *et al.*, 2002). A further enhancement to the decellularisation process was the addition of a nuclease digestion step. DNAase and RNAase were added to the process to minimise residual DNA and RNA (Wilcox *et al.*, 2005). The biocompatibility of decellularised porcine valve tissue was then demonstrated (Wilcox *et al.*, 2005; (Knight *et al.*, 2005).

The process was then applied to a range of tissues including human amniotic membrane (Wilshaw *et al.*, 2006), pericardium (Mirsadraee *et al.*, 2006) and bladder (Bolland *et al.*, 2007).

In later studies, the process was applied to porcine iliac and porcine carotid arteries and it was shown that it was necessary to include an initial high concentration EDTA wash to dislodge endothelial cells and add an additional wash with hypertonic buffer to ensure removal of the α -gal epitope (Ingham *et al.*, 2010). The method developed for the decellularisation of porcine small diameter arteries had no effect on the biomechanical properties of the tissue (Ingham *et al.*, 2010). This process for the decellularisation of porcine carotid arteries was adopted for this study.

3.2 Aims and Objectives

To apply the Leeds decellularisation protocol to batches of porcine carotid arteries to produce biocompatible acellular scaffolds for subsequent studies of the effects of different sterilisation processes.

- To procure and dissect porcine carotid arteries
- To decellularise porcine carotid arteries
- To determine the effectiveness of the decellularisation process using histology and total DNA quantification
- To determine the biocompatibility of the acellular porcine carotid arteries using contact cytotoxicity assay

3.3 Materials and Methods

3.3.1 Tissue Procurement and Dissection

Reagents:

Dulbecco's Phosphate Buffered Saline (DPBS)

See section 2.6.6.4

DPBS and EDTA (2.7 mM; 0.1 %; w/v)

Five Oxoid Dulbecco's PBS tablets and 0.5 g of EDTA were dissolved in 500 ml distilled water, The pH was adjusted to 7.2 – 7.4 using 6 M hydrochloric acid or 6 M sodium hydroxide drop wise whilst using a magnetic stirrer. The solution was sterilised by autoclaving.

Initial Procurement Method:

Porcine external carotid arteries were sourced from an abattoir from 7-8 month old Large White pigs with a carcass weight of 65-85 kg. Arteries were removed during slaughter, frozen at -20 °C and then couriered overnight in ice boxes.

Final Procurement Method:

Porcine external carotid arteries were sourced from an abattoir from 7-8 month old Large White pigs with a carcass weight of 65-85 kg. Arteries were removed during slaughter and delivered on the day of slaughter without freezing.

Dissection Method:

On arrival in the laboratory, the excess tissue and the adventitia was removed from the carotid arteries by blunt dissection to aid the decellularisation process. The arteries were then washed three times for 30 minutes in Dulbecco's PBS containing EDTA (2.7 mM; 0.1 %; w/v) to remove excess blood. After washing any remaining adventitia was removed by blunt dissection (Figure 3.1). The left or right carotid artery was cut as close to the bifurcation as possible. The length and internal diameters of the arteries were then measured and recorded using a purpose built conical ruler. Arteries were labelled and then stored individually at -80 °C wrapped in DPBS soaked filter paper.

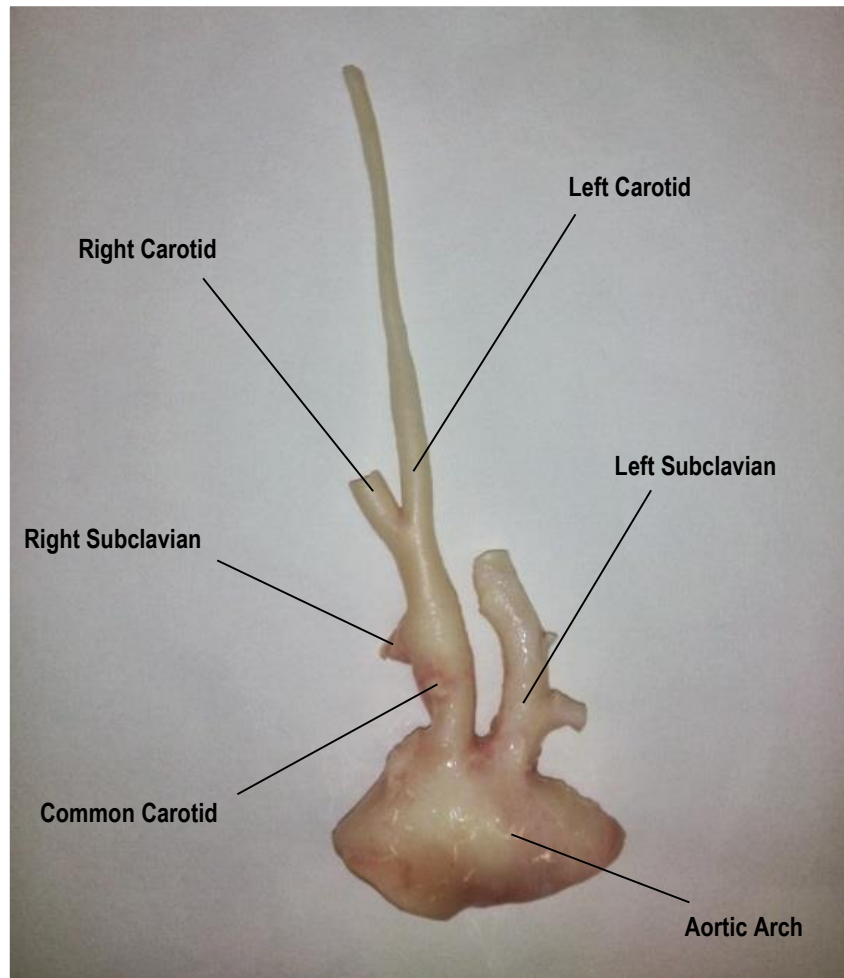


Figure 3.1 : Dissected porcine carotid artery

3.3.2 Decellularisation Process

Reagents:

Sodium hydroxide solution (6 M)

See section 2.6.6.5

Dulbecco's Phosphate Buffered Saline (DPBS)

See section 2.6.6.4. Solutions stored at room temperature and incubated to 4 or 37 °C for 24 hours prior to use.

Disinfection Solution

Sterile DPBS was preheated to 37 °C. Vancomycin, gentamicin and polymyxin B (Table 3.1) were defrosted and added to 100 ml of DPBS. The pH was adjusted to 7.2 – 7.4 using 6 M hydrochloric acid or 6 M sodium hydroxide drop wise whilst using a magnetic stirrer. The solution was filtered through a 0.2 µm pore size filter into a sterile container and the volume made up to 500 ml with sterile DPBS. The solution was used immediately.

Table 3.1: Antibiotic concentrations in the disinfection solution.

Antibiotic	Working concentration	Stock Concentration	Volume of stock required
Vancomycin hydrochloride	0.05 mg.ml ⁻¹	10 mg.ml ⁻¹	2.5 ml
Gentamicin Sulphate	0.5 mg.ml ⁻¹	100 mg.ml ⁻¹	2.5 ml
Polymyxin B	0.2 mg.ml ⁻¹	50 mg.ml ⁻¹	2.5 ml

EDTA solution (200 mM)

EDTA (74.4 g) was dissolved into 1000 ml of distilled water and the pH was adjusted to 7.2 – 7.4 using 6 M hydrochloric acid or 6 M sodium hydroxide drop wise whilst using a magnetic stirrer. The solution was sterilised by autoclaving. Solution stored up to one month at room temperature and cooled to 4 °C 24 hours before use

DPBS and EDTA (2.7 mM; 0.1 %; w/v)

See section 3.3.1

DPBS and EDTA (2.7 mM) containing aprotinin (10 KIU.ml⁻¹)

Aprotinin (500 µl) was withdrawn using a needle and syringe aseptically and added to 500 ml of sterile DPBS and EDTA solution. Solution to be used on same day.

SDS solution (10 %; w/v SDS)

Sodium dodecyl sulphate (10 g) was dissolved into 100 ml of distilled water using a magnetic stirrer and stirrer bar, the solution was passed through a 0.2 µm filter into a sterile container, 5 ml volumes were then aliquoted into sterile universals and stored at room temperature.

BSA solution (5 %; w/v BSA)

Bovine serum albumin (0.25 g) was dissolved into 50 ml of DPBS using a magnetic stirrer and stirrer bar, the solution was then passed through a 0.2 µm filter into a sterile collection container in a class II cabinet. Volumes (5 ml) were then aliquoted into sterile universals and frozen at -20 °C.

Hypotonic buffer (10 mM tris, 2.7 mM EDTA, 10 KIU.ml⁻¹ aprotinin)

Trizma base (1.21 g) and 1 g of EDTA was dissolved into 900 ml of distilled water, the pH was adjusted to 7.2 – 7.4 using 6 M hydrochloric acid or 6 M sodium hydroxide drop wise whilst using a magnetic stirrer. The volume was then made up to a litre and the solution was sterilised by autoclaving. Solution was stored at room temperature. Solution was cooled to 4 °C 24 hours before use. Just prior to use 1 ml of aprotinin solution (10,00 KIU/ml stock) was added.

SDS Hypotonic buffer (0.1 % SDS 10 mM tris, 2.7 mM EDTA, 10 KIU.ml⁻¹ aprotinin)

Autoclaved hypotonic buffer was preheated to 37 °C. SDS solution (10 ml) and aprotinin (1 ml) was added to 990 ml of hypotonic buffer just before use.

DNAase I stock

DNAase I was rehydrated to a final concentration of 10,000 IU.ml⁻¹ using 5 mM sodium acetate, 1 mM calcium chloride and 50 % (v/v) glycerol. The solution was then passed through a 0.2 µm filter into a sterile collection container and stored in aliquots at -20 °C.

RNAase A stock

RNAase I was rehydrated to a final concentration of 100 IU.ml⁻¹ in distilled water the solution was then passed through a 0.2 µm filter into a sterile collection container and stored in aliquots at -20 °C.

Nuclease solution (50 mM tris, 50 µg.ml⁻¹ BSA, 50 IU.ml⁻¹ DNAase, 1 IU.ml⁻¹ RNAase)

This solution was produced aseptically. Trizma base (6.1 g) and 2.0 g of magnesium chloride was dissolved in 80 ml of distilled water using a magnetic stirrer and stirrer bar. The pH was adjusted to 7.5 – 7.7 using 6 M hydrochloric acid or 6 M sodium hydroxide drop wise whilst using a magnetic stirrer. The volume was then made up to 990 ml with distilled water and the solution was sterilised by autoclaving. The solution was stored at room temperature and incubated to 37 °C 24 hours before use. Just prior to use 10 ml of BSA solution, 10 ml of RNAase stock and 5 ml of DNAase stock was added to 975 ml of the buffer.

Hypertonic Solution (50 mM tris, 1.5 M sodium chloride)

Sodium chloride (87.66 g) and tris (6.06 g) was dissolved into 900 ml of distilled water, the pH was adjusted to 7.5 – 7.7 using 6 M hydrochloric acid or 6 M sodium hydroxide drop wise whilst using a magnetic stirrer. The volume was then made up to a litre and the solution was sterilised by autoclaving. Stored at room temperature and incubated at 37 °C for 24 hours prior to use.

Method:

Native porcine carotid arteries sourced using the final procurement method were decellularised in four batches of n=10, n=15, n=21 and n=21. The arteries were thawed at 37 °C. Decellularisation of the arteries was carried out by performing a series of washes; all the incubations were carried out with agitation at 120 rpm except the nuclease step which was agitated at 20 rpm. This method was used on vessels no larger than 200 mm in length and 200 ml of solution was used for each vessel placed in 250 ml sterile pots. The washes were carried out as shown in Table 3.2. Acellular porcine carotid arteries were stored in DPBS at 5 °C for up to one month.

Table 3.2 : Decellularisation process for porcine carotid arteries

Wash	Day	Solution	Temperature	Time
1	Mon.	Disinfection solution	37 °C	0.5 hours
2	Mon.	200 mM EDTA	4 °C	24 hours
3	Tue.	Hypotonic buffer	4 °C	24 hours
4	Wed.	SDS in Hypotonic Buffer	37 °C	24 hours
5	Thu.	Hypotonic buffer	4 °C	24 hours
6	Fri.	DPBS EDTA containing aprotinin	4 °C	56 hours
7	Mon.	SDS in Hypotonic Buffer	37 °C	24 hours
8	Tue.	DPBS x 3	37 °C	0.5 hours
9	Tue.	DPBS	37 °C	~ 16 hours
10	Wed.	Nuclease solution x 2	37 °C	3 hours
11	Wed.	DPBS x 3	37 °C	30 minutes
12	Wed.	DPBS	37 °C	~ 16 hours
13	Thu.	Hypertonic solution	37 °C	24 hours
14	Fri.	DPBS x 3	37 °C	0.5 hours
15	Fri.	Disinfection solution	37 °C	0.5 hours
16	Fri.	DPBS	4 °C	56 hours
17	Mon.	DPBS	4 °C	24 hours
18	Tue.	DPBS	4 °C	24 hours

3.3.3 Tissue Sampling For Biological And Mechanical Evaluation

Native and acellular arteries were divided into smaller tissue samples using one of the following two methods throughout the study. Sampling method I provided tissues for quantitative analyses. Sampling method II was used to provide tissues predominantly for qualitative analysis.

Acellular arteries from batch 1 (n=10) were sampled using method I (n=6) and method II (n=4) for direct comparison with native arteries sampled using the same method. Acellular arteries from batch 2 (n=15) were intended to be used to assess the effects of Gamma

irradiation (n=7 controls; n =8 tests) but were instead used to develop the sterilisation method. The Gamma irradiated arteries were sampled using method I (n=5) and method II (n=3) and were compared against acellular arteries sampled using method I (n=5) and method II (n=2). Acellular arteries from batch 3 (n=21) were used to assess the effects of Gamma (n=7 controls; n =7 tests) and E-Beam (n=7 controls; n =7 tests) irradiation. The acellular Gamma and E-Beam irradiated arteries were sampled using method I (n=5) and method II (n=2) for direct comparison with acellular arteries sampled using the same method. Acellular arteries from batch 4 (n=21) were used to assess the effects of freeze-drying (n=7 controls; n =7 tests) and freeze-drying followed by EO treatment (n=7 controls; n =7 tests) . The freeze-dried acellular arteries were sampled using method I (n=6) and method II (n=1), the EO treated and acellular arteries used for direct comparison were sampled using method I (n=5) and method II (n=2). An overview of the above is displayed in Table 3.3.

Table 3.3 : Overview of the sampling process for each batch and each sterilisation/process

Batch	Acellular		Gamma (1)		Gamma (2)		E-Beam		Freeze Dried		EO	
	SMI	SMII	SMI	SMII	SMI	SMII	SMI	SMII	SMI	SMII	SMI	SMII
1 (n=10)	6	4										
2 (n=15)	5	2	5	3								
3 (n=21)	5	2			5	2	5	2				
4 (n=21)	5	2							6	1	5	2

Gamma (1) group of arteries used for method development, Gamma (2) irradiated arteries used for statistical comparisons.

Reagents:

Dulbecco's Phosphate Buffered Saline (DPBS)

See section 2.6.6.4

Method:

Native arteries were thawed for twenty minutes in a 37 °C water bath; acellular arteries were sampled aseptically in a class II hood.

Sampling method I:

Arteries were sampled as shown in Figure 3.2. Sampling began at the proximal end of the artery on a sterile petri dish for each artery.

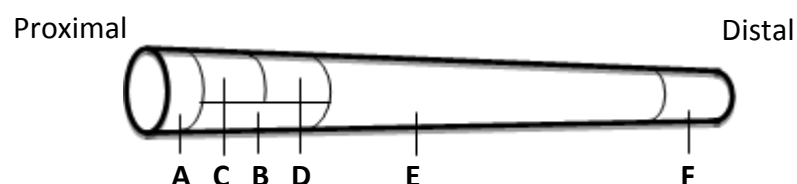


Figure 3.2 : Image depicting sampling method I of porcine carotid arteries

- A. A 5 mm width sample for circumferential stress-strain analysis was removed and placed in a sterile bijou containing 15 ml of DPBS. Stored at 4 °C and used on the same day as sampling. Uniaxial tensile testing is described in section 4.3.4
- B. A 15 mm length x 5 mm width (length is longitudinal) sample for axial stress-strain analysis was removed and placed in a bijou containing 15 ml of DPBS. Stored at 4 °C and used on the same day as sampling.
Uniaxial tensile testing is described in section 4.3.4
- C. For multiphoton imaging a circular disc was removed using a 5 mm diameter hole punch and stored at – 20 °C on DPBS soaked filter paper until used.
The method for multiphoton imaging is later described in section 6.4.5
- D. For differential scanning calorimetry a circular disc was removed using a 5 mm diameter hole punch and stored at – 20 °C on DPBS soaked filter paper until used.
The method for differential scanning calorimetry is later described in section 6.4.6
- E. A 50 mm length was used to carry out compliance and burst pressure testing. These were placed in universals containing 25 ml DPBS. Stored at 4 °C and used on the same day as sampling.
Compliance and burst pressure testing is described in section 4.3.3
- F. The remaining tissue, when sufficient, was used for the denatured collagen assay and stored at – 20 °C on DPBS soaked filter paper until used.
The method for the determination of denatured collagen content is described in section 2.6.10.

Sampling method II:

Arteries were sampled as shown in Figure 3.3. Sampling began at the proximal end of the artery on a sterile petri dish for each artery.

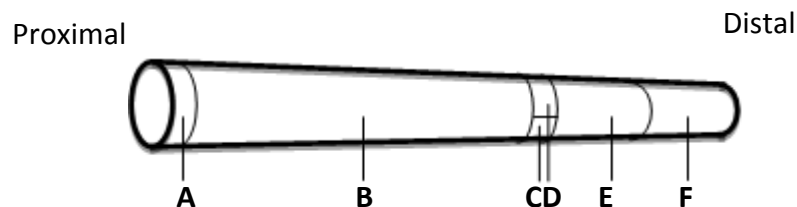


Figure 3.3 : Image depicting sampling method II of porcine carotid arteries.

- A. A 3 mm sample for histological analysis was removed and placed in a histology cassette and fixed in zinc fixative.
The methods used for histological analysis are described in section 2.6.6
- B. A 50 mm length sample was removed either for thrombogenicity assessment or as control tissue. The sampled tissue was placed in universals containing 25 ml DPBS and stored at 4

°C and used same day as sampling, control tissue was stored at -20 °C in a bijou surrounded by PBS soaked filter paper until used.

- C. A 5 mm² square for contact cytotoxicity testing was removed and stored at -20 °C in a bijou surrounded by DPBS soaked filter paper until used.

Methods for determining biocompatibility are described in section 2.6.9.1

- D. A 5 mm length sample for sterility assessment was removed and placed in 25 ml nutrient broth for sterility assessment.

The method used for determining sterility is described 2.6.9.1

- E. A 15 mm length sample was either macerated for DNA quantification or stored as control tissue. These samples were stored at -20 °C in a bijou surrounded by PBS soaked filter paper until used.

The method for DNA quantification was previously described in section 2.6.7

- F. A 15 mm length sample for control tissue was removed and stored at -20 °C in a bijou surrounded by DPBS soaked filter paper until used.

3.3.4 Determination Of The Effectiveness Of The Decellularisation Process And The Biocompatibility Of Acellular Porcine Carotid Arteries

After decellularisation acellular and native porcine carotid arteries were compared by histology using haematoxylin and eosin staining, DAPI staining and immunohistochemical labelling of collagen IV in tissue sections (Section 2.6.6). The DNA was extracted from the tissues for determination of total DNA content (Section 2.6.7). Sterility of the acellular tissues (Section 2.6.9.1) was assessed prior to biocompatibility testing using contact cytotoxicity assays (Section 2.6.8 and 2.6.9.2).

3.4 Results

Porcine carotid arteries were sourced from two abattoirs. Quality assessments were performed to identify arteries suitable for use. Following selection, four batches of arteries were then subjected to the Leeds decellularisation process and were subject to limited analysis to determine the success of the decellularisation process.

Initial Procurement Investigation

Porcine carotid arteries were initially procured from a long distance supplier. The process was not monitored correctly and initially arteries were being removed on the day of slaughter and then frozen at -20 °C after an unknown period at ambient temperature. Arteries were then delivered by overnight courier in ice boxes. Arteries arrived in the laboratory at different stages of the thawing process, ranging from frozen to completely thawed. Arteries were then blunt dissected (Section 3.3.1) and frozen at -80 °C. Histological analysis of the porcine carotid arteries after thawing provided images of the microstructure of the arteries. The images showed repeated areas of perforations in the arteries. An alternative source of arteries enabled delivery of porcine carotid arteries on the day of slaughter, these arteries

were also blunt dissected and frozen at -80 °C and stored for one week before thawing. After thawing the arteries were subject to histological analysis and imaging of histological sections showed that these arteries had normal histo-architecture. Images of histological sections of deteriorated arteries from the first supplier (left) and normal arteries from the second supplier (right) are presented in Figure 3.4.

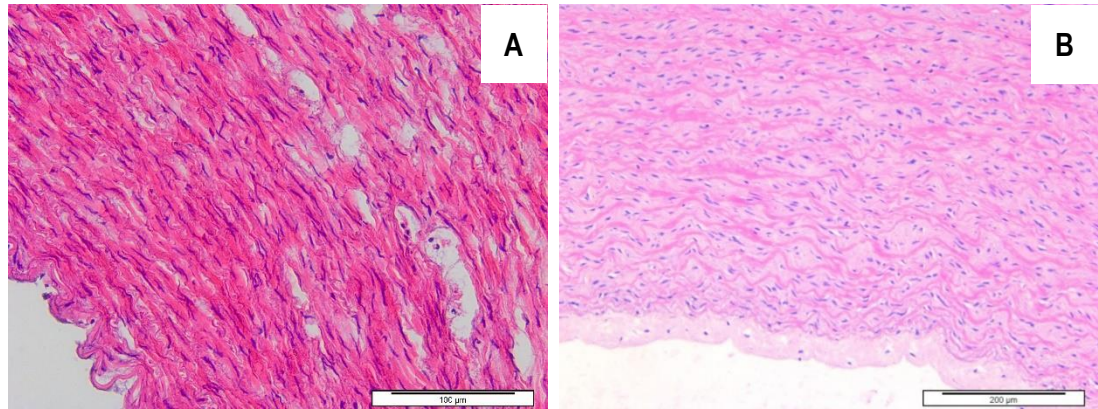


Figure 3.4: Representative images of histological sections of fresh porcine common carotid arteries from two different suppliers.

(A) Long distance tissue supplier (B) tissue supplied on the day of slaughter. The sections were stained with haematoxylin and eosin; the images were captured at 40x and 20x magnification respectively.

3.4.1 Sterility Testing Of Acellular Porcine Carotid Arteries

Samples from each batch of acellular porcine carotid arteries were tested to determine sterility by placing them in nutrient broth and incubating at 37 °C for 48 hours. In the first batch samples were taken from the extra tissue from each artery in sampling method I as well as sampling method II. No contamination was found in any batches

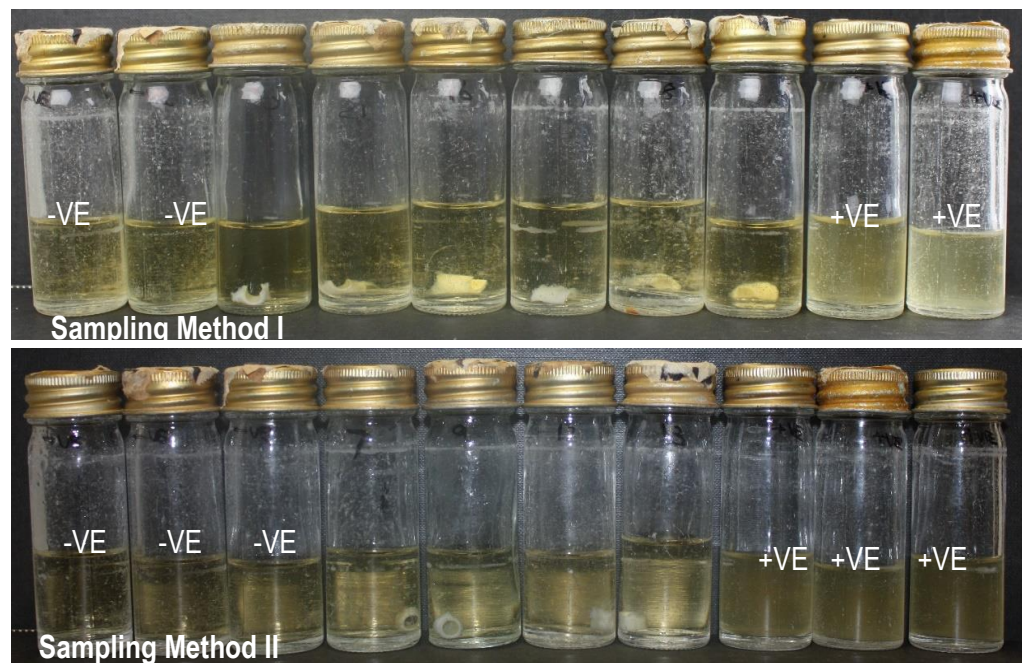


Figure 3.5 : Images of sterility tests carried out on batch 1 of acellular arteries.

Images of sterility testing of acellular porcine carotid arteries from sampling method I and sampling method II. Positive controls of dermal commensal organisms and negative controls of sterile nutrient broth were incubated alongside samples.

3.4.2 Histological Analysis

Haematoxylin and eosin and DAPI stained sections (Figure 3.6) confirmed the presence of cell nuclei and nuclear material in native arteries as well as the typical arterial structure, consisting of the intima, media and adventitia. In acellular arteries there was a distinct absence of cell nuclei and nuclear material; there was also preservation of the arterial structure but collagen and elastin fibres exhibited a wave pattern due to the absence of cells.

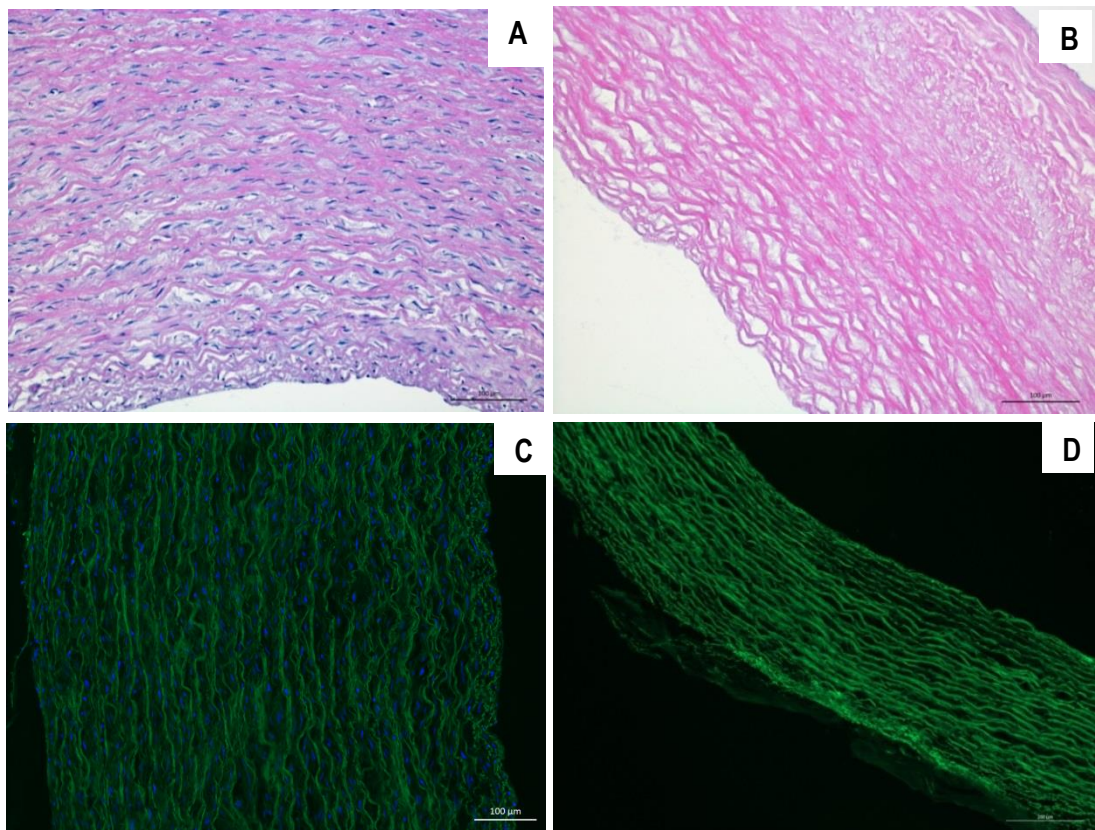


Figure 3.6 : Representative images of histological sections of native and acellular porcine common carotid arteries from batch 1.

Sections were stained with haematoxylin and eosin (A, B) or DAPI (C, D). Native arteries showed the presence of nuclei (A, C) . There was an absence of nuclei in acellular arteries (B, D). The images confirmed the presence of nuclei in native arteries and the absence of nuclei in decellularised arteries as well as the preservation of ECM structure.

3.4.3 Immunohistochemical Labelling Of Collagen IV

Immunohistochemical labelling of collagen IV in tissue sections showed positive staining in regions of native and decellularised arteries (Figure 3.7). Both the intima and media were strongly stained across the whole region with an absence of staining in the adventitial region. There was no observable staining in the section used for either the isotype antibody control or the antibody diluent.

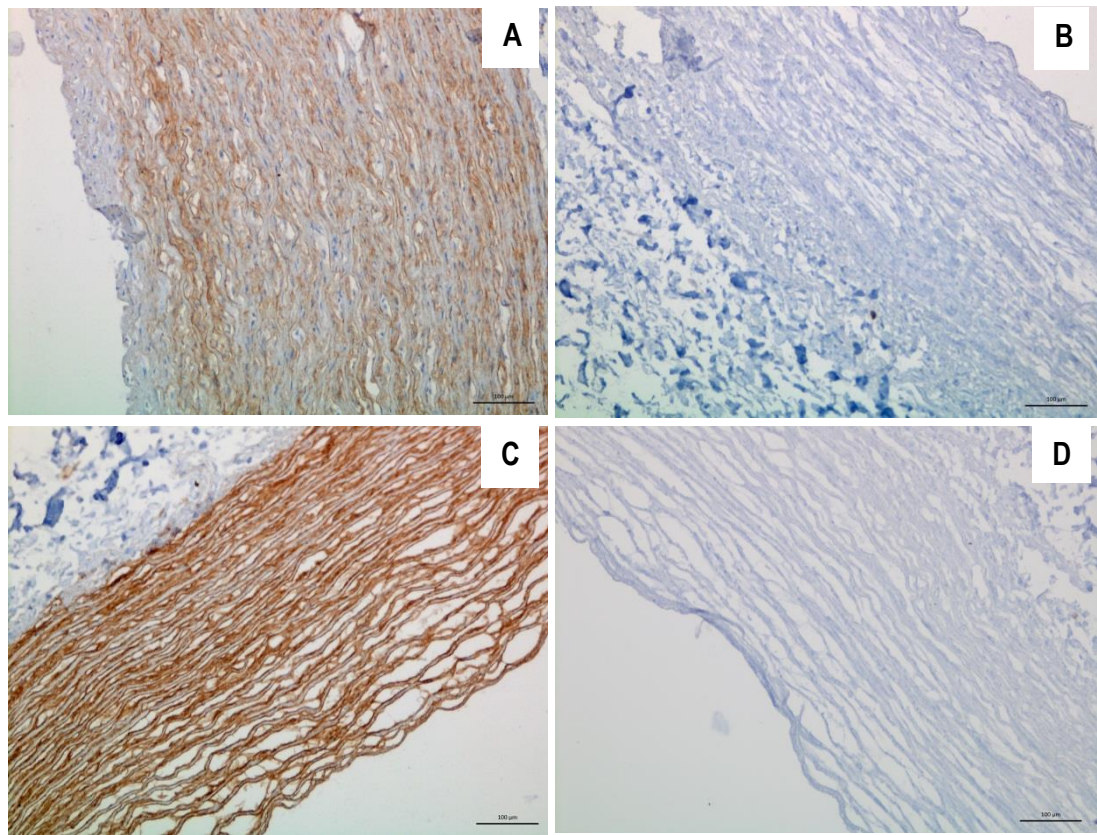


Figure 3.7 : Representative images of sections of native and acellular porcine common carotid arteries (batch 1) labelled using immunohistochemistry with an antibody to collagen IV.

Sections were labelled with antibodies to collagen IV (A, C) and isotype antibody control (B) as well as an antibody diluent control (D). Native (A) and acellular arteries (C) showed positive staining across the intima and media but no staining in the adventitia. Controls showed no positive staining.. The images confirmed the presence of collagen IV in the intima and media of native and decellularised arteries.

3.4.4 DNA Content

DNA was extracted from samples of native (n = 6) and acellular (n = 4) arteries using a DNA isolation kit (Qiagen). The total DNA content was quantified by measuring the absorbance using a nanodrop spectrophotometer at 260 nm (Figure 3.8). Native tissue had 708 ± 184 ng.mg⁻¹ (mean \pm 95 % confidence intervals) DNA per wet weight of tissue and acellular arteries had 8 ± 4 ng.mg⁻¹ DNA per wet weight of tissue demonstrating a 97.6 to 99.6 % (w/w) reduction in DNA content (batch 1).

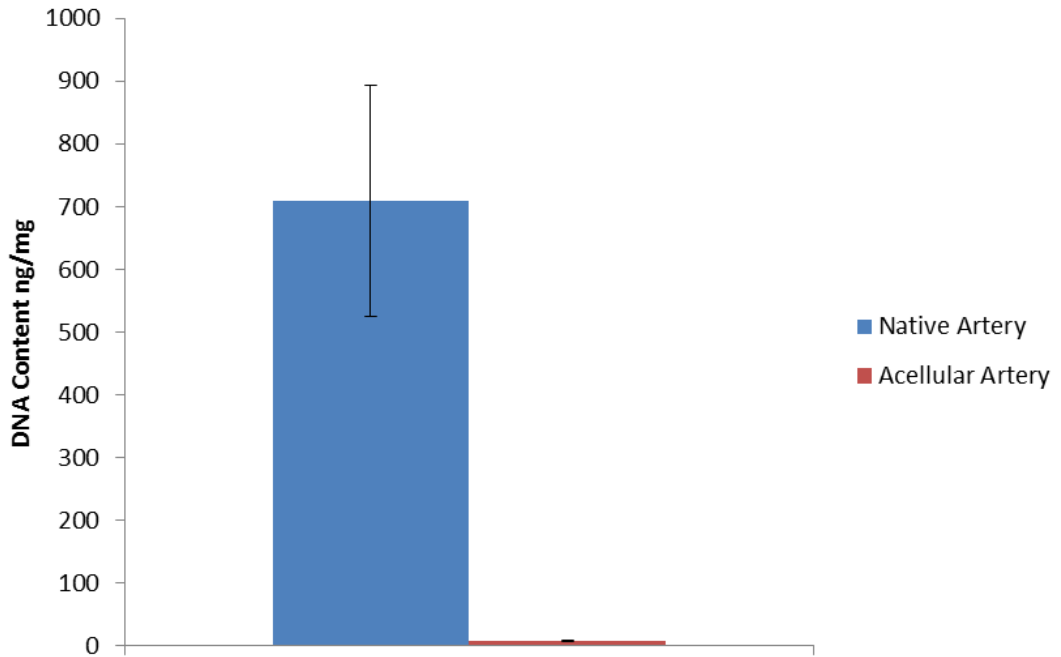


Figure 3.8 : Total DNA content of native and acellular porcine carotid arteries from batch 1. Post decellularisation there was a 97.8 to 99.5 % reduction in total DNA content. Data expressed as the mean (native, n=6; acellular, n=4) \pm 95% C.L.

3.4.5 Contact Cytotoxicity

Acellular arteries were incubated with L929 and BHK cell lines to assess biocompatibility, steri strips were used as a negative control and cyanoacrylate was used a positive control. The phase contrast (Figure 3.9) and giemsa stained (Figure 3.10) images at 48 hours showed that the cell lines grew up to both acellular arteries and steri strips indicating there was no cytotoxic effect on both L929 and BHK cells. Normal cell morphology was observed compared to confluent cells alone and cyanoacrylate was highly cytotoxic and caused cell lysis.

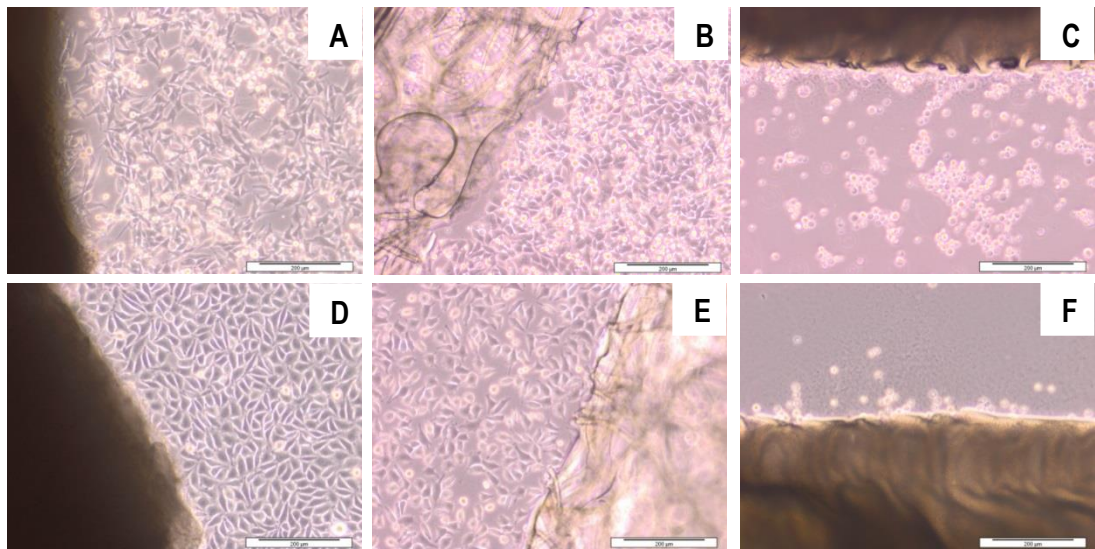


Figure 3.9 : Representative images captured using phase contrast microscopy of BHK and L929 cells growing in contact with acellular porcine carotid artery samples from batch 1.

BHK (A-C) and L929 (D-F) cell lines Incubated with acellular arteries (A, D), steri-strips (B, E) and cyanoacrylate (C, F). Images were captured at x40 magnification.

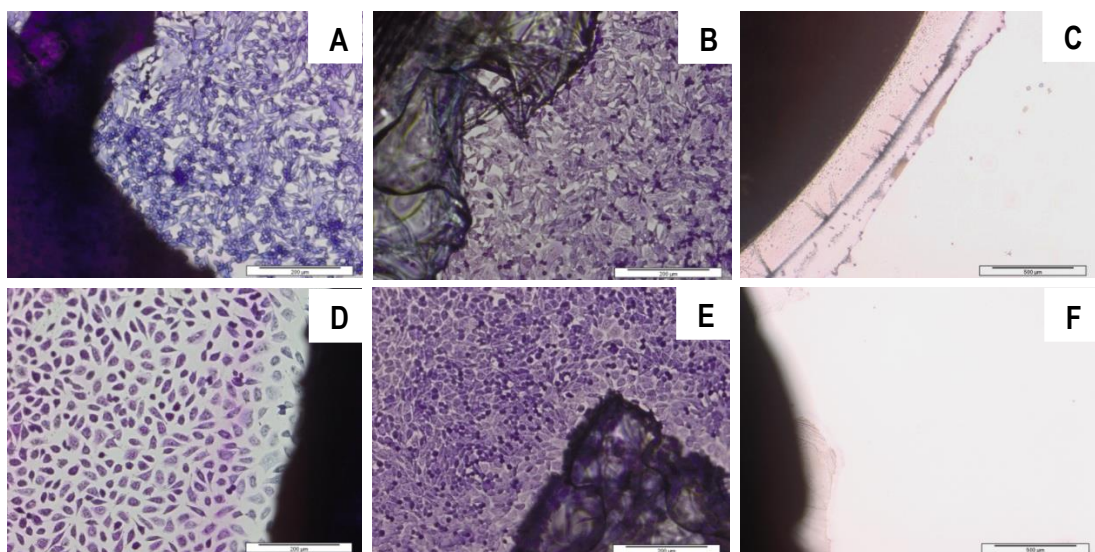


Figure 3.10 : Representative images captured using light microscopy of BHK and L929 cells stained with giemsa growing in contact with acellular porcine carotid artery samples from batch 1.

BHK (A-C) and L929 (D-F) cell lines Incubated with acellular arteries (A, D), steri-strips (B, E) and cyanoacrylate (C, F). Images were captured at x40 magnification.

3.4.6 Summary Of Data On Determination Of The Effectiveness Of Decellularisation Of The Four Different Batches Of Acellular Porcine Carotid Arteries

A summary of the data on the assessment of the effectiveness of decellularisation for the four batches of decellularised arteries used throughout the project is presented in Table 3.4.

Table 3.4 : Summary of analysis of four batches of acellular arteries for the effectiveness of the decellularisation process.

Batch	Absence of nuclei in H&E/DAPI	Positive staining for collagen IV	Total DNA Content (ng.mg ⁻¹)	Biocompatibility contact cytotoxicity
(1), PCA1-6 (n=10)	✓	✓	8.2 ± 4.2	✓
(2), PCA7-12 (n=15)	✓	✓	8.0 ± 23.6	✓
(3), PCA13-33 (n=21)	✓	✓	7.6 ± 1.4	✓
(4), PCA34-54 (n=21)	✓	✓	6.3 ± 2.1	✓

3.5 Discussion

The aim of the research described in this chapter was to produce acellular vascular scaffolds derived from porcine carotid arteries using the patented vascular decellularisation process (Ingham *et al.*, 2010), for use in subsequent studies of the effects of different sterilisation processes.

Once the evidence of damage to porcine carotid arteries had been identified in artery supplies arriving on site, it was important to investigate the cause to prevent further incidences occurring that may have the potential to give false positive results for damage. As the problem was intermittent at first, it was not picked up initially, this highlighted the necessity of monitoring the delivery process of tissues and having routine quality measures in place to check the suitability of the arteries. A large body of work had been carried out before switching supplier and although this was a substantial oversight this knowledge can be passed on to colleagues to prevent similar issues arising.

The cause of the damage to the arteries delivered by the long distance supplier could be attributed to two root causes. Firstly, damage may have been caused by the freezing process of the arteries. Slow freezing rates could have promoted extracellular over intracellular ice crystal formation, which has been shown to cause increased damage to the extracellular matrix (Gage & Baust, 1998; Meryman, 1960; Devireddy *et al.*, 2003). Secondly, damage may have been caused by autolysis. As the time after slaughter that the arteries were frozen was not monitored and the thaw cycle occurring in transit, there was opportunity for the arteries to degrade before freezing or after thawing. After slaughter, cells are subject to ischemic injury to a lethal extent and cells die via necrosis. Cell death via necrosis causes leakage of cellular enzymes such as metalloproteinases and serine proteinases. These proteinases have the

ability to digest the ECM and could have caused the atypical gaps observed in the histological images. The arteries from the local supplier were delivered on the day of slaughter, this enabled control of the freeze-thaw process and prevented any further supply issues.

Once the quality of the source material was established, arteries were decellularised in four separate batches. Although no definitive criteria have been set at which a tissue can be considered decellularised, Crapo *et al.* (2011) has described a set of minimum requirements:

1. < 50 ng dsDNA per mg ECM dry weight
2. < 200 bp DNA fragment length
3. Lack of visible nuclear material in tissue sections with 4',6-diamidino-2-phenylindole (DAPI) or H&E

Previous studies within the department have validated the effectiveness of the decellularisation process on porcine internal carotid arteries and porcine external iliac arteries (Ingham *et al.*, 2010). As this part of the study was not novel or intended to create acellular arteries for clinical trials it was the aim of this chapter to show the effectiveness of the decellularisation process in my hands with a limited set of tests. The acellularity was assessed with the use of total DNA quantification, visual inspection of histological sections stained for nuclear material and a biocompatibility assay.

The test method used in this study for the quantification of DNA content has been used historically within the department. Total DNA content showed a greater than 80 % reduction in all four of the batches. The method determines the total DNA content based on the wet weight of the tissue, this can be approximated as 3 times less than the dry weight concentration meaning all the results were well below the total DNA content specified by Crapo *et al.* (2011). The total DNA content of porcine carotid arteries before and after decellularisation were also similar to those found previously in the department for porcine carotid and iliac arteries (Ingham *et al.*, 2010; Owen *et al.*, 2012).

Both DAPI and H&E staining were used to confirm the absence of visible nuclear material in sections of acellular porcine carotid arteries and positive controls of native porcine carotid arteries were used to demonstrate the validity of the method. H&E/DAPI staining was negative in histological sections of all four batches of acellular arteries and positive in histological sections of native porcine carotid arteries.

The biocompatibility was confirmed through the use of contact cytotoxicity assay. Normal cellular morphology was observed with no zone of inhibition in microscopic images for both cell lines tested using tissue samples from all batches of acellular arteries.

These results demonstrated that decellularisation was effective on porcine carotid arteries and correlated well with previous data from testing on porcine external iliac arteries.

By these assessments the aims of this part of the study had been achieved. Acellular arteries derived from porcine carotid arteries were reproduced consistently, that were biocompatible and sterile, and therefore suitable for subsequent studies. Prior to using the acellular arteries to assess the effects of different sterilisation processes, it was necessary to develop robust methods to determine the biomechanical properties of the acellular arteries. This was the focus of the next part of the study described in Chapter 4.

Chapter 4 Development of Mechanical Testing Methods

4.1 Introduction

Tissues in the body vary in composition and orientation of cells, fibres and extra-cellular matrix, which is dependent on the functional requirement. The main structural components within tissues are elastin, collagen and glycosaminoglycans.

The extension and recoil characteristics of elastin are primarily responsible for the elasticity and compliance properties of a tissue, the triple helical structure of collagen is primarily responsible for the high tensile stiffness and ultimate tensile strength and glycosaminoglycans are primarily responsible for the compressive properties of a tissue.

In arteries the tunica media is the thick central layer and contributes most to the overall mechanics of an artery. It is populated by predominantly smooth muscle cells, organised in the circumferential direction, and surrounded by a dense mesh of collagen and elastin fibres orientated circumferentially.

Determination of the biomechanical properties of vascular grafts is an important aspect to be considered. In order for a graft to be suitable for use it should have adequate strength to resist the extremes of physiological pressure that it will be subjected to and it should also have a compliance that provides a similar or better response to haemodynamics than analogous tissue.

Uniaxial tensile testing, compliance and burst pressure testing are common methods employed to determine the mechanical characteristics in arteries.

With regard to uniaxial tensile testing, it is important to consider preloading. Dependent on the test method employed it can be difficult to ascertain if the tissue is in a zero-stress or natural state before loading. Preloading is a method of applying a small load, usually within 0-10 % of the failure load and then assigning zero to the strain and load at this preload. This is carried out to ensure any slack has been taken up, which could potentially impact the data for the derived parameters. The zero-stress state is critically dependent on the design and setup of the equipment being used, therefore if preloading is being used it is essential to determine the correct level of preloading for that particular piece of equipment. If the preload is set too high it may mask any differences in properties derived from the parameters for different samples.

Dependent on the design of equipment and the method being used, compliance testing can be a very useful tool for determining three dimensional behaviour of the mechanical properties of arteries. Since compliance mismatch has been highlighted as one of the key

failure mechanisms of arterial grafts, development of a reliable method to assess the compliance of the native, acellular and acellular sterilised arteries was essential to this study.

The focus of the research in this chapter was to develop a robust method to determine the compliance of native and acellular porcine carotid arteries and to investigate the required level of preloading using a purpose built rig for the determination of stress-strain parameters of native and acellular vascular grafts.

4.2 Aims and Objectives

The aim of this chapter was to develop robust methods to determine mechanical properties of porcine carotid arteries and evaluate the effects caused by decellularisation by comparing the mechanical properties of native and acellular arteries. The specific objectives were:

- To develop a robust working method for compliance testing of porcine carotid arteries
- To determine the compliance of native and acellular porcine carotid arteries
- To investigate the effects of preloading of porcine carotid artery tissue and determine an acceptance preload for use in uniaxial tensile tests.
- To determine the uniaxial tensile parameters of native and acellular porcine carotid arteries

4.3 Materials and Methods

4.3.1 Tissue Procurement And Dissection

The native porcine carotid arteries used in this chapter were procured and dissected according to the method described in Section 3.3.1.

4.3.2 Decellularisation Of Native Porcine Carotid Arteries

The acellular arteries used in this chapter were from batch 1 (Section 3.4.6) and were processed using the method described in Section 3.3.2.

Tissue sampling for mechanical evaluation

The samples used for mechanical evaluation were obtained as described in Section 3.3.3.

4.3.3 Development Of Compliance And Burst Pressure Testing

4.3.3.1 Preliminary analysis of methods

Reagents:

Dulbecco's Phosphate Buffered Saline (DPBS)

Described in Section 2.6.6.4

Method:

Native arteries were mounted to a custom built rig. The rig consisted of a pressure inlet, a compliance chamber, a pressure gauge and an inflation chamber containing a scale ruler (Figure 4.1).

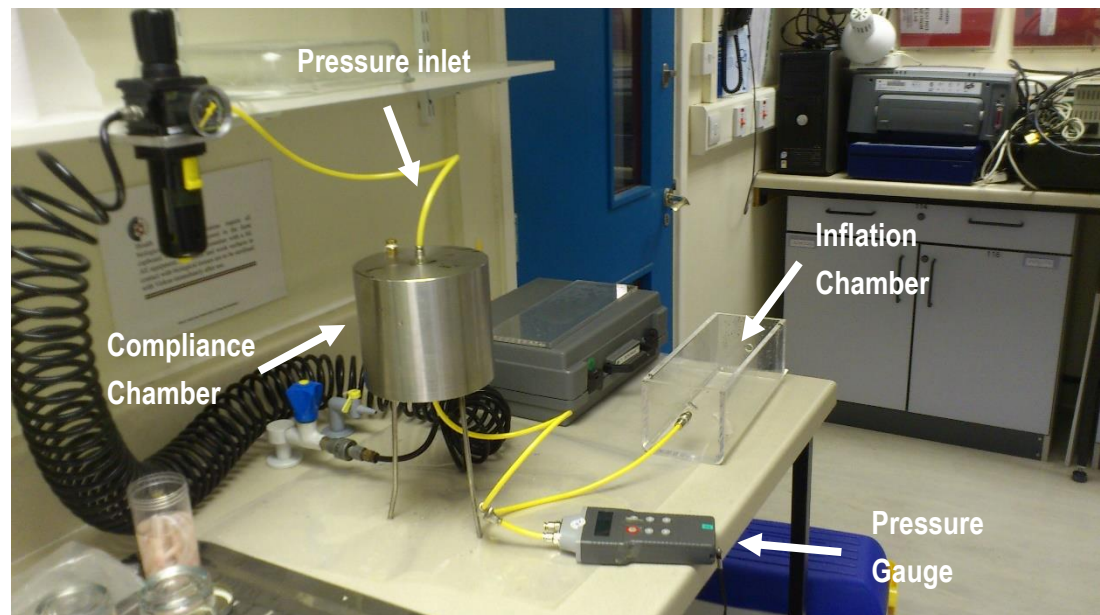


Figure 4.1 : Image of the equipment setup used for determination of the compliance and burst pressure testing.

Four methods for determination of the compliance of the arteries were investigated. In all methods, the proximal end of the artery was attached to the rig inside the inflation chamber. The four methods varied in approach to the mounting of the distal end of the vessel (Figure 4.2). In the first method the distal end was ligated and left to freely orientate in space (Original Method). In the second method the distal end was fixed to a static hose barb (Fixed Position Method). For the third method the distal end was ligated and tension was applied manually along a suture (Manually Adjusted Method). The fourth method involved applying tension along a suture via a constant load of 15 g (Constant Weight Method).

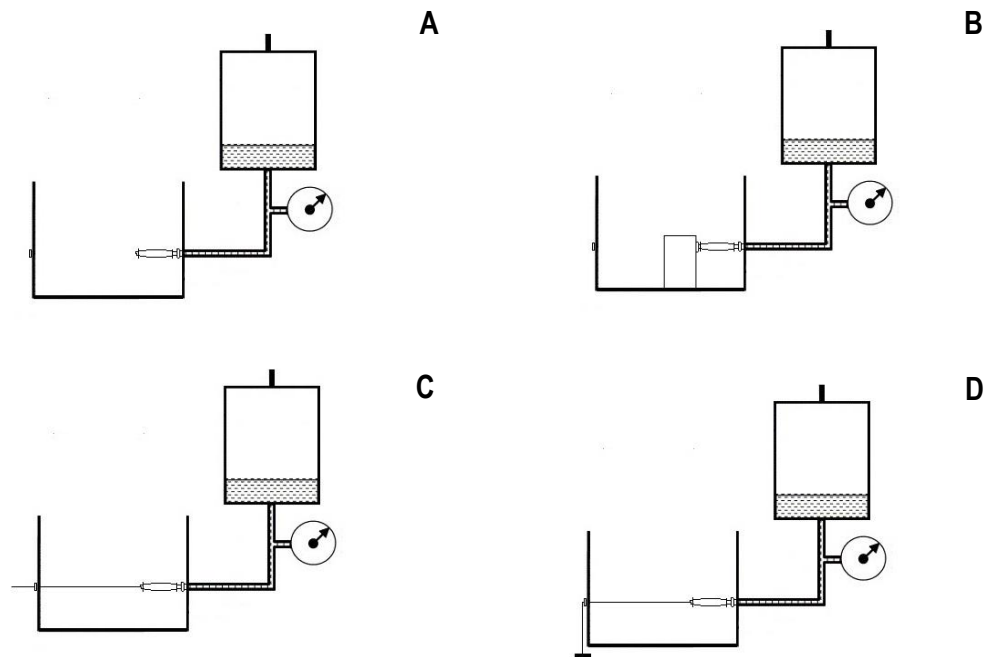


Figure 4.2 : Compliance and Burst Pressure Rig Setup.

Depiction of the four methods investigated for compliance testing of arteries.: Original Method (A), Fixed Position Method (B), Manually Adjusted Method (C), and Constant Weight Method (D).

The arteries were filled with 120 ml DPBS from a compliance chamber and then subjected to increasing pressure in increments of ~20 mmHg up to 200 mmHg at room temperature. At each measurement the pressure was recorded and an image taken using an aerial mounted digital camera. After 200 mmHg the pressure was steadily increased incrementally by 50 mmHg until either bursting or a pressure safety valve of 3700 mmHg was met. The images were then imported into Image Pro Plus (MediaCybernetics) and used to measure the diameter and the length at each pressure increment. The measurements from the final adopted method were used to calculate the percentage diameter and length change using the following equation where X = diameter or length, X' = original diameter or length and P = pressure:

$$\Delta C = \frac{(X_n - X') \times 100}{P'}$$

4.3.3.2 Reproducibility

The constant weight method was repeated with native arteries (n=3) to determine if the method was consistent. The percentage diameter and length change data was arcsine transformed, the means and 95 % confidence intervals calculated and the data was back-transformed for presentation purposes.

4.3.3.3 Sensitivity Analysis

The constant weight method was then investigated to determine its sensitivity to the mass of the constant load for both percentage diameter and length increase. The method was repeated on native arteries (n=5), altering the weight between 5, 10 and 15 g on each artery.

4.3.3.4 Compliance testing of native and acellular arteries

Compliance and burst pressure testing was carried out on native (n=3) and acellular (n=5) arteries using the constant weight method with a 10 g load to determine the effects of decellularisation.

4.3.4 Uniaxial Tensile Testing

Reagents:

Dulbecco's Phosphate Buffered Saline (DPBS)

As described in Section 2.6.6.4

Method:

Uniaxial tensile testing was carried out on an Instron 3365 tensile tester using a 50 N load cell. Samples of native and acellular porcine carotid artery were cut using a purpose built cutter at a constant width of 3 mm. At this point the tissue thickness was measured using a Mitutoyo thickness gauge (± 0.01 mm) and then replaced in PBS until tested. Once all test samples had been prepared individual strips were then mounted using a purpose built rig that allowed the gauge length to be set at 6 mm using a spacer bar. The rig prevented loading until the start of the test (Figure 4.3).

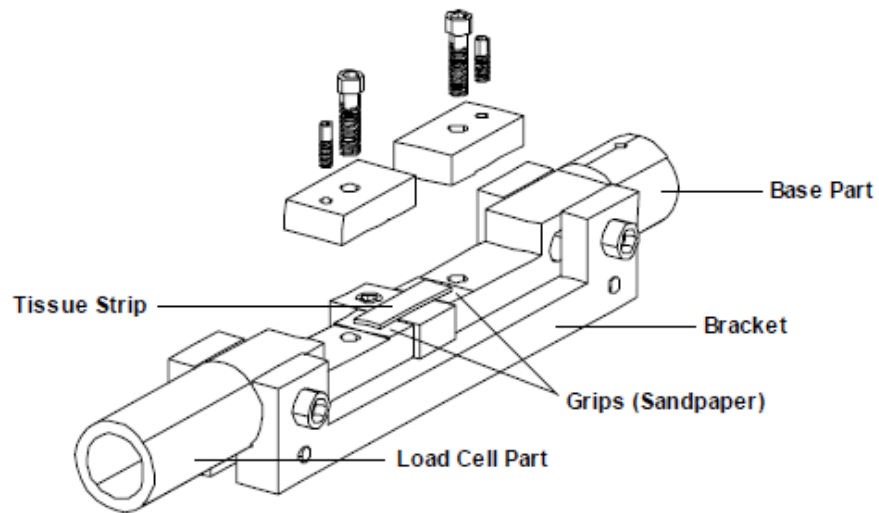


Figure 4.3 : Schematic of the purpose built rig for tensile testing of arteries

The test sample was immersed in PBS at room temperature for the duration of the testing using a water bath (Instron). Samples were then loaded and extended at $10 \text{ mm}\cdot\text{min}^{-1}$ and the load measured using a 50 N load cell. Samples were then loaded to failure (Figure 4.4).

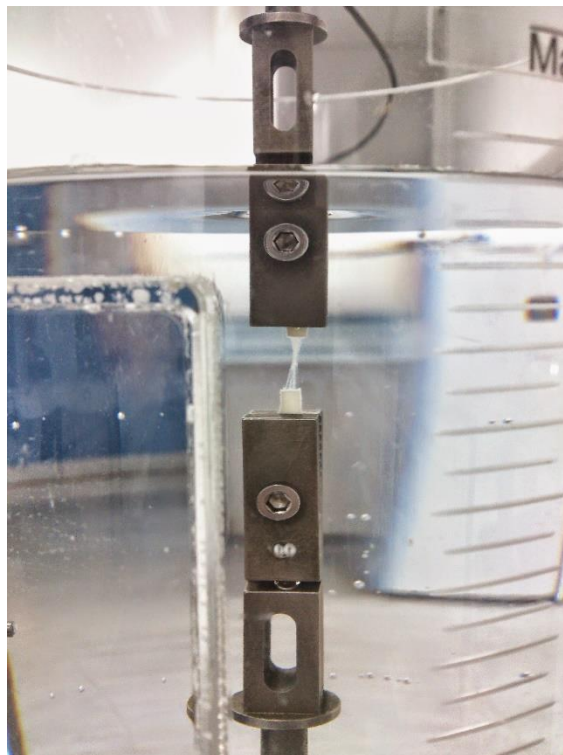


Figure 4.4 : Image of porcine carotid artery loaded to failure using a purpose built rig placed in a waterbath.

The resulting force extension curves were transformed into stress strain curves using the following formulas:

$$\text{Engineering stress } \sigma_{eng} = \frac{F}{A_0}$$

$$\text{Engineering strain } \varepsilon_{eng} = \frac{\Delta L}{L_0}$$

Where, E is the engineering stress in MPa, F is the measured force in N, A₀ is the undeformed cross-sectional area in mm², E_s is the engineering strain ratio, DL is the extension of the specimen in mm and L₀ is the original length of the specimen in mm.

To apply a preloading at ranges of 0.01 N, 0.02 N, 0.05 N, 0.1 N and 0.2 N, data was manipulated by subtracting as a constant the extension at the given preload from all extension data points. The original length was modified by adding the extension at a given preload to create a new original length. The force was zeroed by subtracting the given preload as a constant from all force measurements.

$$\text{Preloaded engineering stress } \sigma_{eng} = \frac{F - PL_F}{A_0}$$

$$\text{Preloaded engineering strain } \varepsilon_{eng} = \frac{\Delta L - PL_e}{L_0 + PL_e}$$

Each stress strain curve was then analysed by means of six parameters: elastin modulus, collagen modulus, transition stress, transition strain, ultimate tensile stress and ultimate tensile strain. The elastin and collagen modulus were determined from the slope of the respective phases using regression analysis to provide the Young's modulus.

The parameters for native and acellular arteries were averaged and expressed as means ± 95 % CL. Using SPSS statistical software, a two way ANOVA was carried out followed by post-hoc Tukey test to compare the group means.

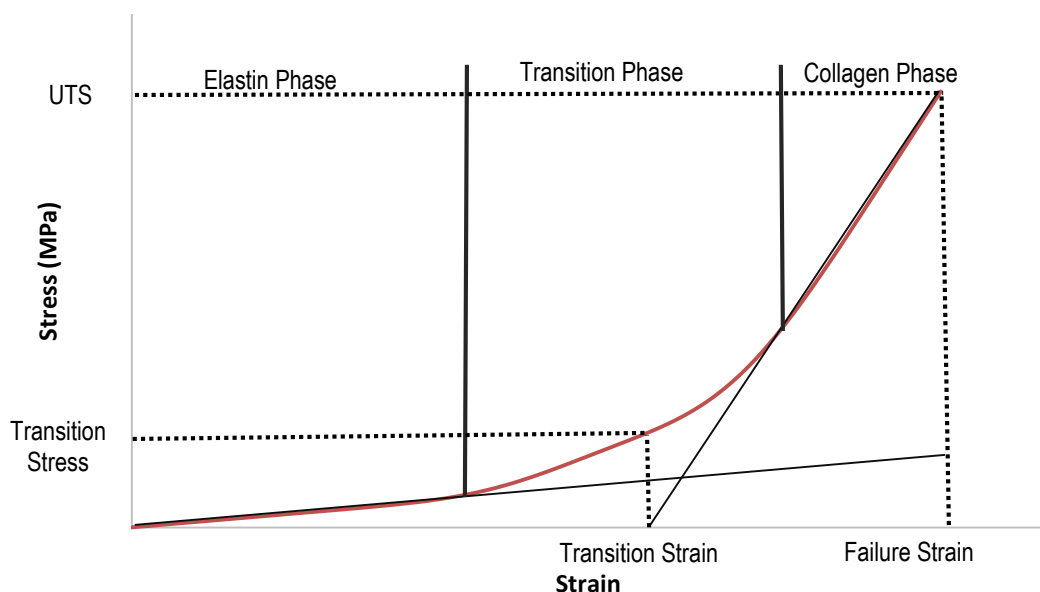


Figure 4.5 : Chart representing the six parameters derived from stress strain curves from uniaxial tensile testing

4.4 Results

4.4.1 Development Of Compliance And Burst Pressure Test Method

In order to develop a burst pressure test method it was first necessary to compare the proposed methods visually and analytically to gain an initial understanding of which method was suitable.

4.4.1.1 Preliminary analysis of methods

Native porcine carotid arteries were tested for compliance using the following four methods:

1. Original Method - distal end of artery ligated and left to freely orientate in space (n=2)
2. Fixed Position Method - distal end of artery fixed to a static hose barb (n=1)
3. Manually Adjusted Method- and tension applied manually along a suture (n=2)
4. Constant Weight Method - distal end of artery ligated and tension applied along a suture via a constant load of 15 g (n=2)

The results are presented in Figure 4.6. Images captured using each test method are presented in Figure 4.7. Testing of the arteries using the original and the manually adjusted methods gave varied and inconsistent measurement of the change in percentage diameter. Visual inspection of the original and fixed position methods showed the artery moving out of the camera view plane. The constant weight method gave rise to data which had less fluctuation. The curves for percentage diameter increase with increase in pressure for the constant weight method exhibited a biphasic pattern with an initial phase of steeper diameter increase followed by a shallower diameter increase.

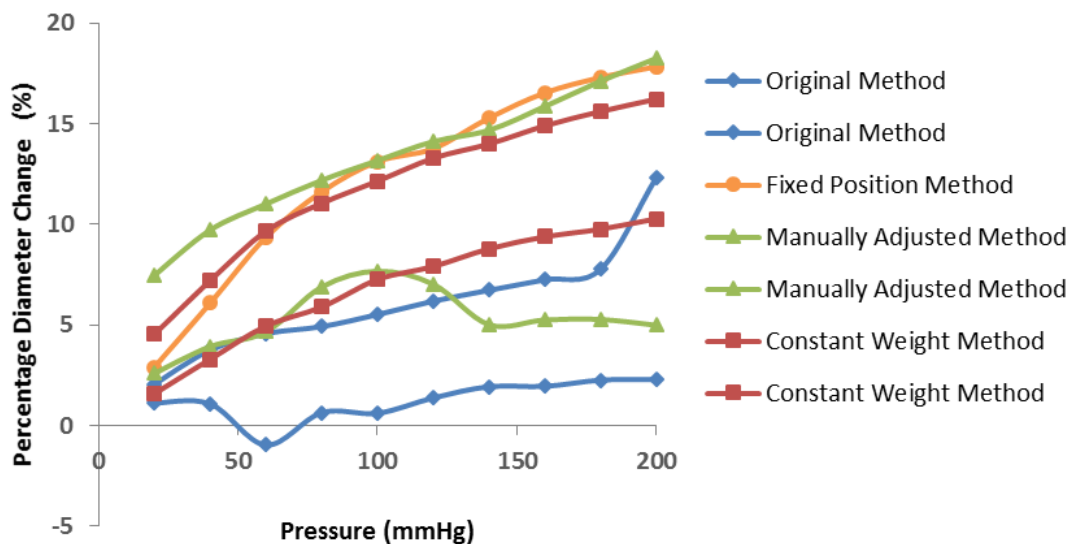


Figure 4.6 : Percentage diameter change in arteries with increasing pressure determined using four methods of compliance measurement.

Curves showing the percentage diameter increase with pressure increase for the four preliminary methods investigated including: Original Method, Fixed Position Method, Manually Adjusted Method, and Constant Weight Method.

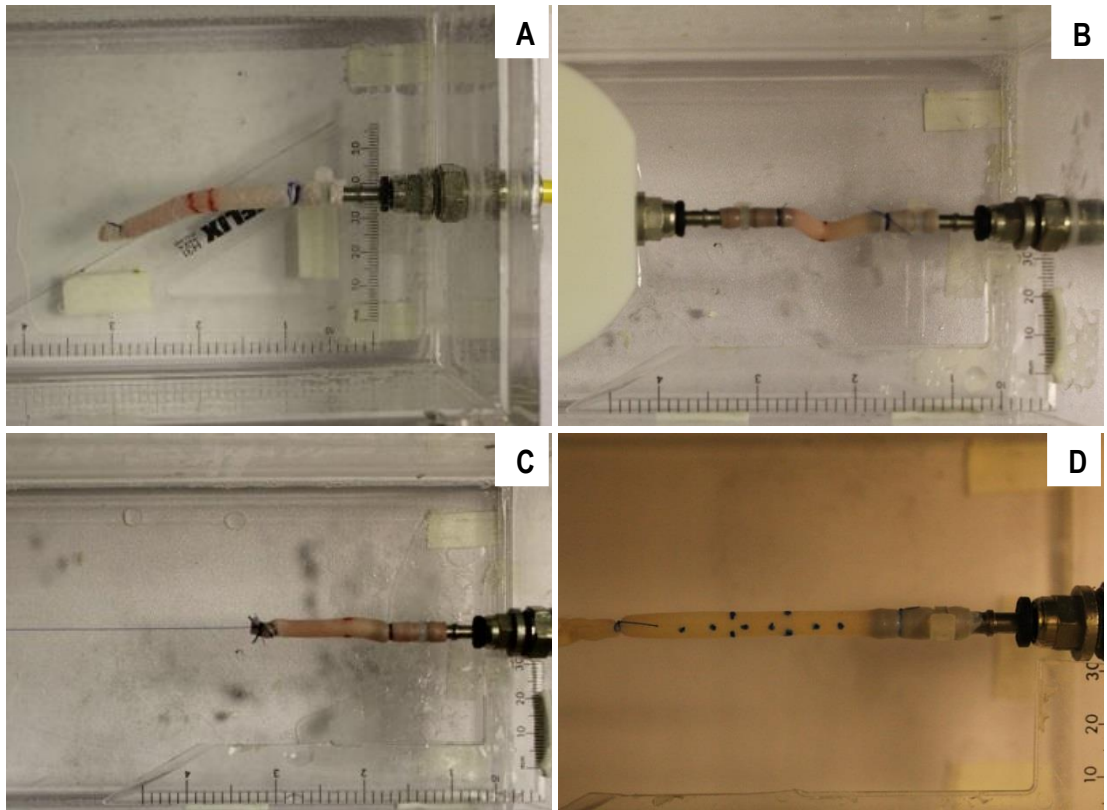


Figure 4.7 : Representative images of arteries captured during testing using the four different methods of measuring compliance.

Original Method (A), Fixed Position Method (B), Manually Adjusted Method (C), and Constant Weight Method (D).

4.4.1.2 Reproducibility of the Constant Weight Method for Measurement of Compliance

The percentage diameter change was measured and compared in three native porcine carotid arteries with increasing pressure using the constant weight method (15 g). The results are presented in Figure 4.8. The compliance curves showed similar patterns with an initial sharper percentage diameter increase with increasing pressure, followed by a shallower gradient. There was greater variation in the percentage diameter increase at low pressures than there was at increased pressure, resulting in a decrease in 95 % confidence levels with increasing pressure.

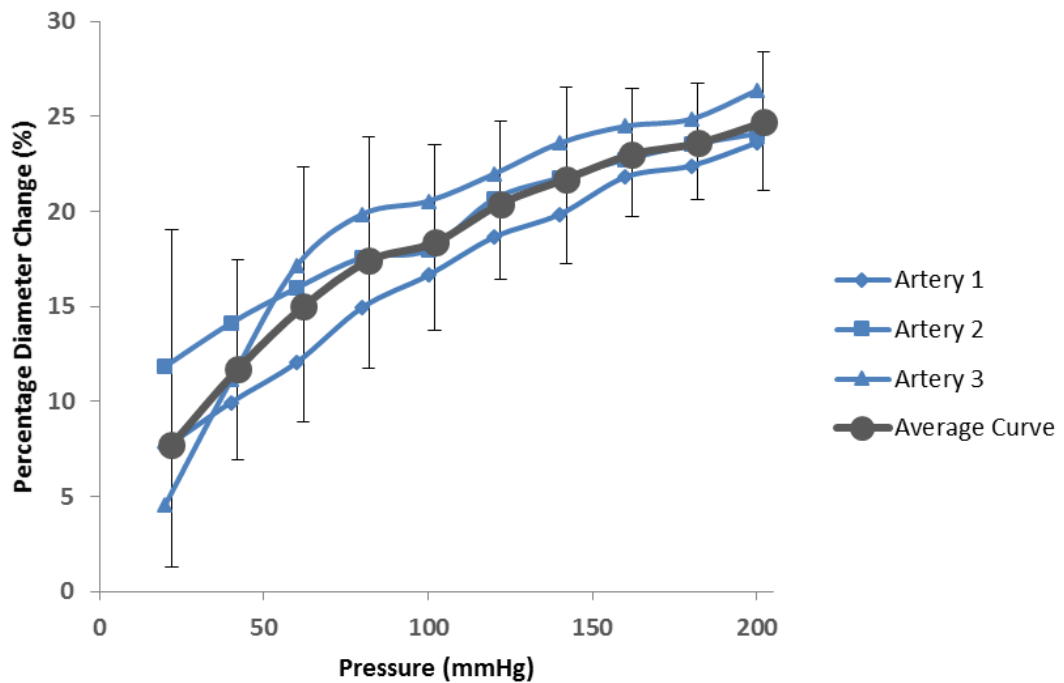


Figure 4.8 : Reproducibility of percentage diameter increase of porcine carotid arteries tested using the constant weight method.

Individual and average curves showing the percentage diameter increase with pressure increase of native arteries using the constant weight method. Data (average curve) expressed as the mean (n=3) \pm 95% C.L.

4.4.1.3 Sensitivity Analysis to Investigate the Impact of Load on Compliance

A sensitivity analysis to investigate the impact of varying load on the compliance of native arteries (n=5) was carried out. The load applied to the arteries was varied using 5, 10 and 15 g for each artery and the percentage diameter and length change with increasing pressure determined. The results are presented in Figure 4.9 and Figure 4.10. All data was arcsine transformed before it was analysed by analysis of variance and Tukey post-hoc testing. The average percentage diameter increase curves showed an initial rapid dilation with increasing pressure, followed by a shallower period of dilation for the three loads tested. With increased load the percentage diameter increase curves became aligned. At 20 mmHg the percentage diameter increase using the 5 g load was significantly less (ANOVA with Tukey post-hoc test; $p < 0.05$) than the percentage diameter change using the 10 and 15 g load. At 40 mmHg and above there was no significant difference between the percentage diameter for the three loads. The average percentage length change curves showed a linear extension for all three loads tested, with length increasing with increasing load. At 20 and 40 mmHg the percentage length change using a 5 g load was significantly less (ANOVA with Tukey post-hoc test; $p < 0.05$) than with the 15 g load. Above 40 mmHg there was no significant difference between the percentage length increase for the three loads (ANOVA with Tukey post-hoc test; $p < 0.05$).

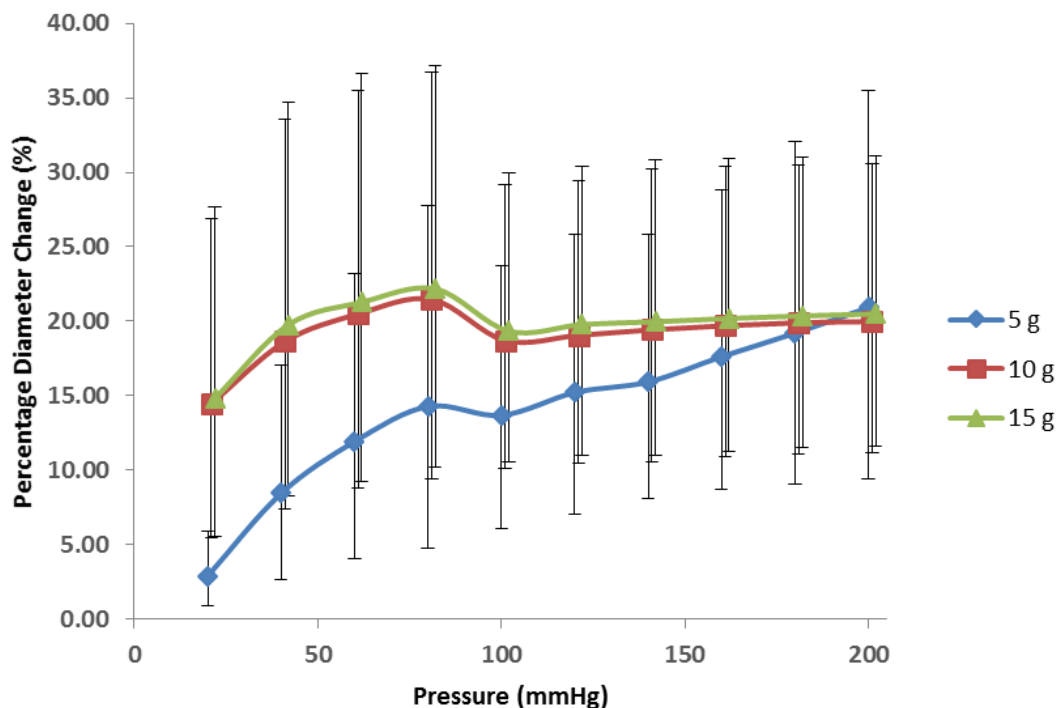


Figure 4.9 : Sensitivity Analysis of Load on Percentage Diameter Change of Arteries with Increasing Pressure.

Averaged percentage diameter increase curves under 5, 10 and 15 g loads with increasing pressure. Data expressed as the mean (n=5) \pm 95 % C.L. Data was arcsine transformed and analysed by analysis of variance and individual differences between group means determined by the Tukey post-hoc test. This showed a significantly lower mean diameter increase with the 5 g load compared to the 10 and 15 g loads at 20 mmHg.

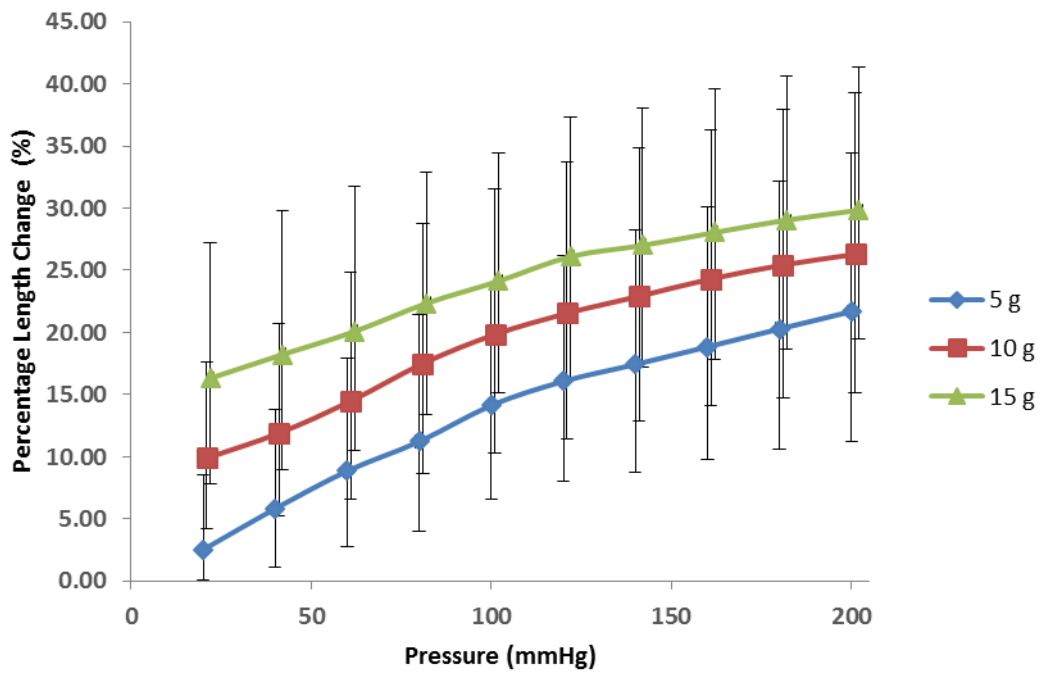


Figure 4.10 : Sensitivity Analysis of Load on Percentage Length Change of Arteries with Increasing Pressure.

Averaged percentage length increase curves under 5, 10 and 15 g loads with increasing pressure. Data expressed as the mean (n=5) \pm 95 % C.L. Data was arcsine transformed and analysed by analysis of variance and individual differences between group means determined by the Tukey post-hoc test. This showed a significantly lower mean length change with the 5 g load compared to the 15 g loads at 20 and 40 mmHg .

Following these results all compliance and burst pressure testing was carried out by attaching a constant weight of 10 g to the ligated artery.

4.4.1.4 Determination of Compliance of Native and Acellular Porcine Carotid Arteries

Using the compliance method developed native (n=3) and acellular (n=5) arteries were subjected to burst pressure and compliance testing. Arteries were inflated incrementally up to 200 mmHg and the length and diameter measured at each increment. From these measurements the percentage diameter change was calculated and is displayed in Figure 4.11, and the percentage length change was calculated and is displayed in Figure 4.12. Means for percentage diameter and length change at 100 mmHg were arcsine transformed before being statistically compared by analysis of variance ; $p>0.05$. The results are shown in Table 4.1 and Table 4.2, respectively. After 200 mmHg arteries were inflated to rupture.

Native and acellular arteries exhibited a slightly steeper incline below 40 mmHg before maintaining a linear increase in percentage diameter change. At 100 mmHg there were no significant differences (ANOVA; $p>0.05$) in percentage diameter change.

Native and acellular arteries exhibited a linear constant rate of percentage length change with increasing pressure there. At 100 mmHg there were no significant differences (ANOVA; $p>0.05$) in percentage diameter length.

All arteries exceeded a burst pressure of 3000 mmHg.

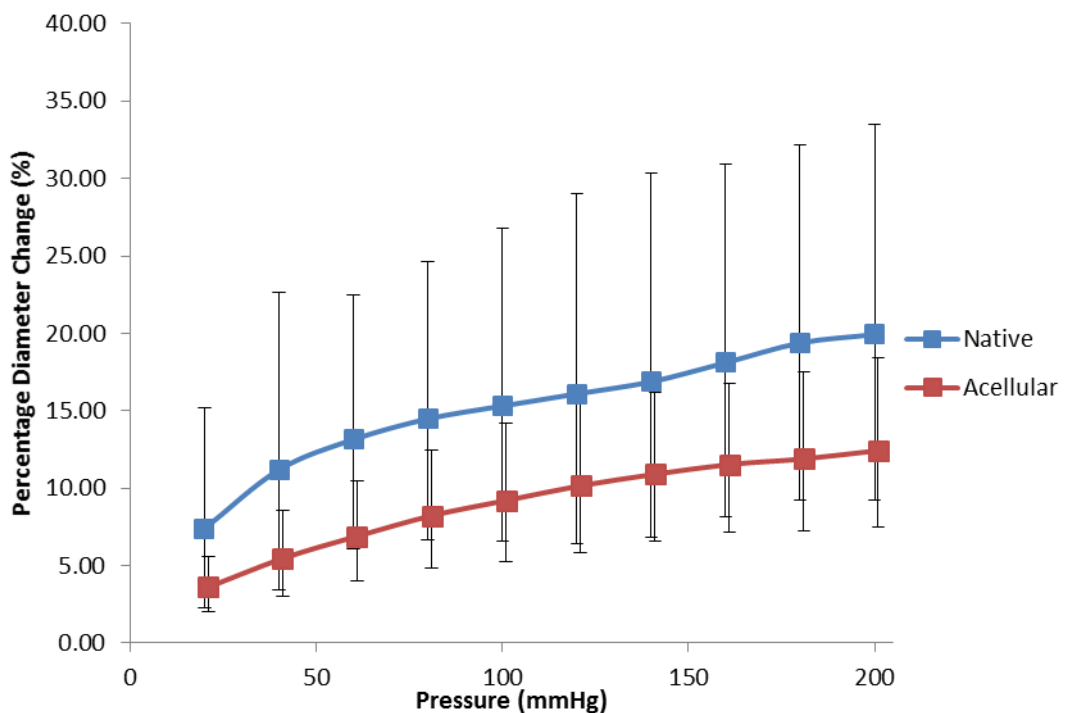


Figure 4.11 : Average Percentage Diameter Change of Native and Acellular Arteries with Increasing Pressure.

Averaged percentage diameter increase curves of native (n=3) and acellular (n=5) arteries with increasing pressure. Data was arcsine transformed and analysed by one way ANOVA, $p>0.05$ and then back transformed for presentation purposes. Data expressed as the mean \pm 95 % C.L.

Table 4.1 : Average Percentage Diameter Change of Native and Acellular Arteries at 100 mmHg

Percentage Diameter Change (100 mmHg)			Acellular		
Native					
Mean	Upper 95 % CL	Lower 95 % CL	Mean	Upper 95 % CL	Lower 95 % CL
15.31	11.47	8.70	9.21	4.98	3.99

Data was arcsine transformed and analysed by one way ANOVA which showed no significant difference ($p>0.05$) and then back transformed for presentation purposes. Data expressed as the mean \pm 95 % C.L. Means were not significantly different.

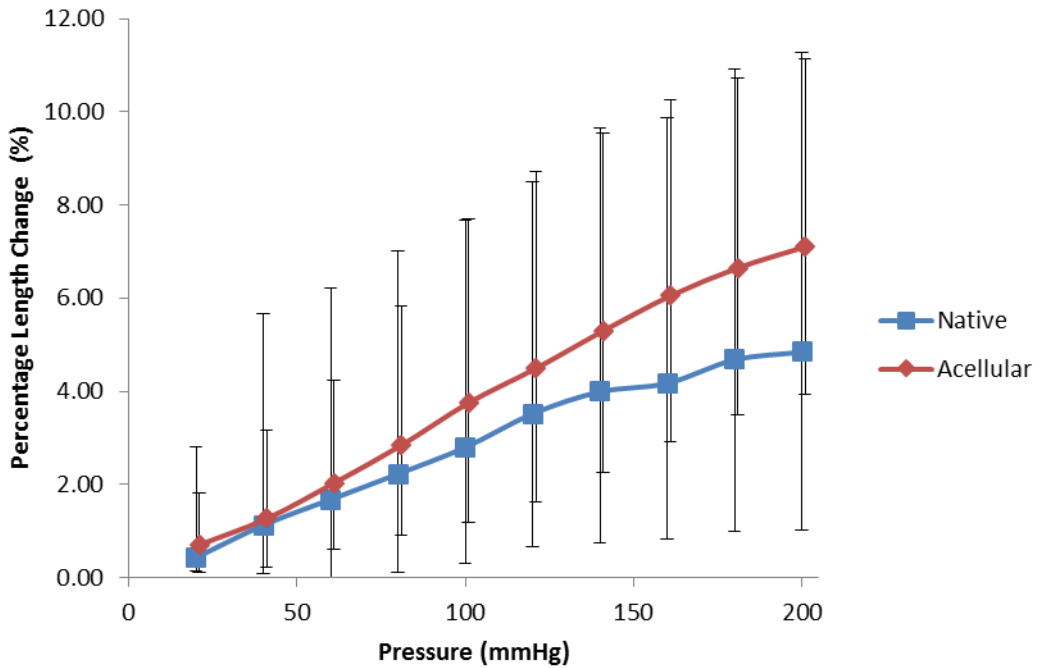


Figure 4.12 : Average Percentage Length Change of Native and Acellular Arteries with Increasing Pressure.

Averaged percentage length change curves of native (n=3) and acellular (n=5) arteries with increasing pressure. Data was arcsine transformed and analysed by one way ANOVA, $p>0.05$ and then back transformed for presentation purposes. Data expressed as the mean \pm 95 % C.L.

Table 4.2 : Average Percentage Length Change of Native and Acellular Arteries at 100 mmHg

Percentage Length Change (100 mmHg)			Acellular		
Native					
Mean	Upper 95 % CL	Lower 95 % CL	Mean	Upper 95 % CL	Lower 95 % CL
2.79	4.88	2.49	3.75	3.94	2.57

Data was arcsine transformed and analysed by one way ANOVA which showed no significant difference ($p>0.05$) and then back transformed for presentation purposes. Data expressed as the mean \pm 95 % C.L. Means were not significantly different.

4.4.2 Investigation Of The Effects Of Preloading In Tensile Testing Of Native And Acellular Porcine Carotid Artery Tissue

4.4.2.1 Effects of Varying Preload on Individual Parameters Extracted from Stress Strain Curves

Three native arteries and six acellular arteries were subjected to uniaxial tensile testing in both the axial and circumferential directions. The data was then manipulated to apply varying levels of preloading. This was carried out by zeroing the force extension curves at increasing levels of loading (0.01, 0.02, 0.05, 0.10 and 0.20 N) and then creating stress strain curves with transformed data. Six parameters: transition strain, transition stress, ultimate tensile strain, ultimate tensile stress, collagen modulus and elastin modulus were extracted from the data at each level of preload and were compared using two way ANOVA (tissue type vs preload) and the Tukey post-hoc test ($p < 0.05$). The results are presented as average stress strain curves in Figure 4.13 and Figure 4.14 and the extracted parameters are displayed in Table 4.3-Table 4.8. Each stress strain curve exhibited biphasic characteristics with an initial shallow gradient in which the artery was more extensible followed by a secondary steep gradient in which the artery became stiffer and less extensible. Varying the levels of preloading had little effect on the transition stress, ultimate tensile stress and collagen modulus parameters; no significant differences between testing without preloading were found below 0.2 N of preloading. Transition strain and ultimate tensile strain parameters were the most sensitive to variations in the level of preload. These parameters were significantly lower at 0.02 N of preload compared to 0 N of preload. There were also significant effects on the elastin modulus but at much higher levels of preload with significantly lower results beginning at 0.1 N of preload when compared to 0 N of preload.

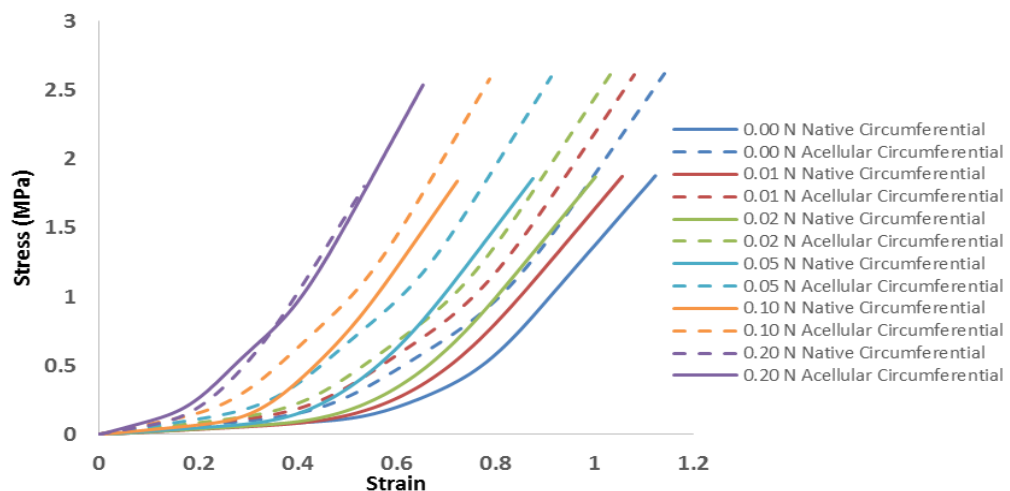


Figure 4.13 Average Stress Strain Curves of Native and Acellular Arteries Tested in the Circumferential Direction at Varying Levels of Preload

Stress strain curves of native ($n=3$) and acellular ($n=6$) arteries exhibited biphasic characteristics. The initial phase had a shallow gradient in which was more extensible under stress. The second phase had a steeper gradient in which the artery became stiffer and less extensible under stress. Applying preload showed little effect on the ultimate tensile stress and the gradient of the second phase however the initial phase showed an increased gradient as well as large reduction in strain parameters.

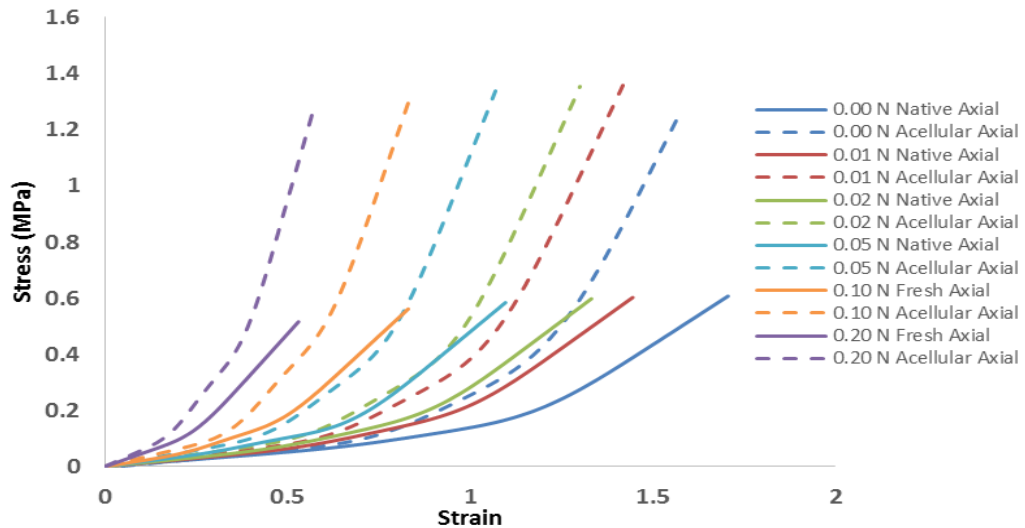


Figure 4.14 Average Stress Strain Curves of Native and Acellular Arteries Tested in the Axial Direction at Varying Levels of Preload

Stress strain curves of native (n=3) and acellular (n=6) arteries exhibited biphasic characteristics. The initial phase had a shallow gradient in which was more extensible under stress. The second phase had a steeper gradient in which the artery became stiffer and less extensible under stress. Applying preload showed little effect on the ultimate tensile stress and the gradient of the second phase however the initial phase showed an increased gradient as well as large reduction in strain parameters.

Table 4.3 : The Average Transition Strain for Native and Acellular Arteries in the Circumferential and Axial Direction at Varying Levels of Preload

Transition Strain Preload	Mean ± 95 % CL					
	0.00 N	0.01 N	0.02 N	0.05 N	0.10 N	0.20 N
Native Circumferential	0.66±0.07	0.61±0.01	0.57±0.11	0.47±0.11*	0.36±0.08*	0.22±0.04*
Native Axial	0.85±0.51	0.67±0.25	0.6±0.22	0.45±0.18*	0.29±0.2*	0.11±0.16*
Acellular Circumferential	0.6±0.09	0.55±0.08	0.52±0.07	0.43±0.06*	0.34±0.05*	0.24±0.04*
Acellular Axial	0.97±0.06	0.85±0.05	0.77±0.06*	0.6±0.07*	0.43±0.09*	0.24±0.09*

Data was analysed by analysis of variance and individual differences between group means determined by the Tukey post-hoc test p<0.05. *significantly different from the same tissue type at 0.00 N preload.

Table 4.4 : The Average Transition Stress for Native and Acellular Arteries in the Circumferential and Axial Direction at Varying Levels of Preload

Transition Stress Preload	Mean ± 95 % CL (MPa)					
	0.00 N	0.01 N	0.02 N	0.05 N	0.10 N	0.20 N
Native Circumferential	0.28±0.14	0.27±0.14	0.27±0.15	0.27±0.16	0.26±0.15	0.24±0.15
Native Axial	0.11±0.04	0.1±0.04	0.1±0.04	0.09±0.05	0.08±0.06	0.05±0.06
Acellular Circumferential	0.46±0.14	0.46±0.14	0.46±0.14	0.46±0.14	0.46±0.14	0.46±0.14
Acellular Axial	0.26±0.07	0.26±0.07	0.26±0.07	0.25±0.07	0.24±0.07	0.21±0.07

Data was analysed by analysis of variance which showed no significant effect of the preload on a given tissue type.

Table 4.5 : The Average Ultimate Tensile Strain for Native and Acellular Arteries in the Circumferential and Axial Direction at Varying Levels of Preload

Ultimate Tensile Strain Preload	Mean ± 95 % CL					
	0.00 N	0.01 N	0.02 N	0.05 N	0.10 N	0.20 N
Native Circumferential	1.12±0.03	1.06±0.03	1±0.05*	0.88±0.06*	0.72±0.04*	0.53±0.02*
Native Axial	1.71±0.52	1.45±0.4	1.33±0.37*	1.1±0.22*	0.83±0.07*	0.53±0.04*
Acellular Circumferential	1.14±0.15	1.08±0.13	1.03±0.12	0.91±0.1*	0.79±0.07*	0.65±0.07*
Acellular Axial	1.57±0.08	1.42±0.1	1.3±0.11	1.07±0.14*	0.83±0.16*	0.57±0.15*

Data was analysed by analysis of variance and individual differences between group means determined by the Tukey posy-hoc test p<0.05. *significantly different from the same tissue type at 0.00 N preload.

Table 4.6 : The Average Ultimate Tensile Stress for Native and Acellular Arteries in the Circumferential and Axial Direction at Varying Levels of Preload

Ultimate Tensile Stress Preload	Mean ± 95 % CL (MPa)					
	0.00 N	0.01 N	0.02 N	0.05 N	0.10 N	0.20 N
Native Circumferential	1.88±1.64	1.87±1.64	1.87±1.64	1.86±1.64	1.84±1.64	1.8±1.64
Native Axial	0.61±0.41	0.6±0.41	0.6±0.41	0.58±0.41	0.56±0.4	0.52±0.39
Acellular Circumferential	2.62±0.67	2.61±0.67	2.61±0.67	2.6±0.67	2.58±0.67	2.54±0.67
Acellular Axial	1.36±0.44	1.36±0.44	1.35±0.44	1.34±0.44	1.31±0.44	1.26±0.44

Data was analysed by analysis of variance which showed no significant effect of the preload on a given tissue type.

Table 4.7 : The Average Collagen Modulus for Native and Acellular Arteries in the Circumferential and Axial Direction at Varying Levels of Preload

Collagen Modulus Preload	Mean ± 95 % CL (MPa)					
	0.00 N	0.01 N	0.02 N	0.05 N	0.10 N	0.20 N
Native Circumferential	4.12±4.12	4.26±4.19	4.38±4.29	4.73±4.69	5.14±5.09	5.78±5.75
Native Axial	0.84±0.63	0.93±0.58	0.97±0.62	1.08±0.66	1.2±0.72	1.43±0.79
Acellular Circumferential	5.19±1.71	5.32±1.71	5.45±1.72	5.75±1.77	6.14±1.86	6.52±1.85
Acellular Axial	2.57±0.84	2.75±0.89	2.9±0.93	3.29±1.06	3.79±1.19	4.54±1.36

Data was analysed by analysis of variance which showed no significant effect of the preload on a given tissue type.

Table 4.8 : The Average Elastin Modulus for Native and Acellular Arteries in the Circumferential and Axial Direction at Varying Levels of Preload

Elastin Modulus Preload	Mean ± 95 % CL (MPa)					
	0.00 N	0.01 N	0.02 N	0.05 N	0.10 N	0.20 N
Native Circumferential	0.22±0.2	0.19±0.07	0.21±0.09	0.25±0.09	0.35±0.08	0.63±0.19*
Native Axial	0.1±0.08	0.12±0.1	0.13±0.1	0.17±0.1	0.21±0.12	0.47±0.38*
Acellular Circumferential	0.32±0.11	0.37±0.1	0.42±0.11	0.54±0.18	0.72±0.28*	0.97±0.31*
Acellular Axial	0.13±0.04	0.15±0.04	0.17±0.05	0.23±0.05	0.31±0.06*	0.57±0.14*

Data was analysed by analysis of variance and individual differences between group means determined by the Tukey posy-hoc test p<0.05. *significantly different from the same tissue type at 0.00 N preload.

4.4.2.2 Preload Selection

The toe region of force extension curves was inspected for extension of hyper relaxed samples (Figure 4.15). Samples inspected were native and acellular porcine carotid arteries in the circumferential and axial direction. Observable extension due to hyper relaxation was only identified in one sample and the sample became taught at less than 0.01 N.

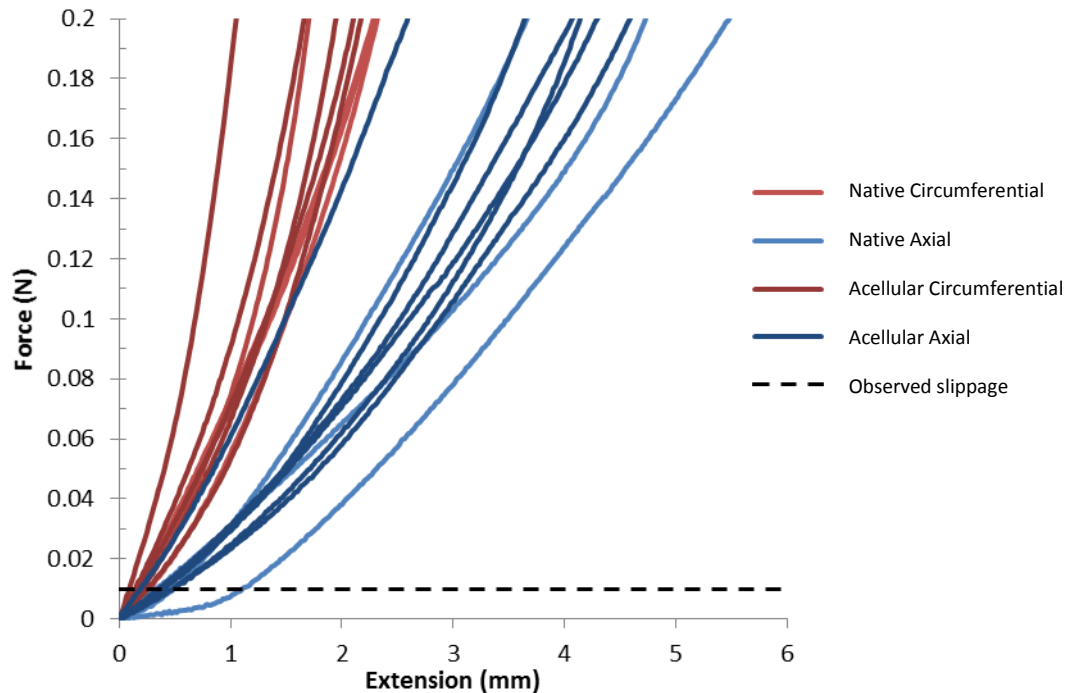


Figure 4.15 : Force Extension Curves of Native and Acellular Porcine Carotid Arteries in the Circumferential and Axial Directions.

4.4.2.3 Comparison of parameters derived from low strain rate to failure testing of native and acellular arteries at 0.01 N

The average stress strain curves at 0.01 N preload for the native and acellular arteries tested in the circumferential and axial directions are presented in Figure 4.16 and Figure 4.17. Analysis of the data presented in Tables 4.3-4.8 using two-way analysis of variance (tissue type vs pre-load) allowed comparison of the parameters derived from the low strain rate to failure testing of native and acellular arteries in the axial and circumferential directions at 0.01N pre-load. Six parameters were compared: transition strain, transition stress, ultimate tensile strain, ultimate tensile stress, collagen modulus and elastin modulus. The elastin modulus of acellular arteries was significantly greater than the elastin modulus of native arteries in the both the circumferential and axial directions (Table 4.8; $p < 0.05$). The collagen modulus of acellular arteries in the circumferential direction was not significantly different than the collagen modulus of the native arteries, however, there was a significant increase ($p < 0.05$) in the axial direction following decellularisation (Table 4.7). The transition strain in acellular arteries was not significantly different in the circumferential direction when compared to native arteries (Table 4.3; $p > 0.05$) but was significantly higher ($p < 0.05$) in the axial

direction when compared to native arteries. The transition stress of acellular arteries was significantly higher (Table 4.4; $p < 0.05$) in both the axial and circumferential directions when compared to native arteries. The ultimate tensile strain was not significantly different in acellular arteries when compared to native arteries in either the circumferential or axial direction. The ultimate tensile stress in the acellular arteries in both the circumferential and axial directions was significantly higher (Table 4.6 ; $p < 0.05$) in acellular arteries when compared to native arteries. A summary of the changes in the material properties of the porcine carotid arteries as a result of the decellularisation process is presented in Table 4.9.

Table 4.9 : Changes in the mechanical parameters of porcine carotid arteries post decellularisation in the circumferential and axial directions.

Native vs Acellular	Significant difference ($P < 0.05$) post decellularisation					
	Elastin Modulus	Collagen Modulus	Transition Strain	Transition Stress	Ultimate Tensile Strain	Ultimate Tensile Stress
Circumferential	↑	×	×	↑	×	↑
Axial	↑	↑	↑	↑	×	↑

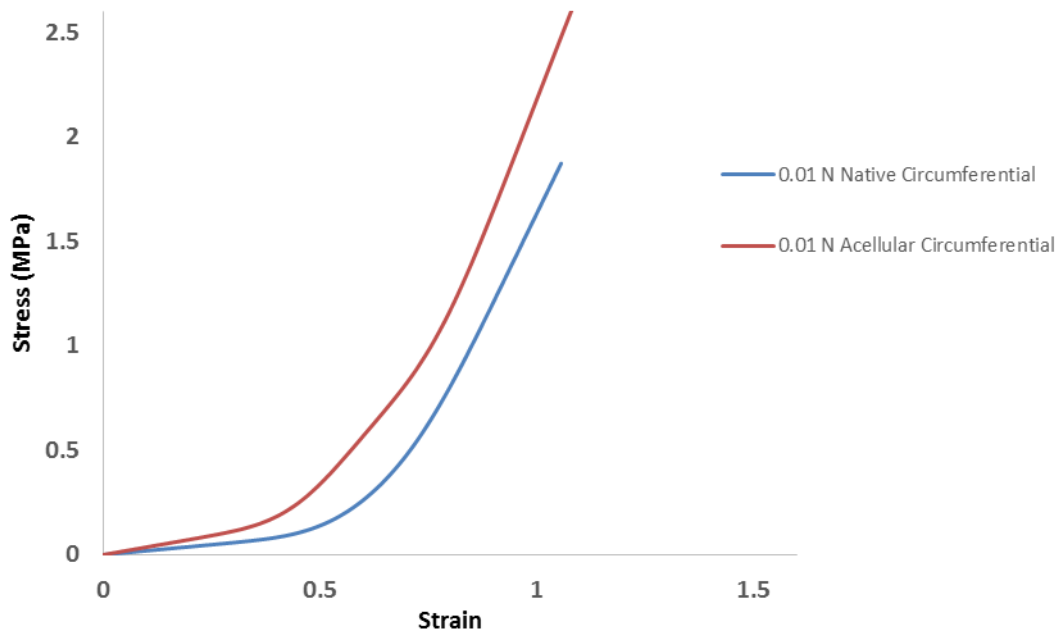


Figure 4.16 : Average Stress Strain Curves of Native and Acellular Arteries Tested in the Circumferential Direction at 0.01 N preload.

Stress strain curves of native ($n=3$) and acellular ($n=6$) arteries exhibited biphasic characteristics. The initial phase had a shallow gradient in which was more extensible under stress. The second phase had a steeper gradient in which the artery became stiffer and less extensible under stress. There was a distinct upward and left shift of the acellular curve compared to the native arteries curve.

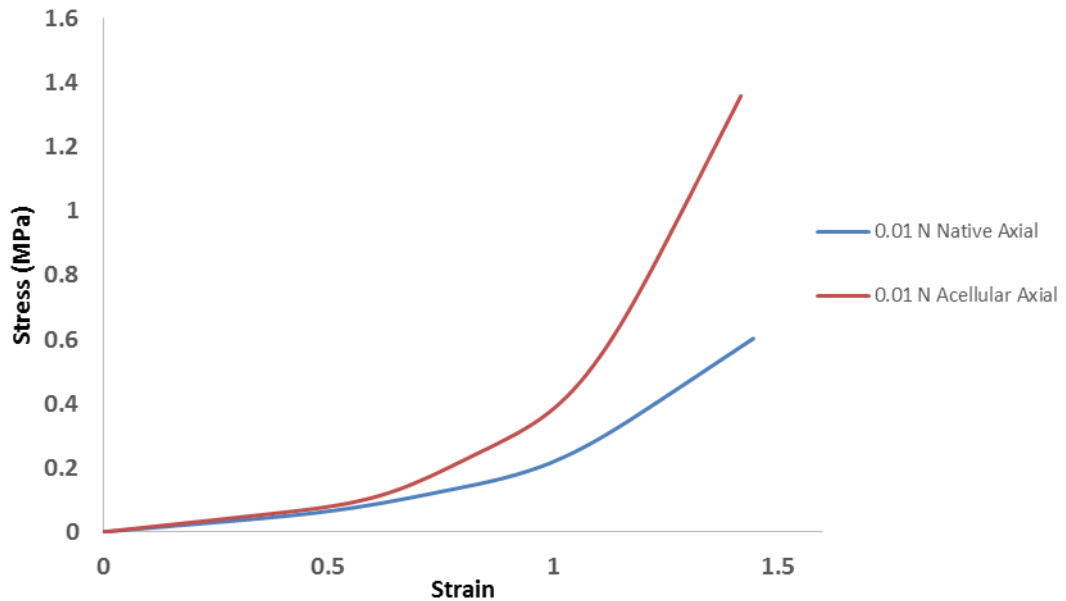


Figure 4.17 : Average Stress Strain Curves of Native and Acellular Arteries Tested in the Axial Direction at 0.01 N preload.

Stress strain curves of native (n=3) and acellular (n=6) arteries exhibited biphasic characteristics. The initial phase had a shallow gradient in which was more extensible under stress. The second phase had a steeper gradient in which the artery became stiffer and less extensible under stress. There was a distinct upward and left shift of the acellular curve compared to the native arteries curve.

4.5 Discussion

The mechanical properties of arteries are largely influenced by the quantity and orientation of collagen and elastin. The compliance properties are attributable to the highly branched and extensible characteristics of elastin. The overall strength of an artery is greatly dictated by the stiffness characteristics of collagen.

It was important to develop a robust method for the determination of mechanical properties so that the effects of decellularisation on native arteries could be assessed and enable further studies of the effects of sterilisation processes on the acellular arteries.

The method that had previously been developed to determine compliance and burst pressure testing was not robust. The arteries were free to orientate in space and would follow the natural curvature of the artery when pressurised and cause exaggerated movement below and across the plane of view making the determination of the compliance subject to large amounts of variance. Equally the fixed position method caused arteries to bend out of plane and therefore it was difficult to take accurate measurements. The manually adjusted method resulted in the artery being taught in the plane of view when images were captured, however it was difficult to control how much tension was being applied and therefore this gave rise to fluctuations in the measurements in between pressure increments. The constant weight method provided a method of applying a consistent load to the arteries and kept them in the plane of view for taking accurate measurements. The load applied can also be considered to replicate the internal tension of the artery under physiological conditions. When the method

was repeated with arteries it was clear by the small 95 % CL that the method was robust. It was then necessary to determine how much load was required to keep the arteries taught under increasing pressure. By measuring the percentage diameter change it was apparent that arteries loaded with 10 or 15 g weights had become aligned and there were no significant differences between data presented using 10 or 15 g weights.. Arteries loaded with 5 g weights resulted in percentage diameter changes that were significantly lower below 40 mmHg than arteries loaded with 10 or 15 g weights.. By examining the percentage length change it was evident that a change in load affected the initial extension on the artery which remained constant over the test. The 5g load produced significantly smaller increase in length than the 10 or 15 g loads below 40 mmHg. The combination of these two observations justified the selection of a 10 g load for future compliance tests as this was the minimum load that provided stability.

Determination of the appropriate preload to apply to a soft tissue is an important factor to be considered before analysing any properties derived from stress strain curves. Preloading is used to negate the effects caused by hyperrelaxation of samples allowing increased extension of a sample without increased load. However, applying too great a preload could cause other effects on the parameters derived from stress strain curves and when making comparison between groups. None of the stress parameters were significantly affected by the level of preloading. The moduli were also minimally affected by the level of preloading. Although there were some significant increases in the elastin modulus at the highest level of preloading, which can be explained by the fact that the elastin phase is subject to larger deformations under load than the collagen modulus. The parameters most affected by the level of preload were the strain parameters since these were concerned with extension and original length. With increased preloading the extension value was reduced and the original length value was increased. The strain is determined by dividing an increasingly smaller number by an increasingly larger number thus leading to a reduction of strain values with increased preload. This effect had the potential to mask differences between groups by causing stress-strain curves to become increasingly aligned.

The correct level of preloading for a particular system can be selected by a combination of two factors. Firstly the lowest value of preload that does not give rise to a significant difference in parameters compared to none preloaded samples. Secondly, the minimum level needed to negate any extension due to hyperrelaxation observed by inspection of the toe region. Ideally each individual curve should be analysed for the correct level of preloading for that curve. It was clear by inspection of the toe region of the stress-strain curves that a minimum of 0.01 N of preloading was required for the system used and at this level there were no significant differences compared to non-preloaded samples.

Having developed robust methods to determine compliance and uniaxial tensile testing a comparison of mechanical properties between native and acellular arteries could be made to

determine the effects of decellularisation. There were significant differences in the mechanical properties of acellular arteries caused by the decellularisation process when compared to native arteries. These effects are seen to varying levels dependent on the orientation of the tissue. However, the characteristic biphasic shape of the arterial stress strain curves remained.

By visual inspection of the percentage length change during compliance testing, both native and acellular arteries increased linearly, but there was a high degree of variation in the data, indicated by the large 95% CL. There was no significant difference between the percentage length change of native and acellular arteries at 100 mmHg. By visual inspection of the percentage diameter change curves with increasing pressure, both native and acellular arteries had an initial steeper slope, where the artery expanded more under pressure followed by a longer shallow slope, where the deformation was less with increasing pressure. When comparing native and acellular arteries it was evident that the acellular arteries dilated less than native arteries and there was a trend towards reduced compliance, however there was no significant difference in the percentage diameter change at 100 mmHg. Albeit using different methods for the determination of compliance, these results correlated well with previous findings, which found no significant differences between the compliance of acellular porcine ureters (Derham *et al.*, 2008) and femoral arteries (Wilshaw *et al.*, 2012) and their respective native tissues.

It is important to maintain compliance in vascular grafts close to that of the analogous tissue which it is replacing. It is widely accepted that compliance mismatch can contribute considerably to the failure of a vascular graft and is reflected in clinical outcomes shown in Table 4.10.

Table 4.10 : Patency Rates and Compliance Values of Clinically Used Vascular Grafts.

Graft Type	Compliance % / 100 mmHg	Patency
Host artery	5.9 ±0.5	
Saphenous vein	4.4 ± 0.8	75
Umbilical Vein	3.7 ±0.5	60
Bovine Heterograft	2.6±0.3	59
Dacron	1.9±0.3	50
PTFE	1.6±0.2	40

Data adapted from Salacinski *et al.* (2001)

Grafts with too great a compliance may become aneurysmal (Khaira & Vohra, 2002; Van Damme *et al.*, 2005) and those that lack compliance develop intimal hyperplasia (Bassiouny *et al.*, 1992). This is a major factor in surgeries in which the artery anastomoses are attached in an end to side configuration. There is an increased incidence in intimal hyperplasia in less compliant grafts at the distal anastomosis (Sottiurai *et al.*, 1989; Trubel *et al.*, 1994), where there are higher stresses at the suture line (Ballyk *et al.*, 1998) and, on the bed floor on the opposing host artery, where stagnation occurs (Morinaga *et al.*, 1985). Interestingly when

looking at autologous grafts used for coronary artery bypass grafts, the saphenous vein has a much higher incidence of intimal hyperplasia related occlusion when compared to the more compliant internal mammary artery (Mitra *et al.*, 2006). Considering this the internal mammary artery has been found to have a compliance of $11.5 \pm 3.9 \% / 100 \text{ mmHg}$ (Konig *et al.*, 2009), which matches closely to acellular porcine carotid arteries ($9.21 + 4.98 - 3.99 \% / 100 \text{ mmHg}$), therefore although native and acellular porcine carotid arteries were not significantly different it may be that the decellularisation process is having a beneficial effect by reducing the compliance closer to the desired compliance of analogous tissue.

However, it is difficult to truly compare these results due to the wide discrepancies in the methods used for the determination of compliance. There are guidelines set out in ISO 7198 (International Standard ISO/DIS 7198, 1998), however, this standard leaves a large amount of interpretation open to the reader. To truly compare results either a standardised model needs to be adopted for compliance testing or a range of data using host arteries needs to be collated using the same test method to identify when ideal properties are being met.

The parameters derived from stress-strain curves created from uniaxial tensile testing data can further help in the understanding of the biomechanics of native and acellular vascular porcine carotid arteries. Perusal of the stress strain curves from the uniaxial tensile tests showed that the curves for the acellular arteries shifted upwards and to the left indicating a decreased extensibility and increased strength compared to native arteries. This could explain the trend in the compliance being lower in acellular porcine carotid arteries than native porcine carotid arteries.

In the circumferential and axial directions the ultimate tensile stress, the transition stress and the elastin modulus were significantly higher in acellular porcine carotid arteries than native porcine carotid arteries. The collagen modulus of acellular porcine carotid arteries was also significantly higher in the axial direction, when compared to native porcine carotid arteries. It is expected to find some differences in the mechanical data owing solely to the natural variance of the porcine arteries between animal to animal, however there is an indication from this data that the decellularisation process is causing an increased stiffness particularly affecting the elastin in the artery, which would again explain the slight trend towards a reduced compliance. This could be due to conformational changes in the structure and the incompressibility of water. With the absence of cells, an intake of water into the interstitial spaces of ECM may be providing a small increase in stiffness.

There were no significant differences in the ultimate tensile strain in either circumferential or axial directions when comparing native and acellular porcine carotid arteries indicating that the extensibility was not compromised significantly by the decellularisation process, which mirrors the results found with the compliance testing. However, the transition strain was significantly higher in the axial direction of acellular porcine carotid arteries when compared to native porcine carotid arteries. This was contrary to the compliance data found. These results

may not be indicative of the true picture; the transition strain is determined to be where the tangent of the collagen slope intercepts with x axis, if the collagen modulus is changed the transition point changes. If the collagen modulus becomes stiffer a greater transition strain will be recorded and if it becomes weaker then a lower transition strain will be recorded, when in reality the transition start may not have actually changed. This observation can also be seen in previous work with parameters derived from stress-strain curves for native and acellular porcine ureter in the circumferential direction where the transition stress has increased but the elastin modulus has decreased. This can only be accounted for by the increase in collagen modulus bringing the transition strain forward (Derham *et al.*, 2008). It is therefore worth considering calculation of the transition point in an alternative manner for future studies. A proposed method to account for this would be to create a line at the intercept between the collagen and elastin slope tangents that is of equal angle to the collagen and elastin slope tangents. This is depicted in Figure 4.18.

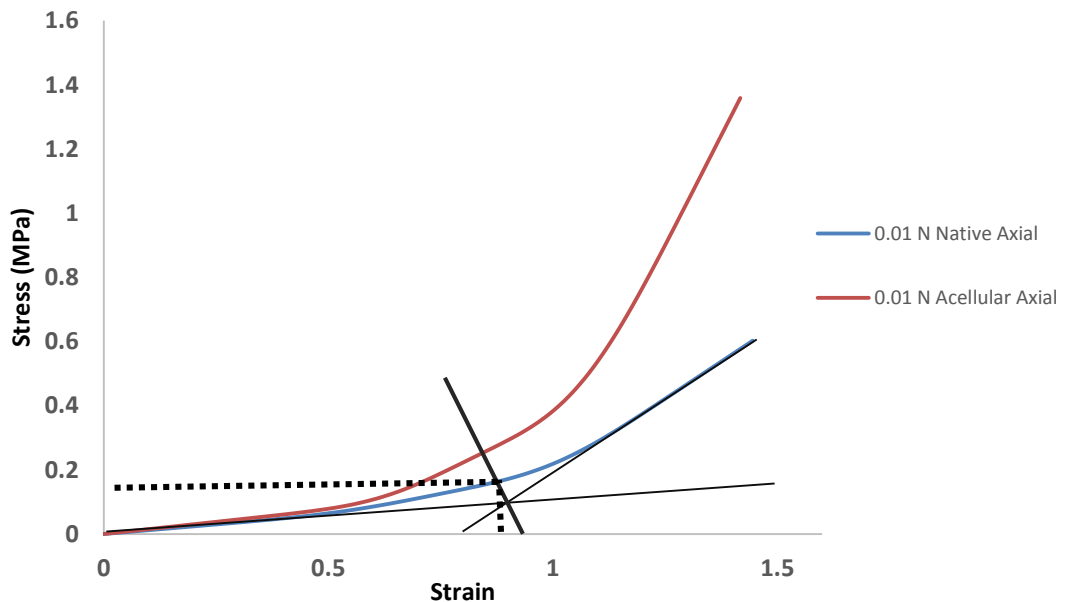


Figure 4.18 : Proposed Method to Calculate the Transition Strain Using a Line of Equal Angle Between the Tangents of the Collagen and Elastin Slopes.

When comparing mechanical properties of the porcine carotid artery obtained using uniaxial tensile testing to data presented by other research groups it is difficult to make true comparisons due to the varied test methods used. The main difference is either testing a ringlet of artery vs a strip of artery being loaded under tension. The ringlet method has limitations since it can only be used for testing mechanical properties in the circumferential direction and the strip method must then be adopted to obtain the properties in the axial direction. One study of the biomechanics of the vertebral artery compared the ringlet method in the circumferential direction with the strip method in the axial direction and the study indicated that the arteries were anisotropic (Johnson *et al.*, 2000). It may have been prudent in addition to compare ringlets and strips in the same direction to establish whether any

differences were found in the methods. The anisotropy correlated well with arterial structure in which longitudinally the strength is weaker than in the circumferential direction. The range in UTS was approximately 0.5 to 2 MPa and the elastic modulus ranged from approximately 1 to 5 MPa. The advantage of the ringlet method is that it eliminates the clamping issues found with the strip method. In the strip method, often failure at the grips can occur if too much compression is applied and slippage occurs if too little tension is applied. If the tissue breaks at the grips then an underestimation of the UTS may occur and so it is important check the break point of a sample, however when dealing with small samples this may be difficult to identify. Another common difference in test methods used by different groups is whether a biobath is used. This can be used to maintain hydration of the sample and the temperature. Alternatively, PBS spray has been used to maintain hydration, however the problem with this method is that it is not possible to determine whether the sample has been fully soaked in PBS and what intervals of spraying are required to maintain hydration.

Overall consideration of the effects of the decellularisation process on the mechanical integrity of the arteries indicated they were maintained. There were changes to the mechanical properties some of which can be attributed to the natural variance in porcine arteries from animal to animal. There is a slight trend to a reduction in compliance and increase in elastic stiffness, however the mechanical properties of the acellular porcine carotid arteries were similar to those of host arteries.

Now that robust methods to establish the mechanical properties of native and acellular porcine carotid arteries had been achieved, the effects of sterilisation processes on the mechanical properties could be compared, and this is the focus of the research described in the following chapter.

Chapter 5 Mechanical properties of Sterilised Acellular Porcine Carotid Arteries

5.1 Introduction

In the research and development of novel biological grafts, sterilisation of the final product is an important aspect to be considered, which is often overlooked during the early phases. It is absolutely necessary for an implantable medical device to be sterile before being used clinically. This is carried out by ensuring that the device has a minimum sterility assurance level of 10^{-6} , this gives the probability of a microorganism being present on the device as 1 in a million. The most common and historical industry practiced sterilisation processes are: dry heat, moist heat, gas plasma, peracetic acid, Gamma irradiation, E-Beam irradiation and ethylene oxide (EO). Each of these processes utilises differing mechanisms and environments to inactivate microorganisms. Variables such as temperature, pressure, humidity and sterilisation mechanism can have detrimental effects on biological materials which could compromise the biological and mechanical function of biological grafts. For the sterilisation of acellular porcine carotid artery vascular grafts, several processes can be excluded from consideration due to: high temperatures, penetration depth and the desire for a terminal sterilisation process rather than chemical sterilisation followed by post-sterilisation aseptic processing. Therefore, the sterilisation processes selected for investigation in this study were limited to Gamma irradiation, E-Beam irradiation and EO sterilisation processes.

These three sterilisation methods inactivate microorganisms by causing structural instability in cells or by interrupting replication (as discussed in Chapter 1). Gamma and E-Beam irradiation ionise molecules and cause cleavage of covalent bonds in DNA. Ionisation and free radical formation, however might also have detrimental effects on the biochemical and biomechanical properties of biological vascular grafts. Ionising radiation has the ability to form crosslinks in elastin and collagen which can increase strength and stiffness. In addition, irradiation can cause chain scission which can shorten the length of the fibres which may have effects on elasticity. The mechanism of action of EO is via direct alkylation. This alkylation process restructures or denatures functional proteins, enzymes and DNA/RNA. This highly reactive alkylation mechanism also has the potential to alter the properties of biological vascular grafts. In order to apply EO sterilisation to acellular porcine carotid artery vascular grafts the graft must first be freeze-dried. Therefore it was necessary to determine the effects of freeze-drying on the graft material in addition to the effects of the EO sterilisation process.

The methods used to assess the biomechanical properties of the acellular porcine carotid artery vascular grafts before and after sterilisation treatment were developed and discussed

in Chapter 4. This chapter focuses on the effects of sterilisation processes on the biomechanical properties of acellular porcine carotid arteries.

5.2 Aims and objectives

The aims of this study were to investigate the effects of Gamma irradiation, E-Beam irradiation, freeze-drying and EO treatment on the biomechanical properties of acellular porcine carotid arteries

The specific objectives were:

- To subject acellular porcine carotid arteries to Gamma irradiation (30 kGy) and determine the effects on the properties of the arteries using uniaxial tensile, compliance and burst pressure testing.
- To subject acellular porcine carotid arteries to E-Beam irradiation (30 kGy) and determine the effects on the properties of the arteries using uniaxial tensile, compliance and burst pressure testing.
- To freeze-dry acellular porcine carotid arteries and determine the effects on the properties of the arteries using uniaxial tensile, compliance and burst pressure testing.
- To subject freeze-dried acellular porcine carotid arteries to EO sterilisation and determine the effects on the properties of the arteries using uniaxial tensile, compliance and burst pressure testing.

5.3 Materials and Methods

5.3.1 Arteries

Native porcine carotid arteries used in this chapter were procured and dissected according to the method described in Chapter 3; Section 3.3.1. Acellular arteries (n=57) were produced in three batches (Batches 2, 3 and 4; Chapter 3, Section 3.4.6) using the method described in Chapter 3; Section 3.3.2. Arteries from batches were then separated to be tested as quality controls or subject to sterilisation as follows:

Arteries from batch 2 were split into two groups:

1. Acellular porcine carotid arteries (n=7)
2. Acellular porcine carotid arteries to be processed by Gamma irradiation (n=8)

Arteries from batch 3 were split into three groups:

1. Acellular porcine carotid arteries (n=7)
2. Acellular porcine carotid arteries to be processed by Gamma irradiation (n=7)
3. Acellular porcine carotid arteries to be processed by E-Beam irradiation (n=7)

Arteries from batch 4 were split into three groups:

1. Acellular porcine carotid arteries (n=7)
2. Acellular porcine carotid arteries to be processed by freeze drying (n=7)
3. Acellular porcine carotid arteries to be processed by freeze drying followed by EO treatment. (n=7)

The sampling method of arteries for biological and mechanical evaluation has been described previously in Chapter 3; Section 3.3.3. Sampling method I was used to provide tissue for quantitative analyses including mechanical testing. Sampling method II was used for primarily qualitative analyses. Below is a table to show the sample size for sampling method I and II for each group within the batch.

Table 5.1: Sample Sizes for sampling method I and II for each batch of acellular arteries

Batch 2	SM I	SM II	Batch 3	SM I	SM II	Batch 4	SM I	SM II
Acellular	5	2	Acellular	5	2	Acellular	5	2
Gamma Irradiated	6	2	Gamma Irradiated	5	2	Freeze-Dried	6	1
			E-Beam Irradiated	5	2	Freeze-Dired EO Treated	5	2

5.3.2 Irradiation Sterilisation

Acellular arteries were placed on polyethyleneglycol (PEG) semi-circular supports to prevent flattening of the artery by the pressure of the packaging itself or from the vacuum process.

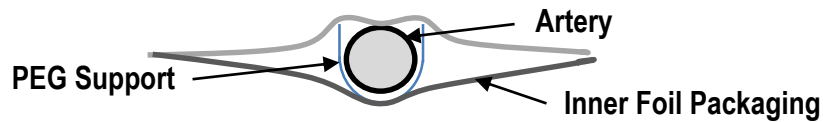


Figure 5.1 : Diagram of the artery support for packaging

Arteries were then vacuum sealed in an inner foil pouch and an outer Tyvek membrane pouch (Figure 5.2). Arteries were then couriered to Synergyhealth PLC and were either Gamma or E-Beam irradiated at a dose of 30 kGy (Minimum, 25 kGy).



Figure 5.2 : Acellular Artery on PEG Support Structure and Vacuum Sealed in Inner Foil Membrane and Outer Tyvek

5.3.3 Freeze Drying

Acellular arteries were placed on PEG semi-circular supports. Arteries were then freeze-dried under vacuum at $-60\text{ }^{\circ}\text{C}$ (Figure 5.3). to a constant weight. A constant weight was determined after three consecutive measurements differed to a resolution of $\pm 0.0001\text{ g}$ measured using a four figure balance



Figure 5.3 : Freeze Dried Acellular Arteries on PEG Support Structure

5.3.4 Ethylene Oxide Sterilisation

Acellular arteries were freeze-dried as described in Section 5.3.3. Arteries were then vacuum sealed in Tyvek membrane pouches, then couriered to Sterigenics International LLC and were treated using a low temperature ($<55\text{ }^{\circ}\text{C}$) ethylene oxide sterilisation cycle.

5.3.5 Rehydration Of Arteries

Reagents:

Physiological saline

Sodium chloride (0.85 g) was dissolved in 800 ml distilled water. The pH was adjusted to 7.0 – 7.4 using 6 M hydrochloric acid or 6 M sodium hydroxide drop wise whilst using a magnetic stirrer. The final volume was adjusted to 1 L using distilled water. The solution was sterilised by autoclaving.

Method:

Acellular freeze-dried and acellular freeze-dried EO treated arteries were rehydrated in physiological saline prior to sampling. Rehydration was determined after a constant weight was achieved using a four figure balance.

5.3.6 Mechanical Testing Of Samples

All sampling of arteries for mechanical testing was performed using sampling method I as described in Section 3.3.3. The sample sizes for mechanical testing deviated from intended; the actual sample sizes are presented in Table 5.2. During the setup of compliance testing, in

some arteries, holes in the arterial walls from arterial branching prevented testing in some samples and were discarded. During the setup of tensile testing, in some arteries, the curvature of the artery when being cut into strips sometimes caused non rectangular strips and therefore these samples were also discarded. The sample size of freeze dried arteries was increased as the determination of the mechanical properties due to freeze drying was more beneficial than the biological evaluation.

Table 5.2 : Intended (I) and Actual (A) Sample Sizes for Mechanical Testing

Batch	Test Method	Native		Acellular		Gamma		E-Beam		Freeze Dried		EO	
		I	A	I	A	I	A	I	A	I	A	I	A
3	Compliance	5	3	5	5	5	5	5	4				
	SS (Circumferential)	5	4	5	4	5	5	5	5				
	SS (Axial)	5	3	5	5	5	5	5	4				
4	Compliance	5	3	5	4					6	6	5	3
	SS (Circumferential)	5	4	5	5					6	6	5	5
	SS (Axial)	5	4	5	5					6	6	5	5

SS=Stress Strain

Native, acellular, acellular freeze-dried, acellular ethylene oxide treated, acellular Gamma irradiated and acellular E-Beam irradiated porcine carotid arteries were subjected to uniaxial tensile testing as described in Section 4.3.4 and compliance testing as described in Section 4.3.3. A sample of native porcine carotid arteries (n=3) fixed in NBF for 16 – 24 hours and were also mechanically tested. The NBF fixed arteries were used as a positive control for damage but were not included in the overall analysis of the data.

5.4 Results

5.4.1 Mechanical Properties of Gamma and E-Beam Irradiated Acellular Porcine Carotid Arteries

5.4.1.1 Uniaxial Tensile Testing of Gamma and E-Beam Irradiated Acellular Porcine Carotid Arteries

Native, native NBF fixed, acellular and acellular Gamma and E-Beam irradiated porcine carotid artery samples were subjected to uniaxial tensile testing in both the axial and circumferential directions. The data was then manipulated to apply a preload of 0.01 N. Six parameters: transition strain, transition stress, ultimate tensile strain, ultimate tensile stress, collagen modulus and elastin modulus were extracted from the data and were compared using one way ANOVA and Tukeys post-hoc test. The control NBF treated arteries were excluded from statistical analysis. The parameters extracted from the stress strain curves obtained for circumferential samples are presented in Table 5.3 and depicted as average stress strain curves in Figure 5.4. The parameters extracted from the stress strain curves obtained for axial samples are presented in Table 5.4 and depicted as stress strain curves in Figure 5.5.

In the circumferential direction, the ultimate tensile stress was significantly increased post decellularisation. Acellular arteries that had been Gamma irradiated had significantly stiffer elastin and collagen moduli and a significantly higher ultimate tensile stress compared to native arteries but were not significantly different to acellular arteries. In addition, acellular arteries that had been Gamma irradiated exhibited a significantly lower transition strain than native arteries but not significantly different than acellular arteries. Acellular arteries that underwent E-Beam irradiation had a significantly higher elastin modulus and a significantly lower transition strain compared to both native and acellular arteries. Acellular arteries that underwent E-Beam irradiation also had a significantly lower ultimate tensile strain compared to native arteries.

In the axial direction there were no significant differences between native and acellular arteries. Acellular arteries that underwent Gamma irradiation had a significantly lower transition strain compared to acellular arteries but otherwise showed no significant differences to native or acellular arteries. Acellular arteries that underwent E-Beam irradiation had significantly higher collagen modulus and transition stress than native and acellular arteries, the ultimate tensile stress was also significantly higher than in native arteries.

Table 5.3 : Parameters Extracted from Stress Strain Curves Derived from Low Strain Rate to Failure Uniaxial Tensile Testing in the Circumferential Direction Of Native, Acellular, Gamma and E-Beam Irradiated Porcine Carotid Arteries.

Tissue	Thickness (mm)	Elastin (MPa)	Collagen (MPa)	TStrain	TStress (MPa)	UTStrain	UTStress (MPa)
Native	0.91±0.29	0.17±0.04	2.7±1.14	0.77±0.15	0.26±0.14	1.68±1.03	1.58±0.52
Acellular	0.9±0.34	0.21±0.14	4.23±2.23	0.57±0.15	0.5±0.49	1.06±0.45	2.6±1.26*
Gamma	0.83±0.18	0.74±0.38*	5.69±2*	0.53±0.18*	0.61±0.14	1.05±0.23	2.74±0.2*
E-Beam	0.98±0.21	1.64±0.5***	4.49±1.14	0.29±0.09***	0.56±0.26	0.8±0.13*	2.27±0.59

Data is presented as the mean (Native, n=4; Acellular, n=4; Gamma, n=5; E-Beam, n=5) ± 95% CL. Data for each parameter was analysed by one way ANOVA and Tukey test (p<0.05). * Significantly different to native, *** Significantly different to native and acellular

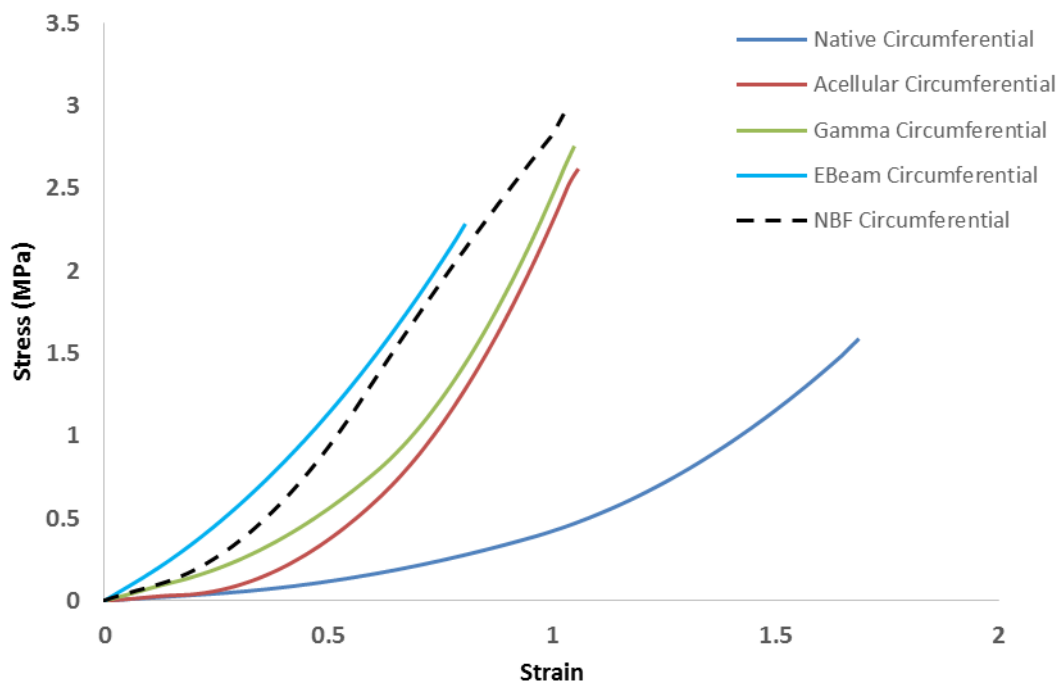


Figure 5.4 : Average Stress Strain Curves Derived From Low Strain Rate To Failure Uniaxial Tensile Testing In The Circumferential Direction Of Native, Acellular, Gamma And E-Beam Irradiated Porcine Carotid Arteries.

Acellular arteries showed a significant increase in ultimate tensile stress compared to native arteries. Acellular Gamma sterilised arteries showed significant stiffening of the collagen and elastin modulus and a significant increase in ultimate tensile stress compared to native arteries as well as a significant reduction in transition strain resulting in an observed shift of the curve upwards and to the left. Acellular E-Beam sterilised arteries had significantly higher collagen modulus and transition stress than native and acellular arteries. The ultimate tensile strain was also significantly higher than in native arteries. This resulted in a shift of the curve upwards and left past that of Gamma sterilised arteries and NBF fixed arteries.

Table 5.4 : Parameters Extracted From Stress Strain Curves Derived From Low Strain Rate To Failure Uniaxial Tensile Testing In The Axial Direction Of Native, Acellular, Gamma And E-Beam Irradiated Porcine Carotid Arteries.

Tissue	Thickness (mm)	Elastin (MPa)	Collagen (MPa)	TStrain	TStress (MPa)	UTStrain	UTStress (MPa)
Native	0.74±0.36	0.1±0.03	0.92±1.04	0.64±0.29	0.09±0.1	1.29±0.47	0.59±0.77
Acellular	0.63±0.16	0.14±0.03	2.06±0.71	0.8±0.21	0.19±0.09	1.43±0.23	1.21±0.4
Gamma	0.75±0.05	0.33±0.19	2.08±0.42	0.48±0.1**	0.21±0.05	1.21±0.43	0.98±0.12
E-Beam	0.84±0.2	0.31±0.2	3.4±1.79***	0.68±0.22	0.37±0.1***	1.17±0.15	1.46±0.7*

Data is presented as the mean (Native, n=3; Acellular, n=5; Gamma, n=5; E-Beam, n=4) ± 95% CL. Data for each parameter was analysed by one way ANOVA and Tukey test (p<0.05). * Significantly different to native, ** Significantly different to Acellular *** Significantly different to native and acellular

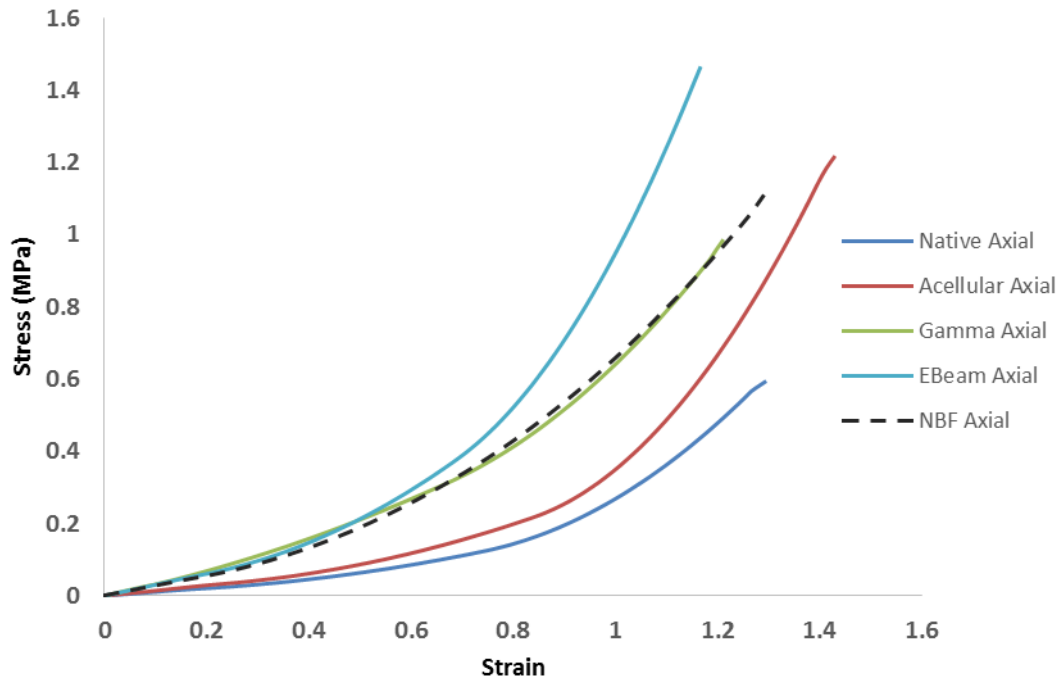


Figure 5.5 : Average Stress Strain Curves From Parameters Extracted From Stress Strain Curves Derived From Low Strain Rate To Failure Uniaxial Tensile Testing In The Axial Direction Of Native, Acellular, Gamma And E-Beam Irradiated Porcine Carotid Arteries.

Acellular arteries were not significantly different from native arteries in any of the six parameters. Acellular arteries sterilised by Gamma or E-Beam showed an upwards and left shift in the stress strain curve. Gamma sterilised arteries showed a significant decrease in transition strain when compared to acellular arteries and E-Beam Sterilised arteries had significant increases in collagen modulus and transition stress compared to native and acellular arteries as well as a significant increase in ultimate tensile stress compared to native arteries.

5.4.1.2 Compliance Testing of Gamma and E-Beam Irradiated Acellular Porcine Carotid Arteries

Native, acellular, acellular Gamma and E-Beam irradiated and NBF fixed porcine carotid arteries were subjected to burst pressure and compliance testing. Arteries were inflated incrementally up to 200 mmHg and the length and diameter measured at each increment. From these measurements the percentage diameter change was calculated and is displayed in Figure 5.6 and the percentage length change was calculated and is displayed in Figure 5.7. Data for the native, acellular, acellular Gamma and E-Beam irradiated artery groups was compared using one way ANOVA with Tukeys post hoc test ($p < 0.05$) at 100 mmHg for percentage diameter and length change and the results are shown in Table 5.5 and Table 5.6 respectively. After 200 mmHg arteries were inflated to rupture and all of the arteries tested burst above 3000 mmHg.

Native, acellular and acellular Gamma sterilised arteries exhibited an initial steeper incline before maintaining a linear increase in percentage diameter change. NBF fixed arteries showed very little increase in percentage diameter change and maintained a near constant value. Acellular E-Beam sterilised arteries had a constant decrease in percentage diameter change and maintained a constant rate with increasing pressure. With regard to percentage diameter change at 100 mmHg change there was no significant difference between native and acellular arteries, however acellular Gamma and E-Beam irradiated arteries had significantly lower percentage diameter change compared to native arteries and acellular E-Beam irradiated arteries also showed significantly lower percentage diameter change than acellular arteries.

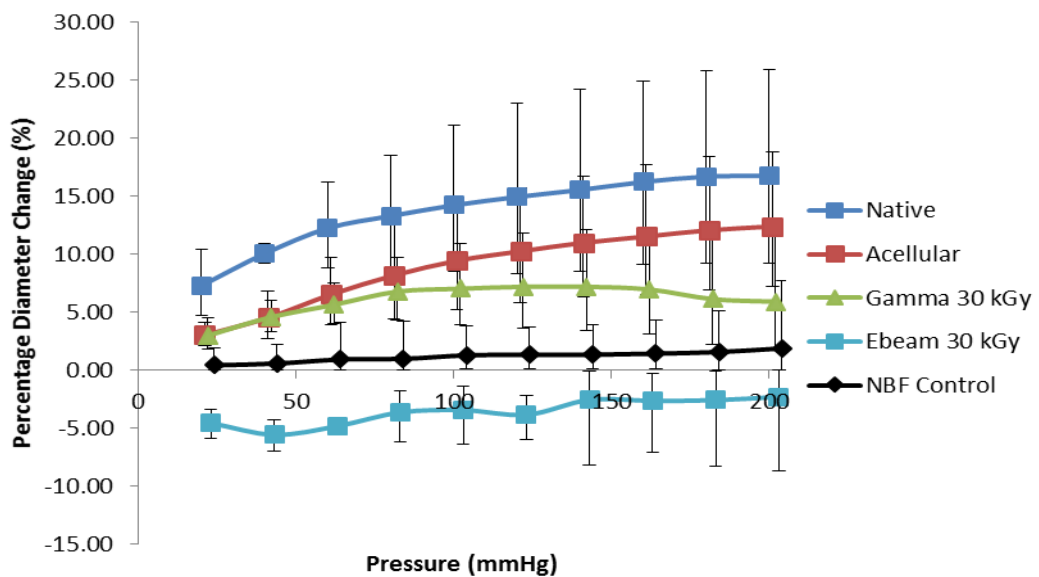


Figure 5.6 : Average Percentage Diameter Change of Native, Acellular, Acellular Gamma and E-Beam Irradiated and NBF fixed Arteries with Increasing Pressure.

Average percentage diameter change of native, acellular, acellular Gamma and E-Beam irradiated and NBF fixed arteries with increasing pressure. Data was arcsine transformed for calculation of the mean \pm 95 % CL and back transformed to percentages for presentation.

NBF fixed, acellular arteries exhibited a linear constant rate of percentage length change. Native and E-Beam sterilised arteries exhibited a linear but increasing percentage length change. Native and E-Beam irradiated arteries had significantly higher percentage length change compared to acellular arteries.

Table 5.5 - Average Percentage Diameter Change Native, Acellular, Acellular Gamma and E-Beam Irradiated Arteries at 100 mmHg

Percentage Diameter Increase (100 mmHg)											
Native			Acellular			Gamma			E-Beam		
Mean	Upper 95 % CL	Lower 95 % CL	Mean	Upper 95 % CL	Lower 95 % CL	Mean	Upper 95 % CL	Lower 95 % CL	Mean	Upper 95 % CL	Lower 95 % CL
14.22	6.89	5.72	9.44	5.24	4.18	7.02*	3.86	3.07	-3.44**	2.06	2.95

Data is presented as the mean (Native, n=3; Acellular, n=5; Gamma, n=5; E-Beam, n=4) ± 95% CL. Following arcsine transformation, data for each parameter was analysed by one way ANOVA and Tukey test (p<0.05). *Significantly different from Native, **Significantly different from native and acellular

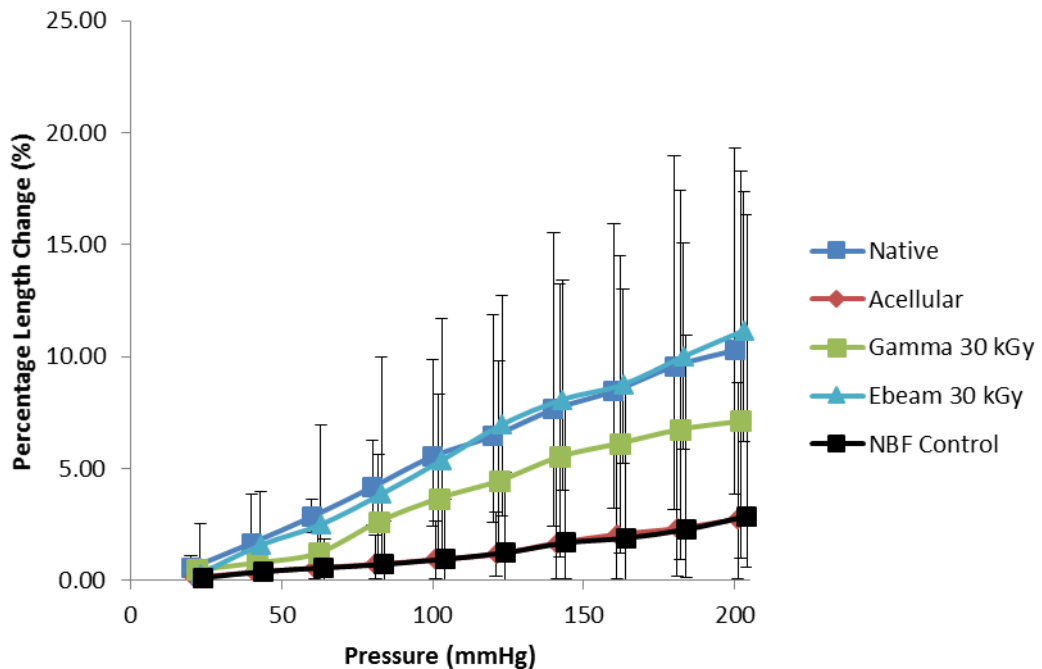


Figure 5.7 : Average Percentage Length Change of Native, Acellular, Acellular Gamma and E-Beam Irradiated and NBF fixed Arteries with Increasing Pressure.

Average Percentage Length Change of Native, Acellular, Acellular Gamma and E-Beam Irradiated and NBF fixed Arteries with Increasing Pressure. Data was arcsine transformed for calculation of mean ± 95% CL and back transformed to percentages for presentation.

Table 5.6 - Average Percentage Length Change of Native, Acellular, Acellular Gamma and E-Beam Irradiated Arteries at 100 mmHg

Percentage Length Increase (100 mmHg)											
Native			Acellular			Gamma			E-Beam		
Mean	Upper 95 % CL	Lower 95 % CL	Mean	Upper 95 % CL	Lower 95 % CL	Mean	Upper 95 % CL	Lower 95 % CL	Mean	Upper 95 % CL	Lower 95 % CL
5.54*	4.30	3.12	0.93	1.70	0.84	3.67	4.66	2.82	5.36**	6.34	3.97

Data is presented as the mean (Native, n=3; Acellular, n=5; Gamma, n=5; E-Beam, n=4) ± 95% CL. Following arcsine transformation, data for each parameter was analysed by one way ANOVA and Tukey test (p<0.05). *Significantly different from acellular, **Significantly different from native and acellular.

5.4.2 Mechanical Properties Of Freeze-Dried and Freeze-dried Ethylene Oxide Treated Acellular Porcine Carotid Arteries

5.4.2.1 Uniaxial Tensile Testing of Freeze-Dried and Freeze-Dried Ethylene Oxide Treated Acellular Porcine Carotid Arteries

Native, native freeze dried, acellular, acellular freeze dried and ethylene oxide sterilised arteries were subjected to uniaxial tensile testing in both the axial and circumferential directions. The data was then manipulated to apply 0.01 N of preload. Six parameters: transition strain, transition stress, ultimate tensile strain, ultimate tensile stress, collagen modulus and elastin modulus were extracted from the data and were compared using one way ANOVA and Tukeys post-hoc test ($p < 0.05$). The parameters extracted from circumferential samples are presented in Table 5.7 and depicted as average stress strain curves in Figure 5.8. The parameters extracted from axial samples are presented in Table 5.8 and depicted as stress strain curves in Figure 5.9.

In the circumferential direction native freeze-dried arteries had no significant differences in mechanical properties compared to native arteries. Acellular freeze dried arteries had no significant differences in mechanical properties when compared to acellular arteries. Acellular arteries had a significantly lower transition strain than native arteries and acellular freeze dried arteries had a significantly lower transition stress than native arteries. Ethylene oxide sterilised arteries had a significantly higher elastin and collagen modulus than native and acellular arteries as well as significantly reduced transition strain. The ultimate tensile strain was significantly lower and the ultimate tensile stress significantly higher when compared to native arteries.

In the axial direction native, native freeze dried, acellular and acellular freeze dried arteries had no significant differences in mechanical properties. Acellular freeze dried ethylene oxide sterilised arteries had significantly higher elastin modulus and ultimate tensile stress than native and acellular arteries. The transition strain was significantly lower when compared to acellular arteries and the transition stress significantly higher when compared to native arteries.

Table 5.7 : Parameters Extracted From Stress Strain Curves Derived From Low Strain Rate To Failure Uniaxial Tensile Testing In The Circumferential Direction Of Native, Native Freeze-Dried, Acellular, Acellular Freeze-Dried And Ethylene Oxide Treated Porcine Carotid Arteries.

Tissue	Thickness (mm)	Elastin (MPa)	Collagen (MPa)	TStrain	TStress (MPa)	UTStrain	UTStress (MPa)
Native	0.96±0.02	0.15±0.06	3.63±2.85	0.84±0.15	0.29±0.16	1.4±0.34	1.87±1.26
Native FD	0.97±0.08	0.22±0.09	3.67±1.26	0.73±0.26	0.32±0.14	1.3±0.24	1.99±0.72
Acellular	0.93±0.08	0.77±0.37	4.13±0.77	0.55±0.17*	0.52±0.18	1.11±0.23	2.32±0.95
Acellular FD	0.94±0.15	0.76±0.34	4.82±0.62	0.6±0.16	0.63±0.16*	1.18±0.3	2.64±0.63
EO	0.81±0.21	2.52±0.93***	6.02±0.63***	0.12±0.05***	0.3±0.12	0.81±0.4*	3.35±0.92*

Data is presented as the mean (Native, n=4; Native Freeze-dried, n=5; Acellular, n=5; Acellular Freeze-dried, n=6; ethylene oxide, n=5) ± 95% CL. Data for each parameter was analysed by one way ANOVA and Tukey test (p<0.05). * Significantly different to native, *** Significantly different to native and acellular

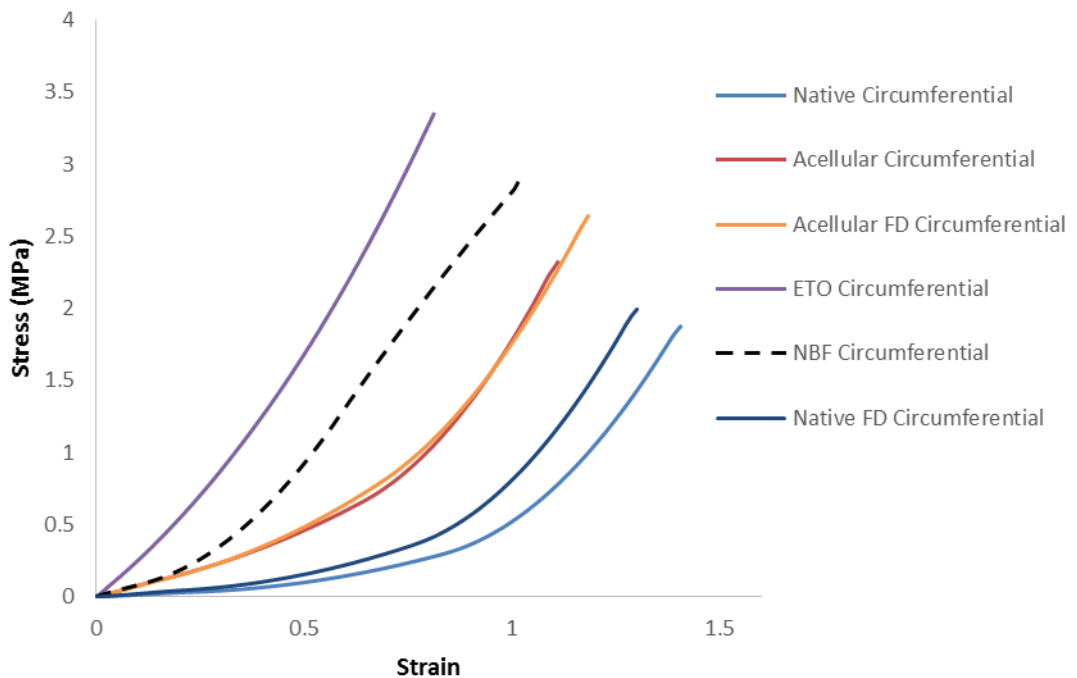


Figure 5.8 Average Stress Strain Curves Derived From Low Strain Rate To Failure Uniaxial Tensile Testing In The Circumferential Direction Of Native, Native Freeze-Dried, Acellular, Acellular Freeze-Dried And Ethylene Oxide Treated Porcine Carotid Arteries

Native, native freeze-dried, acellular, acellular freeze-dried arteries exhibited typical biphasic curves with a observable upwards and left shift in acellular arteries. Ethylene oxide treated arteries had a linear curve. The transition strain was significantly lower in acellular arteries when compared to native arteries and the acellular freeze-dried arteries had significantly higher transition stress than native arteries. Ethylene oxide treated arteries has significantly higher elastin and collagen moduli and significantly lower transition strain when compared to native and acellular arteries . Ethylene oxide treated arteries had a significantly higher ultimate tensile stress and significantly lower ultimate tensile strain when compared to native arteries.

Table 5.8 : Parameters Extracted From Stress Strain Curves Derived From Low Strain Rate To Failure Uniaxial Tensile Testing In The Axial Direction Of Native, Native Freeze-Dried, Acellular, Acellular Freeze-Dried And Ethylene Oxide Treated Porcine Carotid Arteries.

Tissue	Thickness (mm)	Elastin (MPa)	Collagen (MPa)	TStrain	TStress (MPa)	UTStrain	UTStress (MPa)
Native	0.87±0.24	0.1±0.03	1.35±0.84	0.65±0.22	0.1±0.05	1.37±0.48	0.64±0.35
Native FD	0.78±0.11	0.19±0.08	3.07±0.57	0.63±0.15	0.23±0.08	1.13±0.22	1.4±0.6
Acellular	0.73±0.1	0.19±0.05	2.67±1.37	0.82±0.15	0.26±0.1	1.45±0.29	1.09±0.25
Acellular FD	0.79±0.18	0.24±0.09	2.94±2.27	0.68±0.25	0.24±0.1	1.27±0.24	1.21±0.44
EO	0.68±0.11	0.83±0.33***	2.71±1.52	0.39±0.21**	0.38±0.26*	1.21±0.23	1.82±0.52***

Data is presented as the mean (Native, n=4; Native Freeze-dried, n=5; Acellular, n=5; Acellular Freeze-dried, n=6; ethylene oxide, n=5) ± 95% CL. Data for each parameter was analysed by one way ANOVA and Tukey test (p<0.05). * Significantly different to native, ** Significantly different to Acellular *** Significantly different to native and acellular

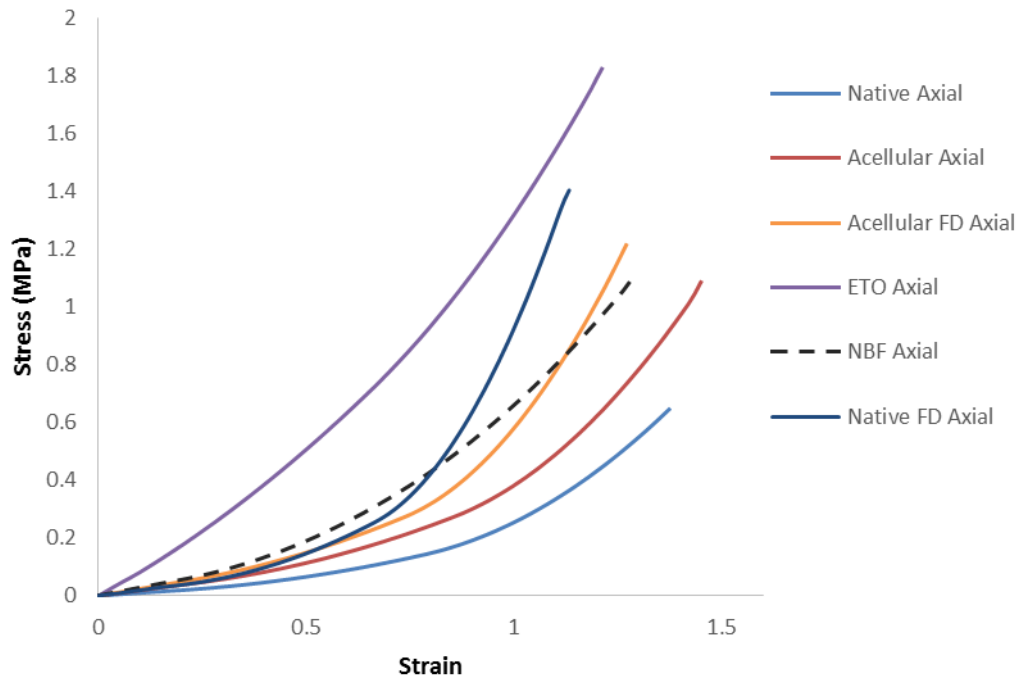


Figure 5.9 Average Stress Strain Curves Derived From Low Strain Rate To Failure Uniaxial Tensile Testing In The Axial Direction Of Native, Native Freeze-Dried, Acellular, Acellular Freeze-Dried And Ethylene Oxide Treated Porcine Carotid Arteries

Native, native freeze-dried, acellular, acellular freeze-dried arteries exhibited typical biphasic curves with a observable upwards and left shift in acellular and freeze dried arteries. Ethylene oxide treated arteries had a linear curve. There were no significant differences between native, native freeze-dried, acellular and acellular freeze-dried arteries. Ethylene oxide treated arteries had a significantly higher elastin modulus and ultimate tensile stress when compared to native and acellular arteries. Ethylene oxide treated arteries had a significantly lower transition strain when compared to acellular arteries and a significantly higher transition stress when compared to native arteries.

5.4.2.2 Compliance

Native, native freeze dried, acellular, acellular freeze dried, ethylene oxide sterilised and NBF fixed porcine carotid arteries were subjected to burst pressure and compliance testing. Arteries were inflated incrementally up to 200 mmHg and the length and diameter measured at each increment. From these measurements the percentage diameter change was calculated and is displayed in Figure 5.10 and the percentage length change was calculated and is displayed in Figure 5.11. Means were statistically compared at 100 mmHg for percentage diameter and length change and the results are shown in Table 5.9 and Table 5.10 respectively. After 200 mmHg arteries were inflated to rupture. All arteries exceeded a burst pressure of 3000 mmHg.

Native, native freeze dried, acellular and acellular freeze dried porcine carotid arteries exhibited an initial steeper incline before maintaining a linear increase in percentage diameter change. NBF fixed porcine carotid arteries showed very little increase in percentage diameter change and maintained a near constant value. Ethylene oxide sterilised arteries had a constant decrease in percentage diameter change and maintained a constant rate with increasing pressure. At 100 mmHg there was no significant difference in percentage diameter change between Native, native freeze dried, acellular and acellular freeze dried arteries. Ethylene oxide sterilised arteries had a significantly lower percentage diameter change than all other groups.

Native, native freeze dried, acellular, acellular freeze dried and ethylene oxide sterilised arteries exhibited a linear but increasing percentage length change. NBF fixed porcine carotid arteries exhibited a constant rate of percentage length change. There was a large amount of variance and no significant differences were found between any of the groups.

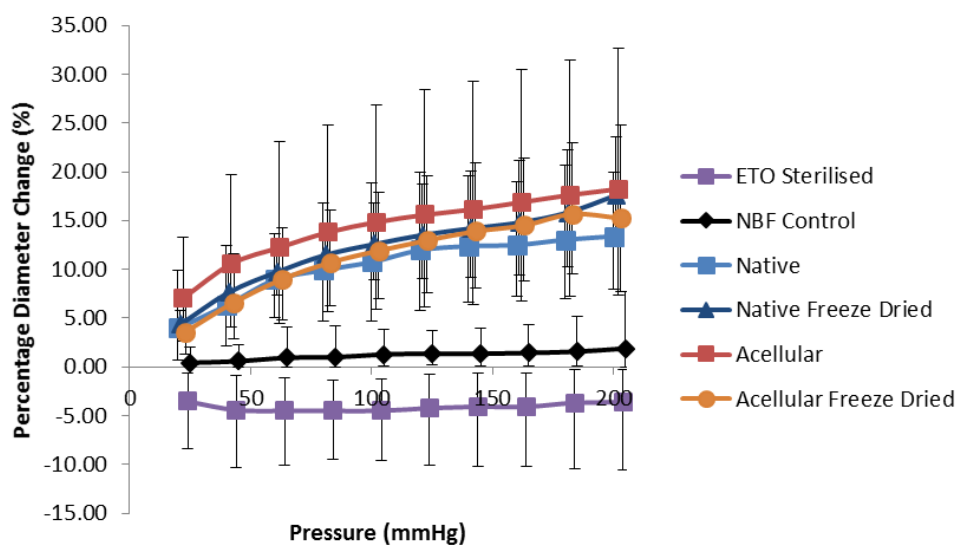


Figure 5.10 : Average Percentage Diameter Change Native, Native Freeze-dried, Acellular, Acellular Freeze-dried, Ethylene Oxide Treated and NBF Fixed Arteries with Increasing Pressure.

Data was arcsine transformed for calculation of mean \pm 95% CL and back transformed to percentages for presentation.

Table 5.9 - Average Percentage Diameter Change Native, Native Freeze-dried, Acellular, Acellular Freeze-dried and Ethylene Oxide Treated Arteries at 100 mmHg

Percentage Diameter Increase														
Native			Native Freeze dried			Acellular			Acellular Freeze Dried			EO Sterilised		
Mean	Upper 95 % CL	Lower 95 % CL	Mean	Upper 95 % CL	Lower 95 % CL	Mean	Upper 95 % CL	Lower 95 % CL	Mean	Upper 95 % CL	Lower 95 % CL	Mean	Upper 95 % CL	Lower 95 % CL
10.75	8.14	6.05	12.57	4.21	3.68	14.84	12.06	8.93	11.92	5.98	4.90	-4.51*	3.23	5.07

Data is presented as the mean (Native, n=3; Native Freeze-dried, n=4; Acellular, n=4; Acellular Freeze-dried, n=6; ethylene oxide, n=3) ± 95% CL. Following arcsine transformation, data for each parameter was analysed by one way ANOVA and Tukey test (p<0.05). *Significantly different from Native, **Significantly different from native and acellular

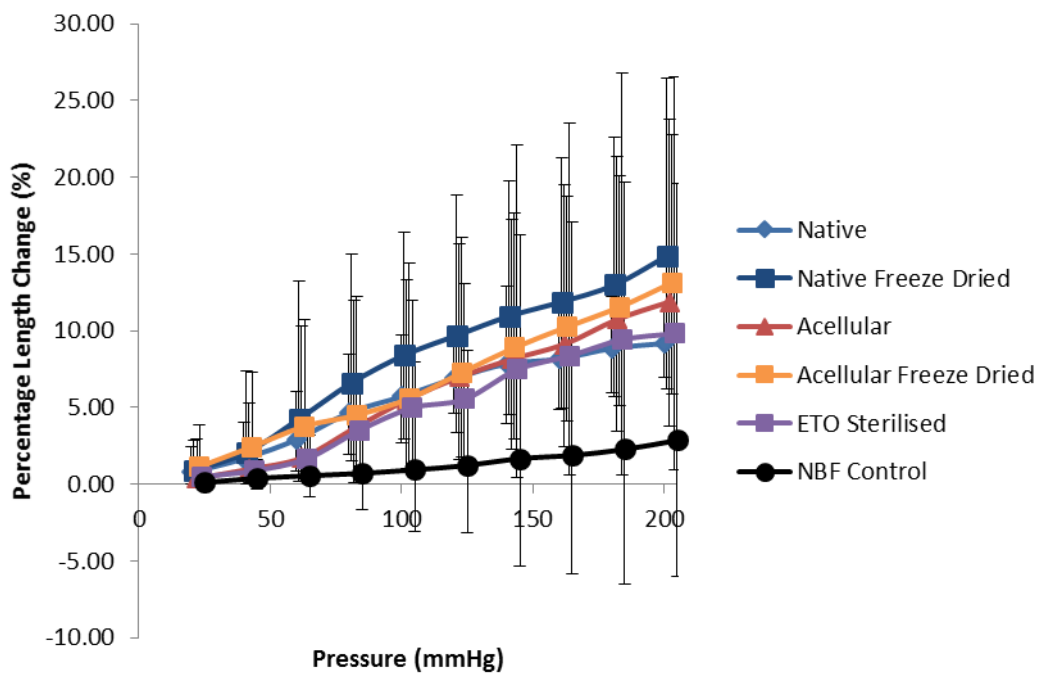


Figure 5.11 : Average Percentage Length Change Native, Native Freeze-dried, Acellular, Acellular Freeze-dried, Ethylene Oxide Treated and NBF Fixed Arteries with increasing pressure.

Data was arcsine transformed for calculation of mean ± 95% CL and back transformed to percentages for presentation

Table 5.10 - Average Percentage Length Change Native, Native Freeze-dried, Acellular, Acellular Freeze-dried and Ethylene Oxide Treated Arteries at 100 mmHg

Percentage Length Increase														
Native			Native Freeze dried			Acellular			Acellular Freeze Dried			EO Sterilised		
Mean	Upper 95 % CL	Lower 95 % CL	Mean	Upper 95 % CL	Lower 95 % CL	Mean	Upper 95 % CL	Lower 95 % CL	Mean	Upper 95 % CL	Lower 95 % CL	Mean	Upper 95 % CL	Lower 95 % CL
5.71	4.04	3.01	8.41	7.98	5.49	5.51	7.82	4.51	5.59	8.83	4.82	4.98	7.00	4.05

Data is presented as the mean (Native, n=3; Native Freeze-dried, n=4; Acellular, n=4; Acellular Freeze-dried, n=6; ethylene oxide, n=3) ± 95% CL. Following arcsine transformation, data for each parameter was analysed by one way ANOVA and Tukey test (p<0.05). *Significantly different from Native, **Significantly different from native and acellular

5.5 Discussion

The mechanical properties of arteries are attributed largely to the content and orientation of elastin and collagen. The elastin and collagen both have the potential to be affected by ionising radiation or EO treatment and therefore the mechanical properties of acellular porcine carotid arteries had the potential to be affected by sterilisation processes. The aims of the work described in this chapter were therefore to determine whether Gamma, E-Beam or EO sterilisation processes had any effect on the mechanical properties of the acellular arteries using the test methods developed in Chapter 4.

The effects of the decellularisation process on the mechanical properties of native porcine carotid arteries from batch 3 and batch 4 described in this Chapter were largely consistent with those found for previous batches of acellular arteries described in Chapter 4 and any differences observed could be attributed to the natural variance that occurs within animal derived tissues.

Observations of the stress-strain curves for the E-Beam irradiated samples revealed that much of the characteristic biphasic nature of native and acellular porcine carotid arteries was removed. Although the elastin and collagen modulus were not the same the stress-strain curves had become linear in comparison to native or acellular porcine carotid arteries. In the circumferential direction the elastin modulus was significantly higher than that of native and acellular porcine carotid arteries. In the axial direction the collagen modulus was significantly higher than that of the native and acellular porcine carotid arteries and the elastin modulus was also elevated. This suggested increased crosslinking due to E-Beam irradiation. In particular a major effect was observed on the elastin phase.

The effects of cross linking on the collagen phase by E-Beam irradiation on acellular porcine carotid arteries were not as noticeable in the circumferential direction but were clearly evident in the axial direction. As there is a higher content of collagen fibres orientated in the circumferential direction, the effects of E-Beam irradiation are likely to be most pronounced in this direction. Therefore any effects caused by chain-scission are also most likely to be most pronounced in this direction. Again, therefore any increased stiffness may have been masked by a reduction in chain length, which would also support the observable reduction in the ultimate tensile stress.

The contribution of elastin to the compliance of an artery was clearly highlighted by the negative effects that the increased elastin modulus had on the percentage diameter change of E-Beam irradiated acellular porcine carotid arteries. The elastin modulus was stiffened to the extent at which when pressurised the vessel would only extend longitudinally and caused a constant narrowing of E-Beam irradiated acellular porcine carotid arteries. The elastin modulus in the axial direction was less than half the elastin modulus in the circumferential direction of E-Beam irradiated acellular porcine carotid arteries making this the easiest route

for expansion. Increased chain scission in the circumferential direction may have also allowed for easier longitudinal movement in E-Beam irradiated acellular porcine carotid arteries.

E-Beam irradiation clearly had detrimental effects on acellular arteries to the point at which it would not be feasible to use them as a functional graft. The most important effect being the large reduction in the compliance of the acellular arteries, which is a recognised factor for the increase in intimal hyperplasia and ultimately failure in vascular grafts (Sarkar *et al.*, 2006).

With regard to the stress strain parameters of Gamma irradiated acellular porcine carotid arteries there was a significant reduction in the transition strain in the axial direction when compared to native and acellular porcine carotid arteries and a significant reduction in the transition strain in the circumferential direction when compared to native porcine carotid arteries. This indicated that the elastin was becoming less distensible and that Gamma irradiation could have increased cross-linking in the elastin phase. In addition, the elastin modulus of Gamma irradiated acellular porcine carotid arteries was significantly stiffer than native but not acellular porcine carotid arteries, providing further evidence that the elastin was susceptible to changes from Gamma irradiation particularly in the circumferential direction. Since, higher quantities of elastin are aligned in the circumferential direction compared to the axial direction, an increase in cross-linking in the circumferential direction could explain the observed increased stiffness.

With regard to the stress strain parameters in the circumferential direction of Gamma irradiated acellular porcine carotid arteries, the collagen modulus and the ultimate tensile strength were significantly higher than native porcine carotid arteries. This might be explained by increased crosslinking occurring as the predominant mechanism over chain-scission in the collagen phase.

The compliance testing of Gamma irradiated acellular porcine carotid arteries showed that the percentage diameter change was not significantly different from acellular porcine carotid arteries but was significantly lower than native porcine carotid arteries. This indicated that the compliance had been reduced which reinforced the findings from the data extracted from stress-strain curves.

The burst pressure for all arteries tested exceeded 3000 mmHg which is in excess of the 2000 mmHg minimum requirement. Unfortunately limitations of the equipment used prevented bursting at higher pressures and therefore statistical comparisons could not be made.

E-Beam and Gamma irradiation both caused significant changes to acellular porcine carotid arteries. The elastin in the circumferential direction was most affected causing an increase in stiffness and a reduction in extensibility. This was more apparent with E-Beam irradiated samples. The collagen modulus and ultimate tensile strength were increased more in Gamma irradiated samples than in E-Beam irradiated samples this could be explained by chain

scission having a greater role in E-Beam irradiated porcine carotid arteries than Gamma irradiated porcine carotid arteries and therefore masking the effects caused by any cross-linking. The high intensity short burst of E-Beam irradiation could be the reason behind this effect. The overall strength of both Gamma and E-Beam irradiated porcine carotid arteries was not compromised but only Gamma irradiated porcine carotid arteries were similarly extendable to native and acellular porcine carotid arteries. In addition to this the compliance of Gamma irradiated arteries at $7.02 + 3.86 - 3.07 \% / 100 \text{ mmHg}$ was still closely matched to that of native human arteries (femoral artery, $5.9 \pm 0.5 \% / 100 \text{ mmHg}$; saphenous vein, $4.4 \pm 0.8 \% / 100 \text{ mmHg}$; Walden *et al.* (1980); Internal mammary artery, $11.5 \pm 3.9 \% / 100 \text{ mmHg}$ Konig *et al.* (2009)).

With regard to ethylene oxide treated arteries, the effects of freeze-drying were initially assessed since if the freeze-drying process adversely effected the mechanics of the arteries there was no value in pursuing ethylene oxide as a potential sterilisation method. Freeze-drying before EO treatment is employed for two reasons, firstly to reduce the water content which in turn reduces the build up of the toxic by-product ethylene glycol and secondly to maximise the penetration of EO gas into the matrix and tissue. Previous studies in bone allografts have shown a lack of penetration in wet tissues (Kearney *et al.*, 1989; Kearney *et al.*, 1993; Prolo *et al.*, 1980). It is also common practice to irrigate tissues prior to EO treatment to reduce chloride content that could react with EO to form another toxic by-product ethylene chlorohydrin. As the decellularisation process is a continual series of washes the probability of a high chloride content was reduced.

There were no significant differences in the mechanical parameters derived from uniaxial tensile testing of native freeze-dried porcine carotid arteries and acellular freeze-dried porcine carotid arteries in the circumferential and axial directions when compared to their respective non freeze-dried native or acellular porcine carotid artery. There were also no significant differences for the percentage diameter change and the percentage length change at 100 mmHg for native freeze-dried porcine carotid arteries and acellular freeze-dried porcine carotid arteries when compared to their respective non freeze-dried native or acellular porcine carotid artery. This suggested that any effects of freeze-drying on acellular and native arteries were negated after adequate rehydration in saline solution and that the arteries returned to their original state in terms of mechanics. Based on this it was possible to assess the effects of ethylene oxide sterilisation on acellular porcine carotid arteries.

Ethylene oxide treatment of acellular porcine carotid arteries had similar effects to E-Beam irradiation but the effects were more pronounced. With regard to the mechanical parameters derived from uniaxial tensile testing of ethylene oxide treated acellular porcine carotid arteries, the elastin modulus in both the circumferential and axial directions was significantly higher than native and acellular porcine carotid arteries and the collagen modulus was also significantly higher in the circumferential direction. The ultimate tensile stress was also

significantly higher in EO treated samples than native porcine carotid arteries. This increase in stiffness and strength could be explained by cross-linking caused by ethylene oxide. Collagen and elastin have a large number of functional groups that are susceptible to alkylation by ethylene oxide. The higher quantities of collagen aligned in the circumferential direction compared to the axial direction was the likely cause of the collagen modulus being effected more in this direction.

In addition to this the transition strain of EO treated porcine carotid arteries was significantly reduced in the circumferential direction when compared to native and acellular porcine carotid arteries and in the axial direction when compared to native porcine carotid arteries. This might be explained by increased crosslinking reducing the extensibility of the artery. This was further supported by observation of the compliance parameters of EO treated acellular porcine carotid arteries. The elastin stiffness increased to such an extent that when under pressure, expansion occurred longitudinally and thinned the artery causing a negative percentage diameter change an effect also seen in E-Beam irradiated arteries. However, unlike E-Beam treated acellular arteries, there was a significant increase in ultimate tensile stress in the circumferential direction of EO treated acellular arteries when compared to native porcine carotid arteries and in the axial direction when compared to native and acellular porcine carotid arteries. This might be explained by no chain scission occurring in ethylene oxide treatment and supports the hypothesis that chain scission is occurring in irradiated samples. Similarly to E-Beam, EO treatment reduced the compliance of the artery to such an extent that it would not be functional as a vascular graft.

The effects of EO treatment, Gamma irradiation and E-Beam irradiation are widely disputed with the later being least investigated. Most of the information about the effects of these sterilisation treatments on the mechanical properties of tissues can be found in the tissue banking literature on the effects on bone or tendon. The differences found by tissue banks in mechanical properties of tendon and bone caused by ionising radiation is well reported (Nather *et al.*, 2007). Some studies have found a decrease in strength and modulus implicating chain scission as the predominant mechanism and some studies have found an increase in strength implicating cross-linking as the predominant mechanism. The structure of bone and tendon is however vastly different compared to soft tissues such as arteries.

A study investigating the effects of Gamma irradiation on an acellular tissue matrix derived from cadaveric human skin also discussed the predominant mechanism (crosslinking/chain-scission) effecting the mechanical parameters with increasing dose (2.5 to 30 kGy). They found that at lower doses of Gamma irradiation there was an initial increase in tensile strength and stiffness and an initial reduction in ultimate tensile strain compared to control tissue. With increasing dose the tensile strength and stiffness decreased and the ultimate tensile strain increased. This supported the hypothesis that chain-scission increased with higher doses reducing the stiffness of the graft and allowing it to extend more (Gouk *et al.*,

2008). Interestingly another study into the effects of Gamma irradiation on collagen coated vicryl meshes reported that the predominance of chain-scission occurred in dry tissues and the predominance of cross-linking occurred in wet tissues. This indicated that the hydration of the tissue during ionising irradiation could be a significant factor in determining what structural changes occur (Gorham *et al.*, 1993).

One study reporting the development of acellular human dermis for clinical use adopted a similar EO treatment to the one used in this chapter. The tissue was freeze-dried before being treated with EO at low temperature (Chakrabarty *et al.*, 1999). The results presented found similar effects to the data in this chapter, the failure strength of acellular human dermis was increased significantly compared to controls and the failure strain was reduced, although not significantly. Conversely Freytes *et al.* (2008) found a decrease in stiffness for EO treated freeze-dried urinary bladder matrix (UBM) compared to non sterilised freeze-dried UBM. They also found that Gamma and E-Beam irradiated freeze-dried UBM had decreased in stiffness and failure strength when compared to non sterilised freeze-dried UBM. However the reduction in mechanical parameters for all these samples including the control might have been attributed to the incomplete rehydration of the sample. A clinical approach for rehydration was taken in which the sample was rehydrated for 5 minutes in 9 % saline whereas the rehydration of freeze-dried acellular porcine carotid arteries in this study was found to require over 1 hour (data not shown).

It is clear that an investigation into each of these industrial standard methods of sterilisation should be carried out for different types of biomaterials and tissues intended for clinical use. The findings from the present study of acellular porcine carotid arteries indicated that Gamma irradiation would be the preferred method for potential sterilisation whereas E-Beam irradiation and EO treatment were shown to have considerable detrimental effects on the tissue. This, however may not be the case for harder or denser tissues such as bone or tendon.

Further characterisation is necessary in order to determine the effects of the different sterilisation processes on the biological characteristics of the porcine carotid arteries. This is the focus of the following chapter.

Chapter 6 Biological Assessment of Acellular Porcine Arteries after Sterilisation using Different Methods

6.1 Introduction

In the previous Chapter, the effect of different methods of sterilisation on the mechanical properties of acellular arteries was assessed. It was also important to consider the effects of sterilisation using the same methods of Gamma irradiation, E-Beam irradiation and ethylene oxide (EO) on the biological properties of the acellular arteries. For example it was important to assess the effects of sterilisation on the microscopical structure, collagen integrity and biocompatibility of the arteries.

It is recognised that EO sterilisation of biomaterials can create toxic residuals such as ethylene glycol and ethylene chlorohydrin and that without proper aeration these residuals can remain within an EO treated product (Prolo *et al.*, 1980). It was therefore considered important to determine whether any of the EO treated or Gamma and E-Beam irradiated acellular porcine carotid arteries were toxic to cells (cytotoxic) since this would adversely affect the capacity of the acellular scaffolds for repopulation and regeneration *in vitro* or *in vivo*.

Evaluation of the sterilised acellular porcine carotid arteries and comparison with non-sterilised arteries using histology with H&E staining of tissue sections was deemed to be a simple approach to determine whether there were any gross effects of the sterilisation methods on the structure of the arteries. Collagen IV is a predominant collagen type present in arteries and is also associated with the basement membrane (Shekhonin *et al.*, 1985; Timpl, 1996). Previous studies of the effects of chemical sterilisation on acellular porcine arteries have indicated that the sterilisation method may lead to a reduction in immunostaining for collagen IV leading to an increase in the thrombogenicity of the scaffold (Wilshaw personal communication). It was therefore considered relevant to assess the effects of Gamma, E-beam and EO sterilisation on the presence of collagen IV by immunostaining..

There are a range of methods available for assessing the integrity of structural collagens in biological materials. These include assays to determine the denatured collagen content (Mirsadraee *et al.*, 2006), assays to assess cross-link density (Schwartz *et al.*, 2006; Jiang *et al.*, 2006), multiphoton microscopy (Williams *et al.*, 2005; Theodossiou *et al.*, 2006) and differential scanning calorimetry (Goissis *et al.*, 2000). In this study, three such methods (multiphoton microscopy, denatured collagen content and DSC) were selected to determine the effects of sterilisation on the integrity of the collagen within the acellular arteries. The use of assays to determine cross-link density was beyond the scope of the initial studies.

Second harmonic generation multiphoton microscopy is a technique that has been adapted previously for the imaging of collagen structures such as rat tendon. The technique works by firing multiple photons at a sample (incident light), the annihilation of two photons occurs on interaction with the material creating a single photon emitted with half the wave length of the original photons (second harmonic light) (Figure 6.1).

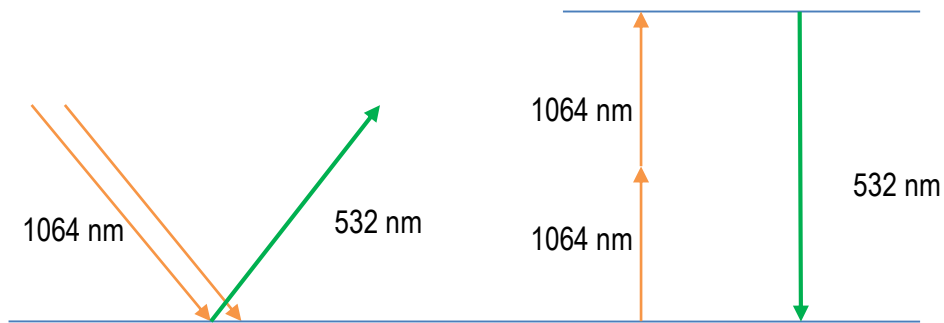


Figure 6.1 : The Second Harmonic Generation of Light

The excitation light is separated from the emitted light through filters and the resultant signal is detected. The technique provides a three dimensional view of the sample with high-resolution and high contrast. The technique is most effective when applied to non-centrosymmetric structures which is why the highly crystalline triple-helix structure of collagen is such a good generator of the second harmonic.

Differential scanning calorimetry (DSC) is a thermo-analytical technique used to analyse the denaturation temperature of materials. DSC is used to measure the enthalpy (change in heat energy) required to increase the temperature of a sample compared to a reference material. The temperature is increased linearly at a constant rate and both the reference material and the sample are maintained at the same temperature. With respect to samples of proteinous nature, the influx of heat disrupts intermolecular hydrogen bonds and disulphide bridges altering the three-dimensional conformational shape (known as denaturation). The structural rearrangement results in a net absorption of heat known as an endotherm and the peak temperature at which this occurs is called the denaturation temperature. Any changes in denaturation temperature could imply structural changes in the acellular porcine carotid artery due to the sterilisation process. It can also provide evidence to preclude certain high temperature sterilisation processes from being tested. The denatured collagen content of tissues can also be determined using simple biological assays such as treating the tissues with alpha chymotrypsin followed by determination of the levels of hydroxyproline released (Mirsadraee *et al.*, 2006)

6.2 Aims and objectives

The aims of this part of the study were to investigate the effects of Gamma irradiation, E-Beam irradiation, freeze-drying and EO treatment on the biological properties of acellular porcine carotid arteries

The specific objectives were:

- To subject acellular porcine carotid arteries to Gamma irradiation (30 kGy) and determine the effects on the properties of the arteries using histology, the contact cytotoxicity assay, immunohistochemical labelling for collagen IV, multiphoton imaging, differential scanning calorimetry and denatured collagen content.
- To subject acellular porcine carotid arteries to E-Beam irradiation (30 kGy) and determine the effects on the properties of the arteries using histology, the contact cytotoxicity assay, immunohistochemical labelling for collagen IV, multiphoton imaging, differential scanning calorimetry and denatured collagen content.
- To freeze-dry acellular porcine carotid arteries and determine the effects on the properties of the arteries using histology, the contact cytotoxicity assay, immunohistochemical labelling for collagen IV, multiphoton imaging, differential scanning calorimetry and denatured collagen content.
- To subject freeze-dried acellular porcine carotid arteries to EO sterilisation and determine the effects on the properties of the arteries using histology, the contact cytotoxicity assay, immunohistochemical labelling for collagen IV, multiphoton imaging, differential scanning calorimetry and denatured collagen content.

6.3 Materials and Methods

6.3.1 Arteries and Sampling

The native porcine carotid arteries used in this chapter were procured and dissected according to the method described in Chapter 3; Section 3.3.1. Acellular arteries were produced in three batches (Chapter 3; Section 3.4.6) using the method described in Chapter 3; Section 3.3.2. The acellular arteries studied in this chapter were from the same groups described in Chapter 5; Section 5.3.1 but here they were used for biological evaluation. The methods used to sample the arteries for biological and mechanical evaluation has been described Chapter 3; Section 3.3.3. Sampling method I was used to provide tissue for quantitative analyses. Sampling method II was used for qualitative analyses.

6.3.2 Irradiation Sterilisation

Acellular porcine carotid arteries from batch 2 were vacuum sealed in an inner foil pouch and an outer Tyvek membrane pouch. Arteries were then couriered to Synergyhealth PLC and were Gamma irradiated at a dose of 30 kGy (Min, 25 kGy).

Acellular porcine carotid arteries from batches 3 and 4 were packaged with a PEG support and then subject to Gamma or E-Beam irradiation as previously described in Section 5.3.2.

6.3.3 Freeze Drying

Acellular porcine carotid arteries from batch 4 were subject to freeze drying as described in Section 5.3.3

6.3.4 EO Method

Freeze dried acellular porcine carotid arteries from batch 4 were subject to EO sterilisation as described in Section 5.3.4

6.3.5 Sterility Testing

Sterility testing of samples (n=2) was carried out according to Section 2.6.9 using tissue obtained using sampling method II for each group as shown in Chapter 5; Section 5.3.1. Arteries from the freeze-dried group were not tested for sterility since they were not freeze dried using aseptic technique.

6.3.6 Histological and Immunohistochemical Analysis

For histological analysis sections of porcine carotid arteries (n=2) from each group were stained using haematoxylin and eosin and immunohistochemically labelled using an antibody to collagen IV as described in Section 2.6.6.

6.3.7 Multiphoton Imaging

For multiphoton analysis 5 mm circular samples (n=2) of porcine carotid arteries from each group were imaged. Images 210 μm by 210 μm were obtained using a Zeiss LSM 510Meta inverted confocal microscope with an EC Plan-Neofluar 40x/1.30 Oil DIC objective, with a pixel dwell time of 12.8 μs . Collagen fluorophores were excited using a two-photon Ti-Sapphire laser with 940 nm wavelength and 10 % transmission. Emission was filtered to detect wavelengths between 458 and 480 nm. All image analysis was performed using Zen 2012 image analysis software. Z-stack images were taken at 1 μm intervals.

6.3.8 Contact Cytotoxicity

Samples (n=2) 5 mm² of porcine carotid arteries from each group that had been shown to be sterile were tested to determine cytotoxicity as described in Section 2.6.9.

6.3.9 Differential Scanning Calorimetry

To determine the denaturation temperature of native, acellular, Gamma irradiated, E-Beam irradiated, freeze-dried EO treated, boiled and NBF fixed porcine carotid arteries samples (n=5) were placed on PBS soaked filter paper in bijoux containers and couriered overnight on ice to the Department of Materials Science at the University of Cambridge. Samples were then tested using modulated differential scanning calorimetry. Samples were placed in

hermetically sealed pans and subjected to a heat flow at a rate of 1 °C.min⁻¹ up to a temperature of 110 °C and the heat energy required for this change was measured.

6.3.10 Denatured Collagen Assay

The denatured collagen content of samples of native (n=8), acellular (n=4), Gamma irradiated (n=4), E-Beam irradiated (n=5), freeze-dried EO treated (n=5), boiled (n=6) and NBF fixed (n=6) porcine carotid arteries was determined using the method described in Section 2.6.10

6.4 Results

6.4.1 Sterility of Sterilised Acellular Porcine Carotid Arteries

It was important to confirm that the arteries were sterile following sterilisation treatment since any contamination would adversely affect the other biological assays to be conducted on the arteries such as contact cytotoxicity testing and denatured collagen assays. Sampling of arteries was therefore carried out after each sterilisation process. Circular samples (5 mm; n=2) from each batch were tested to confirm sterility by placing them in nutrient broth and incubating at 37 °C for 48 hours. No microbial growth was found in any samples tested (Figure 6.2).

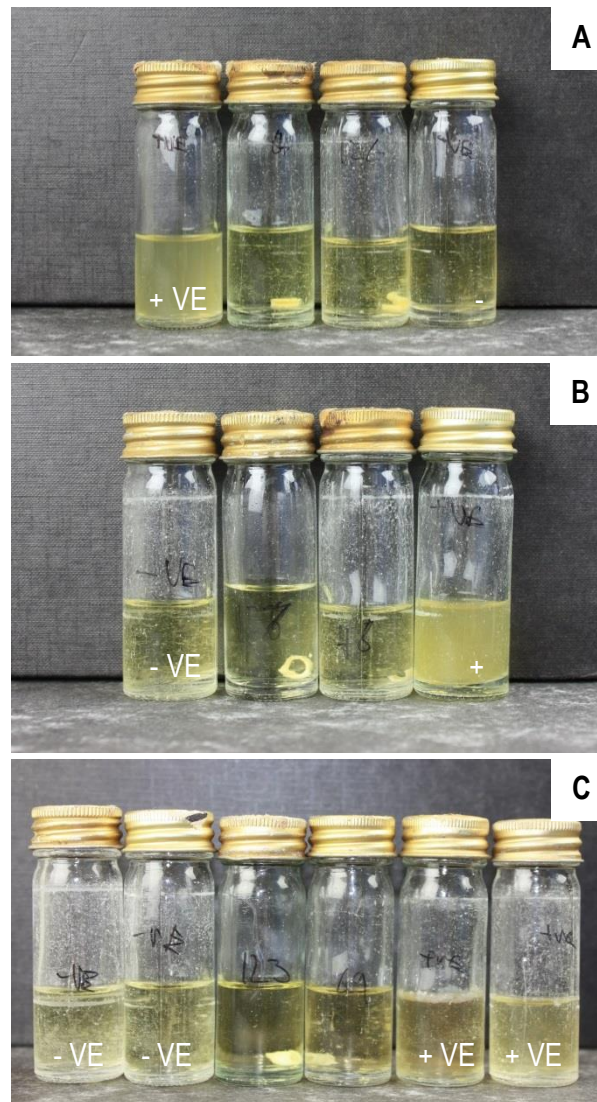


Figure 6.2 : Images of sterility tests carried out on batches of acellular arteries post sterilisation. Images of samples of Gamma (A) and E-Beam (B) irradiated and EO (C) treated porcine carotid arteries incubated in nutrient broth at 37 °C for 48 hours. Positive control was created by immersing a finger in nutrient broth and negative control was a bottle of nutrient broth exposed to the HEPA filtered air.

6.4.2 Histological Evaluation of Sterilised Acellular Porcine Carotid Arteries

Circumferential and longitudinal histological sections of native, acellular, Gamma and E-Beam irradiated and freeze-dried EO treated porcine carotid arteries were stained with haematoxylin and eosin. Representative images are presented in Figures 6.3 and 6.4. The histo-architecture remained consistent in Gamma and E-Beam irradiated acellular arteries when compared to decellularised arteries. EO treated acellular arteries appeared to have some slight contraction and separation between the collagen/elastin layers of the extracellular matrix (Figure 6.3 E; 6.4 E).

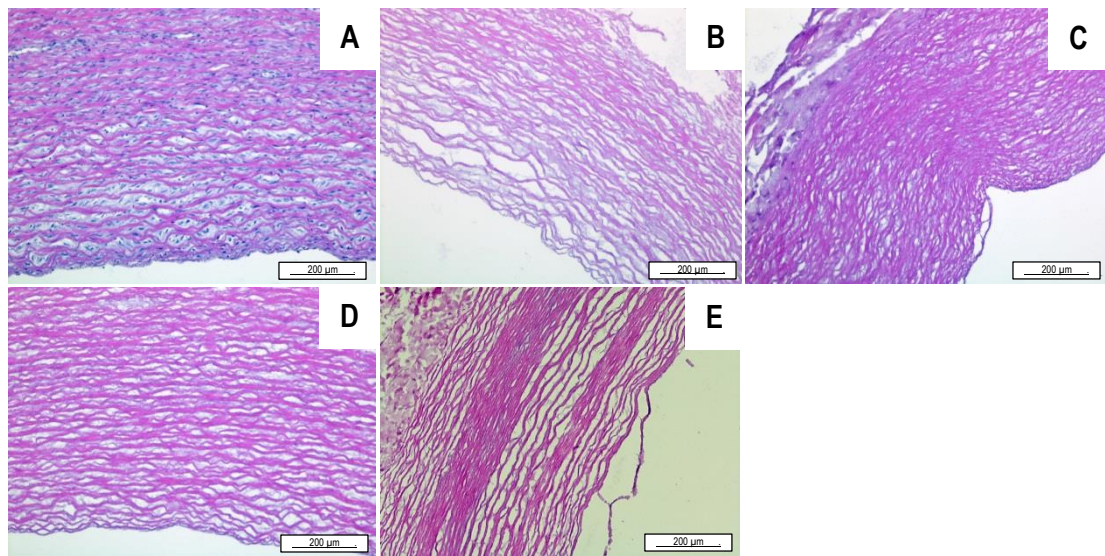


Figure 6.3 Representative images of histological sections of native, acellular, Gamma and E-Beam irradiated and freeze-dried EO treated porcine porcine common carotid arteries in the circumferential direction.

Sections were stained with haematoxylin and eosin. Native arteries showed the presence of nuclei (A). There was an absence of nuclei in acellular arteries (B). Gamma (C) and E-Beam (D) irradiated porcine carotid arteries retained the histo-architecture shown in decellularised arteries. Ethylene oxide (E) treated arteries showed some contraction and separation between layers of the ECM. The images were captured at 40 x magnification.

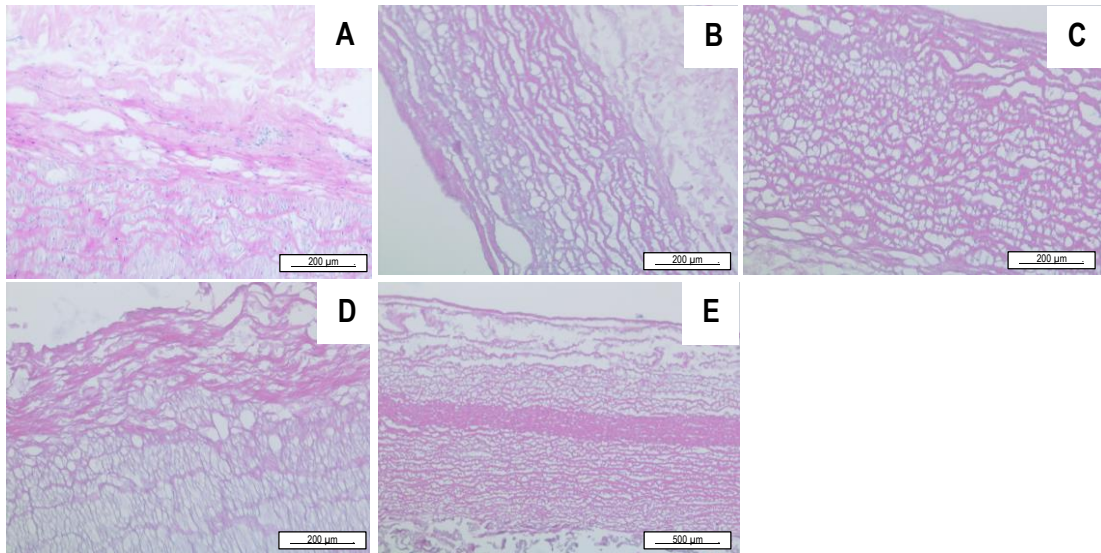


Figure 6.4 : Representative images of histological sections of native, acellular, Gamma and E-Beam irradiated and freeze-dried EO treated porcine porcine common carotid arteries in the longitudinal direction.

Sections were stained with haematoxylin and eosin. Native arteries showed the presence of nuclei (A). There was an absence of nuclei in acellular arteries (B). Gamma (C) and E-Beam (D) irradiated porcine carotid arteries retained the histo-architecture shown in decellularised arteries. Ethylene oxide (E) treated arteries showed some contraction and separation between layers of the ECM. The images were captured at either 40 or 100 x magnification.

6.4.3 Biocompatibility of Sterilised Acellular Porcine Carotid Arteries

Samples of acellular, Gamma and E-Beam irradiated and freeze-dried EO treated acellular porcine carotid arteries were tested for biocompatibility using the contact cytotoxicity assay with L929 and BHK cells. Steri-strips and cyanoacrylate were used as negative and positive controls respectively. The phase contrast (Figure 6.5 and Figure 6.6) and Giemsa stained (Figure 6.7 and Figure 6.8) images captured at 48 hours showed that the cell lines grew up to Gamma and E-Beam irradiated and freeze-dried EO treated acellular porcine carotid arteries indicating there was no cytotoxic effect on both the cell lines. Normal cell morphology was observed. The cyanoacrylate was highly cytotoxic and caused cell lysis.

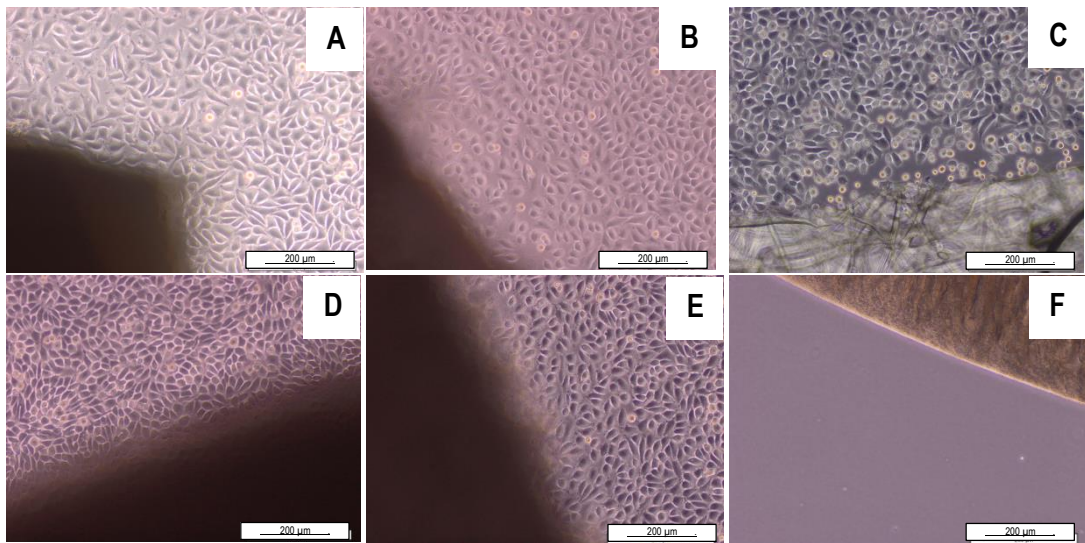


Figure 6.5: Representative images captured using phase contrast microscopy of L929 cells growing in contact with acellular, Gamma and E-Beam irradiated and freeze-dried EO treated acellular porcine carotid arteries from batches 3 and 4.

L929 cells Incubated with acellular (A), Gamma (D) and E-Beam (E) irradiated and freeze-dried EO treated (B) porcine carotid acellular arteries, steri-strips (C) and cyanoacrylate (F). Images captured at x40 magnification.

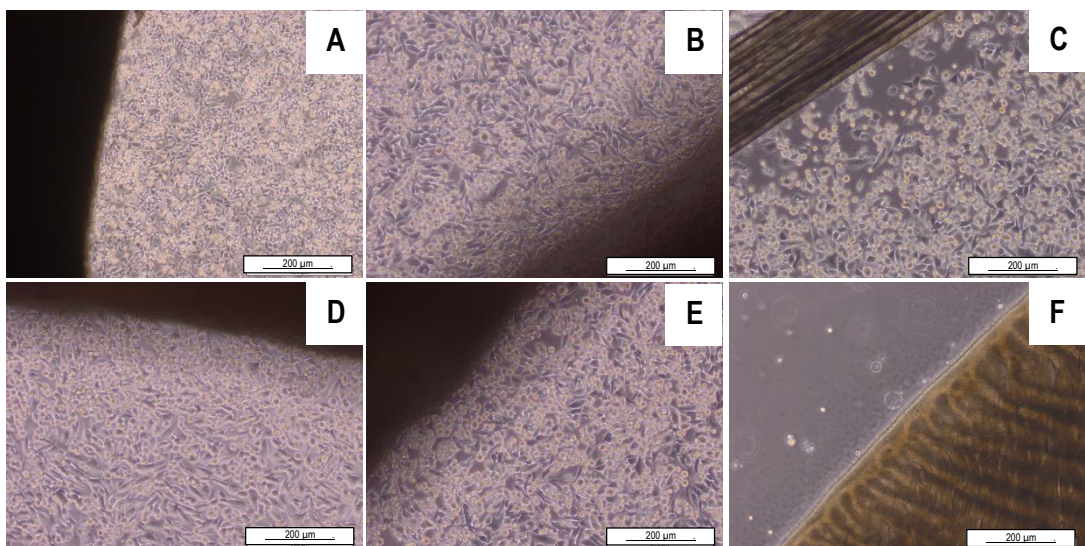


Figure 6.6: Representative images captured using phase contrast microscopy of BHK cells growing in contact with acellular, Gamma and E-Beam irradiated and freeze-dried EO treated acellular porcine carotid arteries from batches 3 and 4.

BHK cells Incubated with acellular (A), Gamma (D) and E-Beam (E) irradiated and freeze-dried EO treated (B) acellular porcine carotid arteries, steri-strips (C) and cyanoacrylate (F). Images captured at x40 magnification

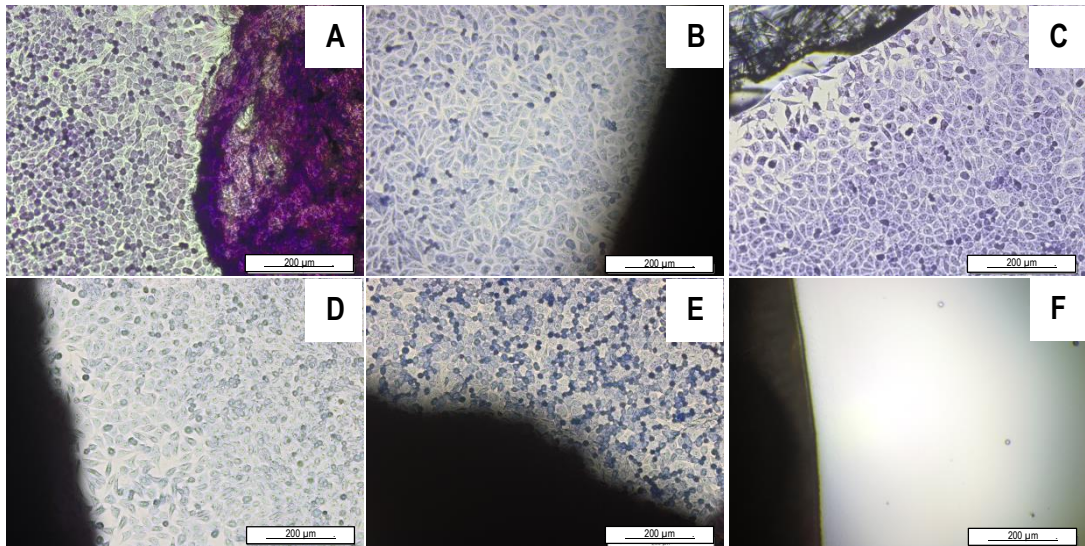


Figure 6.7: Representative images captured using light microscopy of L929 cells stained with Geimsa growing in contact with acellular, Gamma and E-Beam irradiated and freeze-dried EO treated acellular porcine carotid arteries from batches 3 and 4.

L929 cells Incubated with acellular (A), Gamma (D) and E-Beam (E) irradiated and freeze-dried EO treated (B) acellular porcine carotid arteries, steri-strips (C) and cyanoacrylate (F). Images were captured at x40 magnification.

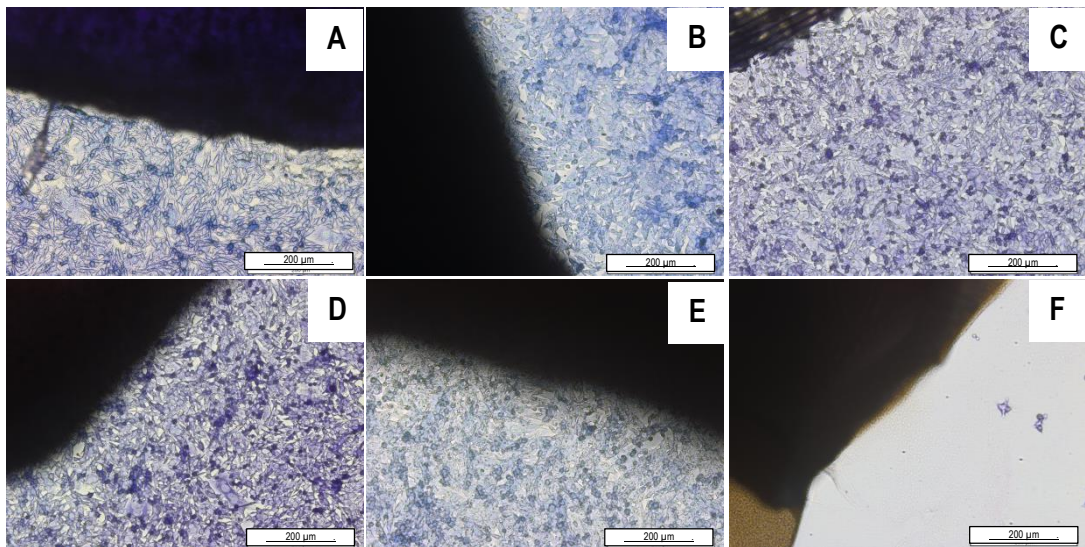


Figure 6.8: Representative images captured using light microscopy of L929 cells stained with Geimsa growing in contact with acellular, Gamma and E-Beam irradiated and freeze-dried EO treated acellular porcine carotid arteries from batches 3 and 4.

L929 cells Incubated with acellular (A), Gamma (D) and E-Beam (E) irradiated and freeze-dried EO treated (B) acellular porcine carotid arteries, steri-strips (C) and cyanoacrylate (F). Images were captured at x40 magnification.

6.4.4 Immunostaining For Collagen IV in Sterilised Acellular Porcine Carotid Arteries

6.4.4.1 Gamma Irradiation Artefacts Without Support Scaffold

On initial testing, acellular arteries to be Gamma sterilised were placed in the appropriate packaging and vacuum sealed. Following sterilisation using Gamma irradiation it was grossly evident that the process had altered the structure of the arteries. A permanent crease remained in the tissue and when sections of the tissue were immuno-stained using antibodies to collagen IV obvious artefacts could be seen. Representative images are presented in Figure 6.9. There was no background labelling present in any control sections of Gamma irradiated tissue including the antibody diluent and isotype control. There was a slight increase in intensity of the collagen IV immuno-staining when acellular tissue was compared to native tissue. In acellular arteries sterilised by Gamma irradiation there was a reduction in the labelling of collagen IV in the central region of the artery but a localised presence around an artefact created by the artery orientation during the sterilisation process.

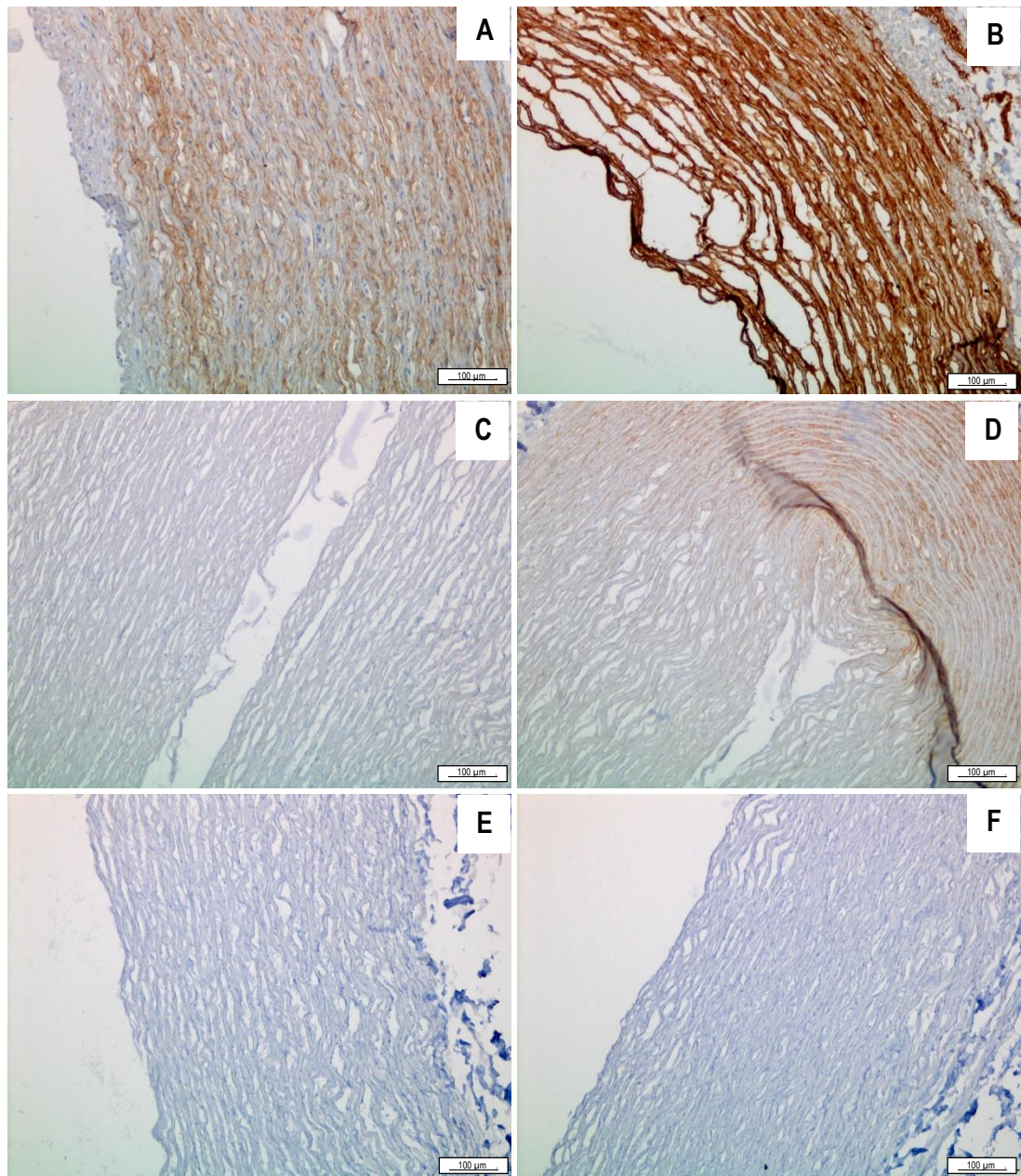


Figure 6.9 : Representative images of collagen IV immuno-stained sections of native (A) , acellular (B) and acellular Gamma (C, D) irradiated porcine carotid arteries. Acellular Gamma irradiated isotype control (F) and antibody diluent control (E).

Arteries post decellularisation were observed to have a slight increase in intensity of collagen IV immunostaining when compared to native arteries. Gamma irradiated acellular arteries were observed to have a reduction on collagen IV presence in the central region but a localised presence remained within artefacts created by the artery orientation in space during Gamma irradiation

6.4.4.2 Gamma Irradiation Effects with Support Scaffold

Due to unwanted artefacts created in Gamma irradiated acellular arteries a new approach was taken. Arteries were rested in a polyethyleneglycol half cylinder support scaffold to maintain and hold the artery structure, the artery was then placed in the appropriate packaging before sterilisation. The addition of this support structure completely removed the visually apparent creasing and when viewed microscopically no artefact could be seen. Sections of native, acellular and Gamma and E-Beam irradiated and EO treated acellular arteries were immunohistochemically labelled for the presence of collagen IV. Representative images are presented in Figure 6.10.

Native arteries exhibited positive immuno-staining for collagen IV. After decellularisation the presence of collagen IV was retained but with a slightly increased intensity observed compared to the native artery. Gamma irradiated arteries also retained positive labelling for collagen IV but with patches of reduced intensity. E-Beam irradiated arteries showed a reduction in intensity of collagen IV immuno-staining with patches of very low intensity staining. Ethylene oxide treated arteries showed no positive labelling for collagen IV. No background staining was observed in any isotype controls or antibody diluent controls.

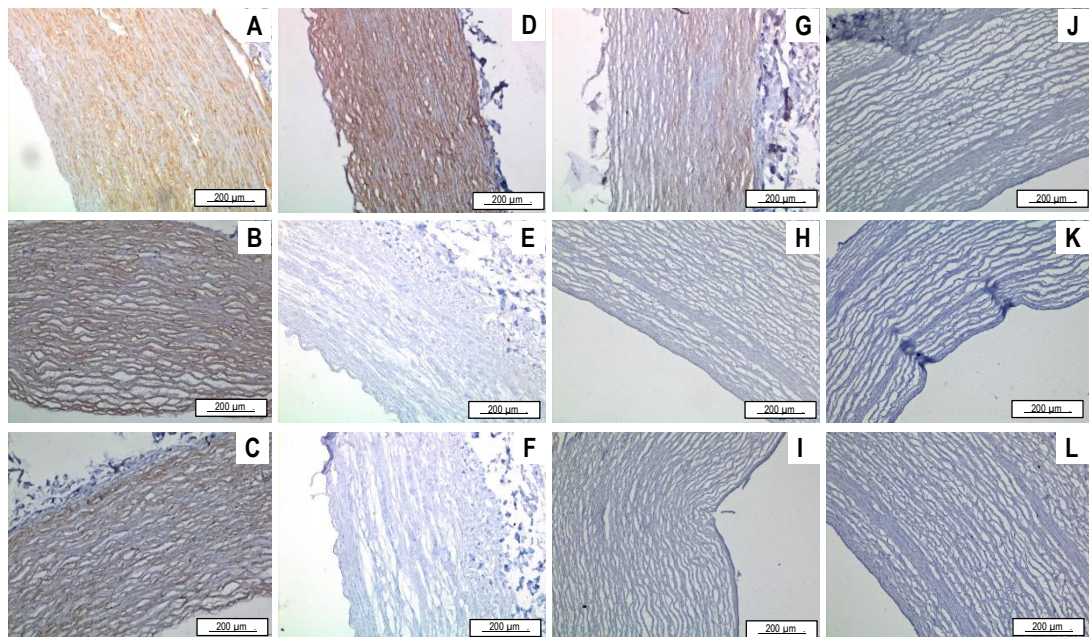


Figure 6.10 : Representative images of collagen IV immune-labelling in sections of native (A), acellular (B, C), acellular Gamma (D) irradiated, acellular E-Beam (G) irradiated, acellular EO (J) treated porcine carotid arteries. Isotype controls (E, H, K) and antibody diluent controls (F, I, L).

Native and acellular arteries exhibited positive immune-labelling for collagen IV but with a slightly increased intensity observed in the acellular artery. Gamma irradiated acellular arteries also retained positive labelling for collagen IV, E-Beam irradiated acellular arteries had a slight intensity reduction and EO treated acellular arteries showed no immune-labelling for collagen IV. No background staining was observed in any isotype controls or antibody diluent controls.

6.4.5 Multiphoton Imaging of Sterilised Acellular Porcine Carotid Arteries

Multiphoton second harmonic generated images were taken of the luminal side of native, acellular, boiled, NBF fixed, acellular Gamma and E-Beam irradiated, acellular freeze-dried and acellular freeze dried EO treated porcine carotid arteries to assess any damage caused to the collagen structure by each of the sterilisation processes. Representative images are depicted in (Figure 6.11-6.15). Z-stacked images of acellular, Gamma and E-Beam irradiated and EO treated porcine carotid arteries were also captured and depicted in Figure 6.16.

Images of native porcine carotid arteries showed the natural crimped collagen structure in a repeated but random pattern orientated in space with a number of small perforations. Acellular porcine carotid arteries also retained this structural pattern, while exhibiting signs of elongation of the crimped structure and slightly larger perforations. Images of boiled porcine carotid arteries showed an absence of the crimped pattern and exhibited a merged sheet containing multiple perforations of various sizes. Images of neutral buffered formalin fixed porcine carotid arteries showed areas of the crimped pattern observed in native tissue with less distinction and a more unidirectional stretched appearance (Figure 6.11).

Images of Gamma irradiated acellular porcine carotid arteries exhibited a reduction in the second harmonic light compared to native arteries and pockets of areas in which the crimped structure could still be observed. The perforations were more frequent and elongated in a particular direction when compared to native or acellular non-sterilised tissue (Figure 6.12).

Similarly E-Beam irradiated acellular porcine carotid arteries exhibited a reduction in second harmonic light compared to native arteries and pockets of areas in which the crimped structure could still be observed. The perforations seemed to be aligned more heavily in one direction and large rifts were evident perpendicular to this arrangement (Figure 6.12).

Prior to EO sterilisation, freeze dried acellular porcine carotid arteries exhibited similar characteristics to acellular tissue but with a reduction in second harmonic light compared to native arteries (Figure 6.14). Multiphoton images of freeze dried EO sterilised acellular porcine carotid arteries had equal second harmonic light compared to images of native and acellular arteries. Elements of the crimped structure remained but appeared in a more condensed mesh. There were also spherical artefacts unique to ethylene oxide sterilised acellular arteries observed in multiple areas of the tissue (Figure 6.15).

Z-stacked images of Gamma irradiated acellular arteries showed pockets of damage in which the collagen structure no longer emitted second harmonic light. This was also observed in the Z-stacked images of E-Beam irradiated acellular arteries but to a far greater extent (Figure 6.16, C). Z-stacked images of EO treated acellular porcine carotid arteries appeared to be similar to acellular arteries however spherical artefacts were observed (Figure 6.16, D).

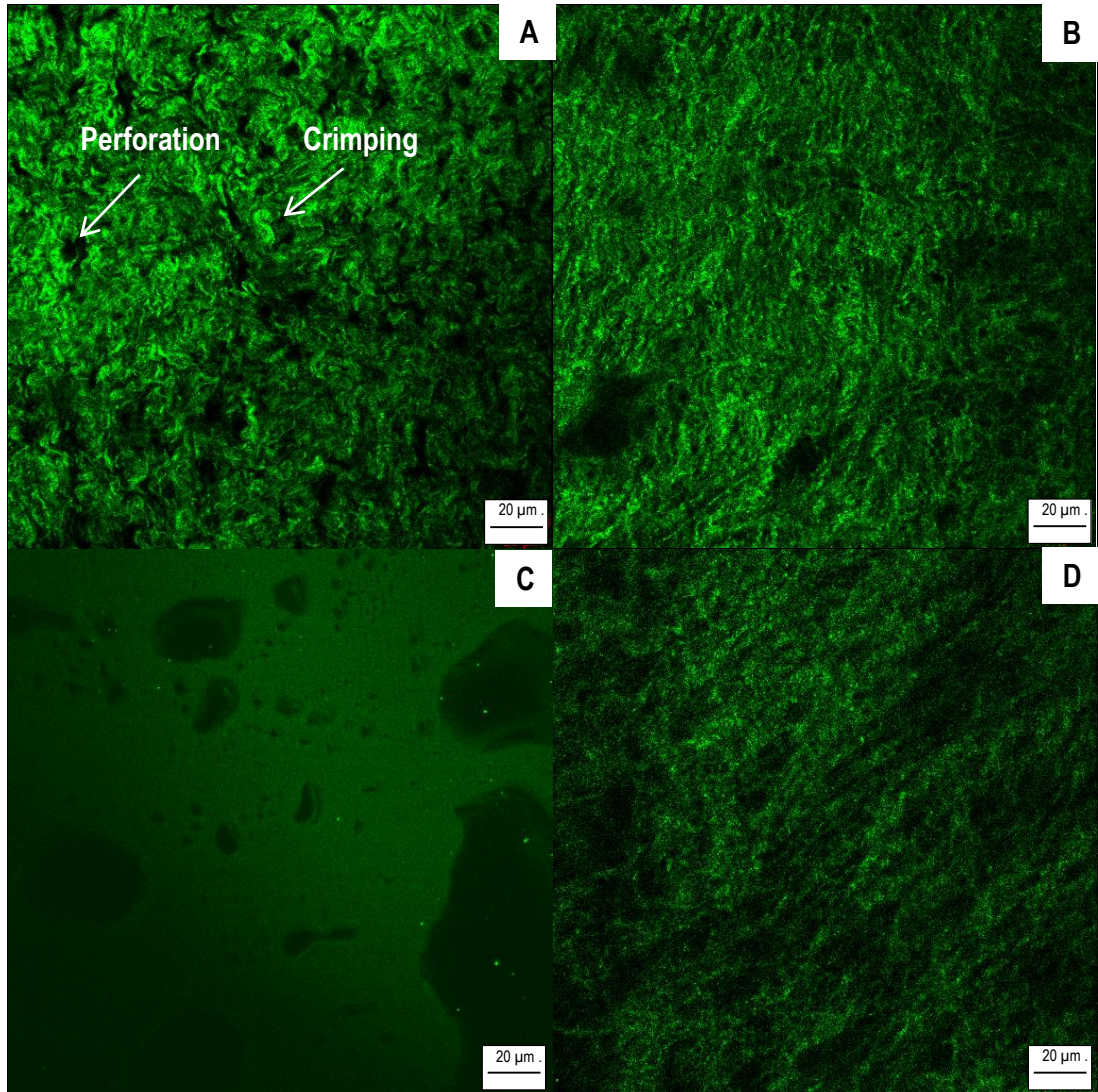


Figure 6.11 Second harmonic image generation of (A) Native, (B) Acellular, (C) Boiled and (D) NBF fixed porcine carotid arteries.

Collagen fluorophores were excited using a two-photon Ti-Sapphire laser with 940 nm wavelength and 10 % transmission. Emission was filtered to detect wavelengths between 458 and 480 nm

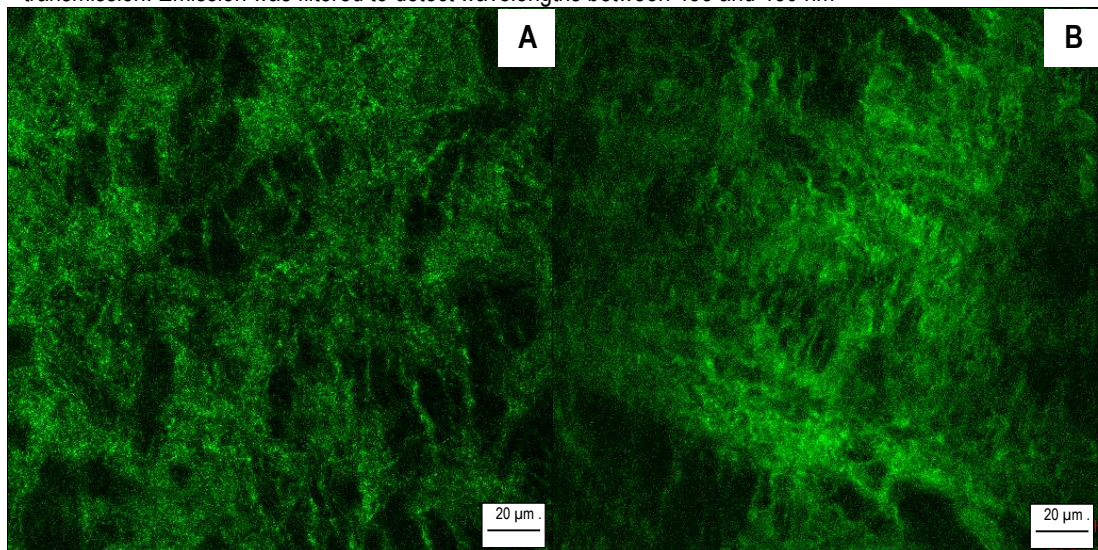


Figure 6.12 : Second harmonic image generation of Gamma irradiated acellular porcine carotid arteries (A,B).

Collagen fluorophores were excited using a two-photon Ti-Sapphire laser with 940 nm wavelength and 10 % transmission. Emission was filtered to detect wavelengths between 458 and 480 nm

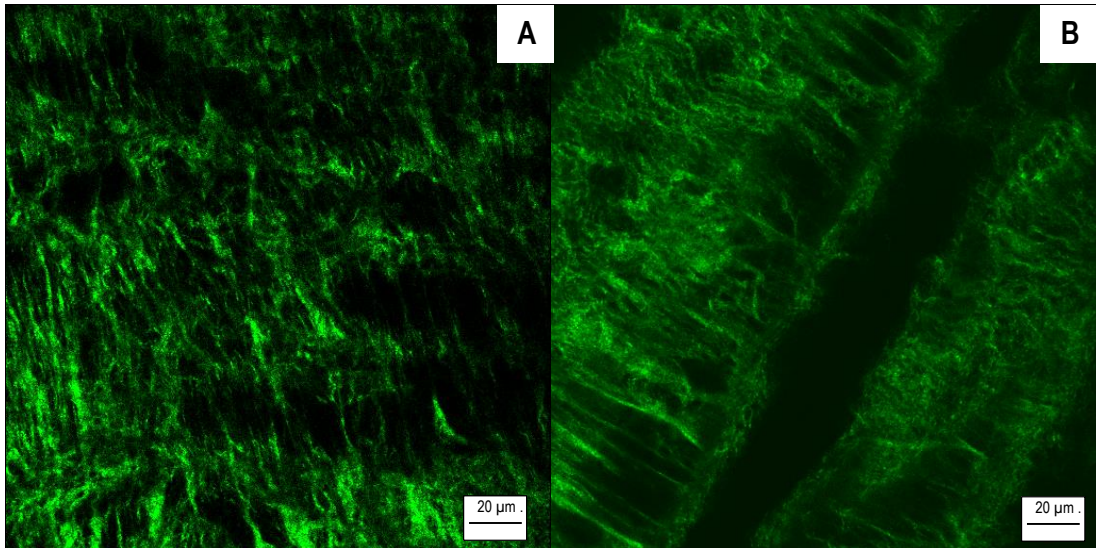


Figure 6.13 : Second harmonic image generation of E-Beam irradiated acellular porcine carotid arteries (A,B).

Collagen fluorophores were excited using a two-photon Ti-Sapphire laser with 940 nm wavelength and 10 % transmission. Emission was filtered to detect wavelengths between 458 and 480 nm

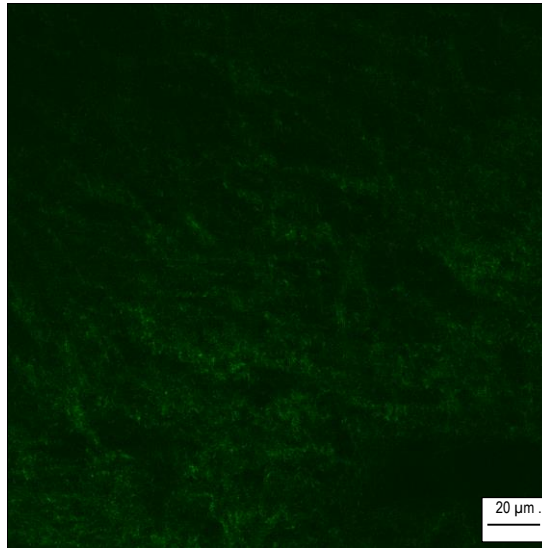


Figure 6.14 : Second harmonic image generation of freeze-dried acellular porcine carotid arteries.

Collagen fluorophores were excited using a two-photon Ti-Sapphire laser with 940 nm wavelength and 10 % transmission. Emission was filtered to detect wavelengths between 458 and 480 nm

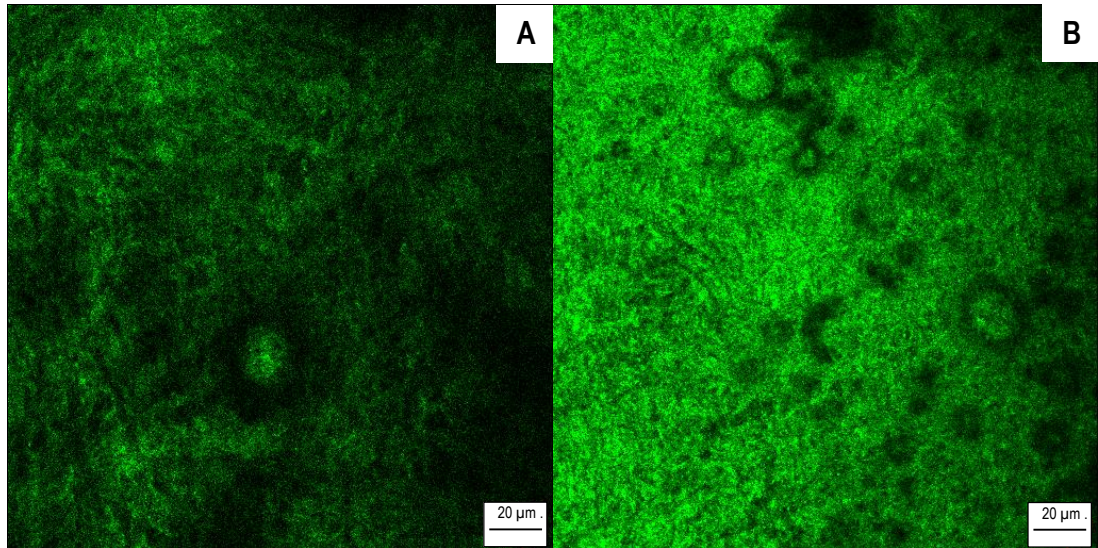


Figure 6.15 : Second harmonic image generation of freeze-dried EO treated acellular porcine carotid arteries (A, B).

Collagen fluorophores were excited using a two-photon Ti-Sapphire laser with 940 nm wavelength and 10 % transmission. Emission was filtered to detect wavelengths between 458 and 480 nm

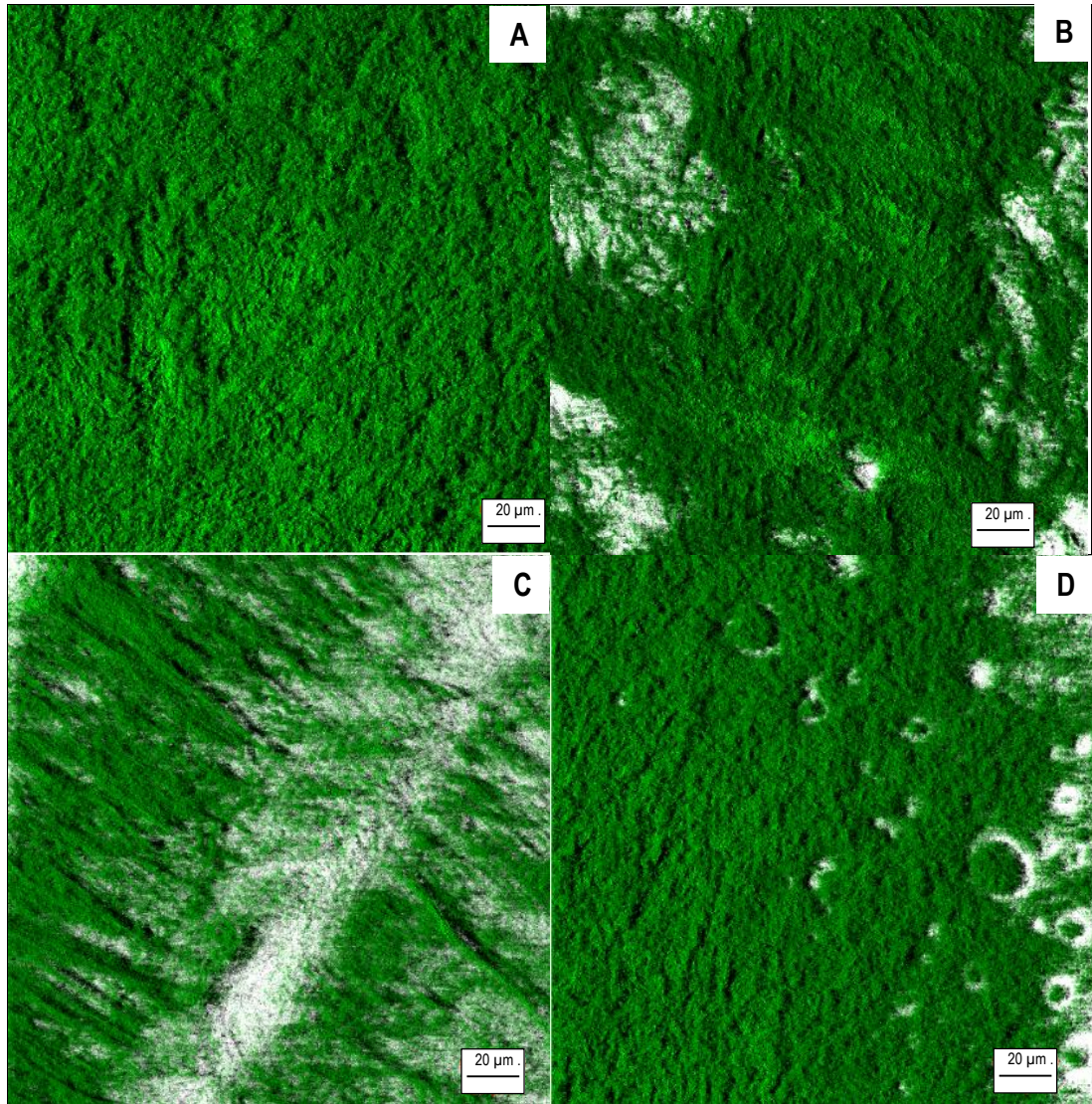


Figure 6.16 : Z stacked Second harmonic image generation of acellular (A), Gamma (B) and E-Beam (C) irradiated and EO (D) treated acellular porcine carotid arteries.

Collagen fluorophores were excited using a two-photon Ti-Sapphire laser with 940 nm wavelength and 10 % transmission. Emission was filtered to detect wavelengths between 458 and 480 nm. Z- stack images were captured at 1 um intervals.

6.4.6 Differential Scanning Calorimetry

Differential scanning calorimetry was used to measure the denaturation temperature of native, acellular, boiled and NBF fixed, Gamma irradiated, E-Beam irradiated, freeze-dried EO treated acellular porcine carotid arteries and the results are depicted in Figure 6.17. The acellular arteries measured were from Batch 3 and Batch 4 (Table 3.3) and were the quality control (QC) samples for the Gamma and E-Beam irradiated group and for the EO treated group. The data was analysed using one way ANOVA ($p < 0.05$). Positive controls demonstrated significant damage to the arteries. DSC could not detect a denaturation point in boiled arteries and showed that the denaturation point for NBF fixed arteries was 95.52 ± 1.11 °C. This was significantly higher ($p < 0.05$) than all other artery groups. The denaturation temperature of native, acellular Gamma irradiated, E-Beam irradiated, freeze-dried EO treated acellular porcine carotid arteries sterilised arteries were approximately 60 °C and were not significantly different from each other $p > 0.05$.

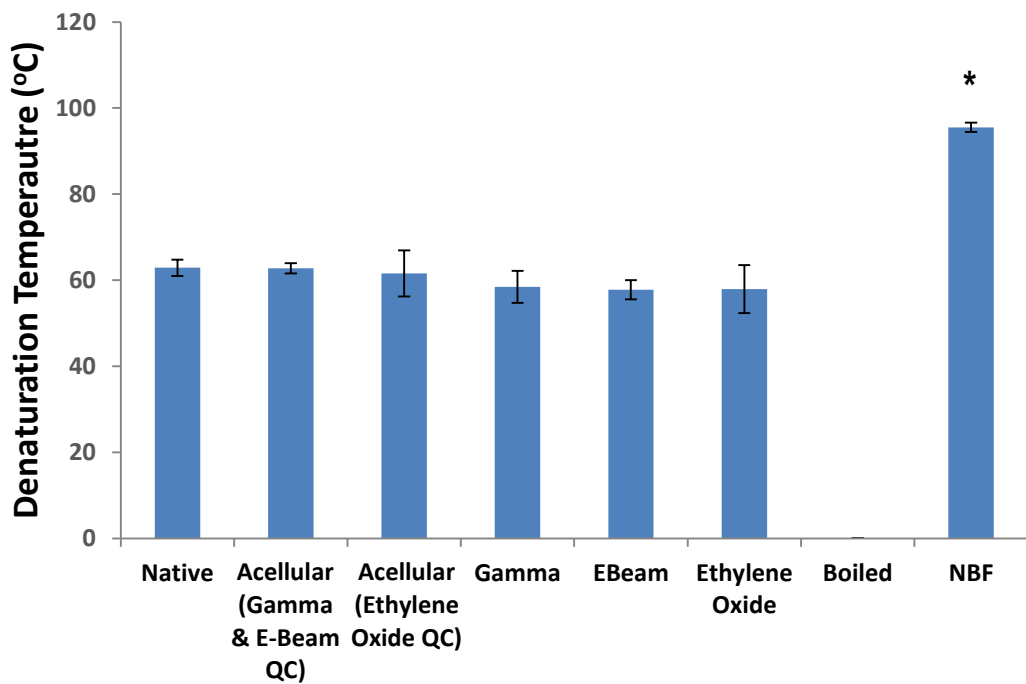


Figure 6.17 : Bar chart depicting denaturation temperatures of native, boiled and NBF fixed, acellular, Gamma irradiated, E-Beam irradiated, freeze-dried EO treated acellular porcine carotid arteries. Data is expressed as the mean ($n=5$; boiled and NBF, $n=4$) \pm 95 % C.L. Data was analysed using one way ANOVA ($p < 0.05$). DSC could not detect a denaturation point in boiled arteries. The denaturation point for NBF fixed arteries was 95.52 ± 1.11 , this was significantly ($p < 0.05$) higher than all other artery groups. The denaturation temperature of native, acellular, Gamma irradiated, E-Beam irradiated, and ethylene Oxide treated arteries were approximately 60 °C and were not significantly different from each other. *Significantly higher than all other arteries.

6.4.7 Denatured Collagen Content

The denatured collagen content was quantified in native, acellular, Gamma irradiated, E-Beam irradiated and freeze-dried EO treated acellular porcine carotid arteries, the denatured collagen content in a second group was quantified to compare positive controls for damage the samples consisted of native, boiled and NBF fixed porcine carotid arteries. Results are depicted in Figure 6.18. Data was analysed using a one way ANOVA and Tukey post-hoc testing. Ethylene oxide sterilised samples were found to contain significantly ($p < 0.05$) more denatured collagen than all other samples. Boiled samples were found to have significantly ($p < 0.05$) higher denatured collagen content than NBF and native samples but significantly ($p < 0.05$) lower than freeze-dried ethylene oxide treated samples. Native, acellular, Gamma and E-Beam irradiated and NBF fixed samples did not show any significant differences ($p > 0.05$) in denatured collagen content.

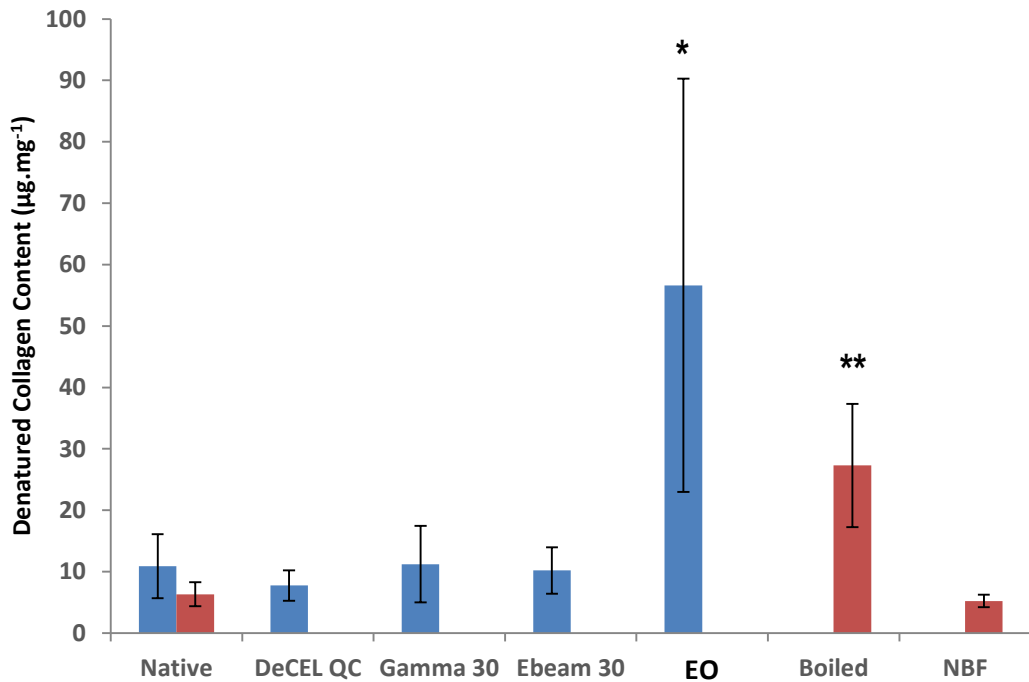


Figure 6.18 : Bar chart of denatured collagen content in native, acellular, acellular Gamma and E-Beam irradiated, EO treated, boiled and NBF fixed porcine carotid arteries

Data expressed as the mean (native, n=8, Blue, n=5, Red ; acellular. n=4; Gamma, n=4; E-Beam, n=5; EO, n=5; boiled, n=6; and NBF, n=6) \pm 95 % C.L. Data was analysed using one way ANOVA and Tukey post-hoc testing. Native, boiled and NBF fixed, acellular, Gamma and E-Beam irradiated, freeze-dried ethylene oxide treated acellular porcine carotid arteries had no significant differences in denatured collagen content. Freeze-dried EO treated acellular samples had significantly higher denatured collagen content than all other samples (*). Boiled samples had significantly more denatured collagen content than NBF fixed and native arteries but significantly less than freeze-dried ethylene oxide treated acellular samples (**).

6.5 Discussion

The research presented in this chapter investigated the biological characteristics of the acellular porcine carotid arteries after treatment with Gamma and E-Beam irradiation or EO.

Initially when the arteries were first sent for Gamma irradiation they were not placed in any support scaffold. On return it was clear that structural changes had occurred. Where the arteries had flattened in the packaging, permanent creases had occurred in the apex. When evaluated by histology with immunohistochemical labelling using an antibody to collagen IV, the creases could be observed and caused an artefact of localised increased intensity of labelling for collagen IV. This also created difficulties in mechanical testing and therefore this batch of arteries was scrapped and a new method to resolve the issue was introduced. A PEG semi-circular scaffold was created from vacuum formed moulds. The arteries were then placed into these scaffolds before packaging and vacuum sealing. On return from sterilisation treatment, the arteries no longer had creases and the artefact was no longer present. The creasing was likely due to the irradiation cross linking the arteries fixed in the flattened position. By placing them in a support structure the arteries were fixed in the natural cylindrical formation.

Histology showed no obvious changes in the structure after any of the sterilisation treatments showing that largely the ECM matrix appeared unchanged. Labelling for collagen IV following Gamma irradiation appeared to show a slight reduction in intensity but the immuno-staining was generally consistent with control acellular arteries, E-Beam irradiation reduced the intensity of collagen IV immuno-staining greatly and EO treatment removed all staining for collagen IV. As mentioned previously biological molecules are highly susceptible to alkylation due to the high incidence of accepting functional groups, it was therefore possible that the collagen IV epitopes recognised by the antibody had undergone conformational changes to such an extent that antibody binding no longer occurred. With respect to Gamma and E-Beam irradiated samples, both had patches of reduced intensity indicating that the collagen IV epitopes may also have been affected by irradiation, to varying extents. Gamma irradiation had far less effect with fewer patches of reduced immuno-staining for collagen IV when compared to E-Beam irradiated samples which showed a much higher reduction in intensity of immunostaining and more patchy areas of reduction. For the same dose of irradiation, E-Beam irradiation occurs as a high intensity electron beam with a short exposure time when compared to Gamma irradiation where a measured dose occurs over a long exposure time. It was perhaps this short burst of higher intensity that has caused E-Beam irradiation to have a more detrimental effect than Gamma irradiation on the collagen and elastin structure. These effects were consistent with those found with multiphoton imaging. When comparing images of Gamma irradiated samples with acellular samples there were small pockets where no signal was produced and an overall reduced intensity showed that significant structural changes had occurred but evidence of a similar pattern compared to the images of the

untreated acellular artery tissue remained. Multiphoton images of the E-Beam irradiated samples showed clear elongated structures of collagen but with large rifts in the tissue, highlighting the fact that E-Beam had significant damaging effects on the collagen structure when compared to images of the acellular control samples. Multiphoton images of freeze-dried acellular porcine carotid arteries showed a very similar pattern to multiphoton images of acellular porcine carotid arteries but with a slight reduction in intensity. This showed that the effects of freeze-drying on the collagen structure were minimal. Multiphoton images of freeze-dried EO treated acellular porcine carotid arteries showed that the intensity of the signal increased compared to freeze-dried arteries but the pattern seemed to represent less of an uncrimped collagen structure and more of a compact mesh. There were also numerous perforations and spherical artefacts. These artefacts could potentially have been caused by alkylation having a shrinking effect where pockets of increased EO concentrations had settled in the artery. This showed that EO treatment drastically changed the architecture of the artery.

It is well known that EO forms toxic residuals (Lucas *et al.*, 2003) and irradiation creates radiolytic by-products (Gehring, 1995). It was therefore necessary to determine if either irradiation or EO treatment resulted in cytotoxic acellular porcine carotid arteries. The results from the incubation of treated arteries with BHK and L929 cells showed that there were no cytotoxic effects from either process. In the EO treatment process the chamber undergoes a degassing period and cycles of nitrogen washes to help dilute the number of EO residuals. Further to this the arteries undergo aeration in which controlled pressure gradients and temperature help to reduce EO residuals over time. It is the addition and control of these steps by industrial sterilisation providers that will help to reduce instances of cytotoxic failure in EO sterilised products (Jackson *et al.*, 1990). In irradiated products the low levels and quick degradation rate of free radicals and radiolytic products may have limited the potential to cause the acellular porcine carotid arteries to become cytotoxic and the results shown here support this.

The differential scanning calorimetry results for the sterilised arteries showed that there were no significant reductions in denaturation temperature of the arteries. This indicated that the structural changes occurring as result of the processes were not sufficient to increase or decrease the peak temperature at which the collagen structure unfolded. In irradiated samples this could have been due to an increase in bonds due to cross-linking being counterbalanced by any reduction in protein length and for EO treated samples the increase in cross-linking showed no significant effect on the denaturation temperature. This also showed that the temperature of the sterilisation processes needed to be below 60 °C as typically EO cycles are carried out at much higher temperatures. Hence, using a low temperature cycle at 55 °C was justified.

The denatured collagen content of all sterilised samples was low in terms of weight per weight content. There were however still significant differences. The positive control of boiled porcine carotid arteries was only significantly higher temperature than NBF fixed porcine carotid arteries and not higher than native or acellular arteries as might be expected. This was probably because as the collagen is boiled at a higher than the denaturation temperature it becomes gelatinous and forms new bonds. A better denatured collagen content control could have been achieved by heating at just above the denaturation temperature for a period of time. It was however significantly lower than the denatured collagen content of the EO treated arteries. This could perhaps have been because at 55 °C, the temperature of the EO sterilisation process, is close to the denaturation temperature of collagen. This coupled with conformational changes occurring due to the EO treatment could have caused an increase in denatured collagen content.

To summarise, all of the sterilisation processes had no effect on the biocompatibility of the acellular arteries but all the process had an effect on the collagen structure to varying degrees. The histo-architecture of the arteries underwent some clearly observable changes, which were most apparent in the E-Beam irradiated and EO treated arteries which was also reflected in the mechanical data reported in Chapter 5. Gamma irradiated acellular arteries also showed definite changes to the collagen structure compared to acellular arteries but remained similar in nature.

The results presented in this chapter give a broader picture of the changes occurring in acellular porcine carotid arteries due to each of the sterilisation processes. This overall picture created by the biomechanical and biological findings for each sterilisation process will be discussed in the final chapter.

Chapter 7 Discussion

There is a clinical need for vascular conduits for a range of applications such as coronary artery bypass grafts, treatment of peripheral arterial disease and kidney dialysis access (Andros et al., 1986; Madden et al., 2005). For small diameter applications the current gold standard is autograft tissue such as the saphenous vein (Goldman et al., 2004). Unfortunately autograft tissue is not available in approximately one third of patients due to previous surgery, donor site morbidity or atherosclerosis (Bourassa, 1994). The major alternative, when no autograft tissue is available, is the use of synthetic graft. Synthetic grafts have limitations of low patency rates and have poor clinical prognosis when used in small diameter applications (Kannan et al., 2005). Therefore the possibility of a functional “off the shelf graft” is highly desirable. The aims of the research presented in this study were to develop a robust set of methods to assess the effects of different sterilisation processes on the mechanical and biological properties of a novel small diameter acellular xenogeneic vascular graft.

The acellular xenogeneic vascular grafts that were utilised during the study were produced from porcine carotid arteries using a previously patented decellularisation method (Ingham et al., 2010). Subsequent work had shown that the acellular porcine carotid arteries had regenerative capacity when tested in a large animal model (Wilshaw S. et al., 2014.). However, in order to translate the acellular porcine carotid arteries into a commercial product for clinical use, it is important that the arteries are sterile. For other acellular xenogeneic biological scaffolds produced using a similar decellularisation process at the University of Leeds, the scaffolds have been sterilised using a chemical sterilant and then aseptically transferred into packaging. This is not ideal and it is highly desirable that a terminal sterilisation process is adopted which has minimal effects on the biological and biomechanical properties of the acellular porcine carotid arteries.

Ideally, a terminal sterilisation method that is industrially available which enables the product to be sterilised in its final packaging should be used. The main industrially available sterilisation processes are Gamma and E-Beam irradiation and ethylene oxide (EO) treatment.

An implantable medical device requires a sterility assurance level (SAL) of 10^{-6} . It was, however beyond the scope of this study to validate the sterilisation processes that were investigated since these were contracted out to industry and were the standard doses and cycles commonly used in industry for the terminal sterilisation of medical devices. Hence the work presented here should be viewed as a feasibility study to determine the compatibility of these sterilisation processes when applied to acellular porcine carotid arteries.

For irradiation sterilisation a commonly practiced method is to apply VDMax 25 to sterilise the product (ISO, 11137-2:2012). This allows a validation using a small number of samples based on the product bioburden being less than 1000 colony forming units. Since the acellular porcine carotid arteries were disinfected and the decellularisation process inherently reduced product bioburden, this approach was adopted in this study. For EO sterilisation a commonly adopted method within industry is the overkill method (ISO, 11135:2014). This entails treating the product with half the concentration of EO required to achieve a SAL of 10^{-6} and then applying a cycle at double this dose giving a SAL of 10^{-12} .

The effects of Gamma and E-Beam irradiation and EO treatment on biological grafts such as bone and tendon have been well documented in the literature with contrasting results. Irradiation processes are well known to induce two mechanisms that can affect the mechanical properties of proteinaceous materials, polypeptide chain scission (Cheung et al., 1990) and cross-linking (Gouk et al., 2008). Chain scission reduces protein length and can reduce the ultimate tensile strength and moduli of proteinaceous materials, whereas cross linking can cause increasing strength and stiffness. Therefore the extent to which either of these mechanisms occurs during the sterilisation process will determine the effect on the mechanical properties. The effects of Gamma and E-Beam irradiation on bone and tendon has been widely reported with differing conclusions. Some comparative studies on the effects of Gamma and E-Beam irradiation have suggested that the treatments have similar effects on the mechanical properties and reduce the elastic modulus and ultimate tensile stress of tendons (Seto et al., 2009), whereas other studies suggest that Gamma irradiation had a greater impact on reducing the stiffness and ultimate tensile strength of tendons compared to E-Beam irradiation (Hoburg et al., 2015).

Acceptable levels of EO residuals for implantable medical devices been set in the ISO standards, however these levels might not reflect the levels required for a regenerative graft to be successful. It was therefore particularly important to assess the biocompatibility of EO treated grafts. The removal of chloride ions through washing pre-sterilisation (Kaku et al., 2002) and the use of heated aeration post sterilisation (Kakiuchi et al., 1996) are two ways to aid in the reduction of EO residuals. It has also been identified that wet tissues reduce the penetration depth of EO gas and that freeze-dried tissues allow better gas penetration (Kearney et al., 1989). Taking this into account, if EO treatment was to be considered as a possible sterilisation method then the effects of freeze-drying on the acellular graft prior to sterilisation also needed to be considered as part of this study. It has been reported that the combined effects of freeze-drying and EO sterilisation on tendon grafts does not have a significant impact on the mechanical properties (Smith et al., 1996; Bechtold et al., 1994).

When considering the literature on the effects of sterilisation on tendons it is important to note that the biological composition of tendons, in terms of elastin and collagen content is quite different compared to elastic soft tissues such as arteries.

Therefore, it was important that both the biological and mechanical effects of the sterilisation processes on the acellular porcine carotid arteries were fully investigated. It was equally important to ensure that the methods used to assess these effects were robust. Hence, a large proportion of the work presented in this study involved development of the methods to establish the effects of the sterilisation processes on the biomechanical properties of the acellular porcine carotid arteries.

Firstly it was necessary to determine whether the acellular porcine carotid arteries could be produced repeatedly and consistently using the previously established decellularisation process. This was demonstrated in Chapter (3) through the production of several batches of acellular porcine carotid arteries with a greater than 80 % reduction in DNA content and preservation of the histoarchitecture when observed in haematoxylin and eosin stained sections. The acellular porcine carotid arteries were also shown to be biocompatible using contact cytotoxicity analysis. These studies also provided sufficient material to conduct the studies described in the subsequent Chapters.

Two sets of mechanical test methods were adopted and developed to assess the mechanical properties of the acellular porcine carotid arteries, uniaxial tensile testing and burst pressure and compliance testing. Uniaxial tensile testing has historically been used to assess the biphasic nature of collagenous tissues (Fung, 1993) although, due to the anisotropy of arteries it was necessary to test samples in both the circumferential and axial directions. The uniaxial tensile testing method was adopted from previous studies and then optimised for performance with porcine carotid arteries. The most significant development was the determination of the correct amount of preloading for the jig being used and new understanding of how overestimating this result could easily mask any differences in properties between groups. The developed uniaxial testing protocol allowed in-depth comparisons to be made of mechanical properties of the arteries that had been subject to different treatments including the collagen and elastin phase modulus and the ultimate tensile strength.

Compliance testing allowed a multi-axial assessment of the arteries to gain an understanding of how the artery might perform physiologically. In addition, it was essential to ensure that the method for determining compliance of the arteries was accurate and reliable since compliance is a known factor for failure of vascular grafts (Walden et al., 1980; Abbott et al., 1987; Seifert et al., 1979). Failure to determine the compliance properties of a potential vascular graft correctly could have a large impact on the functionality of the graft in-vivo. Due to the natural tendency of the arteries to bend under inflation, it was necessary to test various methods in order to keep the artery within the plane of the camera. Similarly, the method of measuring of the artery diameter using image analysis software needed to be repeatable. The final method adopted was robust enough to provide confidence in the results.

The biological methods adopted in this thesis were predominantly well established methods that were readily transferable to the investigation, for example examining the histoarchitecture using histology and immunohistochemical investigation of the collagen IV content. Some of the more novel methods used were multiphoton imaging and DSC. The multiphoton imaging created images based on the ability of the collagen structure to emit second harmonic light. When a collagenous structure is damaged or altered its ability to emit second harmonic light diminishes (Lin et al., 2006; Brockbank et al., 2008; Schenke-Layland, 2008) Hence, this method provided a good tool for visual demonstration of any effects caused by sterilisation on the porcine carotid arteries. DSC is a thermo-analytical technique that has been used to identify the denaturation temperatures of collagenous materials by measuring the heat energy change (Sun & Leung, 2008). This method could be used firstly to provide evidence for the workable temperature ranges of the arteries and whether the temperature conditions of a particular sterilisation process was suitable for the graft and secondly it could potentially identify changes caused by the sterilisation process.

For Gamma and E-Beam irradiation the two predominant mechanisms acting on the biological and mechanical structure are chain-scission and cross-linking. Through examination of the results it was clear that for the same dose of irradiation the mechanisms were not consistent between the two processes.

From a mechanics stand point, the E-Beam irradiation increased the stiffness of the elastin modulus and collagen modulus, with the greatest increase in stiffness on the elastin modulus. E-Beam irradiation also reduced the ultimate strength of the material perhaps indicating that while a large increase in stiffness occurred due to cross-linking, in the elastin modulus a large chain-scission effect could have occurred simultaneously. The increased circumferential elastic stiffness certainly had an impact on the compliance testing, which demonstrated a longitudinal expansion and a circumferential narrowing under pressure giving a negative percentage diameter change. The clear indication that E-Beam irradiation had a significant effect on the ECM was also highlighted in the biological evaluation. The collagen IV immunostaining intensity was greatly reduced with patches of very low intensity and the multiphoton imaging also showed the collagen as segmented with large areas where no second harmonic light was generated. These observations suggested that the collagen structure had been altered resulting in a loss of antibody binding to collagen IV and reduction in ability to emit second harmonic light as usually seen in collagen structures. Although short lived, the temperature of the E-Beam process can rapidly increase to 40 °C above ambient temperature which when considering the DSC data could have raised the temperature above the denaturation point of collagen (~ 60 °C), the denatured collagen content of the treated tissue was however not significantly different to native or acellular porcine carotid arteries. This did not support the hypothesis that the arteries had been over-heated and therefore it was unlikely that that this was the cause of the structural alterations occurring in the matrix. On a

whole the data presented in both chapters 5 and 6 supported the conclusion that E-Beam irradiation is not a compatible choice of sterilisation for acellular vascular grafts.

Gamma irradiation sterilisation of acellular porcine carotid arteries resulted in minimal differences compared to untreated acellular arteries. There were indications of increased stiffness of both the collagen and elastin modulus but the only significant difference was a decrease in transition strain in the axial direction demonstrating a reduced extensibility. As there was no significant reduction in UTS it might be concluded that chain-scission of the proteins in the matrix was not a predominant effect as seen for E-Beam irradiation. Equally when considering the compliance there was no significant difference in the compliance of the Gamma irradiation treated acellular porcine carotid arteries compared to the untreated acellular arteries, demonstrating that Gamma irradiation had far less impact on the elastin modulus compared to E-Beam irradiation. This was not however reflected in the biological evaluation. The collagen IV staining showed a reduction in intensity and the multiphoton imaging showed some distinct changes in structure and reduction in second harmonic light generated compared to acellular arteries. This supports that the combined effects of chain-scission and cross-linking on the mechanical properties of collagen in Gamma irradiated acellular porcine carotid arteries are in effect cancelling each other out but that the process itself is still changing the structure of the proteinaceous material.

Much of the initial literature on the effects of irradiation sterilisation on collagenous materials was carried out at doses above 200 kGy. More recent work has been investigated the effects of lower doses below 50 kGy to reflect the requirements of sterilisation processes. The mechanisms of chain-scission and free-radical formed cross-linking can have varying effects based on tissue structure, process environment conditions, hydrated vs dehydrated tissue and, of course, irradiation dose. Sun & Leung (2008) Gamma irradiated decellularised human dermis (Alloderm, LifeCell Corporation, Branchburg, NJ) at doses from 0 to 32 kGy. They found that the denaturation temperature determined by DSC decreased with increasing dose and hypothesised that chain-scission was the predominant factor at lower doses. Controversially the DSC results from this study suggested that for both E-Beam and Gamma irradiation that either the cross-linking had occurred to an extent that masked the chain-scission or that chain-scission was having little effect on the denaturation temperature of the collagen. This could potentially have been due to the fact that the decellularised human dermis was irradiated in a freeze-dried state in a nitrogen atmosphere with low relative humidity. These conditions reduce the water content present during irradiation and prevent the formation of free radicals such as hydroxyl radicals, that promote the formation of cross-linking (Gorham et al., 1993; Lerouge & Simmons, 2012). Gouk et al. (2008) investigated the mechanics of the same decellularised freeze-dried human dermis, after Gamma irradiation at doses of 0 to 30 kGy, after it had been rehydrated. Again, the mechanical data showed a reduction in UTS and Young's modulus with increasing dose, supporting the conclusion that

chain-scission was the predominant mechanism. A comparison to the results found in this study suggested that the presence of water may have greatly impacted on the occurrence of free-radical induced cross-linking and masked any measurable effects from chain-scission.

In a move away from traditional high dose Gamma irradiation of bone-patella-tendon-bone grafts, Hoburg et al. (2015) compared the effects of E-Beam and Gamma irradiation on bone-patella-tendon grafts at 25 kGy and 34 kGy and found that Gamma irradiation significantly reduced the stiffness and failure load at both 25 kGy and 34 kGy, whereas only the failure load was reduced with E-Beam irradiation at 34 kGy. These findings were again contrary to the results found in the present study for Gamma and E-beam irradiated acellular porcine carotid arteries, this could be attributed to the differences in the parameters used in the process, including temperature and environment. In the Hoburg et al. (2015) study all the irradiation treatments were carried out on dry ice (~ -70 °C) and the E-Beam irradiation of the tendons was carried out in an inert atmosphere of CO₂. Both of these conditions have the ability to reduce the occurrence of free-radical reactions. The differences between the Gamma irradiated and E-Beam irradiated tendons could also potentially be attributed to differences in the process parameters as the Gamma irradiation process was carried out in air and therefore the differences in mechanical properties of the irradiated tendons cannot solely be attributed to the difference in the irradiation mechanisms. The inclusion of a group of tendons Gamma irradiated in CO₂ would have enabled conclusions about the differences in Gamma and E-Beam irradiation more convincingly and provided more insight on the mechanisms occurring. In addition, both irradiation treatments were carried out at -70 °C compared to the ambient temperature used in this study. This reduction in temperature may have reduced the kinetic energy and therefore the incidence of free-radical reactions. The data from the Hoburg et al. (2015) study also suggested that free-radical reactions may have caused chain-scission in the collagen of the tendons, as chain-scission is associated with a reduction in stiffness and strength and these were the effects negated in an atmosphere of CO₂. It is important to note the differences in structure when comparing the effects of sterilisation on tendons vs arteries. There is a much higher proportion of collagen in tendons and limited amounts of elastin compared to the elastin rich artery.

In agreement with the literature (Gorham et al., 1993) neither Gamma or E-Beam irradiation of the acellular porcine carotid arteries resulted in the presence of any cytotoxic residuals in the tissue and on the whole, the histoarchitecture of the irradiated tissues appeared to be unaffected by the treatments as judged by observation of H&E stained tissue sections. .

The main mechanism of action of EO treatment is cross-linking of proteins caused by alkylation. Both collagen and elastin have functional groups susceptible to this mechanism. The biomechanical data presented in this study showed significant increases in the collagen and elastin modulus and ultimate tensile stress of the acellular porcine carotid arteries post EO treatment. This suggested that cross-linking had occurred throughout the ECM. In

contrast to irradiation processes EO treatment does not cause chain-scission and hence a significant increase in strength of the acellular porcine carotid arteries post treatment was observed. This finding was reflected in the compliance data for the EO treated acellular porcine carotid arteries. Similar to E-Beam irradiation, EO treatment increased the elastin modulus to an extent that resulted in a negative percentage diameter change and expansion only occurred longitudinally. These effects of EO treatment of the acellular porcine carotid arteries were only partially reflected in the biological evaluation. Following EO treatment there was an absence of collagen IV immuno-staining indicating that the epitope recognised by the antibody had been altered or lost. Multiphoton imaging of EO treated acellular artery tissue however showed little difference in the treated tissue compared to untreated acellular artery tissue. This suggested that any cross-linking of the collagen caused by EO treatment had not greatly altered the overall collagen structure.. At lower resolution, using light microscopy to assess H&E stained sections; gross separation between the layers of the ECM of the EO treated tissue was observed. This had occurred mostly in the adventitial and luminal areas of the treated tissues where exposure to EO was greatest. There were also spherical artefacts found in the EO treated arteries that were perhaps separation caused by the cross-linking of the collagen structure.

The EO treated acellular porcine carotid arteries also showed significantly higher levels of denatured collagen content compared to the native and acellular arteries. This increase in denatured collagen content could have been due to the fact the sterilisation process was carried out at 55 °C which was close to the denaturation temperature of the acellular porcine carotid arteries as determined by DSC. The amount of denatured collagen present was however, still very low and there were no observable deterioration on the mechanics as might be expected with denaturation of collagen. The EO treated acellular porcine carotid arteries showed no evidence of cellular toxicity in the contact cytotoxicity assays indicating that the controlled aeration of the arteries was sufficient length of time to eliminate any cytotoxic residuals.. In conclusion, with regard to EO sterilisation of the acellular porcine carotid arteries although the collagen structure seemed to be preserved when observed in the multiphoton imaging, the gross histoarchitecture was altered significantly and the biomechanical properties, particularly the compliance data demonstrated that EO treatment is not a feasible sterilisation process for acellular vascular grafts.

The biomechanical test results reported in this study raises the question of whether more attention needs to be paid to the structural changes that might occur in elastin as a result of sterilisation of acellular arterial grafts. Compliance mismatch is one of the key causes of failure in arterial grafts and the structural component associated with this is elastin. Significant changes to the elastin phase in E-Beam irradiated and EO treated arteries caused a complete reversal of compliance. The overall strength of the matrix, which is essential, remained adequate in both EO treated and E-Beam irradiated arteries. It is important for a

vascular graft to reach a threshold of strength to prevent rupture, typically 2000 mmHg is the minimum (Teebken & Haverich, 2002), but once this threshold is met the most important factor is matching the compliance characteristics.

The overall aim of establishing the potential of industrial sterilisation processes for use with acellular vascular grafts in this study was fulfilled. Firstly, it was shown that both E-Beam irradiation and EO treatment were incompatible for use with acellular porcine carotid arteries resulting in significant stiffening of the elastin modulus and negative percentage diameter changes upon compliance testing. It would not be feasible to use these sterilisation methods to produce acellular porcine carotid arteries for clinical use. Gamma irradiation, however, showed promise as a potential sterilisation method for the acellular vascular grafts. The process did cause some stiffening of acellular arteries but had a greater effect on the collagen modulus compared to the elastin modulus. This lesser effect on the elastin modulus compared to E-Beam irradiation and EO treatment could clearly be seen when in the compliance testing data. The percentage diameter change of Gamma irradiated acellular porcine carotid arteries was not significantly different to acellular arteries. Indeed, Gamma irradiation treatment may result in a graft with more desirable characteristics by increasing the overall strength of the tissue without effecting the artery compliance, however further investigation would be required to assess this. In conclusion, it was shown that Gamma irradiation is a feasible sterilisation method for acellular vascular grafts and Gamma irradiation could be further investigated to optimise the sterilisation process.

Future Studies.

In oncology the use of cumulative doses of radiation to target tumours to deliver the therapeutic dose has been practised over many years (Gerbi et al., 2009). It is also accepted in irradiation sterilisation that cumulative doses (ISO, 11137-2:2012) combine to make the total dose. The use of fractionated doses of irradiation has also been investigated in a novel approach to reduce the effects of irradiation on the structure of biological tissue. The theory is that the use of multiple short bursts of lower dose irradiation will reduce the detrimental effects on the tissue. This has been successfully demonstrated using fractionated E-Beam irradiation compared to single dose E-Beam and Gamma irradiation (Hoburg et al., 2011). It would therefore be of interest to study the effects of fractionated Gamma irradiation, to reach the required sterilisation dose, on the biomechanical and biological properties of acellular porcine carotid arteries.. For example, two doses of 12.5 kGy or four doses of 6.25 kGy could be investigated. There are however some limitations to the potential implementation of fractionated Gamma irradiation. In Industrial sterilisation plants the tolerances of the dose mapping for both E-Beam and Gamma irradiation are not as sensitive as the research based facilities. This could pose a barrier to this option due to cost or availability. With reference to industrial irradiation sterilisation validation, VDmax methods are adopted since this reduces the number of samples that have to be destroyed in order to validate the process. The

methods used to validate irradiation sterilisation processes are dependent on the bioburden of the product. With regard to acellular porcine tissue products, the combination of the antibiotic wash and the decellularisation process itself has been shown to disinfect the tissue (Holmes, 2013) It is therefore anticipated that the acellular porcine carotid artery product would have a low bioburden. If this was robustly demonstrated to be less than 1.5 CFU then VDmax 15 could be adopted, reducing the required Gamma irradiation sterilisation dose. There could however be some contention regarding the use of low dose of Gamma irradiation for a graft derived from xenogeneic tissue. It would be necessary to investigate viral clearance in future studies once a sterilisation method has been optimised and found to be compatible with vascular tissues. There is disagreement within the literature regarding the dose of irradiation needed for viral inactivation (Spire et al., 1985; Sullivan et al., 1971; Fideler et al., 1994). As part of ISO 22442-3:2007 "Medical devices utilizing animal tissues and their derivatives", a risk assessment for the tissue must be carried out followed by any validations deemed necessary as a result of the risk assessment. A full literature review would be necessary to determine the best model viruses, however for a porcine derived tissue, potential highly irradiation resistant viruses are porcine parvoviruses (enveloped) and pseudorabies virus (non enveloped) (ISO, 22442-3:2007). An investigation could include spiking native porcine carotid arteries with a known titre of virus, subjecting the arteries to the decellularisation process and the sterilisation process and then measuring recovery of the virus before decellularisation after decellularisation and after sterilisation.

Another method that has been adopted in other studies is the use of radio protectants to reduce damage caused by irradiation to the tissue. Radioprotectants have been used successfully to minimise the effects on mechanical parameters of tendons subjected to high dose (~50 kGy) Gamma irradiation (Grieb et al., 2006) and E-Beam irradiation (Seto et al., 2009). The idea behind radioprotectants is that free-radicals that are produced during sterilisation have the ability to cause either cross-linking or chain-scission in the graft, a radioprotectant interacts with these free-radicals limiting the damage potential to the graft. It would be interesting to evaluate the effects one or a combination of radioprotectants might have on preserving the biological and mechanical parameters of acellular vascular grafts when irradiated.

The methods that have been developed or adopted during the present study were adequate for the initial investigation of the effects of sterilisation processes on the biological and biomechanical properties of the acellular porcine carotid arteries; however, other techniques could have been used. Gouk et al. (2008) employed techniques such as scanning electron microscopy (SEM), swelling ratio and enzyme degradation to assess the effects of sterilisation on biological tissue. These techniques have advantages and disadvantages compared to techniques such as multiphoton imaging for example, the use of SEM would allow observation of the tissue structure when it has been damaged, whereas the use of

multiphoton imaging is limited to changes in the capacity of the tissue to emit second harmonic light. Enzymatic degradation is a technique employed to assess either the increase in stability of a biological material due to cross-linking or the decrease in stability due to chain scission. The theory is based on the concept that if cross-linking has occurred, the resistance to enzymatic digestion would increase and if polypeptide fragmentation has occurred due to chain-scission then the resistance to enzymatic digestion may decrease. This method also may allow determination of the particular protein damaged by using enzymes specific to a certain sequences of amino acids in the protein. Determination of the swelling ratio has been used as an estimation of cross-linking density based on the equations used for a polymeric network (Jiang et al., 2006). A decrease in swelling ratio can be estimated as increase in cross-linking density as the matrix becomes more tightly packed together, however this type of evaluation may not be sensitive enough to detect changes in a product with high natural variability but could be a simple method to assess an increase in cross-linking as a result of sterilisation.

Although cross-linking mechanisms have been established in (Eyre et al., 1984) collagen and elastin, it would be useful to further investigate the differences in radiation induced cross-linking. One method that could potentially highlight the structural changes due to cross-linking is infrared spectroscopy (Jiang et al., 2006; Zhang et al., 2014). Again, due to the natural variability between products when using animal tissues it may be necessary to do matched testing by using tissue from the same sample before and after sterilisation.

High performance liquid chromatography (HPLC) has also been used to evaluate cross-links in collagen and elastin (Eyre et al., 1984). HPLC can be used to evaluate enzymatic digest products and with the use of reverse phase HPLC it may be possible to identify the mechanism of irradiation induced cross-linking collagenous materials.

Other future studies that should be undertaken include the assessment of the thrombogenic potential of the acellular porcine carotid arteries before and after gamma sterilisation. Damage to the basement membrane and intima layer could potentially alter the thrombogenic potential of the graft. There are simple in vitro methods available to assess the thrombogenicity of a material, for example the Chandler loop method (Guilliatt RS *et al.*, 2011; Tatterton *et al.*, 2012). This would involve placing the artery in-line with circular tubing filled with citrated sheep's blood and after a period of incubation with rotation, the weight of any clot formed would then be assessed.

Once a sterilisation process has been established the long-term shelf life and stability of the acellular porcine carotid arteries post-sterilisation would need to be assessed. Free-radical reactions can continue to occur in the final packaging post sterilisation and the extent of this would need to be evaluated. Real time shelf life could be assessed at intervals over the period of a year using the methods developed in this study to evaluate if the biological and mechanical properties were stable over time. In addition to the methods already developed,

the thrombogenicity could also be assessed and new methods for determining cross-linking density could be investigated.

Another vital piece of information that could be investigated in future studies is to carry out mechanical and biological evaluation of human arteries at the graft site. Arteries to be included would be coronary arteries of the heart, femoral and popliteal arteries of the leg and ulnar and radial arteries of the arm. This would then provide comparative data on the desired biological and mechanical properties to match the acellular graft against. Limitations to this will be down to careful screening of cadaveric material to obtain non-diseased arteries.

Finally in-vivo studies in an animal model would be a huge benefit. This has the potential to demonstrate that post sterilisation the combined biological and mechanical characteristics of the sterile acellular vascular graft are adequate for purpose. A comparison of the patency rates of sterile acellular vascular grafts vs synthetic alternatives would provide a good indicator as to the potential of the process.

To conclude Gamma irradiation presents a potential method for sterilisation of acellular vascular grafts.

List of References

- ABBOTT, W. M., J. MEGERMAN, J. E. HASSON, G. L'ITALIEN and D. F. WARNOCK. 1987. Effect of compliance mismatch on vascular graft patency. *Journal of Vascular Surgery*, **5**(2), pp.376-382.
- ANDROS, G., R. W. HARRIS, S. X. SALLES-CUNHA, L. B. DULAWA, R. W. OBLATH and R. L. APYAN. 1986. Arm veins for arterial revascularization of the leg: Arteriographic and clinical observations. *Journal of Vascular Surgery*, **4**(5), pp.416-427.
- ANSI. 2011. *ANSI/AAMI ST67 Sterilization of health care products Requirements and guidance for selecting a sterility assurance level (SAL) for products labeled 'sterile'*. American National Standards Institute.
- ARIZONO, T., Y. IWAMOTO, K. OKUYAMA and Y. SUGIOKA. 1994. Ethylene oxide sterilization of bone grafts. Residual gas concentration and fibroblast toxicity. *Acta Orthop Scand*, **65**(6), pp.640-2.
- BADYLAK, S. F., D. O. FREYTES and T. W. GILBERT. 2009. Extracellular matrix as a biological scaffold material: Structure and function. *Acta Biomater*, **5**(1), pp.1-13.
- BALLESTRA, P. and J.-L. CUQ. 1998. Influence of Pressurized Carbon Dioxide on the Thermal Inactivation of Bacterial and Fungal Spores. *LWT - Food Science and Technology*, **31**(1), pp.84-88.
- BALLYK, P. D., C. WALSH, J. BUTANY and M. OJHA. 1998. Compliance mismatch may promote graft-artery intimal hyperplasia by altering suture-line stresses. *J Biomech*, **31**(3), pp.229-37.
- BARNES, C. P., S. A. SELL, E. D. BOLAND, D. G. SIMPSON and G. L. BOWLIN. 2007. Nanofiber technology: designing the next generation of tissue engineering scaffolds. *Adv Drug Deliv Rev*, **59**(14), pp.1413-33.
- BASSIOUNY, H. S., S. WHITE, S. GLAGOV, E. CHOI, D. P. GIDDENS and C. K. ZARINS. 1992. Anastomotic intimal hyperplasia: Mechanical injury or flow induced. *Journal of Vascular Surgery*, **15**(4), pp.708-717.
- BAULMANN, W. L. 1985. *ELECTRON BEAM CURING OF UNSATURATED COATING MATERIALS*. Patent number:
- BECHTOLD, J. E., D. T. EASTLUND, M. K. BUTTS, D. F. LAGERBORG and R. F. KYLE. 1994. The effects of freeze-drying and ethylene oxide sterilization on the mechanical properties of human patellar tendon. *Am J Sports Med*, **22**(4), pp.562-6.
- BERGER, K., L. R. SAUVAGE, A. M. RAO and S. J. WOOD. 1972. Healing of arterial prostheses in man: its incompleteness. *Ann Surg*, **175**(1), pp.118-27.
- BERGLUND, J. D., M. M. MOHSENI, R. M. NEREM and A. SAMBANIS. 2003. A biological hybrid model for collagen-based tissue engineered vascular constructs. *Biomaterials*, **24**(7), pp.1241-1254.
- BOLLAND, F., S. KOROSSIS, S.-P. WILSHAW, E. INGHAM, J. FISHER, J. N. KEARNEY and J. SOUTHGATE. 2007. Development and characterisation of a full-thickness acellular porcine bladder matrix for tissue engineering. *Biomaterials*, **28**(6), pp.1061-1070.

- BOOTH, C., S. A. KOROSSIS, H. E. WILCOX, K. G. WATTERSON, J. N. KEARNEY, J. FISHER and E. INGHAM. 2002. Tissue engineering of cardiac valve prostheses I: development and histological characterization of an acellular porcine scaffold. *J Heart Valve Dis*, **11**(4), pp.457-62.
- BOU-GHARIOS, G., M. PONTICOS, V. RAJKUMAR and D. ABRAHAM. 2004. Extra-cellular matrix in vascular networks. *Cell Proliferation*, **37**(3), pp.207-220.
- BOURASSA, M. G. 1994. Long-term vein graft patency. *Current Opinion in Cardiology*, **9**(6), pp.685-691.
- BROCKBANK, K. M., W. R. MACLELLAN, J. XIE, S. HAMM-ALVAREZ, Z. CHEN and K. SCHENKE-LAYLAND. 2008. Quantitative second harmonic generation imaging of cartilage damage. *Cell and Tissue Banking*, **9**(4), pp.299-307.
- BROTHERS, T. E., J. C. STANLEY, W. E. BURKEL and L. M. GRAHAM. 1990. Small-caliber polyurethane and polytetrafluoroethylene grafts: A comparative study in a canine aortoiliac model. *J Biomed Mater Res*, **24**(6), pp.761-771.
- BRUCE ALBERTS, DENNIS BRAY, ALEXANDER JOHNSON, JULIAN LEWIS, MARTIN RAFF, KEITH ROBERTS and AND PETER WALTER. 2004. Essential Cell Biology. *Garland Science*
- CAMPBELL, D. G. and P. LI. 1999. Sterilization of HIV with irradiation: relevance to infected bone allografts. *Aust N Z J Surg*, **69**(7), pp.517-21.
- CARLSON, B. E., J. C. ARCIERO and T. W. SECOMB. 2008. Theoretical model of blood flow autoregulation: roles of myogenic, shear-dependent, and metabolic responses. *American Journal of Physiology - Heart and Circulatory Physiology*, **295**(4), pp.H1572-H1579.
- CHAKRABARTY, K. H., R. A. DAWSON, P. HARRIS, C. LAYTON, M. BABU, L. GOULD, J. PHILLIPS, I. LEIGH, C. GREEN, E. FREEDLANDER and S. MAC NEIL. 1999. Development of autologous human dermal-epidermal composites based on sterilized human allodermis for clinical use. *Br J Dermatol*, **141**(5), pp.811-23.
- CHEUNG, D. T., N. PERELMAN, D. TONG and M. E. NIMNI. 1990. The effect of gamma-irradiation on collagen molecules, isolated alpha-chains, and crosslinked native fibers. *J Biomed Mater Res*, **24**(5), pp.581-9.
- CHLUPÁČ, J., E. FILOVÁ and L. BACÁKOVÁ. 2009. Blood vessel replacement: 50 years of development and tissue engineering paradigms in vascular surgery. *Physiological research / Academia Scientiarum Bohemoslovaca*, **58 Suppl 2**, pp.S119-S139.
- COLLINS, R. G., R. VELJI, N. V. GUEVARA, M. J. HICKS, L. CHAN and A. L. BEAUDET. 2000. P-Selectin or Intercellular Adhesion Molecule (Icam)-1 Deficiency Substantially Protects against Atherosclerosis in Apolipoprotein E-Deficient Mice. *The Journal of Experimental Medicine*, **191**(1), pp.189-194.
- COOPER, G. M. 2000. *The Cell: A Molecular Approach*. Sunderland (MA): Sinauer Associates.
- COURTMAN, D. W., C. A. PEREIRA, V. KASHEF, D. MCCOMB, J. M. LEE and G. J. WILSON. 1994. Development of a pericardial acellular

- matrix biomaterial: biochemical and mechanical effects of cell extraction. *J Biomed Mater Res*, **28**(6), pp.655-66.
- CRAPO, P. M., T. W. GILBERT and S. F. BADYLAK. 2011. An overview of tissue and whole organ decellularization processes. *Biomaterials*, **32**(12), pp.3233-3243.
- CYRUS, T., J. L. WITZTUM, D. J. RADER, R. TANGIRALA, S. FAZIO, M. F. LINTON and C. D. FUNK. 1999. Disruption of the 12/15-lipoxygenase gene diminishes atherosclerosis in apo E-deficient mice. *The Journal of Clinical Investigation*, **103**(11), pp.1597-1604.
- DARDIK, H., N. MILLER, A. DARDIK, I. IBRAHIM, B. SUSSMAN, S. M. BERRY, F. WOLODIGER, M. KAHN and I. DARDIK. 1988. A decade of experience with the glutaraldehyde-tanned human umbilical cord vein graft for revascularization of the lower limb. *J Vasc Surg*, **7**(2), pp.336-46.
- DARDIK, H., K. WENGERTER, F. QIN, A. PANGILINAN, F. SILVESTRI, F. WOLODIGER, M. KAHN, B. SUSSMAN and I. M. IBRAHIM. 2002. Comparative decades of experience with glutaraldehyde-tanned human umbilical cord vein graft for lower limb revascularization: an analysis of 1275 cases. *J Vasc Surg*, **35**(1), pp.64-71.
- DAS, N., M. J. BRATBY, V. SHRIVASTAVA, A. J. CORNALL, C. R. DARBY, P. BOARDMAN, S. ANTHONY and R. UBEROI. 2011. Results of a seven-year, single-centre experience of the long-term outcomes of bovine ureter grafts used as novel conduits for haemodialysis fistulas. *Cardiovasc Intervent Radiol*, **34**(5), pp.958-63.
- DAVIS, E. C. 1993. Endothelial cell connecting filaments anchor endothelial cells to the subjacent elastic lamina in the developing aortic intima of the mouse. *Cell and Tissue Research*, **272**(2), pp.211-219.
- DEBELLE, L. and A. M. TAMBURRO. 1999. Elastin: molecular description and function. *The International Journal of Biochemistry & Cell Biology*, **31**(2), pp.261-272.
- DERHAM, C., H. YOW, J. INGRAM, J. FISHER, E. INGHAM, S. A. KORROSI and S. HOMER-VANNIASINKAM. 2008. Tissue engineering small-diameter vascular grafts: preparation of a biocompatible porcine ureteric scaffold. *Tissue Eng Part A*, **14**(11), pp.1871-82.
- DESAI, M., A. M. SEIFALIAN and G. HAMILTON. 2011. Role of prosthetic conduits in coronary artery bypass grafting. *European Journal of Cardio-thoracic Surgery*, **40**(2), pp.394-398.
- DEVIREDDY, R. V., M. R. NEIDERT, J. C. BISCHOF and R. T. TRANQUILLO. 2003. Cryopreservation of collagen-based tissue equivalents. I. Effect of freezing in the absence of cryoprotective agents. *Tissue Eng*, **9**(6), pp.1089-100.
- DEWEESE, J. A., H. B. BARNER, E. B. MAHONEY and C. G. ROB. 1966. Autogenous venous bypass grafts and thromboendarterectomies for atherosclerotic lesions of the femoropopliteal arteries. *Ann Surg*, **163**(2), pp.205-14.
- DINGEMANS, K. P., P. TEELING, J. H. LAGENDIJK and A. E. BECKER. 2000. Extracellular matrix of the human aortic media: An ultrastructural histochemical and immunohistochemical study of the adult aortic media. *The Anatomical Record*, **258**(1), pp.1-14.

- DONG, Z. M., S. M. CHAPMAN, A. A. BROWN, P. S. FRENETTE, R. O. HYNES and D. D. WAGNER. 1998. The combined role of P- and E-selectins in atherosclerosis. *The Journal of Clinical Investigation*, **102**(1), pp.145-152.
- EMA. 1996. *Note for Guidance on Virus Validation Studies: The Design, Contribution and Interpretation of Studies Validating the Inactivation and Removal of Viruses*. European Medicines Agency: Committee for Human Medicinal Products (CHMP) and the Biotechnology Working Party (BWP).
- EUROPE, C. 2004. *European Pharmacopoeia 5.0: Vol-2*. Council of Europe.
- EYRE, D. R., M. A. PAZ and P. M. GALLOP. 1984. Cross-linking in collagen and elastin. *Annu Rev Biochem*, **53**, pp.717-48.
- F.D.A. 2007. *Guidance for Industry and FDA Staff - Biological Indicator*. Center for Devices and Radiological Health
- FEBBRAIO, M., E. A. PODREZ, J. D. SMITH, D. P. HAJJAR, S. L. HAZEN, H. F. HOFF, K. SHARMA and R. L. SILVERSTEIN. 2000. Targeted disruption of the class B scavenger receptor CD36 protects against atherosclerotic lesion development in mice. *The Journal of Clinical Investigation*, **105**(8), pp.1049-1056.
- FIDELER, B. M., C. T. VANGSNESS, JR., T. MOORE, Z. LI and S. RASHEED. 1994. Effects of gamma irradiation on the human immunodeficiency virus. A study in frozen human bone-patellar ligament-bone grafts obtained from infected cadavera. *J Bone Joint Surg Am*, **76**(7), pp.1032-5.
- FINEGOLD, J. A., P. ASARIA and D. P. FRANCIS. 2013. Mortality from ischaemic heart disease by country, region, and age: Statistics from World Health Organisation and United Nations. *International Journal of Cardiology*, **168**(2), pp.934-945.
- FISHER, J., C. BOOTH and E. INGHAM. 2001. *Decellularisation of matrices*. Google Patents.
- FREYTES, D. O., R. M. STONER and S. F. BADYLAK. 2008. Uniaxial and biaxial properties of terminally sterilized porcine urinary bladder matrix scaffolds. *J Biomed Mater Res B Appl Biomater*, **84**(2), pp.408-14.
- FUNG, Y. C. 1993. *Biomechanics: mechanical properties of living tissues*. 2nd ed.
- FUSSENEGGER, M., J. MEINHART, W. HOBLING, W. KULLICH, S. FUNK and G. BERNATZKY. 2003. Stabilized autologous fibrin-chondrocyte constructs for cartilage repair in vivo. *Ann Plast Surg*, **51**(5), pp.493-8.
- GAGE, A. A. and J. BAUST. 1998. Mechanisms of tissue injury in cryosurgery. *Cryobiology*, **37**(3), pp.171-86.
- GALILI, U. and K. SWANSON. 1991. Gene sequences suggest inactivation of alpha-1,3-galactosyltransferase in catarrhines after the divergence of apes from monkeys. *Proc Natl Acad Sci U S A*, **88**(16), pp.7401-4.
- GEHRING, J. 1995. The influence of ionising radiation (Beta/gamma) on various polymers based on the result of the cytotoxicity test. *Radiation Physics and Chemistry*, **46**(4-6, Part 1), pp.617-622.
- GERBI, B. J., J. A. ANTOLAK, F. C. DEIBEL, D. S. FOLLOWILL, M. G. HERMAN, P. D. HIGGINS, M. S. HUQ, D. N. MIHAILIDIS, E. D. YORKE, K. R. HOGSTROM and F. M. KHAN. 2009. Recommendations for clinical electron beam dosimetry: supplement

- to the recommendations of Task Group 25. *Med Phys*, **36**(7), pp.3239-79.
- GILBERT, T. W., T. L. SELLARO and S. F. BADYLAK. 2006. Decellularization of tissues and organs. *Biomaterials*, **27**(19), pp.3675-3683.
- GOISSIS, G., S. SUZIGAN, D. R. PARREIRA, J. V. MANIGLIA, D. M. BRAILE and S. RAYMUNDO. 2000. Preparation and Characterization of Collagen-Elastin Matrices From Blood Vessels Intended as Small Diameter Vascular Grafts. *Artificial Organs*, **24**(3), pp.217-223.
- GOLDMAN, S., K. ZADINA, T. MORITZ, T. OVITT, G. SETHI, J. G. COPELAND, L. THOTTAPURATHU, B. KRASNICKA, N. ELLIS, R. J. ANDERSON, W. HENDERSON and V. A. C. S. GROUP. 2004. Long-term patency of saphenous vein and left internal mammary artery grafts after coronary artery bypass surgery: results from a Department of Veterans Affairs Cooperative Study. *J Am Coll Cardiol*, **44**(11), pp.2149-56.
- GORHAM, S. D., S. SRIVASTAVA, D. A. FRENCH and R. SCOTT. 1993. The effect of gamma-ray and ethylene oxide sterilization on collagen-based wound-repair materials. *Journal of Materials Science: Materials in Medicine*, **4**(1), pp.40-49.
- GOUK, S. S., T. M. LIM, S. H. TEOH and W. Q. SUN. 2008. Alterations of human acellular tissue matrix by gamma irradiation: histology, biomechanical property, stability, in vitro cell repopulation, and remodeling. *J Biomed Mater Res B Appl Biomater*, **84**(1), pp.205-17.
- GRAINGER, D. J., P. R. KEMP, A. C. LIU, R. M. LAWN and J. C. METCALFE. 1994. Activation of transforming growth factor-[beta] is inhibited in transgenic apolipoprotein(a) mice. *Nature*, **370**(6489), pp.460-462.
- GRASSL, E. D., T. R. OEGEMA and R. T. TRANQUILLO. 2002. Fibrin as an alternative biopolymer to type-I collagen for the fabrication of a media equivalent. *J Biomed Mater Res*, **60**(4), pp.607-12.
- GRAY, H., C. M. GOSS and D. M. ALVARADO. 1973. *Anatomy of the human body*. Lea & Febiger Philadelphia.
- GREENWALD, S. E. and C. L. BERRY. 2000. Improving vascular grafts: the importance of mechanical and haemodynamic properties. *The Journal of Pathology*, **190**(3), pp.292-299.
- GREISLER, H. P., E. D. ENDEAN, J. J. KLOSAK, J. ELLINGER, J. W. DENNIS, K. BUTTLE and D. U. KIM. 1988. Polyglactin 910/polydioxanone bicomponent totally resorbable vascular prostheses. *Journal of vascular surgery : official publication, the Society for Vascular Surgery [and] International Society for Cardiovascular Surgery, North American Chapter*, **7**(5), pp.697-705.
- GREISLER, H. P., C. W. TATTERSALL, J. J. KLOSAK, E. A. CABUSAO, J. D. GARFIELD and D. U. KIM. 1991. Partially bioresorbable vascular grafts in dogs. *Surgery*, **110**(4), pp.645-54; discussion 654-5.
- GRIEB, T. A., R. Y. FORNG, S. BOGDANSKY, C. RONHOLDT, B. PARKS, W. N. DROHAN, W. H. BURGESS and J. LIN. 2006. High-dose gamma irradiation for soft tissue allografts: High margin of safety with biomechanical integrity. *J Orthop Res*, **24**(5), pp.1011-8.
- GRIMES, M., J. T. PEMBROKE and T. MCGLOUGHLIN. 2005. The effect of choice of sterilisation method on the biocompatibility and

- biodegradability of SIS (small intestinal submucosa). *Biomed Mater Eng*, **15**(1-2), pp.65-71.
- GUILLIATT RS, DAVIES RPW, WILSHAW SP, AGGELI A. and INGHAM E. 2011. Peptide β -sheet self-assembly for the modification of acellular vascular grafts. *European Cells and Materials*, **22**, p57.
- H.S.C.I.C. 2011. *Hospital episode statistics: Total procedures and interventions*.
- HAMILTON, G., J. MEGERMAN, G. J. L'ITALIEN, D. F. WARNOCK, T. SCHMITZ-RIXEN, D. C. BREWSTER and W. M. ABBOTT. 1988. Prediction of aneurysm formation in vascular grafts of biologic origin. *J Vasc Surg*, **7**(3), pp.400-8.
- HEGYI, L., J. N. SKEPPER, N. R. B. CARY and M. J. MITCHINSON. 1996. Foam cell apoptosis and the development of the lipid core of human atherosclerosis. *The Journal of Pathology*, **180**(4), pp.423-429.
- HERTZER, N. R., E. G. BEVEN, J. R. YOUNG, P. J. O'HARA, W. F. RUSCHHAUPT, 3RD, R. A. GRAOR, V. G. DEWOLFE and L. C. MALJOVEC. 1984. Coronary artery disease in peripheral vascular patients. A classification of 1000 coronary angiograms and results of surgical management. *Ann Surg*, **199**(2), pp.223-33.
- HIEMSTRA, H., M. TERSMETTE, A. H. VOS, J. OVER, M. P. VAN BERKEL and H. DE BREE. 1991. Inactivation of human immunodeficiency virus by gamma radiation and its effect on plasma and coagulation factors. *Transfusion*, **31**(1), pp.32-9.
- HMS.HARVARD.EDU. 2011. *Diseased Aorta*. Television advertisement, hms.harvard.edu. Screened
- HOBURG, A., S. KESHLAF, T. SCHMIDT, M. SMITH, U. GOHS, C. PERKA, A. PRUSS and S. SCHEFFLER. 2011. Fractionation of high-dose electron beam irradiation of BPTB grafts provides significantly improved viscoelastic and structural properties compared to standard gamma irradiation. *Knee Surg Sports Traumatol Arthrosc*, **19**(11), pp.1955-61.
- HOBURG, A., S. KESHLAF, T. SCHMIDT, M. SMITH, U. GOHS, C. PERKA, A. PRUSS and S. SCHEFFLER. 2015. High-dose electron beam sterilization of soft-tissue grafts maintains significantly improved biomechanical properties compared to standard gamma treatment. *Cell and Tissue Banking*, **16**(2), pp.219-226.
- HOBURG, A. T., S. KESHLAF, T. SCHMIDT, M. SMITH, U. GOHS, C. PERKA, A. PRUSS and S. SCHEFFLER. 2010. Effect of electron beam irradiation on biomechanical properties of patellar tendon allografts in anterior cruciate ligament reconstruction. *Am J Sports Med*, **38**(6), pp.1134-40.
- HODDE, J. and M. HILES. 2002. Virus safety of a porcine-derived medical device: evaluation of a viral inactivation method. *Biotechnol Bioeng*, **79**(2), pp.211-6.
- HOENIG, M. R., G. R. CAMPBELL, B. E. ROLFE and J. H. CAMPBELL. 2005. Tissue-Engineered Blood Vessels: Alternative to Autologous Grafts? *Arterioscler Thromb Vasc Biol*, **25**(6), pp.1128-1134.
- HOGSTROM, K. R. and P. R. ALMOND. 2006. Review of electron beam therapy physics. *Phys Med Biol*, **51**(13), pp.R455-89.

- HOLMES, R. V. 2013. *Assessing microbial proliferation and its prevention in the preparation of decellularised human dermis grafts*. Submitted in accordance with the requirements for the degree of MSc by Research thesis, The University of Leeds
- HU, Y., Z. ZHANG, E. TORSNEY, A. R. AFZAL, F. DAVISON, B. METZLER and Q. XU. 2004. Abundant progenitor cells in the adventitia contribute to atherosclerosis of vein grafts in ApoE-deficient mice. *The Journal of Clinical Investigation*, **113**(9), pp.1258-1265.
- HUMPHREY, J. D. and C. A. TAYLOR. 2008. Intracranial and Abdominal Aortic Aneurysms: Similarities, Differences, and Need for a New Class of Computational Models. *Annual Review of Biomedical Engineering*, **10**(1), pp.221-246.
- HUYNH, T., G. ABRAHAM, J. MURRAY, K. BROCKBANK, P. O. HAGEN and S. SULLIVAN. 1999. Remodeling of an acellular collagen graft into a physiologically responsive neovessel. *Nat Biotechnol*, **17**(11), pp.1083-6.
- ICH. 1997. *Q5A(R1) Viral Safety Evaluation of Biotechnology Products Derived From Cell Lines of Human or Animal Origin*. International Conference on Harmonisation.
- IJIRI, S., T. YAMAMURO, T. NAKAMURA, S. KOTANI and K. NOTOYA. 1994. Effect of sterilization on bone morphogenetic protein. *J Orthop Res*, **12**(5), pp.628-36.
- INGHAM, E., J. FISHER and S. P. WILSHAW. 2010. *Acellular vascular products*. Patent number: WO/2012/042250.
- INTERNATIONAL STANDARD ISO/DIS 7198. 1998. *Cardiovascular implants -- Tubular vascular prostheses*.
- ISHIKAWA, H., M. SHIMODA, K. TAMAYA, A. YONEKURA, T. KAWANO and Y. OSAJIMA. 1997. Inactivation of Bacillus spores by the supercritical carbon dioxide micro-bubble method. *Biosci Biotechnol Biochem*, **61**(6), pp.1022-3.
- ISO. 11135:2014 *Sterilization of health-care products -- Ethylene oxide -- Requirements for the development, validation and routine control of a sterilization process for medical devices*.
- ISO. 11137-2:2012. *Sterilization of health care products — Radiation. Part 2: Establishing the sterilization dose*.
- ISO. 22442-3:2007. *Medical devices utilizing animal tissues and their derivatives. Part 3: Validation of the elimination and/or inactivation of viruses and transmissible spongiform encephalopathy (TSE) agents*. International Organization for Standardization.
- ISO. 10993-7:2008 *ISO. Biological evaluation of medical devices. Ethylene oxide sterilization residuals*. International Organization for Standardization.
- JACKSON, D. W., G. E. WINDLER and T. M. SIMON. 1990. Intraarticular reaction associated with the use of freeze-dried, ethylene oxide-sterilized bone-patella tendon-bone allografts in the reconstruction of the anterior cruciate ligament. *Am J Sports Med*, **18**(1), pp.1-10; discussion 10-1.
- JAN, K.-M. 2010. *Physiology : Hemodynamics* [online]. [Accessed 2011]. Available from: <http://www.columbia.edu/~kj3/Chapter2.htm>.

- JESCHKE, M. G., V. HERMANUTZ, S. E. WOLF and G. B. KOVEKER. 1999. Polyurethane vascular prostheses decreases neointimal formation compared with expanded polytetrafluoroethylene. *J Vasc Surg*, **29**(1), pp.168-76.
- JIANG, B., Z. WU, H. ZHAO, F. TANG, J. LU, Q. WEI and X. ZHANG. 2006. Electron beam irradiation modification of collagen membrane. *Biomaterials*, **27**(1), pp.15-23.
- JOHNSON, C. P., T. HOW, M. SCRAGGS, C. R. WEST and J. BURNS. 2000. A biomechanical study of the human vertebral artery with implications for fatal arterial injury. *Forensic Sci Int*, **109**(3), pp.169-82.
- JOHNSON, L. R. and J. H. BYRNE. 1998. *Essential medical physiology*. Lippincott-Raven.
- JORDY, A., R. HOFF-JORGENSEN, A. FLAGSTAD and E. LUND. 1975. Virus inactivation by ethylene oxide containing gases. *Acta Vet Scand*, **16**(3), pp.379-87.
- KAKIUCHI, M., K. ONO, A. NISHIMURA and H. SHIOKAWA. 1996. Preparation of bank bone using defatting, freeze-drying and sterilisation with ethylene oxide gas. *International Orthopaedics*, **20**(3), pp.142-146.
- KAKU, N., H. TSUMURA, M. KATAOKA, H. TAIRA and T. TORISU. 2002. Influence of aeration, storage, and rinsing conditions on residual ethylene oxide in freeze-dried bone allograft. *J Orthop Sci*, **7**(2), pp.238-42.
- KAMIHIRA, M., M. TANIGUCHI and T. KOBAYASHI. 1987. Sterilization of Microorganisms with Supercritical Carbon Dioxide(Food & Nutrition). *Agricultural and biological chemistry*, **51**(2), pp.407-412.
- KANNAN, R. Y., H. J. SALACINSKI, P. E. BUTLER, G. HAMILTON and A. M. SEIFALIAN. 2005. Current status of prosthetic bypass grafts: a review. *J Biomed Mater Res B Appl Biomater*, **74**(1), pp.570-81.
- KAULITZKI, S. 2011. *Cardiovascular System*. Television advertisement, www.dreamstime.com. Screened
- KEARNEY, J. N., R. BOJAR and K. T. HOLLAND. 1993. Ethylene oxide sterilisation of allogenic bone implants. *Clin Mater*, **12**(3), pp.129-35.
- KEARNEY, J. N., U. C. FRANKLIN, V. AGUIRREGOICOA and K. T. HOLLAND. 1989. Evaluation of ethylene oxide sterilization of tissue implants. *J Hosp Infect*, **13**(1), pp.71-80.
- KENNEALEY, P. T., N. ELIAS, M. HERTL, D. S. KO, R. F. SAIDI, J. F. MARKMANN, E. E. SMOOT, D. A. SCHOENFELD and T. KAWAI. 2011. A prospective, randomized comparison of bovine carotid artery and expanded polytetrafluoroethylene for permanent hemodialysis vascular access. *J Vasc Surg*, **53**(6), pp.1640-8.
- KER, R. F. 1981. Dynamic tensile properties of the plantaris tendon of sheep (*Ovis aries*). *J Exp Biol*, **93**, pp.283-302.
- KHAIRA, H. S. and H. VOHRA. 2002. True aneurysm in a femoro-popliteal dacron graft - A case report and literature review. *Cardiovascular Surgery*, **10**(6), pp.644-646.
- KLABUNDE, R. E. 2005. *Cardiovascular Physiology Concepts*. Lippincott Williams & Wilkins.
- KLINKERT, P., P. N. POST, P. J. BRESLAU and J. H. VAN BOCKEL. 2004. Saphenous vein versus PTFE for above-knee femoropopliteal

- bypass. A review of the literature. *Eur J Vasc Endovasc Surg*, **27**(4), pp.357-62.
- KLOSE, B. Z. E., D-34431 MARSBERG, DE), GOHS, UWE (WEINBERGSTRASSE 68 F, D-01129 DRESDEN, DE), BARTEL, RAINER (STANGE STRASSE 2, 01324 DRESDEN, DE). 2007. A PROCESS FOR THE PREPARATION OF A PACKAGE COMPRISING A STERILISED BULK OF A DRUG SUBSTANCE, AND A PACKAGE COMPRISING A STERILISED BULK OF A PENICILLIN. Patent number:
- KNIGHT, R. L., C. BOOTH, H. E. WILCOX, J. FISHER and E. INGHAM. 2005. Tissue engineering of cardiac valves: re-seeding of acellular porcine aortic valve matrices with human mesenchymal progenitor cells. *J Heart Valve Dis*, **14**(6), pp.806-13.
- KOCH, S., T. C. FLANAGAN, J. S. SACHWEH, F. TANIOS, H. SCHNOERING, T. DEICHMANN, V. ELLA, M. KELLOMAKI, N. GRONLOH, T. GRIES, R. TOLBA, T. SCHMITZ-RODE and S. JOCKENHOEVEL. 2010. Fibrin-poly lactide-based tissue-engineered vascular graft in the arterial circulation. *Biomaterials*, **31**(17), pp.4731-9.
- KONIG, G., T. N. MCALLISTER, N. DUSSERRE, S. A. GARRIDO, C. IYICAN, A. MARINI, A. FIORILLO, H. AVILA, W. WYSTRYCHOWSKI, K. ZAGALSKI, M. MARUSZEWSKI, A. L. JONES, L. CIERPKA, L. M. DE LA FUENTE and N. L'HEUREUX. 2009. Mechanical properties of completely autologous human tissue engineered blood vessels compared to human saphenous vein and mammary artery. *Biomaterials*, **30**(8), pp.1542-1550.
- KOROSSIS, S. A., C. BOOTH, H. E. WILCOX, K. G. WATTERSON, J. N. KEARNEY, J. FISHER and E. INGHAM. 2002. Tissue engineering of cardiac valve prostheses II: biomechanical characterization of decellularized porcine aortic heart valves. *J Heart Valve Dis*, **11**(4), pp.463-71.
- L'HEUREUX, N., N. DUSSERRE, A. MARINI, S. GARRIDO, L. DE LA FUENTE and T. MCALLISTER. 2007a. Technology insight: the evolution of tissue-engineered vascular grafts--from research to clinical practice. *Nat Clin Pract Cardiovasc Med*, **4**(7), pp.389-95.
- L'HEUREUX, N., L. GERMAIN, R. LABBE and F. A. AUGER. 1993. In vitro construction of a human blood vessel from cultured vascular cells: a morphologic study. *J Vasc Surg*, **17**(3), pp.499-509.
- L'HEUREUX, N., T. N. MCALLISTER and L. M. DE LA FUENTE. 2007b. Tissue-Engineered Blood Vessel for Adult Arterial Revascularization. *New England Journal of Medicine*, **357**(14), pp.1451-1453.
- LAING, S. T. and D. D. MCPHERSON. 2009. Cardiovascular therapeutic uses of targeted ultrasound contrast agents. *Cardiovasc Res*, **83**(4), pp.626-35.
- LANTZ, G. C., S. F. BADYLAK, A. C. COFFEY, L. A. GEDDES and W. E. BLEVINS. 1990. Small intestinal submucosa as a small-diameter arterial graft in the dog. *J Invest Surg*, **3**(3), pp.217-27.
- LANTZ, G. C., S. F. BADYLAK, M. C. HILES, A. C. COFFEY, L. A. GEDDES, K. KOKINI, G. E. SANDUSKY and R. J. MORFF. 1993. Small intestinal submucosa as a vascular graft: a review. *J Invest Surg*, **6**(3), pp.297-310.

- LEE, Y. and K. B. SONG. 2002. Effect of gamma-irradiation on the molecular properties of myoglobin. *J Biochem Mol Biol*, **35**(6), pp.590-4.
- LEROUGE, S. and A. SIMMONS. 2012. *Sterilisation of Biomaterials and Medical Devices*. Elsevier Science.
- LI, A. C. A. C. and C. K. C. K. GLASS. 2002. The macrophage foam cell as a target for therapeutic intervention. *Nature medicine*, **8**(11), pp.1235-1242.
- LIN, M.-G., T.-L. YANG, C.-T. CHIANG, H.-C. KAO, J.-N. LEE, W. LO, S.-H. JEE, Y.-F. CHEN, C.-Y. DONG and S.-J. LIN. 2006. Evaluation of dermal thermal damage by multiphoton autofluorescence and second-harmonic-generation microscopy. *Journal of Biomedical Optics*, **11**(6), pp.064006-064006-6.
- LIU, M. and J. YANG. 2009. Electrokinetic effect of the endothelial glycocalyx layer on two-phase blood flow in small blood vessels. *Microvascular Research*, **78**(1), pp.14-19.
- LOMAS, R. J., H. L. GILLAN, J. B. MATTHEWS, E. INGHAM and J. N. KEARNEY. 2001. An evaluation of the capacity of differently prepared demineralised bone matrices (DBM) and toxic residuals of ethylene oxide (EtOx) to provoke an inflammatory response in vitro. *Biomaterials*, **22**(9), pp.913-21.
- LUCAS, A. D., K. MERRITT, V. M. HITCHINS, T. O. WOODS, S. G. MCNAMEE, D. B. LYLE and S. A. BROWN. 2003. Residual ethylene oxide in medical devices and device material. *J Biomed Mater Res B Appl Biomater*, **66**(2), pp.548-52.
- LUSIS, A. J. 2000. Atherosclerosis. *Nature*, **407**(6801), pp.233-241.
- MADDEN, R., G. LIPKOWITZ, B. BENEDETTO, A. KURBANOV, M. MILLER and L. BOW. 2002. Decellularized cadaver vein allografts used for hemodialysis access do not cause allosensitization or preclude kidney transplantation. *Am J Kidney Dis*, **40**(6), pp.1240-3.
- MADDEN, R. L., G. S. LIPKOWITZ, B. J. BROWNE and A. KURBANOV. 2005. A comparison of cryopreserved vein allografts and prosthetic grafts for hemodialysis access. *Ann Vasc Surg*, **19**(5), pp.686-91.
- MARANTO, A. R. and F. J. SCHOEN. 1988. Phosphatase enzyme activity is retained in glutaraldehyde treated bioprosthetic heart valves. *ASAIO Trans*, **34**(3), pp.827-30.
- MARRECO, P. R., P. D. L. MOREIRA, S. C. GENARI and Â. M. MORAES. 2004. Effects of different sterilization methods on the morphology, mechanical properties, and cytotoxicity of chitosan membranes used as wound dressings. *Journal of Biomedical Materials Research Part B: Applied Biomaterials*, **71B**(2), pp.268-277.
- MARTIN, R. S., 3RD, W. H. EDWARDS, J. L. MULHERIN, JR., W. H. EDWARDS, JR., J. M. JENKINS and S. J. HOFF. 1994. Cryopreserved saphenous vein allografts for below-knee lower extremity revascularization. *Ann Surg*, **219**(6), pp.664-70; discussion 670-2.
- MCALLISTER, T. N., M. MARUSZEWSKI, S. A. GARRIDO, W. WYSTRYCHOWSKI, N. DUSSEYRE, A. MARINI, K. ZAGALSKI, A. FIORILLO, H. AVILA, X. MANGLANO, J. ANTONELLI, A. KOCHER, M. ZEMBALA, L. CIERPKA, L. M. DE LA FUENTE and N. L'HEUREUX. 2009. Effectiveness of haemodialysis access with an

- autologous tissue-engineered vascular graft: a multicentre cohort study. *The Lancet*, **373**(9673), pp.1440-1446.
- MCDONNELL, G. E. 2007. *Antisepsis, Disinfection, and Sterilization: Types, Action, and Resistance*. ASM Press.
- MCPHERSON, T. B., H. LIANG, R. D. RECORD and S. F. BADYLAK. 2000. Galalpha(1,3)Gal epitope in porcine small intestinal submucosa. *Tissue Eng*, **6**(3), pp.233-9.
- MERYMAN, H. T. 1960. General principles of freezing and freezing injury in cellular materials. *Ann N Y Acad Sci*, **85**, pp.503-9.
- MESTAS, J. and K. LEY. 2008. Monocyte-Endothelial Cell Interactions in the Development of Atherosclerosis. *Trends in Cardiovascular Medicine*, **18**(6), pp.228-232.
- MEYERS, M. A., P.-Y. CHEN, A. Y.-M. LIN and Y. SEKI. 2008. Biological materials: Structure and mechanical properties. *Progress in Materials Science*, **53**(1), pp.1-206.
- MILLS, N. L. and C. T. EVERSON. 1989. Rigt gastroepiploic artery: A third arterial conduit for coronary artery bypass. *The Annals of Thoracic Surgery*, **47**(5), pp.706-711.
- MIRSADRAEE, S., H. E. WILCOX, S. A. KOROSSIS, J. N. KEARNEY, K. G. WATTERSON, J. FISHER and E. INGHAM. 2006. Development and characterization of an acellular human pericardial matrix for tissue engineering. *Tissue Eng*, **12**(4), pp.763-73.
- MITRA, A. K., D. M. GANGAHAR and D. K. AGRAWAL. 2006. Cellular, molecular and immunological mechanisms in the pathophysiology of vein graft intimal hyperplasia. *Immunol Cell Biol*, **84**(2), pp.115-24.
- MOORE, T. M., E. GENDLER and E. GENDLER. 2004. Viruses adsorbed on musculoskeletal allografts are inactivated by terminal ethylene oxide disinfection. *J Orthop Res*, **22**(6), pp.1358-61.
- MORINAGA, K., K. OKADOME, M. KUROKI, T. MIYAZAKI, Y. MUTO and K. INOKUCHI. 1985. Effect of wall shear stress on intimal thickening of arterially transplanted autogenous veins in dogs. *Journal of Vascular Surgery*, **2**(3), pp.430-433.
- NAKAGAWA, Y., K. OTA, Y. SATO, S. TERAOKA and T. AGISHI. 1995. Clinical trial of new polyurethane vascular grafts for hemodialysis: compared with expanded polytetrafluoroethylene grafts. *Artif Organs*, **19**(12), pp.1227-32.
- NATHER, A., N. YUSOF and N. HILMY. 2007. *Radiation in Tissue Banking: Basic Science and Clinical Applications of Irradiated Tissue Allografts*. World Scientific Publishing Company.
- NEVEN, E. and P. C. D'HAESE. 2011. Vascular Calcification in Chronic Renal Failure: What Have We Learned From Animal Studies? *Circulation Research*, **108**(2), pp.249-264.
- NEWBY, A. C. and A. B. ZALTSMAN. 2000. Molecular mechanisms in intimal hyperplasia. *The Journal of Pathology*, **190**(3), pp.300-309.
- NIKLASON, L. E., W. ABBOTT, J. GAO, B. KLAGGES, K. K. HIRSCHI, K. ULUBAYRAM, N. CONROY, R. JONES, A. VASANAWALA, S. SANZGIRI and R. LANGER. 2001. Morphologic and mechanical characteristics of engineered bovine arteries. *J Vasc Surg*, **33**(3), pp.628-38.
- OKUHN, S. P., D. P. CONNELLY, N. CALAKOS, L. FERRELL, P. MAN-XIANG and J. GOLDSTONE. 1989. Does compliance mismatch alone

- cause neointimal hyperplasia? *Journal of Vascular Surgery*, **9**(1), pp.35-45.
- OLDE DAMINK, L. H., P. J. DIJKSTRA, M. J. VAN LUYN, P. B. VAN WACHEM, P. NIEUWENHUIS and J. FEIJEN. 1995. Influence of ethylene oxide gas treatment on the in vitro degradation behavior of dermal sheep collagen. *J Biomed Mater Res*, **29**(2), pp.149-55.
- OWEN, K., S. P. WILSHAW, S. HOMER-VANNIASINKAM, R. A. BOJAR, H. BERRY and E. INGHAM. 2012. Assessment of the antimicrobial activity of acellular vascular grafts. *Eur J Vasc Endovasc Surg*, **43**(5), pp.573-81.
- PANKAJAKSHAN, D. and D. K. AGRAWAL. 2010. Scaffolds in tissue engineering of blood vessels. *Canadian Journal of Physiology and Pharmacology*, **88**(9), pp.855-873.
- PARISI, A. and A. D. ANTOINE. 1974. Increased radiation resistance of vegetative *Bacillus pumilus*. *Appl Microbiol*, **28**(1), pp.41-6.
- PARK, I. S., S.-H. KIM, Y. H. KIM, I. H. KIM and S. H. KIM. 2009. A Collagen/Smooth Muscle Cell-Incorporated Elastic Scaffold for Tissue-Engineered Vascular Grafts. *Journal of Biomaterials Science, Polymer Edition*, **20**(11), pp.1645-1660.
- PARKER, W., S. SAADI, S. S. LIN, Z. E. HOLZKNECHT, M. BUSTOS and J. L. PLATT. 1996. Transplantation of discordant xenografts: a challenge revisited. *Immunol Today*, **17**(8), pp.373-8.
- PHILLIPS, C. R. and S. KAYE. 1949. The sterilizing action of gaseous ethylene oxide; a review. *Am J Hyg*, **50**(3), pp.270-9.
- PONTICELLI, C. 2012. The mechanisms of acute transplant rejection revisited. *J Nephrol*, **25**(2), pp.150-8.
- PREVENTING-A-HEART-ATTACK.COM. 2011. *Anatomy of the heart*. Television advertisement. Screened
- PROLO, D. J., P. W. PEDROTTI and D. H. WHITE. 1980. Ethylene Oxide Sterilization of Bone, Dura Mater, and Fascia Lata for Human Transplantation. *Neurosurgery*, **6**(5), pp.529-539.
- QIU, Q. Q., P. LEAMY, J. BRITTINGHAM, J. POMERLEAU, N. KABARIA and J. CONNOR. 2009. Inactivation of bacterial spores and viruses in biological material using supercritical carbon dioxide with sterilant. *J Biomed Mater Res B Appl Biomater*, **91**(2), pp.572-8.
- RADER, D. J. and A. DAUGHERTY. 2008. Translating molecular discoveries into new therapies for atherosclerosis. *Nature*, **451**(7181), pp.904-913.
- RANDON, C., B. JACOBS, F. DE RYCK, H. BEELE and F. VERMASSEN. 2010. Fifteen years of infrapopliteal arterial reconstructions with cryopreserved venous allografts for limb salvage. *J Vasc Surg*, **51**(4), pp.869-77.
- ROLL, S., J. MULLER-NORDHORN, T. KEIL, H. SCHOLZ, D. EIDT, W. GREINER and S. N. WILLICH. 2008. Dacron vs. PTFE as bypass materials in peripheral vascular surgery--systematic review and meta-analysis. *BMC Surg*, **8**, p22.
- ROTHSCHILD, M. F., A. RUVINSKY and C. A. B. INTERNATIONAL. 2011. *The Genetics of the Pig*. CABI.
- SAGOO, P., G. LOMBARDI and R. I. LECHLER. 2012. Relevance of Regulatory T cell Promotion of Donor-specific Tolerance in Solid Organ Transplantation. *Frontiers in Immunology*, **3**.

- SAHA, P., B. MODARAI, J. HUMPHRIES, K. MATTOCK, M. WALTHAM, K. G. BURNAND and A. SMITH. 2009. The monocyte/macrophage as a therapeutic target in atherosclerosis. *Current Opinion in Pharmacology*, **9**(2), pp.109-118.
- SALACINSKI, H. J., S. GOLDNER, A. GIUDICEANDREA, G. HAMILTON, A. M. SEIFALIAN, A. EDWARDS and R. J. CARSON. 2001. The Mechanical Behavior of Vascular Grafts: A Review. *Journal of Biomaterials Applications*, **15**(3), pp.241-278.
- SARAZIN, P., X. ROY and B. D. FAVIS. 2004. Controlled preparation and properties of porous poly(-lactide) obtained from a co-continuous blend of two biodegradable polymers. *Biomaterials*, **25**(28), pp.5965-5978.
- SARKAR, S., H. J. SALACINSKI, G. HAMILTON and A. M. SEIFALIAN. 2006. The mechanical properties of infrainguinal vascular bypass grafts: their role in influencing patency. *Eur J Vasc Endovasc Surg*, **31**(6), pp.627-36.
- SAUVAGE, L. R., K. E. BERGER, S. J. WOOD, S. G. YATES, II, J. C. SMITH and P. B. MANSFIELD. 1974. Interspecies healing of porous arterial prostheses: Observations, 1960 to 1974. *Archives of Surgery*, **109**(5), pp.698-705.
- SCHANER, P. J., N. D. MARTIN, T. N. TULENKO, I. M. SHAPIRO, N. A. TAROLA, R. F. LEICHTER, R. A. CARABASI and P. J. DIMUZIO. 2004. Decellularized vein as a potential scaffold for vascular tissue engineering. *Journal of Vascular Surgery*, **40**(1), pp.146-153.
- SCHENKE-LAYLAND, K. 2008. Non-invasive multiphoton imaging of extracellular matrix structures. *Journal of Biophotonics*, **1**(6), pp.451-462.
- SCHERZER, T. and A. BECKERT. 1997. Electron beam curing of methacrylated gelatin studied by EPR and FT-Raman spectroscopy. *Macromolecular Symposia*, **119**(1), pp.299-307.
- SCHMITZ-RIXEN, T., S. LEPIDI and G. HAMILTON. 1993. [Compliance: a fundamental biomechanical property in the maintenance of an arterial reconstruction?]. *Ann Ital Chir*, **64**(1), pp.15-27.
- SCHOEN, F. J. 1987. Cardiac valve prostheses: pathological and bioengineering considerations. *J Card Surg*, **2**(1), pp.65-108.
- SCHULZE-BAUER, C. A. J., P. REGITNIG and G. A. HOLZAPFEL. 2002. Mechanics of the human femoral adventitia including the high-pressure response. *American Journal of Physiology - Heart and Circulatory Physiology*, **282**(6), pp.H2427-H2440.
- SCHWARTZ, H. E., M. J. MATAVA, F. S. PROCH, C. A. BUTLER, A. RATCLIFFE, M. LEVY and D. L. BUTLER. 2006. The Effect of Gamma Irradiation on Anterior Cruciate Ligament Allograft Biomechanical and Biochemical Properties in the Caprine Model at Time Zero and at 6 Months After Surgery. *The American Journal of Sports Medicine*, **34**(11), pp.1747-1755.
- SEIFERT, K. B., D. ALBO, JR., H. KNOWLTON and D. J. LYMAN. 1979. Effect of elasticity of prosthetic wall on patency of small-diameter arterial prostheses. *Surg Forum*, **30**, pp.206-8.
- SETO, A., C. J. GATT, JR. and M. G. DUNN. 2009. Improved tendon radioprotection by combined cross-linking and free radical scavenging. *Clin Orthop Relat Res*, **467**(11), pp.2994-3001.

- SHANAHAN, C. M. 2013. Mechanisms of vascular calcification in CKD[mdash]evidence for premature ageing? *Nat Rev Nephrol*, **9**(11), pp.661-670.
- SHEKHONIN, B. V., S. P. DOMOGATSKY, V. R. MUZYKANTOV, G. L. IDELSON and V. S. RUKOSUEV. 1985. Distribution of Type I, III, IV and V Collagen in Normal and Atherosclerotic Human Arterial Wall: Immunomorphological Characteristics. *Collagen and Related Research*, **5**(4), pp.355-368.
- SIMON, P., M. T. KASIMIR, G. SEEBACHER, G. WEIGEL, R. ULLRICH, U. SALZER-MUHAR, E. RIEDER and E. WOLNER. 2003. Early failure of the tissue engineered porcine heart valve SYNERGRAFT™ in pediatric patients. *European Journal of Cardio-thoracic Surgery*, **23**(6), pp.1002-1006.
- SMITH, C. W., I. S. YOUNG and J. N. KEARNEY. 1996. Mechanical properties of tendons: changes with sterilization and preservation. *J Biomech Eng*, **118**(1), pp.56-61.
- SMITH, J. D., E. TROGAN, M. GINSBERG, C. GRIGAUX, J. TIAN and M. MIYATA. 1995. Decreased atherosclerosis in mice deficient in both macrophage colony-stimulating factor (op) and apolipoprotein E. *Proceedings of the National Academy of Sciences*, **92**(18), pp.8264-8268.
- SOKAL, R. R. and F. J. ROHLF. 1981. *Biometry: The Principles and Practice of Statistics in Biological Research*. W. H. Freeman.
- SOLDANI, G., P. LOSI, M. BERNABEI, S. BURCHIELLI, D. CHIAPPINO, S. KULL, E. BRIGANTI and D. SPILLER. 2010. Long term performance of small-diameter vascular grafts made of a poly(ether)urethane-polydimethylsiloxane semi-interpenetrating polymeric network. *Biomaterials*, **31**(9), pp.2592-605.
- SOTTIURAI, V. S., J. S. YAO, R. C. BATSON, S. L. SUE, R. JONES and Y. A. NAKAMURA. 1989. Distal anastomotic intimal hyperplasia: histopathologic character and biogenesis. *Ann Vasc Surg*, **3**(1), pp.26-33.
- SPARK, J. I., S. YELURI, C. DERHAM, Y. T. WONG and D. LEITCH. 2008. Incomplete cellular depopulation may explain the high failure rate of bovine ureteric grafts. *Br J Surg*, **95**(5), pp.582-5.
- SPIILIMBERGO, S. and A. BERTUCCO. 2003. Non-thermal bacterial inactivation with dense CO(2). *Biotechnol Bioeng*, **84**(6), pp.627-38.
- SPIRE, B., D. DORMONT, F. BARRE-SINOUSI, L. MONTAGNIER and J. C. CHERMANN. 1985. Inactivation of lymphadenopathy-associated virus by heat, gamma rays, and ultraviolet light. *Lancet*, **1**(8422), pp.188-9.
- STENMARK, K. R., E. NOZIK-GRAYCK, E. GERASIMOVSKAYA, A. ANWAR, M. LI, S. RIDDLE and M. FRID. 2006. *The Adventitia: Essential Role in Pulmonary Vascular Remodeling*. Comprehensive Physiology. John Wiley & Sons, Inc.
- SULLIVAN, R., A. C. FASSOLITIS, E. P. LARKIN, R. B. READ, JR. and J. T. PEELER. 1971. Inactivation of thirty viruses by gamma radiation. *Appl Microbiol*, **22**(1), pp.61-5.
- SUMPIO, B. E., J. TIMOTHY RILEY and A. DARDIK. 2002. Cells in focus: endothelial cell. *The International Journal of Biochemistry & Cell Biology*, **34**(12), pp.1508-1512.

- SUN, W. Q. and P. LEUNG. 2008. Calorimetric study of extracellular tissue matrix degradation and instability after gamma irradiation. *Acta Biomater*, **4**(4), pp.817-26.
- SUZUKI, H. H., Y. Y. KURIHARA, M. M. TAKEYA, N. N. KAMADA, M. M. KATAOKA, K. K. JISHAGE, O. O. UEDA, H. H. SAKAGUCHI, T. T. HIGASHI, T. T. SUZUKI, Y. Y. TAKASHIMA, Y. Y. KAWABE, O. O. CYNISHI, Y. Y. WADA, M. M. HONDA, H. H. KURIHARA, H. H. ABURATANI, T. T. DOI, A. A. MATSUMOTO, S. S. AZUMA, T. T. NODA, Y. Y. TOYODA, H. H. ITAKURA, Y. Y. YAZAKI and T. T. KODAMA. 1997. A role for macrophage scavenger receptors in atherosclerosis and susceptibility to infection. *Nature*, **386**(6622), pp.292-296.
- SWARTZ, D. D., J. A. RUSSELL and S. T. ANDREADIS. 2005. Engineering of fibrin-based functional and implantable small-diameter blood vessels. *Am J Physiol Heart Circ Physiol*, **288**(3), pp.H1451-60.
- TATTERTON, M., S. P. WILSHAW, E. INGHAM and S. HOMER-VANNIASINKAM. 2012. The use of antithrombotic therapies in reducing synthetic small-diameter vascular graft thrombosis. *Vasc Endovascular Surg*, **46**(3), pp.212-22.
- TEEBKEN, O. E. and A. HAVERICH. 2002. Tissue Engineering of Small Diameter Vascular Grafts. *European Journal of Vascular and Endovascular Surgery*, **23**(6), pp.475-485.
- THEODOSSIOU, T. A., C. THRASIVOULOU, C. EKWOBI and D. L. BECKER. 2006. Second Harmonic Generation Confocal Microscopy of Collagen Type I from Rat Tendon Cryosections. *Biophysical Journal*, **91**(12), pp.4665-4677.
- TILANUS, H. W., H. OBERTOP and H. VAN URK. 1985. Saphenous vein or PTFE for femoropopliteal bypass. A prospective randomized trial. *Ann Surg*, **202**(6), pp.780-2.
- TILLMAN, B. W., S. K. YAZDANI, S. J. LEE, R. L. GEARY, A. ATALA and J. J. YOO. 2009. The in vivo stability of electrospun polycaprolactone-collagen scaffolds in vascular reconstruction. *Biomaterials*, **30**(4), pp.583-8.
- TIMPL, R. 1996. Macromolecular organization of basement membranes. *Current Opinion in Cell Biology*, **8**(5), pp.618-624.
- TIWARI, A., K. S. CHENG, H. SALACINSKI, G. HAMILTON and A. M. SEIFALIAN. 2003. Improving the Patency of Vascular Bypass Grafts: the Role of Suture Materials and Surgical Techniques on Reducing Anastomotic Compliance Mismatch. *European Journal of Vascular and Endovascular Surgery*, **25**(4), pp.287-295.
- TIWARI, A., H. SALACINSKI, A. M. SEIFALIAN and G. HAMILTON. 2002. New prostheses for use in bypass grafts with special emphasis on polyurethanes. *Cardiovascular Surgery*, **10**(3), pp.191-197.
- TRANQUILLO, R. T., T. S. GIRTON, B. A. BROMBEREK, T. G. TRIEBES and D. L. MOORADIAN. 1996. Magnetically orientated tissue-equivalent tubes: application to a circumferentially orientated media-equivalent. *Biomaterials*, **17**(3), pp.349-57.
- TRUBEL, W., A. MORITZ, H. SCHIMA, F. RADERER, R. SCHERER, R. ULLRICH, U. LOSERT and P. POLTERAUER. 1994. Compliance and formation of distal anastomotic intimal hyperplasia in Dacron mesh

- tube constricted veins used as arterial bypass grafts. *ASAIO Journal*, **40**(3), pp.M273-M278.
- TSCHOEKE, B., T. C. FLANAGAN, S. KOCH, M. S. HARWOKO, T. DEICHMANN, V. ELLA, J. S. SACHWEH, M. KELLOMAKI, T. GRIES, T. SCHMITZ-RODE and S. JOCKENHOEVEL. 2009. Tissue-engineered small-caliber vascular graft based on a novel biodegradable composite fibrin-poly lactide scaffold. *Tissue Eng Part A*, **15**(8), pp.1909-18.
- VALENTE, M., U. BORTOLOTTI and G. THIENE. 1985. Ultrastructural substrates of dystrophic calcification in porcine bioprosthetic valve failure. *Am J Pathol*, **119**(1), pp.12-21.
- VAN DAMME, H., M. DEPRez, E. CREEMERS and R. LIMET. 2005. Intrinsic structural failure of polyester (Dacron) vascular grafts. A general review. *Acta Chirurgica Belgica*, **105**(3), pp.249-255.
- VAN DET, R. J., B. H. VRIENS, J. VAN DER PALEN and R. H. GEELKERKEN. 2009. Dacron or ePTFE for femoro-popliteal above-knee bypass grafting: short- and long-term results of a multicentre randomised trial. *Eur J Vasc Endovasc Surg*, **37**(4), pp.457-63.
- VANGSNESS, C. T., JR., I. A. GARCIA, C. R. MILLS, M. A. KAINER, M. R. ROBERTS and T. M. MOORE. 2003. Allograft transplantation in the knee: tissue regulation, procurement, processing, and sterilization. *Am J Sports Med*, **31**(3), pp.474-81.
- VEITH, F. J., C. M. MOSS, S. SPRAYREGEN and C. MONTEFUSCO. 1979. Preoperative saphenous venography in arterial reconstructive surgery of the lower extremity. *Surgery*, **85**(3), pp.253-6.
- VESELY, I., R. NOSEWORTHY and G. PRINGLE. 1995. The hybrid xenograft/autograft bioprosthetic heart valve: In vivo evaluation of tissue extraction. *The Annals of Thoracic Surgery*, **60**, Supplement 2(0), pp.S359-S364.
- W.H.O. 2011. *World Health Organisation: Global Health Observatory - Number of deaths : World by cause (2000-2011)*.
- WAGENSEIL, J. E. and R. P. MECHAM. 2009. Vascular Extracellular Matrix and Arterial Mechanics. *Physiol Rev*, **89**(3), pp.957-989.
- WALDEN, R., G. J. L'ITALIEN, J. MEGERMAN and W. M. ABBOTT. 1980. Matched elastic properties and successful arterial grafting. *Archives of surgery (Chicago, Ill. : 1960)*, **115**(10), pp.1166-1169.
- WEINBERG, C. B. and E. BELL. 1986. A blood vessel model constructed from collagen and cultured vascular cells. *Science*, **231**(4736), pp.397-400.
- WESTERHOF, N., N. STERGIOPULOS, M. I. M. NOBLE and N. STERGIOPULOS. 2010. Law of Laplace. *Snapshots of Hemodynamics*. Springer US, pp.45-48.
- WHITE, A., D. BURNS and T. W. CHRISTENSEN. 2006. Effective terminal sterilization using supercritical carbon dioxide. *Journal of Biotechnology*, **123**(4), pp.504-515.
- WIGHT, T. 1989. Cell biology of arterial proteoglycans. *Arterioscler Thromb Vasc Biol*, **9**(1), pp.1-20.
- WILCOX, H. E., S. A. KOROSSIS, C. BOOTH, K. G. WATTERSON, J. N. KEARNEY, J. FISHER and E. INGHAM. 2005. Biocompatibility and recellularization potential of an acellular porcine heart valve matrix. *J Heart Valve Dis*, **14**(2), pp.228-36; discussion 236-7.

- WILLIAMS, R. M., W. R. ZIPFEL and W. W. WEBB. 2005. Interpreting Second-Harmonic Generation Images of Collagen I Fibrils. *Biophysical Journal*, **88**(2), pp.1377-1386.
- WILSHAW S., LUO J., FISHER J., HOMER-VANNIASINKAM S and INGHAM E. 2014. Regenerative Potential of An Acellular Xenogeneic Small Diameter Artery In Vivo. *In: TERMIS NA (Americas), Washington D.C.*, 13th - 15th December.
- WILSHAW, S. P., J. N. KEARNEY, J. FISHER and E. INGHAM. 2006. Production of an acellular amniotic membrane matrix for use in tissue engineering. *Tissue Eng*, **12**(8), pp.2117-29.
- WILSHAW, S. P., P. ROONEY, H. BERRY, J. N. KEARNEY, S. HOMER-VANNIASINKAM, J. FISHER and E. INGHAM. 2012. Development and characterization of acellular allogeneic arterial matrices. *Tissue Eng Part A*, **18**(5-6), pp.471-83.
- WU, H. C., T. W. WANG, P. L. KANG, Y. H. TSUANG, J. S. SUN and F. H. LIN. 2007. Coculture of endothelial and smooth muscle cells on a collagen membrane in the development of a small-diameter vascular graft. *Biomaterials*, **28**(7), pp.1385-92.
- WWW.COLUMBIA.EDU. 2011. *Pressure volume relationship of arteries and veins*. Television advertisement, www.columbia.edu. Screened
- WWW.INTECHOPEN.COM. 2011. *arteriovenous graft in forearm* Television advertisement, www.intechopen.com. Screened
- WWW.MAYFIELDCLINIC.COM. 2011. *Stenotic Artery*. Television advertisement, www.mayfieldclinic.com. Screened
- WWW.NHS.UK. 2011. *CABG Suregry*. Television advertisement, www.nhs.uk. Screened
- WWW.SHINONGLOBAL.COM. 2011. *Femeropopliteal Bypass Graft*. Television advertisement, www.shinonglobal.com. Screened
- WWW.VASCULARCONCEPTS.COM. 2011. *artery layers*. Television advertisement, www.vascularconcepts.com. Screened
- WWW.VEININFO.CO.UK. 2011. *Thrombosis*. Television advertisement. Screened
- WWW.VWMIN.ORG. 2011. *Artherosclerosis*. Television advertisement, www.vwmin.org. Screened
- WYSTRYCHOWSKI, W., T. N. MCALLISTER, K. ZAGALSKI, N. DUSSERRE, L. CIERPKA and N. L'HEUREUX. 2014. First human use of an allogeneic tissue-engineered vascular graft for hemodialysis access. *Journal of Vascular Surgery*, (0).
- ZARINS, C., D. GIDDENS, B. BHARADVAJ, V. SOTTIURAI, R. MABON and S. GLAGOV. 1983. Carotid bifurcation atherosclerosis. Quantitative correlation of plaque localization with flow velocity profiles and wall shear stress. *Circ Res*, **53**(4), pp.502-514.
- ZHANG, J., S. BURROWS, C. GLEASON, M. A. MATTHEWS, M. J. DREWS, M. LABERGE and Y. H. AN. 2006a. Sterilizing *Bacillus pumilus* spores using supercritical carbon dioxide. *Journal of Microbiological Methods*, **66**(3), pp.479-485.
- ZHANG, J., N. DALAL, C. GLEASON, M. A. MATTHEWS, L. N. WALLER, K. F. FOX, A. FOX, M. J. DREWS, M. LABERGE and Y. H. AN. 2006b. On the mechanisms of deactivation of *Bacillus atrophaeus* spores using supercritical carbon dioxide. *The Journal of Supercritical Fluids*, **38**(2), pp.268-273.

- ZHANG, W. J., W. LIU, L. CUI and Y. CAO. 2007. Tissue engineering of blood vessel. *J Cell Mol Med*, **11**(5), pp.945-57.
- ZHANG, Y., X. ZHANG, L. XU, S. WEI and M. ZHAI. 2014. Radiation cross-linked collagen/dextran dermal scaffolds: effects of dextran on cross-linking and degradation. *Journal of Biomaterials Science, Polymer Edition*, **26**(3), pp.162-180.
- ZHAO, Y., S. ZHANG, J. ZHOU, J. WANG, M. ZHEN, Y. LIU, J. CHEN and Z. QI. 2010. The development of a tissue-engineered artery using decellularized scaffold and autologous ovine mesenchymal stem cells. *Biomaterials*, **31**(2), pp.296-307.
- ZILLA, P. and H. P. GREISLER. 1999. *Tissue engineering of vascular prosthetic grafts*. R.G. Landes Co.

Appendix A

Lists of general equipment, chemicals, reagents and consumables used throughout the project are presented here:

A.1 Equipment

A list of general equipment and supplier used throughout this project.

Table A-1: General Equipment

Equipment	Model	Supplier
1L, 2L graduated bottles borosilicate glass	FB33147, FB33148	Fisher Scientific Ltd.
250 ml filter unit (0.2 µm)	Nalgene	126-0020
Adjustable spanners x 2	N/A	N/A
Automatic pipettes	Various	Gilson
Balance	GR-200-EC	AND
Bench top autoclave	5 L	Kuhn Rikon
Burst pressure apparatus	N/A	N/A
Cell^AB	Cell ^A B	Olympus UK
Centrifuge	Harrier 15/80	Sanyo Biomedical
Centrifuge	Microcentaur	MSE
Class II safety cabinet	CL2	Heraeus
Class II safety cabinet	CL2	Heraus
Cutting tool	N/A	N/A
Digital colour camera	Evolution MP5	Media Cybernetics
Digital colour camera	XC50	Olympus UK
Dissection Kit	Various	Thackeray
Freeze dryer	Modulo	Thermo Scientific
Glass troughs	E105	Raymond A Lamb
Histology water bath	MH8515	Barnstead Electrothermal
Hole punch 5 mm diameter	N/A	In-house
Hot wax oven	E18/31	Raymond A Lamb
Hotplate	E18/1	Raymond A Lamb
Image-pro plus	Version 5.1	Media Cybernetics
Incubator	Heraeus	Jencons PLC
Inverted microscope	IX71	Olympus UK
Magnetic stirrer	CB161	Stuart Scientific
Materials testing machine	3365	Instron

Equipment	Model	Supplier
Micro plate spectrophotometer	Multiskan spectrum	Thermo Scientific
Micro shaker	AM69	Cooke
Microtome	RM2125 RTF	Leica
Nanodrop spectrophotometer	ND-100	Labtech
Orbital Shaker	KS 130	IKA
pH meter	3510	Jenway
Pipette boy	Integra acu	Integra Bioscience
Pressure gauge	C9557	Comark
Slide holder	E102	Raymond A Lamb
Thickness measurement gauge	7323	Mitutoyo
Tissue processor	TP11020	Leica
Top Count	C9902 NXT	Perkin Elmer
Upright microscope	BX40	Olympus UK Ltd.
Vernier callipers	N48AA	Maplin
Water bath	G 352	Grant
Wax dispenser	E66	Raymond A Lamb
Whrli mixer	CM-1	Thermo Fisher Scientific

A.2 Chemicals and Reagents

A list of general equipment and supplier used throughout this project.

Table A-2 : Chemicals and Reagents

Chemical/Reagent	Cat No.	Supplier
10 % Neutral buffered formalin (NBF)	RRFF4000-G	Atom scientific
3M Steri-Strip SkinClosure 3x75 mm	R1540C	Medisave
Acetone	LS8/1970/G	European Bios
Aprotonin (10000 KI ml ⁻¹)	AP012	Mayfair House
ATPLite-M assay	6016941	Perkin-Elmer
Bovine serum albumin (BSA)	A7030-100G	Sigma-Aldrich
Calcium acetate (anhydrous)	C/0920/50	Thermo Fisher Scientific Ltd.
Calcium chloride	ALFA12316.A1	VWR International
Chloramine T	C9887	Sigma-Aldrich
Citric acid	100814N	VWR International
Collagen IV isotype IgG1	X0931	Dako
Collagen IV mouse monoclonal antibody	M0785	Dako
Cyanoacrylate contact adhesive	Z105902-1EA	Sigma-Aldrich
Dako fluorescence mounting medium	S3023	Dako
Dimethyl sulfoxide (DMSO)	D26650	Sigma

Chemical/Reagent	Cat No.	Supplier
Disodium ethylenediaminetetraacetic acid (EDTA)	E/P140/53	Thermo Fisher Scientific Ltd.
DNase	DN25-1	Sigma-Aldrich
DNeasy kit	69504	Qiagen
DPX mountant	M81330/C	Thermo Fisher Scientific Ltd.
Dulbecco's minimal essential medium (DMEM)	D6546	Sigma
Dulbecco's PBS tablets	BR0014	Oxoid
Dulbecco's PBS with Ca²⁺ & Mg²⁺	D8662	Sigma
Eosin	1.09844.1000	VWR International
Ethanol	E/0555DF/25	Thermo Fisher Scientific Ltd.
Foetal bovine serum (FBS)	EU-000	Sera Lab
Gentamycin sulphate	345810	VWR International
Giemsa solution	352603R	VWR International
Glacial acetic acid	10001	VWR International
Glasgow's minimal essential medium (GMEM)	G5154	Sigma
Glycerol	BPE229-1	Thermo Fisher Scientific Ltd.
Haematoxylin	PS50/C	Thermo Fisher Scientific Ltd.
Histo-clear III	HS-204	National Diagnostics
Hydrochloric acid 6 M	2611.5000	VWR International
Hydrogen peroxide	H1009	Sigma-Aldrich
ImmEdge hydrophobic barrier pen	H-4000	Vector Laboratories
L-Glutamine (200 mM)	G7513	Sigma
Magnesium chloride	22321-1000	Thermo Fisher Scientific Ltd.
Molecular grade water	W4502-1L	Sigma Aldrich
Paraffin wax	PS138/E	Thermo Fisher Scientific Ltd.
PBS without Ca²⁺/Mg²⁺	D8537	Sigma
p-dimethylaminobenzaldehyde	S647861	Sigma-Aldrich
Penicillin (5000 U/ml) / streptomycin (5 mg/ml)	P4458	Sigma
Perchloric acid (60 %)	294582D	Sigma-Aldrich
Polymyxin B	81334-5G	Sigma-Aldrich
Propan-1-ol	103456A	VWR International
Proteinase K	S3020	Dako
RNAse	123879	Sigma-Aldrich
Scott's tap water	PS138/E	Thermo Fisher Scientific Ltd.
Sodium acetate	S/2080/60	Thermo Fisher Scientific Ltd.
Sodium azide 1% solution	786-299	G-Biosciences
Sodium chloride	42429-5000	Thermo Fisher Scientific Ltd.

Chemical/Reagent	Cat No.	Supplier
Sodium dodecyl sulphate (SDS)	71727	Sigma-Aldrich
Sodium hydroxide 6M	S/4920/53	Thermo Fisher Scientific Ltd.
Trans-4-hydroxy-L-proline	H7279	Sigma-Aldrich
Trigene	CLE1312	SLS
Trizma base	T-1503	Sigma-Aldrich
Trypsin/EDTA	T3924	Sigma
Tryptone phosphate broth (TPB)	T8782	Sigma
Tween 20	P1379	Sigma-Aldrich
Ultra Vision one detection system: HRP Polymer DAB Plus substrate	TL-125-HLJ TA-125-HDX	Thermo Scientific
Vancomycin hydrochloride	861987-1G	Sigma-Aldrich
Zinc acetate	383317	Sigma-Aldrich
Zinc chloride	96470	Fluka
α -chymotrypsin	C4129-10	Sigma-Aldrich

A.3 Consumables

A list of general equipment and supplier used throughout this project.

Table A-3 : Consumables

Material	Cat No.	Supplier
2 ml cryovials	72.380.992	Sarstedt
250ml sterile containers	CON7580S	Scientific Laboratory Supplies
30 ml universal bottles	CON9000	SLS
75 ml tissue culture flask	TKT-130-210-T	Thermo-Fisher scientific
Bijoux tubes	SLS7522	SLS
Cable ties	Small	Wilkinsons
Culture slides tissue culture 4 wells	734-0088	VWR International
Fresh blood agar plates	N/A	FBS Media Services
Glass cover slips	MIC3228	Scientific Laboratory Supplies
Histology moulds	E10.8/4161	Raymond Lamb
Mersilk sutures size 3-0	W502H	Medisave
Micro tube I 1.5 ml, loop cap – Simport	212-9573	VWR International
Microtome blades	SD3050835	Fisher Scientific
Nutrient agar plates	N/A	FBS Media Services
Plastic histology cassettes	CMB-160-030R	Thermo Fisher Scientific Ltd.
Sabauroud agar	N/A	FBS Media Services

Material	Cat No.	Supplier
Six well tissue culture plates	140675	Thermo Fisher Scientific Ltd.
Stanley knife blades	N/A	N/A
Sterile glass universal tube	N/A	FBS Media Services
Superfrost microscope slide	MIC3040	SLS
Superfrost Plus microscope slide	MIC3022	SLS
TopSeal 96 well plate	6005185	Perkin Elmer
White, 96 well optiplate	6005680	Perkin Elmer

Appendix B

B.1 Statistical Analysis

Table B-1 : Basic statistical analysis terms.

Term	Equation
Sum of Value	$\sum x$
Sample number	n
Mean (\bar{x})	$\frac{\sum x/n}{n}$
Standard deviation (S)	$\sqrt{\frac{\sum x^2}{n}}$
Standard error (SE)	S/\sqrt{n}
95 % Confidence limit (CL)	$SE \times t - value$
Minimum significant difference (MSD)	$Critical\ value \times SE$

Table B-2 Statistical analysis using minimum significant difference.

Term	Equation
Minimum significant difference (MSD)	$Critical\ value \times SE$
SE	$\sqrt{\frac{mean\ square\ within\ groups}{n}}$
Critical value	$Q_{0.05} [k, v]$ the studentised range
Number of group means to be compared	k
Degrees of freedom	v